PACEMAKER ACTIVITY AND INTERCELLULAR COMMUNICATION IN THE INTESTINAL MUSCULATURE

by

Louis W. C. Liu, B. Eng., M. Eng. (McMaster University)

A Thesis

Submitted to the School of Graduate Studies

in Partial Fulfillment of the Requirements

for the Degree

Ph.D. Eng. in Electrical and Computer Engineering

McMaster University

© Copyright by Louis W. C. Liu, September 1995.

PACEMAKER ACTIVITY AND INTERCELLULAR COMMUNICATION IN THE INTESTINAL MUSCULATURE

PHD IN ENGINEERING (1995) McMASTER UNIVERSITY
(Electrical and Computer Engineering) Hamilton, Ontario

TITLE: Pacemaker Activity and Intercellular Communication in the Intestinal Musculature.

AUTHOR: Louis Wing Cheong Liu, B. Eng., M. Eng. (McMaster University)

SUPERVISOR: Dr. Jan D. Huizinga

NUMBER OF PAGES: xxii, 234

Abstract

Knowledge of the origin and characteristics of the intestinal pacemaker activity, and the characteristics of intercellular communication throughout the musculature is instrumental for the understanding of the mechanisms through which gastrointestinal (GI) motility is regulated. This thesis makes a significant contribution to provide electrophysiological and morphological evidence supporting the hypothesis that interstitial cells of Cajal (ICCs) are the GI pacemaker cells. The pacemaker activity of the GI tract triggers the slow-wave-type action potentials (slow waves) which are coherent with the phasic contractions for facilitating peristaltic movement. Origins of the slow waves at different portions of the GI tract always coincide with the locations of the ICCs. The objectives of this study were to identify the cellular origin of the pacemaker activity and to thoroughly investigate the mechanism of intercellular communication in the canine colon using electrophysiological and microscopic techniques. The cellular origin of the pacemaker activity was further examined by studying simultaneously the ontogenesis of the pacemaker activity and the ICCs in the neonatal mouse small intestine.

The cellular origin of the pacemaker activity was studied by employing the photodynamic property of methylene blue (Chapter 3). We previously demonstrated that the submuscular ICCs of the canine colon selectively accumulate methylene blue. In this undertaken study, we further illustrated that incubation with 50 μM methylene blue and subsequent intense illumination resulted in abolition of the pacemaker activity. Following methylene blue incubation, intense illumination first changed the

mitochondrial conformation in the ICCs from very condensed to orthodox, and progressively imposed more severe damages, such as swollen and ruptured mitochondria, loss of cytoplasmic contrast and detail, and rupture of the plasma membrane. No damage was seen in smooth muscle cells and nerves. The correlation between selective lesioning of ICCs and loss of the pacemaker activity strongly supports that ICCs play an essential role in the generation of the pacemaker activity.

The regulatory mechanism of the pacemaker frequency was investigated with a focus on the effects of cyclopiazonic acid (CPA), a specific inhibitor of the endoplasmic reticulum (ER) Ca^{2+}-pump (Chapter 4). CPA dose dependently decreased the pacemaker frequency. Similarly, chelating cytosolic Ca^{2+} with BAPTA also decreased the pacemaker frequency. The pacemaker frequency was also decreased by neomycin (inhibiting inositol 1,4,5-triphosphate (IP_3) synthesis) and caffeine (inhibiting the IP_3-sensitive Ca^{2+} channels in the ER membrane). Electron microscopy showed that the smooth ER forms an extensive network of subsurface cisternae which is closely associated with large areas of the cytoplasmic face of the plasma membrane. These structures were the most extensive in the ICCs, slightly less in branching smooth muscle cells and far less in circular muscle cells. Based on the electrophysiological and morphological observations, we hypothesize that the Ca^{2+} refilling cycle of the IP_3-sensitive calcium stores associated with the plasma membrane, determines the frequency of the pacemaker activity generated by the submuscular ICC-smooth-muscle network of the canine colon.

The ontogenesis of the pacemaker activity and the ICCs in the small intestine of neonatal mice was studied to further substantiate the pacemaker role of ICCs (Chapter 5). The pacemaker component of the slow waves was fingerprinted by its resistance to L-type Ca^{2+}-channel blockers and sensitivity to cyclopiazonic acid, CPA,

(Chapter 4). All isolated musculature of the neonatal mouse small intestine (newborn, unfed–7 days old) spontaneously generated action potentials. The presence of the pacemaker component in different age groups was examined by verapamil, a L-type Ca^{2+} channel blocker, and CPA. In conclusion, electrophysiological and morphological evidences were obtained to demonstrate that both the pacemaker activity and the ICC network were immature at birth but fully developed in 2 days old neonatal mice.

Communication between the longitudinal and the circular muscle layers are essential for producing co-ordinated motility in the musculature. Through electrophysiological measurements with microelectrodes, the study of neurobiotin spread using confocal microscopy and the investigation of the cellular structure at the electron-microscopic level, the cellular mechanisms of communication between the two muscle layers was studied. We positively demonstrated the existence of low-resistance pathways. We also provided evidence that the ICCs associated with the myenteric plexus facilitated electrotonic coupling between the two muscle layers across the myenteric plexus of the canine colon (Chapter 7).

In the longitudinal muscle layer, no positive evidence for electrical coupling between smooth muscle cells has yet been presented. We thoroughly examined the properties of electrical coupling in the longitudinal muscle layer of the canine colon (Chapter 8). The properties of electrical coupling between longitudinal muscle cells were compared with that between the circular muscle cells. Three electrical coupling parameters were measured: (i) the input resistance, (ii) the space constant (determined by the method developed with a double-electrode technique (Chapter 6)), and (iii) the phase relationship of simultaneously recorded electrical activities. Furthermore, a detailed electron microscopic investigation revealed the absence of

gap junctions in the longitudinal muscle layer; whereas, numerous close apposition contacts were observed. These observations put forward the hypothesis that the pathways for electrical coupling between longitudinal muscle cells are consituted by close apposition contacts.

Communication between circular muscle (CM) lamellae is necessary to generate propulsive phasic contractions for facilitating peristalsis along the longitudinal axis of the GI tract. The submuscular ICCs are extensively coupled to the underlying branching smooth muscle (bSM) cells forming an ICC-bSM network covering the entire submucosal surface of the canine colon. There is another ICC network located in the myenteric plexus. The roles of the submuscular ICC-bSM network, the myenteric ICC network and the longitudinal muscle layer in mediating communication across the CM lamellae were studied by simultaneous recordings with surface electrodes using different types of muscle strip preparations (Chapter 9). Electrophysiological evidence demonstrated that, within the pure circular musculature, circular muscle cells were electrically coupled along a CM lamella, oriented circumferentially around the lumen, but electrically insulated across CM lamellae. The submuscular ICC-bSM network, but not the longitudinal muscle nor the myenteric plexus, was shown to be essential for mediating communication between CM lamellae such that co-ordinated motility can be exhibited with neighbouring CM lamellae through excitation-contraction coupling.

In summary, employing a number of electrophysiological and microscopic techniques, this dissertation presents novel evidence (i) to substantiate the pacemaker role of ICCs in the GI tract; (ii) to put forward a hypothesis that the pacemaker-frequency regulatory mechanism is synchronized with the ER Ca^{2+} refilling cycle; and, (iii) on the heterogeneity of mechanisms through which intercellular communication occurs

along the radial, circumferential and longitudinal axes of the intestinal musculature.

Acknowledgements

I would like to express my deepest thanks to my supervisor, Dr. Jan D. Huizinga, for his unremitting guidance and yet allowing me the freedom to stretch my speculation and to explore various areas of research for satisfying my curiosity which made my learning experience more joyful and fulfilling.

My thanks also extend to other members of my supervising committee, Dr. Hubert DeBruin and Dr. Colin Nurse, for their time and expertise in helping me to complete this dissertation.

I would also like to express my thanks to Lars Thuneberg, Irene Berezin, Laura Farraway, Russell Ruo, David Richardson, Jon Lee, Areles Molleman, and John Malysz for their support and collaboration during the course of my PhD study. Because of the collaboration with these collegues, my research has been able to cover a wider spectrum and has become more complete.

Last but not the least, I would like to thank my family: my mother, my sisters (Louisa, Julianna, Patricia and Vicky), and Anthony for their support and encouragement.

This work was financially supported by the Medical Research Council of Canada (MRC) and McMaster University. I received a Studentship from MRC, and Teaching Assistantships and Centennial Scholarships from McMaster University.

Contents

List of Figures

List of Tables

Nomenclature

AMP	adenosine monophosphate
BAPTA/AM	*bis*-(*o*-aminophenoxy)-ethane-*N*,*N*,*N*′,*N*′-tetra-acetic acid, tetra (acetoxymethyl)-ester
CM	circular muscle
CPA	cyclopiazonic acid
D600	methoxyverapamil
DMSO	dimethyl sulfoxide
EM	electron microscopy
FT	full thickness
ICC	interstitial cell of Cajal
IP_3	inositol 1,4,5-triphosphate
ISWI	inter-slow wave interval
LM	longitudinal muscle
MB	methylene blue
RMP	resting membrane potential
PA	plateau amplitude
PP	plateau potential
R_i	input resistance
R_j	junctional resistance
R_m	membrane resistance

RMP	resting membrane potential
SEM	standard error of the mean
SLAP	spike like action potential
TEA	tetraethylammonium chloride
TTX	tetrodotoxin
UA	upstroke amplitude
bSM	branching smooth muscle
cpm	cycle(s) per minute
cAMP	cyclic adenosine monophosphate
min	minute(s)
n	number of samples
p	probability of a false-positive conclusion
r^2	pearson product moment correlation coefficient
rER	rough endoplasmic reticulum
sER	smooth endoplasmic reticulum
s	second(s)
λ	space constant

Chapter 1

Introduction

The *muscularis externa* of the gastrointestinal tract exhibits a large variety of motor activities for facilitating different physiological functions. In the small intestine, the motility is organized to provide mixing movements for optimal digestion and absorption of nutrients, and to generate propulsive peristaltic movement for transiting the chyme received from the stomach in the aboral direction. The large intestine, apart from providing mixing movements for optimally extracting water and electrolytes from the fluid content received from the ileum, also allows temporary storage of its luminal contents in the distal portion before defecation, during which co-ordinated propulsive contractions are generated under voluntary control.

The versatility of intestinal motility relies on the manifestation of co-ordinated contractions from the musculature. The intestinal musculature is composed of the longitudinal and the circular muscle layers which are oriented roughly orthogonal to one another. The overall motor pattern exhibited by the intestine results from the summation of contractile activities generated in both muscle layers which are regulated mainly by the mechanism of excitation-contraction coupling [53, 108, 176].

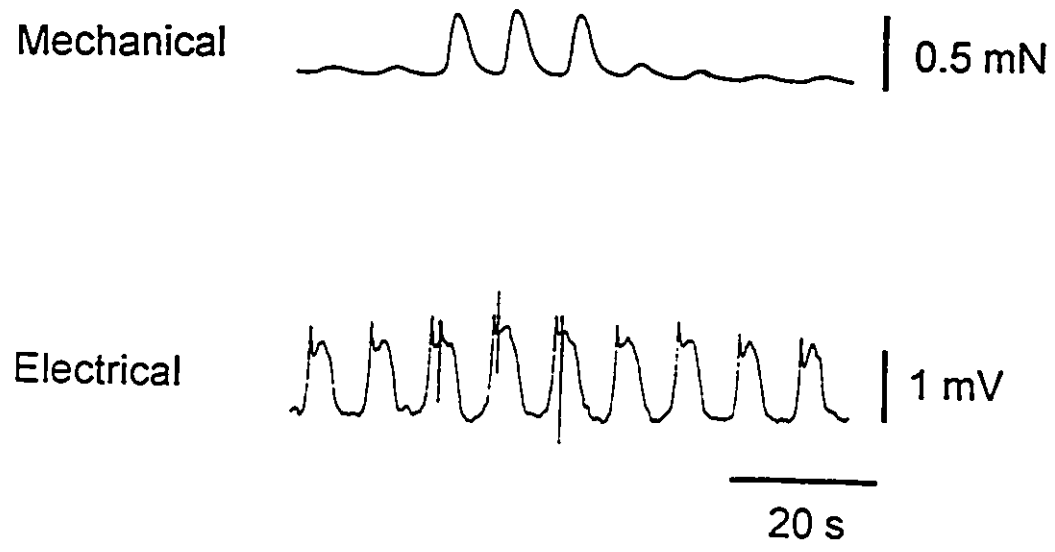

Figure 1.1: *Simultaneous electrical and mechanical recordings from the canine colonic circular muscle*

The top panel illustrates the phasic contractions recorded in the isolated circular muscle layer (with the intact submuscular ICC network) of the canine colon. The bottom panel depicts the slow wave activity simultaneously recorded at the submucosal surface by a suction electrode (see references [108, 113] and Chapter 9 for experimental set up). Note the force of phasic contractions was significantly larger when spikes were superimposed on the plateau phase of the slow waves.

Excitation-contraction coupling involves calcium ions[1] (Ca^{2+}), which enter the cells during the depolarizing phase of electrical oscillations, causing these cells to contract by activating the intracellular contractile filaments (Figure 1.1). This calcium influx is mainly mediated by L-type calcium channels [3, 4, 7, 93, 112, also see Chapters 3, 4 and 5]. In addition, the contractile activity of smooth muscle cells can also be modulated by the Ca^{2+} released from the endoplasmic reticulum (see discussion in Chapter 4).

Aboral propagation of ring-like contractions of the intestine revealed by radiology studies effectively move its luminal contents in the same direction. Becasue these contractions can occur in a very regular manner with the frequency similar to the estimated *in vivo* slow wave frequency, it is generally assumed that the slow wave activity plays a significant role in the mechanism through which the intestinal motility is controlled. The precise mechanism of this excitation-contraction coupling, however, is not understood. Better understanding of the mechanism of the intestinal motility requires (i) identification of the pacemaker cells, (ii) understanding of the mechanism through which the pacemaker activity is generated, and (iii) characterization of intercellular coupling mechanisms. Before presenting experimental evidence to unravel these enigmas, a brief account of the history in reaching the current hypotheses of the pacemaker activity and intercellular communication in the intestinal musculature will be given in the next section.

[1]Since Ringer's discovery of the peculiar importance of calcium salts for the heart contractile activity in 1883 (Practitioner, XXXI, p.81), the first detailed quantitative account of the importance of calcium ions in mechanical contractions was not performed until 1913 by Mines [129]. His results confirmed Locke's earlier conclusion which stated that "calcium is necessary for the conversion of the heart's chemical energy into the mechanical energy of its beat" [121, page 213].

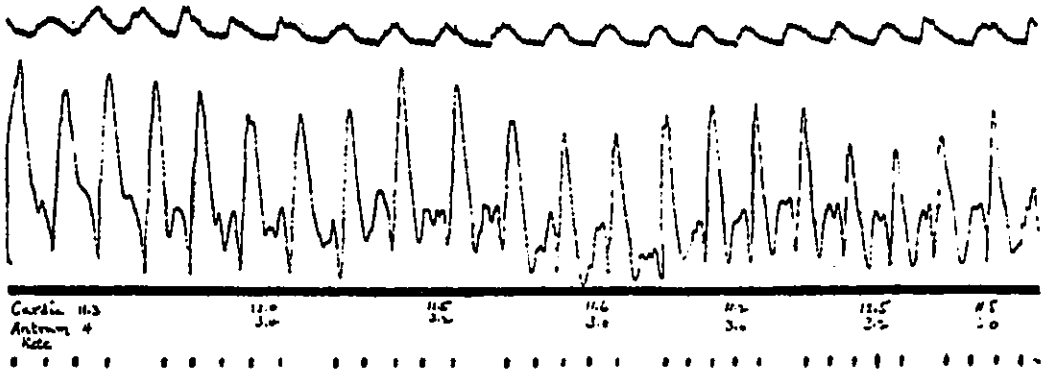

Figure 1.2: *The first published simultaneous recordings of electrical and mechanical activities recorded from the pyloric antrum*

The top panel shows mechanogram at the upper end of the pyloric antrum. The smaller waves on the mechanogram are respiratory in origin. The large ones represent gastric peristalsis. The bottom panel shows the simultaneously recorded electrogram from the pyloric antrum. Electrical recordings were made by a small calomel electrode whose output currents were registered by an Einthoven galvanometer. Recordings were made by directing the beam of light reflected from the galvanometer mirrors through the slit of a camera on to a revolving drum covered with bromide paper. Adapted from reference [2].

1.1 A conspectus of the early history of intestinal physiology

In 1899, Bayliss and Starling first described the peristaltic movement in details in the canine small intestine *in vivo* [11]. In 1902, Cannon demonstrated 6 cycle per min (cpm) phasic contractions in the feline colon using a radiography technique [37]. A subsequent study performed in 1904 by Elliott and Barclay-Smith [65] confirmed Cannon's observations and found similar contractile patterns in other mammals, such as dogs, ferrets, guinea pigs, hedgehogs, rabbits and rats.

"Electro-enterograms[2]" novelly presented by Alvarez[3] and Mahoney in 1922 [2] landmarks the forefront of today's gastrointestinal electrophysiology. The periodic electrical potential oscillations were termed as "action currents" because, most of the time, each oscillation (current) was observed to be associated with a contraction (action). This association was demonstrated by simultaneously obtained "electrograms" and "mechanograms" (Figure 1.2). This pioneer study also described the frequency gradient of the action currents in the small intestine. An additional intriguing, albeit unintentional, observation was the temperature dependence of the action current frequency.

---

[2]The term, "electro-enterogram", was conceivably chosen in parallel with the electro-cardiogram.

[3]Alvarez's first efforts to show the action currents in the bowel were made in 1913 with the help of Dr. Alexander Forbes. A few recordings were made with the string galvanometer in the Physiological Laboratory at Harvard. In 1917, collaborating with Dr. Robert Newell, a few good electrical recordings were obtained from the rabbit small intestine with an Einthoven galvanometer through zinc-zinc sulfate moist thread electrodes. Unfortunately, the study was forced to be suspended until better electrodes could be secured.

Alvarez proclaimed that "the most remarkable thing about these action currents is that they are produced constantly in the stomachs and intestines which, so far as the eye can detect, are absolutely motionless [2, page 482]." This observation stimulated Berkson to perform a series of studies with an objective to determine the cellular origin of the action currents. Berkson observed that the action currents[4] were associated with contractions only periodically [18]. Such an uncoupling of the electrical and the mechanical activities challenged the concept of action currents [14]. He concluded that although the action currents were independent of the extrinsic nervous system [15], these "electrical changes are not true action currents of muscle ... (and) ... the characteristic cycles ... originate in a physiological rhythm within the intrinsic nervous plexus [16, 17]." Furthermore, Berkson was probably the first one to hypothesize the excitation-contraction coupling mechanism in the gastrointestinal tract; he postulated that the generation of mechanical contractions was triggered by the rising phase of electrical oscillations [18].

Having the knowledge of the cellular origin of the action potentials[5], Bozler was interested in the nature of intercellular communication. Bozler intuitively speculated that because "the muscular coat of the viscera contains an enormous number of fibers, uncoordinated activity of the small muscle cells, therefore, could never produce the regular movements which are observed in these organs" [31, page 614]. Being inspired by Engelmann's observations[6], Bozler performed a series of experiments and

[4]The action currents were recorded from anaesthetized rabbits with non-polarizable electrodes made of steel piano wire electroplated with silver and then chloridizing the silver electrolytically. This was probably the first employment of the Ag-AgCl non-polarizable electrodes for recording bio-potentials.

[5]The action potentials were later found to be non-neuronal in origin.

[6]Engelmann observed, in 1869-70, that mechanical and electrical stimulations of the ureter produced contraction waves propagating in either direction from the source of stimulation (Pflüger's

concluded that the visceral muscles, like cardiac muscle, are syncytia [31, 33]. The mechanism of intercellular communication also fascinated Prosser later. His approach to understanding this question was by means of both structural and electrophysiological investigations. Using low power electron micrographs, he demonstrated the presence of "intercellular bridges" between circular muscle cells which provided a structural basis for intercellular communication [145]. Prosser also observed that the conduction velocity of the action potentials decreased with an increase in the intercellular space [138]. In 1962, with the development of high power electron microscopes, Dewey and Barr identified nexuses[7] which "comprised of three dark lines of uniform thickness separated by two light regions [57]." A nexus, "meaning a region where the plasma membranes of two excitable cells are fused", provides "direct electrical connection between cell interiors without intervening extracellular space [57, page 672]" and intracellular integrity.

These pioneer studies initiated the era of research into gastrointestinal physiology to identify the cellular origin of the pacemaker activity and to determine the mechanism of intercellular communication. Before proceeding to the discussion of the current hypotheses and the advancement contributed by the undertaken thesis, a definition of the nomenclature used to describe the gastrointestinal action potentials is indispensable to avoid confusion.

Arch. 2: 243, 1869; and, Pflüger's Arch. 3: 248, 1870).

[7]Nexuses are now commonly known as gap junctions.

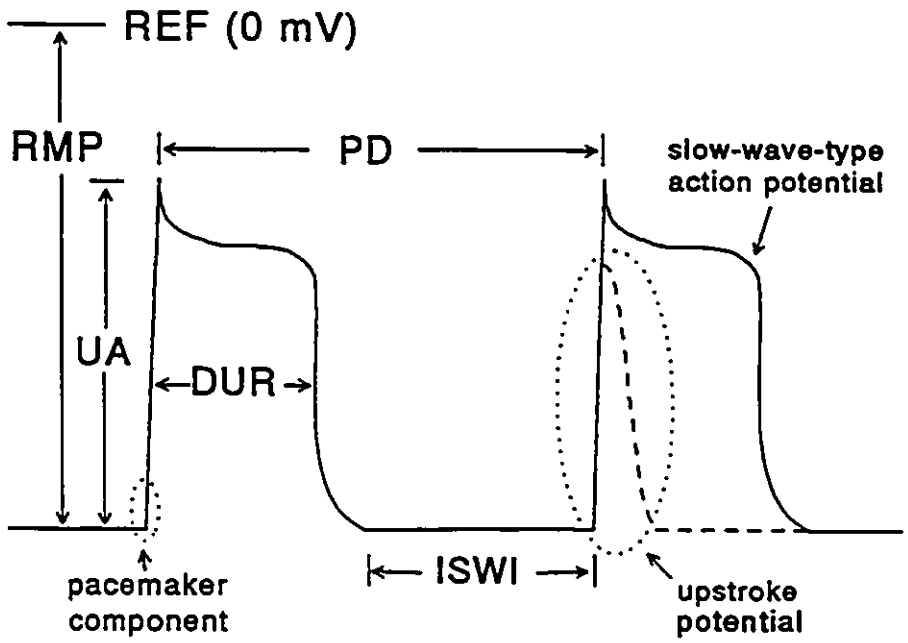

Figure 1.3: *Schematic illustration defining the terminology used to characterize the slow wave activity*

The slow-wave-type action potentials (slow waves; solid line) are initiated by a biochemical clock which triggers the initial depolarization (pacemaker component) during the rising phase. The duration (DUR) is the time interval at the half maximum of the plateau amplitude. The inter-slow-wave interval (ISWI) is the time interval at the resting membrane potential between the end of the repolarization phase of a slow wave and the initial depolarization of the next slow wave. The frequency is the inverse of the period (PD). As illustrated in the second slow wave, the dashed line outlines the L-type calcium channel-blocker resistance component of the slow waves. This component consists mainly of the upstroke phase of the slow waves and contains the pacemaker component; it is termed "upstroke potential". REF — reference potential; RMP — resting membrane potential; UA — upstroke amplitude.

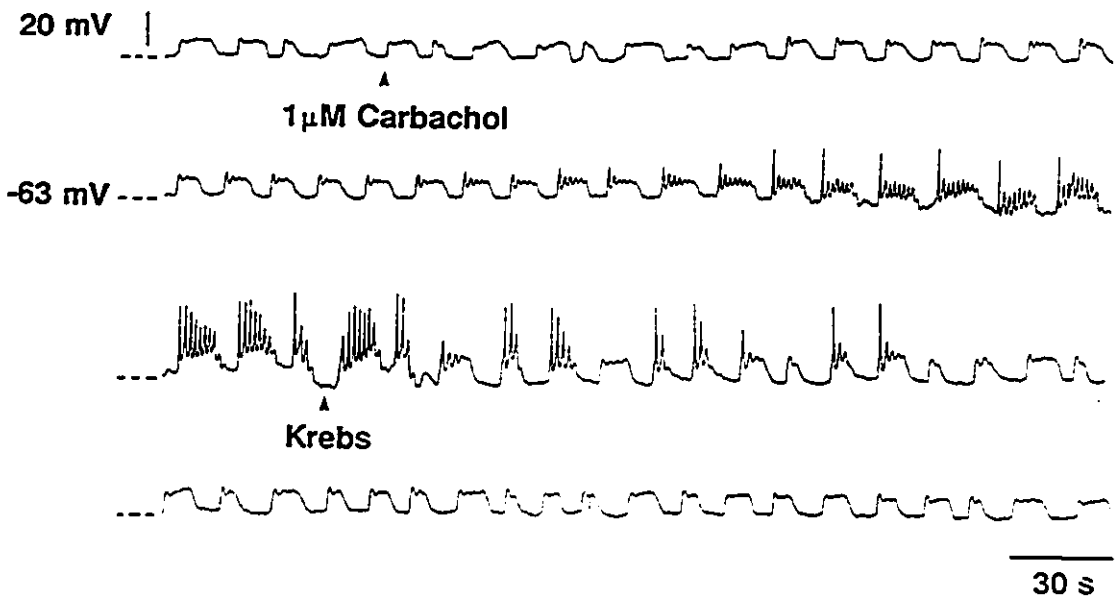

Figure 1.4: *Induction of spike-like action potentials by carbachol in the canine colonic circular muscle*

Intracellular recording was made from a circular muscle cell approximately in the middle of the circular muscle layer between the submucosal and the myenteric borders. The longitudinal muscle layer and the myenteric plexus were removed. Circular muscle cells were exposed for impalements, by mounting the preparation sideways, as described previously [110]. Carbachol (1 μM) increased the slow wave duration and induced spike-like action potentials superimposed on the plateau phase. Effects of carbachol were completely reversible after washout.

1.2 Nomenclature of the gastrointestinal action potentials

The terminology employed today to describe the gastrointestinal action potentials evolved from studies presented by Alvarez, Bozler and Posser. During 1938-42, Bozler redefined Alvarez's "action currents." Bozler identified two distinguishable components of the action potentials: (i) the "spike potentials" whose amplitude and abundance strongly correlated with the strength of the contractions [32, also see Figure 1.1]; and, (ii) the "slow potential waves" which were present in all regions of the gastrointestinal tract [34]. Spikes were very often observed "at the negative crest ...(plateau phase) ...of such waves" [34]. This relationship between the spikes and the slow waves is also illustrated in Figure 1.4. Unlike *in vivo* observations made by Alvarez [2] and Berkson [14, 15, 18, 16], the slow waves[8] are always associated with phasic contractions in *in vitro* studies [3, 4, 176, also see Figure 1.1]. Hence, the slow waves are also termed as slow-wave-type action potentials[9] [87, 176].

In summary, the two types of action potentials prevailingly recorded in the gastrointestinal musculature are the *slow-wave-type action potentials* (*slow waves* in short) and the *spike-like action potentials* (*SLAPs*). Furthermore, electrophysiological observations characterized two distinct components in the slow waves: (i) a L-type calcium channel blocker sensitive component which contributes mainly to the plateau phase and is associated with contractions; and (ii) an *upstroke potential* which em-

[8]The term, slow waves, was probably first used by Nagai and Prosser [138] which referred to the "slow potential waves" identified by Bozler.

[9]The slow waves and spikes had previously been named electrical control activity (ECA) and electrical response activity (ERA), respectively, because contractions were thought to be triggered by ERA but not by ECA.

bodies the *pacemaker component* (Figure 1.3). The slow wave duration is directly related to the level of excitation [3, 4, 87, 91]. When the level of excitation was increased pharmacologically [91], SLAPs can frequently be observed superimposed on the lengthened plateau phase of slow waves (Figure 1.4). The SLAPs, whose occurrence is strongly correlated to the force of phasic contractions (Figure 1.1), are generated by activation of L-type calcium channels [87, 90, 88].

1.3 Cellular origin of the pacemaker activity in the intestinal tract

After the neural origin hypothesis of the slow wave activity was defeated [144], it was thought for a long time that the slow waves are *myogenic* in nature. That is, the generation mechanism of the slow waves is an intrinsic property of smooth muscle cells. In the small intestine, early experimental evidence obtained from cats [24, 26, 138], and dogs [54] form the basis for the hypothesis that the slow waves were generated by the longitudinal muscle. In the colon, it was first observed in cats that the slow waves were generated in the isolated circular muscle but not in the isolated longitudinal muscle [44]. It was concluded that the slow waves were generated in the circular muscle. In view of these observations, Tomita speculated that "it is thus possible that some particular cells located between the muscle layers act as pacemakers for the slow waves. ... The slow waves are fundamentally of myogenic origin. ... If this kind of specialized pacemaker cells exists in all parts of the gastrointesinal tract, then it may be that when the longitudinal and circular muscle layers are separated from each other, these cells tend to attach to the longitudinal muscle in the cat small intestine and stomach, to the circular muscle in the cat colon ... and this determined

the activity of the preparations." [186].

The myogenic origin of the slow waves had been widely accepted until the publication of an instrumental paper written by Thuneberg [179] in 1982. Based on the histological characteristics of interstitial cells of Cajal (ICCs) and their topographical association with nerves and smooth muscle cells, Thuneberg hypothesized ICCs to be the pacemaker cells of the gastrointestinal tract after accounting the electrophysiological observations of the origin of the slow waves. Since its conception by Thuneberg in 1982 [179], the hypothesis that ICCs regulate the rhythmicity of the slow wave activity of the gastrointestinal tract has received increasing attention. In the stomach, an ICC network is observed to be associated with the myenteric plexus [45, 180]. In the small intestine, ICC networks are present in both the myenteric plexus and the deep muscular plexus [42, 153, 154, 179, 180]. In the canine colon, a complete and relatively dense network of ICCs is found at the submuscular surface of the circular muscle layer [12, 45, 119, 180, 188], whereas ICCs are more scattered in the myenteric plexus [13]. The organization of the ICC network in the submuscular plexus of the canine colon was recently made visible under the light microscope after selective accumulation of methylene blue by ICCs [119].

Studies using different types of isolated muscle strips demonstrated that the slow waves originate from the locations where the ICCs are found. In the stomach, the slow wave activity orginates at the myenteric border between the longitudinal and the circular muscle layers [9, 10]. In the small intestine, evidence was obtained for formulating a hypothesis that the slow waves are generated by non-neural cells situated at the boundary between the longitudinal and the circular muscle layers [82, 175]; whereas, in the colon, the pacemaker activity originates from the submucosal surface [5, 38, 58, 60, 112, 113, 172]. Another set of experiments addressed the

pacemaker role of the ICCs more sepecifically by directly correlating the ability of the tissue to generate the pacemaker activity to the integrity or the presence of the ICCs; evidence put forward the hypothesis that the pacemaker potential is generated by the ICCs associated with the myenteric plexus of the small intestine [85, 183], and by the ICCs associated with the submuscular plexus of the colon [189, also see Chapter 3,]. Additional evidence supporting the pacemaker role of ICCs are presented in Chapters 4 and 5. As the evidence of ICCs being the gastrointestinal pacemaker cells is progressively mounting, the myogenic origin of the slow wave activity becomes *questionable* since ICCs are not classified as smooth muscle cells.

1.4 Metabolic regulation of the pacemaker activity

Metabolic regulation of the pacemaker activity was probably first stated in 1941 by Bozler who stated that "the degree of polarization of the cell surface probably is closely related to the metabolic changes within the cells [33, page 559]." Recent experimental observations acquired from the canine colon lead to a hypothesis that the slow wave frequency is paced by an intracellular biochemical clock sensitive to intracellular processes rather than by a voltage driven cyclic activation-inactivation of ionic channels intrinsic to the plasma membrane. This hypothesis is supported by: (i) there is no consistent diastolic depolarization[10]; (ii) the slow wave frequency is

[10]The slow waves arise abruptly from a stable resting potential, without a diastolic potential like the cardiac action potentials. Because of our knowledge about the location of the ICC networks, many investigators have purposefully recorded from these areas and no consistent slow depolarization can be observed before the initiation of slow waves.

Figure 1.5: *The gap junction density gradient in the canine colonic musculature* Immunohistochemical localization of connexin 43 (a gap junction protein) was performed on the canine colonic musculature using the method described previously by Mikkelsen *et al.* [128]. The locations of gap junction protein are depicted as bright dots in the micrographs. (a) Distribution of gap junctions in the first quarter of the circular muscle layer away from the submucosal border is shown. Strong immunoreactivity of connexin 43 (Cx 43) was observed at the submucosal border of the circular muscle layer (arrow heads) indicating that the gap junction density is significantly higher at the submucosal border. The gap junction density decreases abruptly in the radial direction of the colon. This observation is consistent with the electron microscopic observations that gap junctions can only be abundantly found in the first 5–7 layers of the circular muscle cells away from the submucosal border. The density of gap junctions is usually higher along the septa (arrow). SMP — submuscular plexus, × 2,600, Bar — 5 μm.

(b) Distribution of gap junctions in three quarters of the circular muscle layer away from the myenteric border (arrow). Gap junction density is higher in the circular muscle layer near the myenteric border than in the body of the circular muscle. Immunoreactivity of Cx43 was not observed in the longitudinal muscle layer (LM). × 1640, Bar — 5 μm.

Figure 1.5

very sensitive to changes in intracellular second messengers, such as cAMP [92], but not to voltage; and, (iii) the slow wave frequency is extremely sensitive to changes in temperature. Importantly, the reduction in the slow wave frequency by a decrease in temperature [6] cannot be sufficiently explained by the temperature dependence of voltage activated ionic currents [146]. In Chapter 4, the slow wave frequency is further demonstrated to be sensitive to changes in intracellular Ca^{2+}. The specific mechanism and the source of Ca^{2+} will be discussed later.

1.5 Heterogeneity in intercellular junctions

In spite of a remarkable cell heterogeneity, gastrointestinal smooth muscle produces synchronized action potentials for generating coordinated motility. Not only are the intrinsic electrical activities displayed by different cell types markedly different, but the gastrointestinal musculature also shows a significant heterogeneity in the distribution of intercellular junctions.

It is widely accepted that gap junctions constitute the structural basis for intercellular communication [52, 77, 84] through which individual cells can function in harmony as a tissue. However, the distribution of gap junctions is extremely non-uniform in the musculature. In the small intestine, gap junctions are abundantly found throughout the entire outer circular muscle layer but not in the inner circular muscle layer nor in the longitudinal muscle layer[11]. In the colon, gap junctions have never been observed in the longitudinal muscle layer [76, 184]. Even within the circular muscle layer of the canine colon, the distribution of gap junctions is extremely

[11]In a single study, a gap junction has been demonstrated in a slightly oblique section obtained from the longitudinal muscle of the cat small intestine [178]. The presence of gap junctions in the longitudinal muscle layer of the small intestine is awaiting to be confirmed.

non-uniform. Gap junction density is found to be the highest at the submucosal surface and then decreases abruptly along the radial axis of the colon (Figure 1.5). In the human intestine, no gap junctions has ever been observed in the entire musculature [153, 155]. The physiological significance of such a heterogeneity in the distribution of gap junctions is unclear. In the canine colon, the abundant amount of gap junctions at the submuscosal border of the circular muscle layer may be related to the metaboiic regulation of the pacemaker activity [67, 107]. In Chapters 7 and 8, experimental evidence is presented to demonstrate possible physiological significance of such an heterogeneity in intercellular junctions in the canine colonic musculature.

1.6 Evidence of electrical coupling within the intestinal musculature of the colon

Since the majority of research described in this thesis was performed on the canine colon, an overview of what is known in the colon is deemed to be sufficient to formulate the objectives conferred in the next section. Comparison of the experimental observations made in the colon to other systems is presented elsewhere in subsequent Chapters.

1.6.1 Submuscular ICC-circular muscle interactions

Electrical communication between the submuscular ICC network and the body of the circular muscle becomes evident when one records from the whole circular muscle layer including the submuscular ICC network [110]. The isolated circular muscle layer, devoid of the submuscular ICC network, is spontaneously quiescent with a resting membrane potential uniformly at approximately -62 mV (Figure 1.6a). If

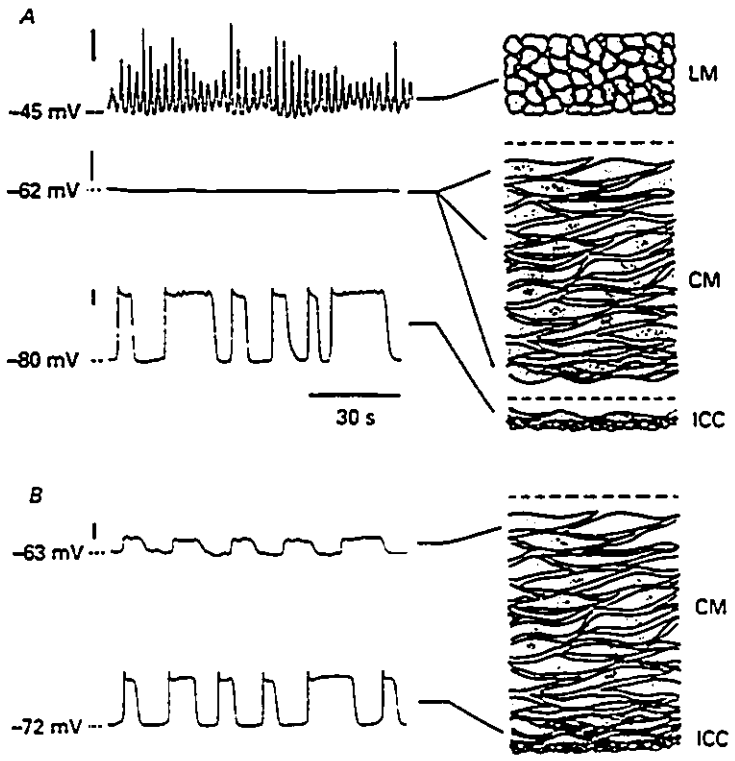

Figure 1.6: *Electrical oscillations in isolated muscle strips of canine colon*
a) Microelectrode recordings were made at the myenteric surface of an isolated longitudinal muscle (LM) preparation (first panel), various locations in circular muscle (CM) preparations (second panel) and the submucosal surface of an ICC-rich preparation (third panel). The ICC-rich preparations consist of the submuscular ICC network and a few layers of adjoining smooth muscle cells. b) Recordings were made at the myenteric and submucosal surfaces of the ICC-CM preparations. Note the resting potential gradient in the circular muscle layer. Such a gradient is absent in the CM preparations.

the submuscular ICC network is attached, the slow wave activity can be recorded throughout the entire circular muscle layer (Figure 1.6b).

As a consequence of electrical coupling, the resting membrane potentials of the submuscular ICC network (−80 mV) and the circular muscle (−62 mV) converge towards a rather uniform resting potential of −72 mV for the first 7% of the circular muscle layer (Figure 1.7). This area of uniform resting membrane (up to $\approx$ 75 μm away from the submuscular surface) is characterized by a high density of gap junctions, as determined by electron microscopy [12] and immunohistochemistry [128, also see Figure 1.5]. Furthermore, excellent electrotonic current spread is measured at the submuscular surface [89, 114, Chapter 8]. Since this is blocked by octanol [89], it seems likely that gap junctional coupling is responsible for the averaging effect of the membrane potential in cells near the submuscular border.

1.6.2 Longitudinal-circular muscle interactions

Electrical communication between the longitudinal and the circular muscle layers is illustrated by comparing the intrinsic resting membrane potential of the circular muscle cells near the myenteric border to that of the full thickness preparations (Figures 1.6 and 1.7). With the circular muscle coupled to the longitudinal muscle in the full thickness preparations, the resting potential is $\approx$ −48 mV in the myenteric plexus area. As discussed, in isolated muscle strips, the circular muscle has a resting potential of −62 mV and the longitudinal muscle of −45 mV in the myenteric plexus [110]. Coupling of longitudinal muscle to circular muscle apparently depolarizes the myenteric circular muscle cells by 14 mV but hyperpolarizes longitudinal muscle cells by only 3 mV. The mechanism of electrical communication leading to a greater influence on the resting membrane potential of the circular muscle compared to the

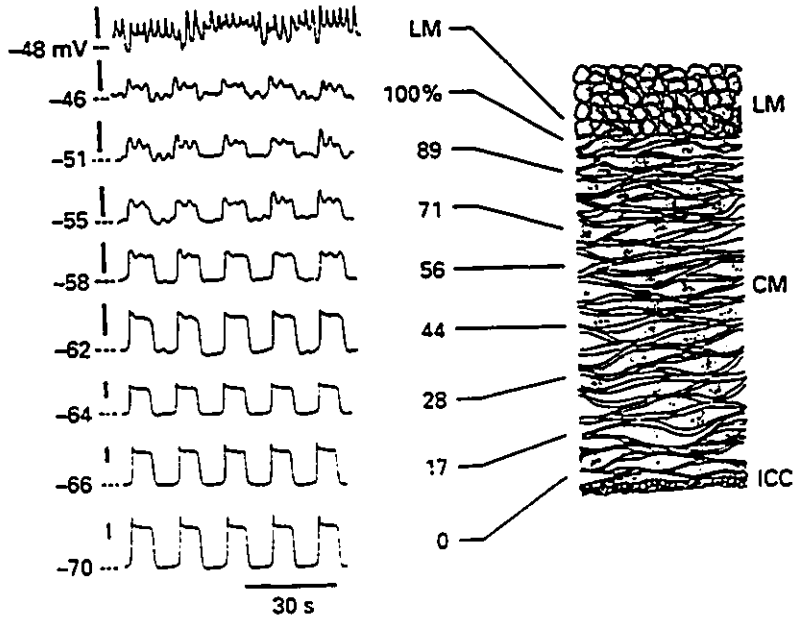

Figure 1.7: *Electrical oscillations in a full thickness preparation of canine colon* Microelectrode recordings were made at different locations of the circular muscle layer as well as the myenteric border of the longitudinal muscle. 0% indicates the submuscular surface; 100% is the myenteric interface. The slow wave pattern remains distinguishable throughout the entire circular muscle layer despite the change in resting membrane potential. Note that the frequency and duration of slow waves are very similar throughout the entire circular muscle although recordings were not made simultaneously. Spike like action potentials start to appear at about 56% in this preparation. Also note that the resting potential in the myenteric border of the longitudinal muscle fluctuated as compared to the more steady resting potential in the isolated LM preparations (see Figure 1.6). Calibration bars represent 10 mV.

longitudinal muscle is unclear. A hypothesis is postulated in Chapter 7 to account for such an anisotropic coupling based on the different degree of electrotonic coupling in the longitudinal and circular smooth muscle adjacent to the myenteric plexus.

Another evidence of longitudinal-circular muscle interaction is the exhibition of spike-like action potentials (SLAPs) in the myenteric half of the circular muscle layer. The frequency and duration of SLAPs in the circular muscle were very similar to those observed in the longitudinal muscle. Furthermore, the SLAPs recorded simultaneously in a longitudinal and a circular muscle cell near the myenteric borders appear to be entrained [172, 160, unpublished observations, Liu and Huizinga]. However, it is noteworthy that the maximum SLAP amplitude was found between 70% and 80% of the circular muscle thickness away from the submuscular surface [110]. Hence, the amplitude of SLAPs superimposed on the slow wave plateaus of the circular muscle did not follow an exponential decay function starting from the myenteric plexus; it indicates that SLAPs observed on the plateaus of slow waves do not propagate passively into the circular muscle from the longitudinal muscle. Although it is likely that the SLAPs, generated in the longitudinal muscle, propagate into the circular muscle and modify its electrical activity (since the two muscle layers are electrically coupled), this illustrates that circular muscle cells can actively generate SLAPs. Their appearance in the circular muscle depends on the level of excitation (Figure 1.4).

1.6.3 Communication between circular muscle lamellae

The circular muscle layer of the intestine is hypothesized to be divided into discrete circumferentially oriented groups of smooth muscle bundles (lamellae) that are separated by connective tissue septa [108, 119, 140, 155, 153, 184]. This organization

brings into question how the activity among circular muscle lamellae is synchronized to provide propulsive contractions in the longitudinal direction of the intestine. *In vivo* recordings from the dog colon revealed a cyclic occurrence of bursts of contractions propagating in the aboral direction at a speed of 3–20 cm/min [163]. Similarly, Fioramonti *et al.* [73] reported propagation of spike bursts at 14 cm/min. These observations suggest that circular muscle lamellae are electrically coupled. Using transection techniques, an *in vitro* study in the cat colon showed that slow waves were phase locked and propagated at a velocity of $\approx$ 18 cm/min in the longitudinal direction through the "interface between the submucosa and muscularis propria" [48]. In the canine colon, the submuscular ICCs are in intimate contact with the underlying branching smooth muscle cells (bSM) by an abundant amount of gap junctions. The presence of a continuous ICC-bSM network covering the entire submuscular surface of the dog colon [119] provides a structural basis for a role of the ICC-bSM network in inter-lamellar communication in the circular muscle layer. This hypothesis is supported by experimental evidence presented in Chapter 9.

1.7 Objectives

It still remains obscure why the pacemaker activity is generated by the ICCs associated with the myenteric plexus of the small intestine but by the ICCs associated with the submuscular plexus of the large intestine. What are the physiological significances of the ICC network located in the deep muscular plexus of the small intestine and that located in the myenteric plexus of the large intestine? These networks apparently do not play a role in generating the pacemaker activity. Furthermore, once the pacemaker activity is generated, how does it then propagate to the rest of the musculature

to command a co-ordinated contraction in the musculature with an ostensible heterogeneity in intercellular junctions? I have tried to address some of these questions in this dissertation. The explicit objectives of the undertaken research are: (i) to identify the cellular origin of the pacemaker activity in the canine colonic musculature using the photodynamic property of methylene blue, (ii) to reveal the relationship between the pacemaker-frequency regulatory mechanism and the intracellularly stored Ca^{2+}, (iii) to extend the hypothesis established in (ii) and apply it to the mouse small intestine, (iv) to substantiate the pacemaker role of the ICCs by following the ontogenesis of the ICCs and the pacemaker activity, (v) to unravel the mechanism of communication between the circular and the longitudinal muscle layers, (vi) to determine the degree of electrical coupling in different areas of the canine colonic musculature, and (vii) to access roles of the longitudinal muscle layer, the myenteric plexus and the submuscular ICC-bSM network in mediating communication across the circular muscle lamellae.

Chapter 2

Methodology and Thesis Outline

2.1 Choice of animal models

The advantages of choosing the canine colon as the animal model in the undertaken study are: (i) different muscle strips ,such as the circular muscle layer with or without the intact submuscular ICC network and the longitudinal muscle layer, can easily be dissected; and, (ii) our existing knowledge of the electrical activities. The rationale of the use of different muscle strip preparations has been discussed in my Master's thesis [108]. In each of the following research Chapters, the strip preparations and methodology employed in various studies will again be justified separately for their appropriateness in meeting the stated objectives. Experimentaticns on the pacemaker role of ICCs and the frequency-regulatory mechanism of the pacemaker activity were extended to the neonatal mouse small intestine. The pacemaker role of the ICCs was demonstrated by the simultaneous development of the myenteric-ICC network and the pacemaker component of the slow waves.

2.2 Electrophysiological studies

Both the intracellular microelectrode technique and the suction surface-electrode technique were employed in this work. Box diagrams of the experimental set-up and description of various components have been discussed in my Master's thesis [108]. Brief descriptions of the experimental set-up and the technique employed in various studies will be discussed in corresponding chapters. The suction-electrode experiments shown in Chapter 9 were implemented by Russell Ruo.

2.3 Morphological studies

The electron microscopic examinations described in various research chapters were performed by Irene Berezin (Chapters 7 and 8) and Lars Thuneberg (Chapters 3, 4 and 5). The neurobiotin experiments described in Chapter 7 were performed by Laura Farraway.

2.4 Thesis outline

The research chapters (3–9) are written in the format of independent manuscripts[1] and are self-explanatory. Each chapter is started with an Epitome which highlights the essence of each study and ended with a Discussion which relates the undertaken study to relevant literature in other systems. The method section in each chapter

[1]Chapter 3 is published in the American Journal of Physiology and presented as is. Chapter 4 is published in the Journal of Pharmacology and Experimental Therapeutics and presented as is. Chapter 6 is in revision and to be submitted to the Canadian Journal of Physiology and Pharmacology. Chapter 7 is submitted to Cell and Tissue Research. Chapters 5, 8 and 9 are in the final editing stage prior to submission.

is sufficiently described for the understanding and interpretation of the results presented. The Introduction and Discussion sections contain extensive references to the literature. These discussions are not repeated in the general introduction (Chapter 1) and discussion of this dissertation (Chapter 10).

Chapter 3

Selective Lesioning of Interstitial Cells of Cajal by Methylene Blue and Light Leads to Loss of Slow Waves

3.1 Epitome

Incubation with 50 μM methylene blue (MB) and subsequent intense illumination resulted in abolition of the slow wave activity in ICC-CM preparations (the circular musculature with the submuscular interstitial cells of Cajal network) of canine colon. This was often accompanied by a decrease in resting membrane potential.

This chapter was published in the American Journal of Physiology, 266: G485-G496, 1994, by Louis Liu, Lars Thuneberg and Jan Huizinga. Contributions of Lars Thuneberg are discussed in section 2.3 of Chapter 2.

Repolarization of cells back to −70 mV did not restore the slow wave activity indicating that methylene blue plus light directly interrupted the generation mechanism of slow waves. Following MB incubation, a 2 min illumination consistently changed the mitochondrial conformation in the ICCs from very condensed to orthodox, without inducing any obvious changes in smooth muscle cells. After 4–10 min illumination, ICCs became progressively more damaged with swollen and ruptured mitochondria, loss of cytoplasmic contrast and detail, loss of caveolae, and rupture of the plasma membrane. No damage was seen in smooth muscle cells and nerves. Gap junctional ultrastructure was preserved. Intense illumination without pre-incubation with MB left the slow waves and the ultrastructure of ICC-CM preparations unaffected. In CM preparations, without the submuscular ICC-smooth-muscle network, MB plus light induced no changes in electrical activity. We conclude that the correlation between selective damage to ICCs (relative to smooth muscle) and selective loss of the slow wave activity (relative to other electrical activity of the circular muscle) strongly indicates that ICCs play an essential role in the generation of slow waves.

3.2 Introduction

The concept of a regulatory role of interstitial cells of Cajal (ICCs) in the function of gastrointestinal (GI) tract was pioneered by Stach in 1972 [173], Duchon *et al.* in 1974 [59] and Faussone-Pellegrini *et al.* in 1977 [71]. It was not until 1982 that ICCs were hypothesized to play a role in the generation of the auto-rhythmicity in the GI tract by Thuneberg [179]. Evidence that ICCs contribute to the generation of pacemaker activity and subsequent generation of slow-wave-type action potentials (slow waves) has been obtained in a number of tissues, including the small intestine [82, 175], and

the colon [38, 58, 60, 113, 172]. Significantly, an ICC network can be found in areas (the myenteric plexus of the small intestine [97, 179] and the submuscular plexus of the colon [12, 119, 180]) where slow waves originate.

In the canine colon, evidence that the submuscular ICCs play a role in the generation of pacemaking activity comes from the following observations: (a) when the ICC network is removed, the circular muscle layer does not generate the slow wave activity [60, 113, 172]; and (b) in very thin preparations consisting of the ICC network and some associated smooth muscle cells, spontaneous slow waves are consistently recorded [110, 166, 172]. We have shown that the electrical activity recorded at the submuscular surface is a consequence of electrical interactions between the body of the circular muscle and the ICC network with associated smooth muscle cells [110]. Because of the extensive coupling of ICCs to smooth muscle cells by gap junctions [12], the relative roles of each cell type in the generation of the slow wave activity cannot be deduced with certainty from electrophysiological studies using isolated muscle strips alone.

Before the advent of electron microscopy, the most selective method for the recognition of ICCs relied upon the ability of ICCs to accumulate the dye, methylene blue,under physiological conditions [150, 177]. Depending on conditions, methylene blue may primarily stain ICCs or nerve tissue (with or without glial cells), or give rise to an unspecific staining pattern [182, 183]. Previously, the identification of ICCs using vital methylene blue staining was limited to the small intestine of mice, guinea pigs, and rabbits. In a recent paper, we have demonstrated the feasibility of obtaining a selective methylene blue accumulation in ICCs of the submuscular plexus in canine colon [119]. In the same study, we showed that, in subdued light, methylene blue per se induced no ultrastructural changes to the stained ICCs and did not significantly

affect the slow wave characteristics of cells impaled at the submuscular border.

In earlier studies, disappearance of the slow wave activity in the mouse small intestine was observed when the selectively methylene blue stained ICCs at the myenteric border were illuminated [183]. Furthermore, illumination of methylene blue stained ICCs in cultured explants of the mouse small intestine resulted in a loss of spontaneous rhythmic contractile activity; this effect was reversible for a short period of low intensity illumination, but otherwise irreversible [182].

Our objective was to find a method to specifically lesion canine colonic ICCs associated with the submuscular plexus. The photo-toxic properties of methylene blue were used to study possible effects on the slow wave activity and changes in the ultrastructure of different cell types associated with the submuscular ICC network.

3.3 Materials and methods

3.3.1 Tissue acquisition and preparation

Dogs of either sex were killed by an overdose of pentobarbital sodium (100 mg/kg) given intravenously. Approximately 5 cm of proximal colon was taken starting from 5 cm distal to the ileocecal junction. The colon was then opened by a longitudinal cut. A cleaned segment was pinned flat to the Sylgard bottom of a dissecting dish filled with continuously oxygenated (95% O_2 and 5% CO_2) Krebs solution.

To study the specificity of the actions of methylene blue plus light, we examined the effects on both *ICC-CM preparations* (submuscular ICC network plus circular muscle) and *CM preparations* (circular muscle devoid of the submuscular ICC-smooth-muscle network). The procedures for obtaining these preparations have been described previously [113].

Approximately 2 × 2 mm of the tissue, with the submucosal surface facing up, was pinned onto the Sylgard bottom of a transfer holder. The tissue was then cut along the pinned edges, except one edge from which a strip of 10 mm in length (3 mm wide at the pinned edge and gradually reduced to 2 mm at the free end) was cut along the long axis of the circular muscle cells. The free end of the strip was tied to a surgical silk (0.5 mm in diameter). The holder was transferred to a partitioned chamber with the pinned tissue in the recording chamber and the free end in the stimulating chamber. The free end was also tied to a force transducer.

3.3.2 Drugs and solutions

All the solutions perfused into the partitioned chamber were prewarmed to 37.0±0.5 °C and oxygenated with 95% O_2 and 5% CO_2. The composition (in mM) of the Krebs solution was: NaCl — 120.3; KCl — 5.9; $CaCl_2$ — 2.5; $MgCl_2$ — 1.2; $NaHCO_3$ — 20.2; NaH_2PO_4 — 1.2 and glucose — 11.5. Methylene blue (Sigma) was dissolved directly into Krebs solution. $BaCl_2$ (Fisher Scientific Company) stock solution (1 M) was prepared in deionized distilled water. Bay K8644 (Sigma) was dissolved in dimethyl sulfoxide (DMSO) to prepare a stock solution of 1 mM. DMSO in the concentration applied did not have any effect.

3.3.3 Intracellular recordings

Intracellular recordings were made with microelectrodes that had 30–50 MΩ tip resistances. Microelectrodes were then filled with 3 M KCl. A filled microelectrode was inserted into a microelectrode holder connected to an electrometer (WPI Duo773). The output of the electrometer was displayed on a Gould oscilloscope (1421) and recorded on a Gould inkwriting recorder (2400S). Electrotonic pulses were introduced through

a Grass isolation unit (SIU5) into the muscle strips by applying potential differences (generated by a Grass stimulator (S88)) across a pair of Ag-AgCl plates separated by 10 mm. The field strength was measured by a pair of electrodes, 2 mm apart, located in the middle of the stimulating chamber. The electric field strength (represented by the voltage gradient across the recording electrodes) was displayed on the oscilloscope and recorded on the inkwriting recorder. The muscle strips were allowed to equilibrate with continuously oxygenated Krebs solution, perfusing at a rate of 500 ml/h, in the partitioned chamber for at least 2 hours at 37.0±0.5 °C before experimentation started.

During the incubation with methylene blue (50 μM), light intensity was kept low. Preparations were then washed with Krebs solution for approximately 5 min. The preparations were illuminated by a MKII fibre optic lamp (the maximum intensity refers to 50 mW/cm^2 at the surface of the tissue situated at 3.5 cm away from the light source). The light intensity was measured by a digital photometer (model 815 series, Newport). After the experiment, the strip was immediately transferred to an aldehyde/picrate fixative.

3.3.4 Light- and electron-microscopy

After the experimental procedure, the Sylgard was removed from the holder with the tissue still in place. The mounted tissue was immersed in a fixative (pH 7.5), containing formaldehyde (2%), glutaraldehyde (2%) and picric acid (0.2%) in a phosphate buffer (0.1 M). The strips were stored at 4 °C in this fixative. Each strip had the pinned edges trimmed away, the remainder being divided in 4–6 pieces of tissue. Before further processing, the degree of MB staining was assessed by stereo microscopy. The tissue was then washed with 0.1 M phosphate buffer, postfixed with 2% osmic

Table 3.1: *Effects of 50 μM methylene blue (45 min) on the electrical activity of ICC-CM preparations with or without illumination*

	Krebs	+ Methylene blue	+ Light
Resting Membrane Potential (mV)	−72.8±0.8	−70.6±0.9*	−47.3±1.9† / −69.7±1.6§
Frequency (cpm)	5.3±0.2	5.0±0.2	- - -
Duration (s)	3.8±0.3	4.9±0.7*	- - -
Upstroke Amplitude (mV)	38.6±1.4	37.4±1.5	- - -
Plateau Amplitude (mV)	34.1±1.3	33.2±1.6	- - -
Rate of Rise (mV/s)	192.3±23.8	169.4±18.7	- - -

n=12; *: significantly different from the corresponding slow wave parameters in Krebs solution ($P < 0.01$); †: significantly different from the RMP in Krebs solution and in 50 μM of methylene blue ($P < 0.001$); and, §: RMP during repolarizing pulses (n=4).

acid in 0.1 M phosphate buffer for 1 h, dehydrated in a graded series of ethanol, block-stained for 1 h in 1% uranyl acetate in absolute alcohol, and taken through propylene oxide to epon (Merck). 1 μm-sections were stained with toluidine blue and examined under a Leitz Orthoplan microscope. Ultra-thin sections were post-stained with alcoholic uranyl acetate and lead citrate, and examined under a Philips 300 electron microscope.

3.3.5 Data presentation and statistical analysis

Data are presented as mean ± SEM. The statistical significance of the data sets under different conditions was obtained by Student's t-test.

3.4 Results

3.4.1 Electrophysiological studies

Effects of light on methylene blue stained ICC-CM preparations

Incubation of ICC-CM preparations with 50 μM methylene blue for 45 min depolarized the circular muscle cells by 2 mV and increased the slow wave duration (n = 12, Table 3.1), which was consistent with previous observations [119]. To minimize non-specific effects of extracelluiar methylene blue during illumination, the tissue was washed with Krebs solution for about 5 min. During this time, the effects of methylene blue on the slow wave activity remained. This part of the experiments was done in subdued light.

After incubation with methylene blue and washout, intense illumination abolished the slow wave activity in the ICC-CM preparations. The abolition of slow waves was accompanied by depolarization of the cells to a membrane potential of -47.3 ± 1.9 mV (ranging from -64 mV to -42 mV, n = 12, $P < 0.001$). Concurrently, phasic contractions were abolished and the tone of the muscle strips increased. The slow wave activity was not affected when the ICC-CM preparations were illuminated at the maximum intensity for 10 min without pre-incubation with methylene blue.

Abolition of slow waves was not a direct effect of depolarization since repolarization did not restore the slow wave activity (Figure 3.1A) even when repolarization was applied before the slow waves amplitude was completely diminished (Figure 3.2A). These observations indicated that the effects of methylene blue plus light on the generation mechanism of the slow wave activity was independent of the membrane potential. In contrast, changes in slow wave activity caused by increasing the

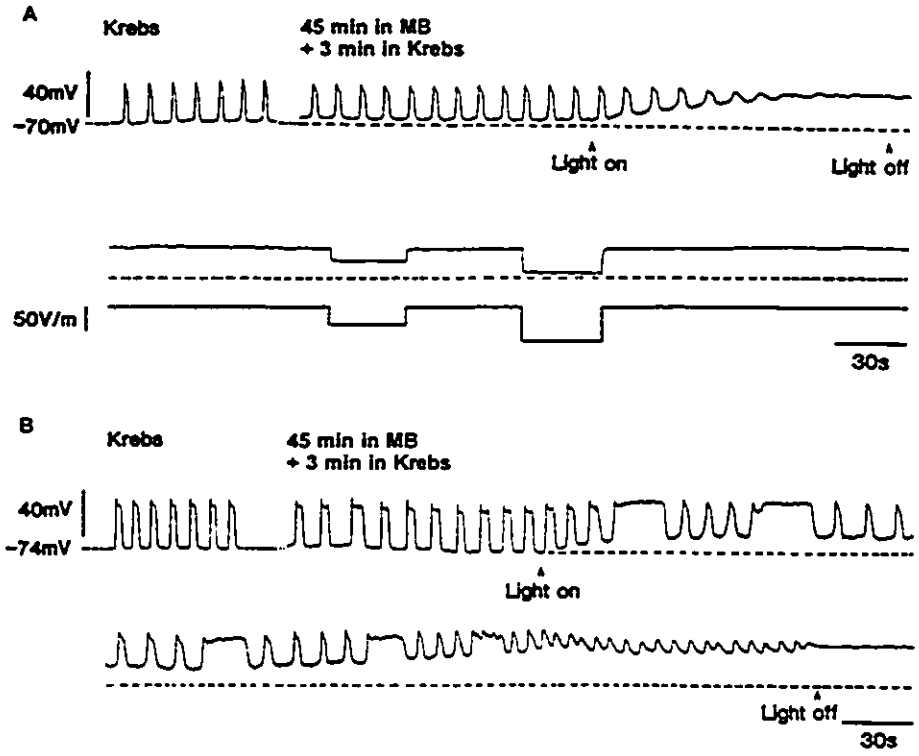

Figure 3.1: *Electrophysiological effects of illumination on methylene blue (MB) stained ICC-CM preparations*

(A) MB (45 min incubation period) per se slightly decreased the resting membrane potential and increased the slow wave duration. These effects remained after washout of MB with Krebs solution. The preparation was then illuminated at the maximum intensity. As a consequence, the resting membrane potential decreased to −44 mV. Concomitantly, the slow wave amplitude decreased. Repolarization of the membrane did not restore the slow wave activity indicating that the abolition of slow waves was due to inhibition of the slow wave generation mechanism and not caused by depolarization.

(B) Reducing the light intensity to 1/3 of that in (A) significantly prolonged the illumination duration required for abolishing the slow waves. Longer duration slow waves were observed intermittently during the period of depolarization in this experiment. Similar observations in introducing intermittent long duration slow waves were observed in 3 other experiments. Slow waves were abolished at a resting membrane potential of −42 mV.

extracellular potassium concentration were solely due to depolarization since repolarization of the muscle strip completely reversed the effects (Figure 3.2B). In addition, abolition of the slow wave activity could be observed with depolarization of only 8–12 mV (slow waves abolished at membrane potential of -60.4 ± 1.5 mV, $P < 0.001$, Figure 3.3) in 3 experiments.

The rate at which the slow waves were abolished varied directly with the light intensity. With illumination at the maximum intensity, the slow waves were abolished between 0.8 min and 3 min (Figure 3.1A). Reducing the light intensity by 3 times increased the illumination duration required for abolishing the slow waves to 3–12 min (Figures 3.1B and 3.3).

The time required for abolishing the slow waves was also dependent on the duration of incubation with methylene blue. When ICC-CM preparations were incubated with methylene blue for 7 min with a subsequent washout period of 5 min (a procedure that produced no effects on the slow wave activity), illumination at the maximum intensity abolished the slow waves between 4–8 min (n=5). The effects of methylene blue plus light were irreversible.

Effects of methylene blue plus light on CM preparations

The specificity of the action of methylene blue was studied using CM preparations that did not contain the submuscular ICC network. Incubation with methylene blue for 45 min produced no effect on the electrical parameters of the spontaneously quiescent CM preparations (resting membrane potential = -62.8 ± 0.5 mV), nor was any effect observed by illumination at the maximum intensity for as long as 6 min ($n = 4$, Figure 3.1) which was twice the maximum amount of time required for abolishing the slow waves in ICC-CM preparations under the same conditions.

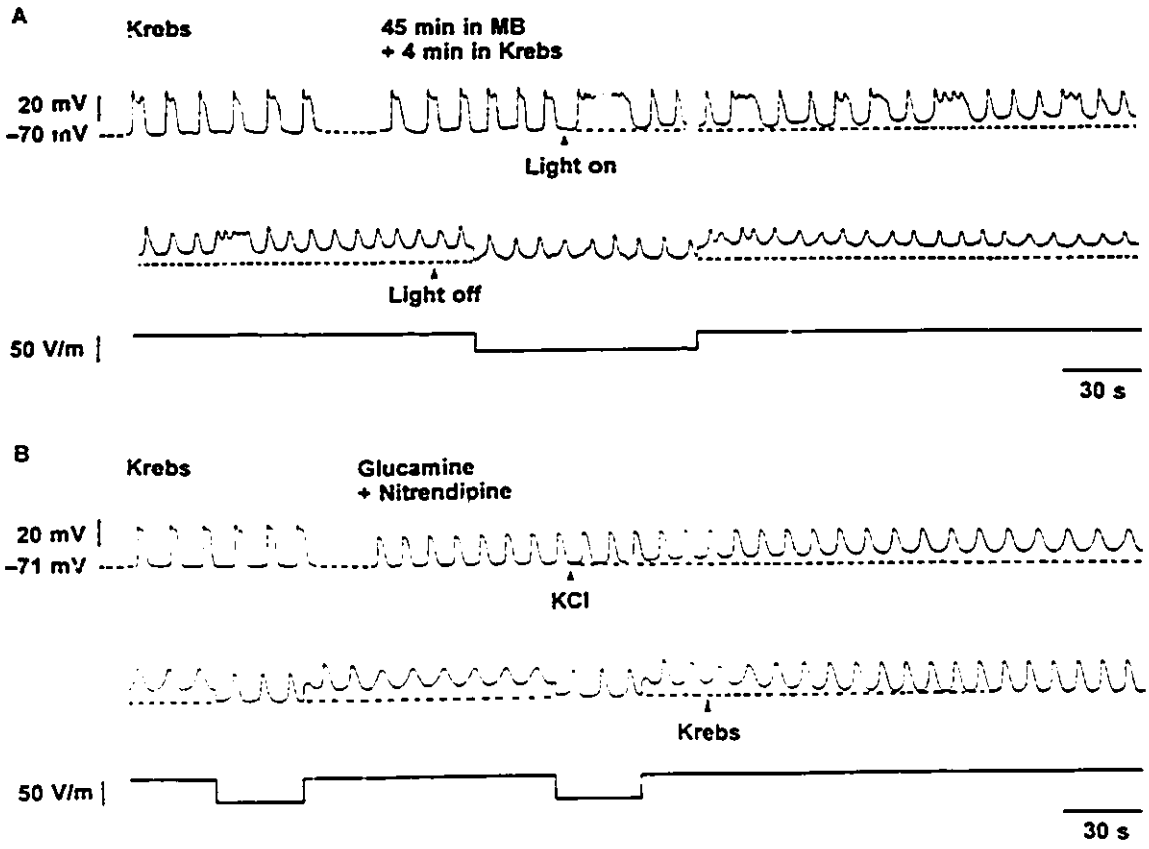

Figure 3.2: *Effects of membrane potential on the slow wave activity*

(A) After 45 min incubation with methylene blue (MB) and washing with Krebs solution, the ICC-CM preparation was illuminated at 1/3 of the maximum intensity until the slow wave amplitude was reduced to about half of that in Krebs solution. The preparation was repolarized to the same resting membrane potential as in Krebs solution. There was no restoration of the slow wave amplitude.

(B) In contrast, when depolarization was caused by increasing the extracellular potassium concentration to 15 mM (at arrow) in glucamine-nitrendipine-Krebs solution, repolarization of the ICC-CM preparation using the same method as in (A) completely restored the slow wave amplitude. In addition, the slow wave amplitude was also restored after washout.

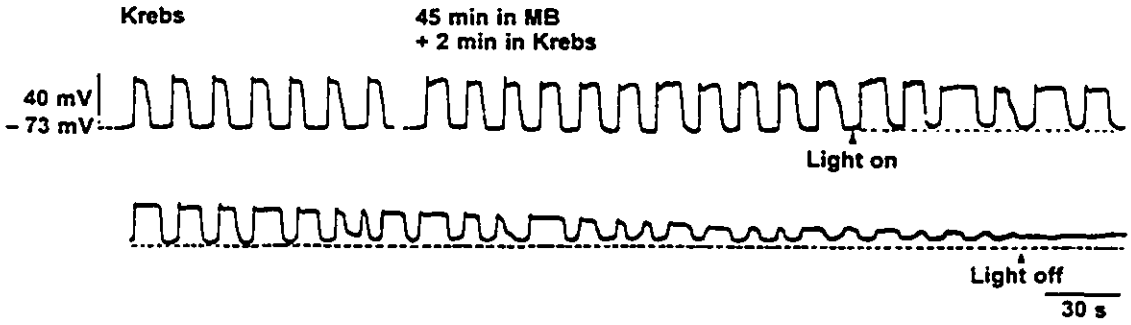

Figure 3.3: *Abolition of the slow wave activity by methylene blue (MB) plus light in ICC-CM preparations without marked depolarization*

Slow waves were abolished in MB stained ICC-CM preparation when illuminated at 1/3 of the maximum intensity for 8.5 min. Slow waves were abolished at −64 mV which is the same as the intrinsic resting membrane potential of the circular muscle preparations in Krebs solution (Figure 3.4).

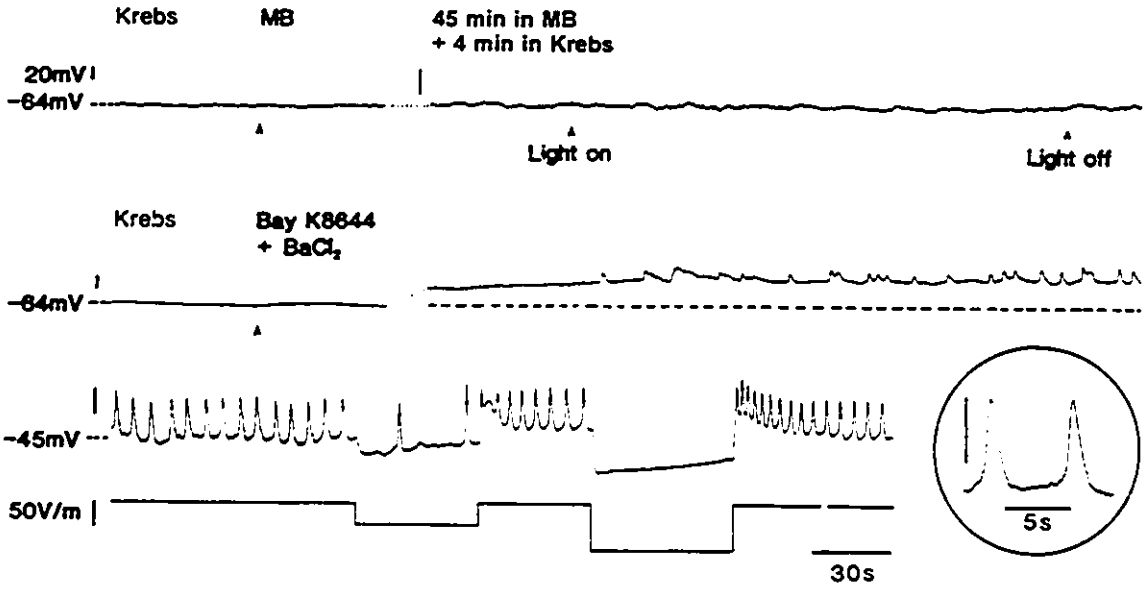

Figure 3.4: *Electrophysiological effects of methylene blue plus light on circular muscle (CM) preparations*

CM preparations, devoid of the submuscular ICC network and a few adjoining layers of circular muscle cells, were spontaneously quiescent in Krebs solution. Incubation with 50 μM methylene blue for 45 min produced no change to the membrane potential, neither did illumination at the maximum intensity for 3 min. The CM preparation was shown to be viable by stimulating with 0.5 mM $BaCl_2$ + 0.1 μM Bay K 8644, during which voltage dependent spike-like action potentials were induced. The preparation was allowed to equilibrate for 15 min in Krebs solution before perfusion of $BaCl_2$ and Bay K 8644. There is a gap of 3 min between the first and the second traces of the second panel.

Figure 3.5: *Electron micrographs of the submuscoal border in control tissue and tissue with 2 min illumination after incubation with methylene blue*
(A) An electron micrograph of the submucosal border in control tissue. Illumination at the maximum intensity for 10 min, without pre-incubation with MB, had no effect on the ultrastructure of interstitial cells of Cajal (IC) (note condensed mitochondria), thin, irregular branching smooth muscle cells (bSM), nerves (N) and circular muscle proper (CM); SUB: submucosa. (B,C) Note that ICCs, after incubation with MB for 45 min, not followed by illumination (B) or 2 min illumination at the maximum intensity (C), shift their mitochondrial conformation from condensed to orthodox. Apart from this, the ultrastructure is preserved, including gap junctions (GJ). All calibration bars represent 1 μm.

While the ability of the ICC-CM preparations to generate slow waves was irreversibly abolished by methylene blue plus light, typical activities of circular muscle preparations were unaffected. After treatment with methylene blue plus light and washout with Krebs solution, addition of $BaCl_2$ (0.5 mM) and Bay K8644 (0.1 μM) decreased the resting membrane potential to -46.1 ± 0.7 mV and evoked spike-like action potentials with a frequency, amplitude and duration of 18.7 ± 1.3 cpm, 16.5 ± 1.1 mV and 1.6 ± 0.3 s, respectively. The frequency of the induced action potentials was decreased when the cells were repolarized by 8–12 mV and completely abolished by repolarizing the cells back to the same resting membrane potential as in Krebs solution (Figure 3.4). These observations were typical responses of CM preparations in the presence of $BaCl_2$ and Bay K8644 [83, 112].

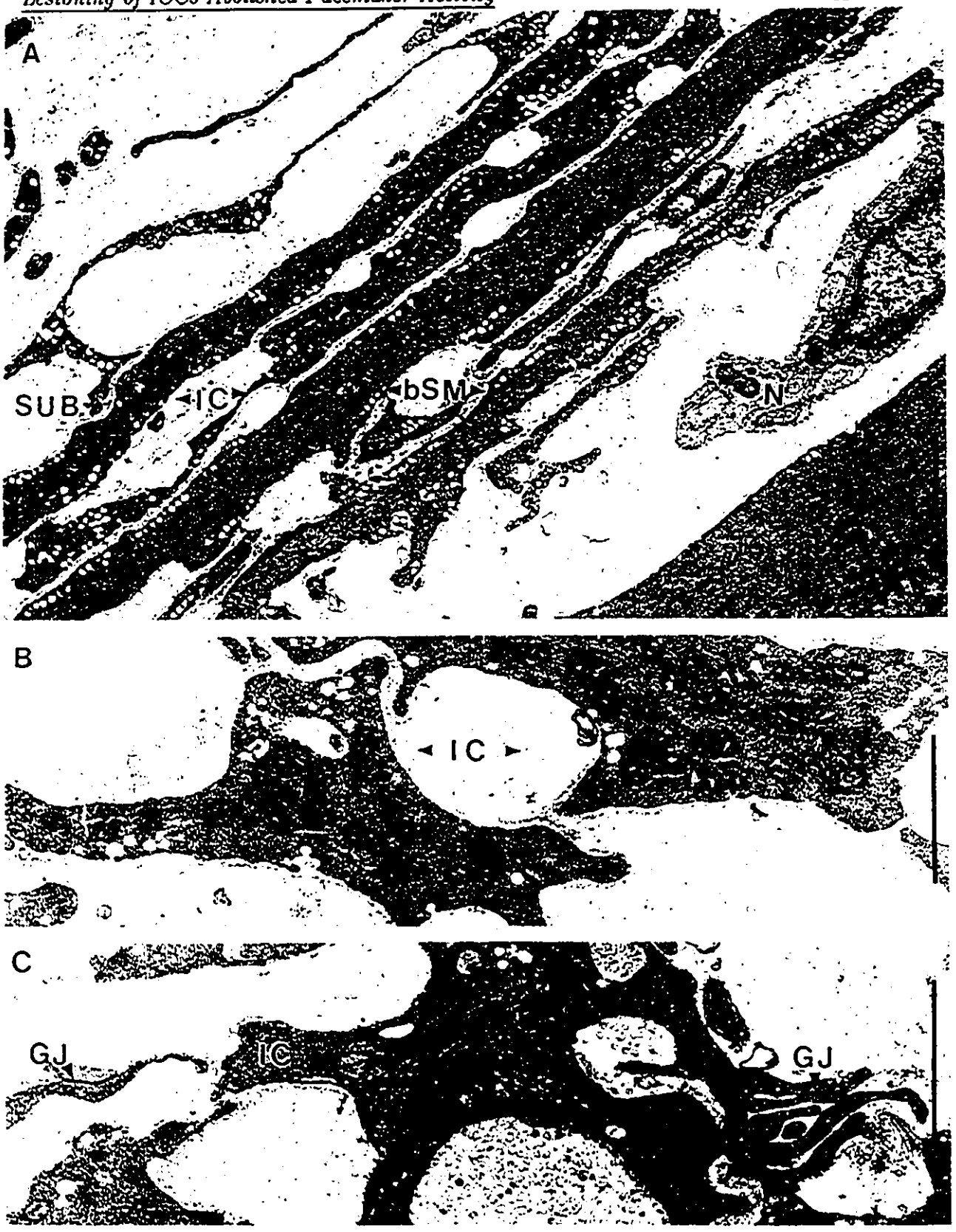

Figure 3.5

3.4.2 Structural correlations

Light microscopy

Incubation with 50 μM methylene blue for 7 min produced no visible dye-uptake in any strips (n = 12), whereas a 45 min incubation resulted in a distinct pattern of staining in all strips (n = 10). This pattern was conspicuous in areas where the residual submucosal layer was very thin, and obscured by remaining submucosa in other parts. In initial experiments, we observed a complete loss of stainable ICCs, when the inner surface of the circular muscle layer was exposed by pulling away the submucosal connective tissue. Therefore, in all experiments, the submucosa was removed as completely as possible by cutting with scissors with the mechanical stretch reduced to a minimum. From inspection and dissection of similarly stained larger sheets of colonic tissue, we conclude that, as long as the remaining submucosa was very thin, there was a general coloration of ICCs at the submucosal border though in some places this was clearly seen only after sharp dissection of remaining submucosa from the fixed tissue.

After 45 min incubation with methylene blue, in addition to ICCs and a small number of axons, staining was also observed in red blood cells inside capillaries and venules, in mast cells in the submucosa, and in interstices of the circular muscle. The smooth muscle cells were unstained, except for a few, very thin, cells scattered adjacent to the submucosal border. In 1μm-sections, the circular muscle was contracted in all methylene blue-treated strips, as determined by the cell dimensions and irregular surface patterns. The tissues were well preserved. Although ICC-CM preparations that had been pre-incubated with methylene blue for 7 min did not show visible stain, the contrast of the submucosal ICC layer was diminished after illumination at the maximum intensity for 4–10 min, as observed with the toluidine blue

Figure 3.6: *Tissue incubated with MB for 7 min, followed by illumination at the maximum intensity for 2 min (A) and 10 min (B)*

(A) After 2 min of illumination, the only conspicuous ultrastructural change is a change of mitochondrial appearance to typical orthodox configuration (compare to Figure 3.5C: 45 min MB, 2 min light). IC: interstitial cells of Cajal; bSM: thin, irregular branching smooth muscle cell; CM: circular muscle proper; N: nerve of the submuscular plexus. (B) After 10 min of illumination, the ICCs are severely damaged with disintegration of cytoplasmic organelles and ruptured plasma membranes. The basal lamina (arrows) is still intact. Processes of thin, irregular branching muscle cells and circular muscle cells are markedly less affected. All calibration bars represent 1 μm.

---

stain. These observations were correlated with changes in ultrastructural appearance.

Electron microscopy

a. Control data: illumination without methylene blue.

No ultrastructural changes were observed in ICC-CM preparations (n = 11, 2–10 min illumination) that had been illuminated for as long as 10 min (n = 3, Figure 3.5A) at the maximum intensity without incubation with methylene blue. Three cell types, intimately connected by gap junctions and intermediate contacts, were present along the entire inner border; ICCs were connected to thin, irregularly branching smooth muscle cells (bSM), which in turn formed gap junctional and intermediate contacts with the innermost, larger cells of the circular muscle (CM) proper.

The distinction between these cell types was important since we found that the staining with methylene blue, as well as the conspicuous damage after methylene

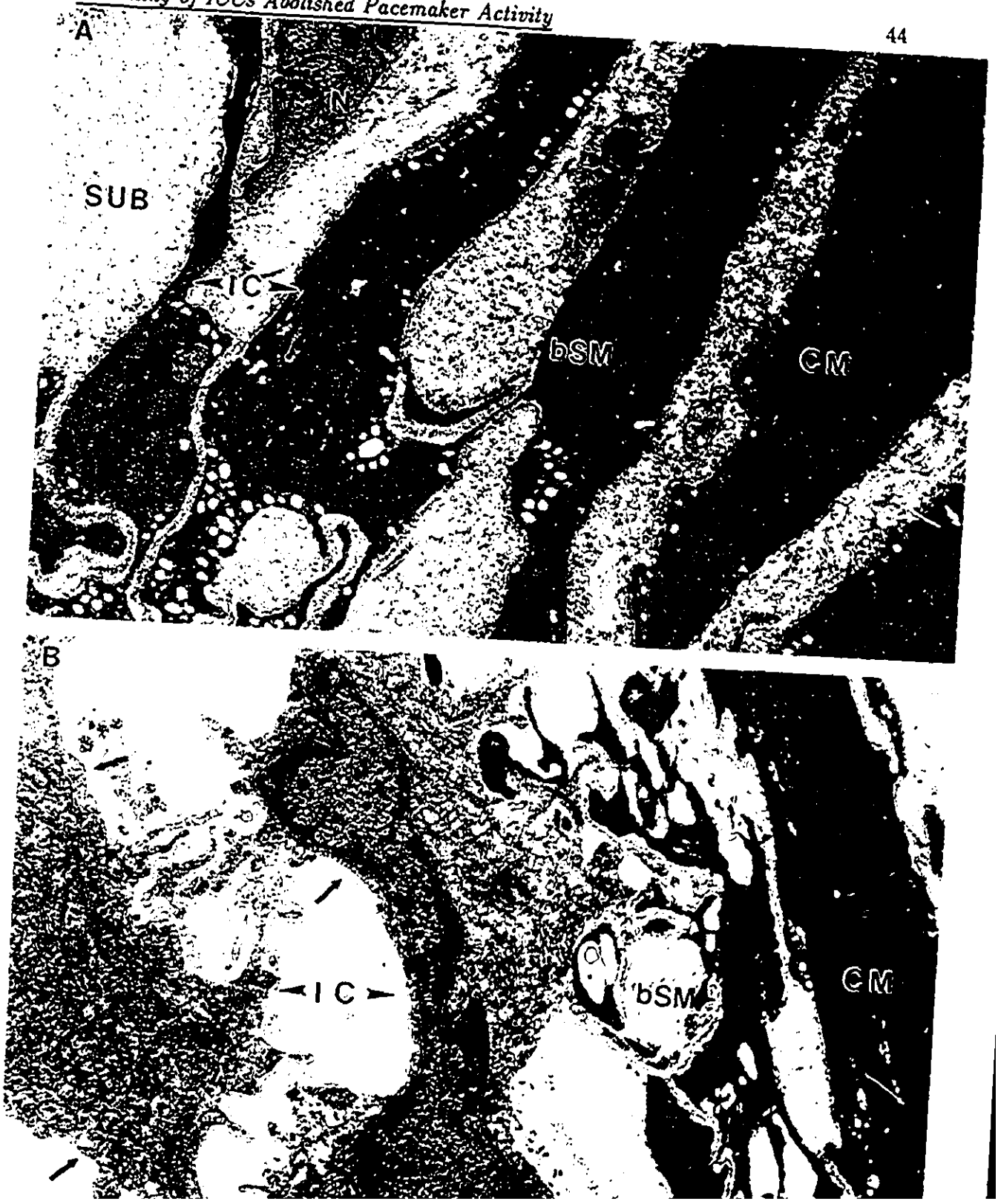
A
N
SUB
IC
bSM
CM
B
IC
bSM
CM

blue plus illumination were restricted to ICCs, rather than the branching and the typical smooth muscle cells. Although individual profiles of cell processes seen in single sections were often impossible to classify with confidence, the three cell types could be sorted out by comparing cross-sectioned, nucleated parts of the cells:
(1) ICCs were highly branched cells with 2–5 primary processes; profiles, which included the nucleus, generally also included the origin of 1–2 primary processes. The perinuclear cytoplasm between the origin of processes was very thin and partly had the thickness of the size of caveolae, which were present in large numbers at all surfaces of the ICCs. At the origin of processes, the perinuclear cytoplasm was dominated by large accumulations of mitochondria. Part of the cytoplasm was occupied by filament bundles (thin and intermediate but no thick filaments) with small cytoplasmic and membrane-associated dense bodies. When compared with the conspicuous array of dense bodies in smooth muscle cells (bSM and CM), these were a minor constituent in ICC cytoplasm. Scattered microtubules were always present in the perinuclear cytoplasm. An extensive endoplasmic reticulum was composed of a system of interconnected flattened cisternae, organized partly in between and around mitochondria, partly connecting to smooth subsurface cisternae. The cisternae were largely of the smooth type, with the rough part being characterized by widely scattered ribosomes.
(2) bSM and CM: the above described features were typical for ICCs but not for bSM or CM. Mitochondria were far less in number and randomly scattered in bSM and CM. Profiles like those of Figures 3.5A and 3.6A were common where the mitochondrial density in bSM is less than 10% of that of the adjacent ICC. The perinuclear cytoplasm was dominated by a dense array of filaments (thin, thick and intermediate types) with a similar organization of dense bodies (cytoplasmic and membrane-associated) in bSM and CM. bSM could be distinguished from CM by

Figure 3.7: *Low power electron micrographs of tissue illuminated for 10 min at the maximum intensity*

(A) A low power electron micrograph of tissue illuminated for 10 min at the maximum intensity after 7 min of pre-incubation with MB. There is no indication of structural damage to the circular muscle proper, intramuscular capillaries (C) and fibroblasts (F), while the layer of cells bordering the submucosa (SUB) is severely affected. (B) At higher magnification (same conditions), it is observed that the major damage is limited to the mitochondria-rich ICCs, while the thin, irregular smooth muscle cells (bSM), circular muscle cells (CM) and nerves (N) are unaffected. Gap junctional structure is preserved between inner circular-muscle cells and between ICCs (inset). All calibration bars represent 1 μm, except in the inset, it represents 0.1 μm.

---

the size difference (thinner perinuclear filament area and thinner processes of bSM), and the irregular branching appearance of bSM. The nuclear morphology was similar in ICCs, bSM and CM. Similar to ICCs, the bSM and CM were enveloped by a continuous basal lamina.

Although some variations of ultrastructure could be observed by inspection of semiserial sections, profiles of major processes of the three cell types could in general be distinguished by the criteria given above.

b. Ultrastructure after incubation with methylene blue

The overall preservation of cells and subcellular detail was unaffected by methylene blue as previously reported [119]. After 7 min incubation with methylene blue, no ultrastructural changes were observed in any cell type (n = 3). After 45 min incubation with methylene blue, the only changes noted were in ICCs (n = 3, Figure 3.5B),

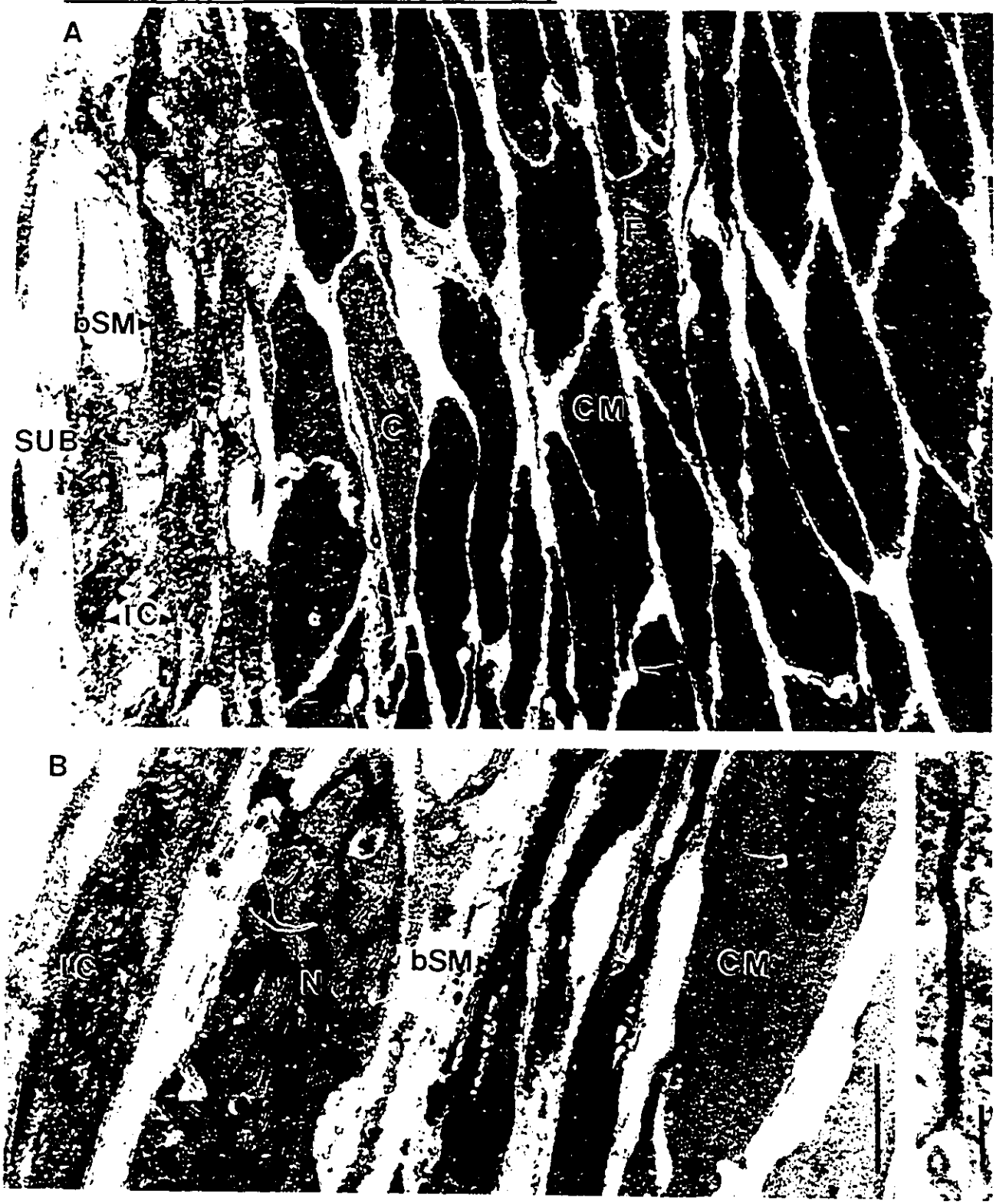

Figure 3.7

namely, (1) an increased occurrence of a moderately dilated endoplasmic reticulum, part of which contained small deposits of an electron-dense material, and (2) an increased number of large, electron-dense cytoplasmic deposits, which might be partly of lysosomal origin and partly related to picrate-precipitated methylene blue. With (Figure 3.5B) or without (Figure 3.5A) methylene blue incubation, mitochondria of ICCs were consistently preserved in a highly condensed conformation while this mitochondrial conformation was less pronounced and more variable in smooth muscle cells (bSM and CM).

c. Ultrastructural changes after incubation with methylene blue followed by illumination

After 2 minutes illumination, ultrastructural changes were limited, and similar in preparations pre-incubated with methylene blue for 45 min (Figure 3.5C, n = 7) or 7 min (Figure 3.6A, n = 3). The only consistent change, observed in all specimens, was a mitochondrial transition from the condensed (widened intracristal spaces and a dense matrix) to the orthodox (narrow cristae and a light matrix) conformation in ICCs. In contrast, smooth muscle cells have mitochondria in variable conformational states before and after treatment with methylene blue plus light. No evidence could be obtained for transformation of mitochondrial configurations in smooth muscle cells.

After incubation with methylene blue, illumination for 4 and 10 min induced severe damage in ICCs and in a small number of smooth muscle cells scattered close to the submucosal border. However, smooth muscle cells of both types (bSM and CM) generally appeared intact (Figures 3.6B & 3.7A,B). After 4 min of light, the prominent changes in ICCs were mitochondrial swelling, together with increasing vacuolization of the cytoplasm (n = 3). After 10 min of light (n = 3, Figures 3.6B & 3.7A,B), the

ICCs were swollen with low cytoplasmic contrast, barely discernible mitochondria, few caveolae, and punctated plasma membranes which were presumably ruptured. The identification of the ICCs was still possible by the preservation of continuous basal laminae (Figures 3.6B & 3.7B) together with cytoplasmic features (such as mitochondrial number) and preserved intercellular relations with the innermost muscle cells. Gap junctions were preserved in unchanged numbers and morphology. Under these conditions, the extent of damage to nerves appeared to match the observed extent of axonal dye-uptake. That is, most nerve bundles were structurally intact; however, a few nerve bundles exhibited damage (swelling) which was restricted to 1–2 axons.

3.5 Discussion

3.5.1 Selective lesioning of colonic ICCs by methylene blue plus light

We provide strong evidence that the submuscular interstitial cells of Cajal (ICCs) are essential for the generation of slow-wave-type action potentials in the canine colon circular muscle by showing a direct relationship between selective damage to ICCs and abolition of the slow waves. In a recent study [119], we have shown that ICCs in the submuscular plexus of canine colon selectively accumulate methylene blue, and that methylene blue per se does not produce any electron microscopically observable changes to any cell types nor does it induce any significant effect on the slow wave activity. In the present study, we showed that intense illumination after incubation with methylene blue resulted in specific lesions of ICCs verified by electron microscopy. Furthermore, when CM preparations, from which the submuscular

ICC-smooth-muscle network had been removed, were incubated with methylene blue followed by illumination, the spontaneous and inducible electrical activities were unaffected. These observations indicate that the effects of methylene blue plus light in ICC-CM preparations were specific to ICCs since only ICCs, but not the associated smooth muscle cells, in the submuscular ICC-smooth- muscle network were damaged by methylene blue plus light.

Although the abolition of slow wave activity by methylene blue plus light was accompanied by depolarization, depolarization was not responsible for the inhibition of the slow wave activity since repolarization of the cells to its original resting membrane potential did not restore the slow waves. In addition, slow waves were observed to be abolished over a large range of membrane potentials, including the resting membrane potential intrinsic to the circular muscle, indicating that changes in slow wave activity were not caused by changes in membrane potential. In contrast, ouabain also depolarizes the membrane and abolishes the slow wave activity [6]; however, repolarization of the membrane to the original resting membrane potential (carried out by the same method as applied in the present study) completely restores the slow wave activity. This indicates that in the presence of ouabain, inhibition of the slow wave activity is a direct effect of depolarization.

The site of methylene blue accumulation within the ICCs is very specific. When the precipitation of methylene blue was monitored in such a way that displacement and formation of coarse precipitates was avoided, electron dense deposits were observed to be present only in endoplasmic reticulum (ER) and not in any other cytoplasmic components [181]. This may indicate that methylene blue enters the ER directly by way of the smooth subsurface cisternae. However, it remains unclear as to why methylene blue accumulates in the ER of ICCs but under the same circumstances

does not enter the ER of smooth muscle cells. Under the experimental conditions of the present study, changes in the mitochondrial conformation as well as the slow wave activity were observed with minimal methylene blue incubation (7 min) and minimal illumination duration (2 min) suggesting that the primary cause of abolition of the slow waves was mitochondrial damage.

The photodynamic, cytotoxic action of methylene blue has been known for many years [8]. Recently, the cytotoxic efficacy of photo-inactivation of methylene blue-sensitized bladder cancer cells was studied [79], including accompanying ultrastructural changes [198]. After short periods of illumination (5 min), ultrastructural changes reported were similar to our findings (mitochondrial disintegration and early signs of damage to the plasma membranes) and increasing illumination duration led to membrane rupture and cell fragmentation. In a study of the photodynamic action of methylene blue on DNA [127], it was shown that a reversible pre-lesion in DNA induced by methylene blue in darkness became irreversible when illuminated in the presence of methylene blue. Similarly, in the present study, the electrophysiological and ultrastructural effects of methylene blue plus light were also found to be irreversible.

3.5.2 Roles of ICCs in the generation of slow waves

The present study strengthens the hypothesis that ICCs are essential for the generation of the pacemaking activity in the gut. In a related study using the mouse small intestine, illumination with red laser light abolished slow wave activity recorded intracellularly after incubation with methylene blue [183]. It was shown that the slow wave activity was affected in areas where ICCs were stained, but not in unstained areas. In another study [182], spontaneous contractile activity at the slow-wave fre-

quency was preserved when cultured explants of mouse small-intestinal musculature with selectively methylene blue-stained ICCs were viewed under very dim light; but, these explants rapidly became quiescent in strong light.

The present study specifically establishes a crucial role for ICCs in the generation of slow waves in the canine colon as proposed previously [87, 109, 110, 113, 172]. We hypothesized that cyclic intracellular activity periodically activates pacemaker current [92]. In this case, the ICCs could harbour either the biochemical clock or both the biochemical clock and the ion channels responsible for generating the pacemaker current. Although spontaneous oscillations have been recorded in isolated smooth muscle cells [143] and cells tentatively identified as ICCs [104, 148], these oscillations were abolished by L-type calcium channel blockers and hence did not show the slow-wave pacemaker component which is not abolished by these blockers [93]. Also, the spontaneously occurring oscillations do not have the characteristic slow wave frequency.

The next question concerns the role of smooth muscle cells in generating the pacemaker component of the slow waves. The branching smooth muscle cells, which are intimately connected to ICCs by gap junctions, are of particular interest. If solely the ICCs are responsible for the generation of pacemaker current, the amount of current that each ICC must generate to depolarize all the low-resistantly coupled cells will be enormous. An alternate possibility is that ICCs harbour the biochemical clock and send intracellular metabolites through gap junctional contacts to the intimately associated smooth muscle cells. Through metabolic coupling [66], the associated smooth muscle cells could be in synchrony with the ICCs when the pacemaker channels in both ICCs and associated smooth muscle cells are activated. Validation of this hypothesis requires identification of the pacemaker channels and verification

of the presence of such channels in ICCs and smooth muscle cells. Interestingly, in the presence of TEA, $BaCl_2$ and carbachol, the isolated circular muscle layer without the submuscular ICC-smooth-muscle network exhibits action potentials, which have a similar frequency to the slow waves, but are abolished by the L-type channel blocker (D600) [113]. This and a subsequent study [112] show that circular muscle, without the submuscular ICC-smooth-muscle- network, can generate action potentials with characteristics similar to the slow wave activity but lacking the spontaneous rhythmic pacemaker component of slow waves.

The slow wave activity also disappears after uptake of Rhodamine 123 in full thickness muscle preparations [195]. Rhodamine 123 is a specific marker for mitochondria; thus, it is not specific to ICCs although ICCs are particularly rich in mitochondria [12]. After uptake into the mitochondria, Rhodamine 123 becomes cytotoxic by interfering with the generation of ATP [133]. Hence, the effect of Rhodamine 123 suggests that the slow wave activity is strongly dependent on intracellular metabolic activity. This is consistent with the observations that the slow wave activity is highly temperature sensitive [6], blocked by metabolic inhibitors such as dinitrophenol and carbonyl cyanide (Preiksaitis and Huizinga, unpublished), and affected by changes in mitochondrial conformations (present study). This supports our hypothesis that the pacemaker component of slow waves is initiated by an intracellular metabolic clock [92].

Chapter 4

Cyclopiazonic Acid, Inhibiting the Endoplasmic Reticulum Calcium Pump, Reduces the Canine Colonic Pacemaker Frequency

4.1 Epitome

The slow wave frequency of the canine colon has previously been hypothesized to be paced by an intracellular biochemical clock. We investigated the relationship between the endoplasmic reticulum (ER) Ca^{2+} and the periodicity of the biochemical clock. Cyclopiazonic acid (CPA), a specific inhibitor of the ER Ca^{2+}-pump,

This chapter was published in the Journal of Pharmacology and Experimental Therapeutics, 275: 1058-68, 1995, by Louis Liu, Lars Thuneberg and Jan Huizinga. Contributions of Lars Thuneberg are discussed in section 2.3 of Chapter 2.

dose dependently decreased the pacemaker frequency. Similarly, chelating cytosolic Ca^{2+} with BAPTA also decreased the pacemaker frequency. These observations suggest that delaying the Ca^{2+} uptake into the ER decreases the pacemaker frequency. The pacemaker frequency was similarly decreased by neomycin (inhibiting inositol 1,4,5-triphosphate (IP_3) synthesis) and caffeine at concentrations higher that 5 mM (inhibiting the IP_3-sensitive Ca^{2+} channels in the ER membrane). Hence, the IP_3-sensitive Ca^{2+} stores are involved in the biochemical clock. Ryanodine (up to 60 μM) did not affect the pacemaker frequency indicating that a ryanodine-sensitive store, if it exits, is not coupled to the biochemical clock. Electron microscopy showed that the smooth ER forms an extensive network of subsurface cisternae which is closely associated with large areas of the cytoplasmic face of the plasma membrane. These structures were the most extensive in interstitial cells of Cajal, slightly less in branching smooth muscle cells and far less in circular muscle cells. In summary, based on these electrophysiological and morphological observations, we hypothesize that the Ca^{2+} refilling cycle of the IP_3-sensitive calcium stores associated with the plasma membrane, determines the frequency of the pacemaker activity generated by the submuscular ICC-smooth-muscle network of the canine colon.

4.2 Introduction

The motility of the gastrointestinal tract is associated with action potentials through excitation-contraction coupling. Spike-like action potentials and slow-wave-type action potentials (slow waves) are the two main types of action potentials generated by the musculature (see reviews by [87, 161, 176]). The slow wave activity regulates the timing and the propagation characteristics of circular muscle contractions [161].

When spiking activity occurs superimposed on the slow waves, the force of contractions increases markedly. There is a strong direct correlation between the intensity of the spiking activity and the force of phasic contraction *in vivo* [36, 161, 164] as well as *in vitro* [62, 63, 90, 91].

In the canine colon, the slow waves are initiated through the activation of Ca^{2+}-dependent pacemaker channels [7, 93, 194] sensitive to intracellular metabolic components such as cAMP [92] rather than to voltage changes [92]. In addition, the reduction in the slow wave frequency by a decrease in temperature [6] cannot be sufficiently explained by the temperature dependence of voltage activated ionic currents [146]. These observations lead to the hypothesis that the slow wave frequency is paced by an intracellular biochemical clock rather than by a voltage driven cyclic activation-inactivation of ionic channels intrinsic to the plasma membrane.

A role of the endoplasmic reticulum (ER) Ca^{2+} in the regulation of the periodicity of the biochemical clock was suggested by preliminary experiments showing that cyclopiazonic acid (CPA) significantly reduced the slow wave frequency [116]. CPA, a mycotoxin from *Aspergillus* and *Penicillium*, is a potent and specific inhibitor of the ER Ca^{2+}- ATPase [56, 80, 102]. Using the microsomal fraction isolated from the smooth muscle of rat vas deferens, Darby *et al.* [55] reported that CPA dose-dependently inhibited the oxalate-stimulated Ca^{2+} uptake in the ER fraction, reaching a maximum inhibition of 98% at a concentration of 10 μM; but, CPA (up to 30 μM) did not affect the saponin-sensitive Ca^{2+} uptake in the plasma membrane enriched fraction. It demonstrates that CPA selectively inhibits the ER Ca^{2+}- pump. CPA has been widely used to reversibly suppress Ca^{2+} uptake into the ER of dog airway smooth muscle [29], rat arterial smooth muscle [56, 167], dog mesenteric artery [123], and guinea-pig ileum and urinary bladder smooth muscle cells [174]. An ob-

jective of our study was to unravel the role of ER Ca^{2+} in the regulation of the slow wave frequency.

In the canine colon, the slow waves originate from the submucosal surface of the circular muscle [60, 110, 172] where a network of interstitial cells of Cajal (ICCs) is found [12, 119, 188]. It has recently been demonstrated that the pacemaker component of the slow waves is generated within the submuscular ICC-smooth-muscle network [112, 113, 172]. Specifically, when the submuscular ICCs are lesioned selectively by methylene blue and light, the pacemaker activity can no longer be generated [117]; this observation leads to the conclusion that the submuscular ICCs are essential for the generation of the pacemaker component. To develop a hypothesis about the role of ER Ca^{2+} in the mechanism regulating the pacemaker frequency, it was essential to investigate the plasma-membrane associated ER in the submuscular ICCs.

4.3 Materials and methods

4.3.1 Preparation of muscle strips

Dogs of either sex were killed by an overdose of sodium pentobarbital (100 mg/kg) given intravenously. Approximately 10 cm of proximal colon was taken from 5 cm distal to the ileocecal junction. The colon was opened flat. Colonic contents were carefully removed in a beaker containing Krebs solution equilibrated with 95% O_2/ 5% CO_2. The clean segment was then pinned flat onto the Sylgard of a dissecting dish which was filled with continuously aerated Krebs solution. After removing the mucosa, the segment was turned over; the longitudinal muscle layer together with a few cell layers of circular muscle near the myenteric border were carefully removed. This preparation was composed of the circular muscle with the intact submuscular

ICC network, referred to as *ICC-CM preparation*.

Approximately 2×2 mm of the tissue, with the ICC network facing up, was pinned onto the Sylgard bottom of a transfer holder which was then placed in a partition chamber [1] allowing voltage control of the muscle strips [92, 112].

4.3.2 Intracellular recordings

Intracellular recordings were made by microelectrodes (30–50 MΩ) filled with 3 M KCl. A microelectrode was inserted into a microelectrode holder which was connected to an electrometer (WPI Duo773). The output of the electrometer was displayed on a Gould oscilloscope (1421) and recorded on a Gould ink-writing recorder (2400S). Electrotonic pulses were introduced, through a Grass isolation unit (SIU5), into the muscle strips by applying potential differences (generated by a Grass stimulator (S88)) across a pair of Ag-AgCl plates separated by 10 mm. The field strength was measured by a pair of electrodes, 2 mm apart, located in the middle of the stimulating chamber. The electric field strength (represented by the voltage gradient across the recording electrodes) was displayed on an oscilloscope and recorded on an ink-writing recorder. Before experimentations started, the muscle strips were allowed to equilibrate for at least 2 hours at 37.0±0.5 °C in the partition chamber with continuously aerated Krebs solution perfusing at a rate of 500 ml/h (Pharmacia LKB-Pump P-1).

4.3.3 Force of contraction measurements

The method used to quantify the force of phasic contractions has previously been described by Huizinga *et al.* [86]. The characteristics of the phasic contractions were described by frequency, basal tone, amplitude (difference between the basal tone and the peak of contraction) and duration (measured at the half maximal amplitude;

similar convention was used for the electrical activity). Each parameter under different experimental solutions was normalized to the corresponding parameter in Krebs solution.

4.3.4 Drugs and solutions

All solutions perfused into the partition chamber were prewarmed to 37.0±0.5 °C and equilibrated with 95% O_2 and 5% CO_2. The composition (in mM) of the Krebs solution was: NaCl — 120.3; KCl — 5.9; $CaCl_2$ — 2.5; $MgCl_2$ — 1.2; $NaHCO_3$ — 20.2; NaH_2PO_4 — 1.2 and glucose — 11.5. Cyclopiazonic acid (CPA; Sigma, St. Louis) and *bis-(o*-aminophenoxy)-ethane-*N,N,N',N'*-tetra-acetic acid, tetra(acetoxymethyl)-ester (BAPTA/AM; Molecular Probes, Inc, Eugene, Oregon) were dissolved in dimethyl sulfoxide (DMSO, Sigma, St. Louis) to prepare stock solutions of 10 mM and 25 mM, respectively. Ryanodine (AgriSystems International) was first dissolved in absolute ethanol and then diluted to a stock solution of 3 mM with deionized distilled water to obtain a solution containing 12% ethanol. Stock solutions of neomycin (Sigma, St. Louis) and D600 (Sigma, St. Louis) were 0.4 M and 1 mM. Vehicles in the concentrations applied did not have any effect on the electrical activity.

4.3.5 Result presentation and statistical analysis

All data were expressed as mean ± S.E.M. 'n' represented the number of dogs used in each set of experiments. Statistically significant differences between data sets were determined by one-way repeated measures ANOVA (KWIKSTAT 4, TexaSoft). The slow-wave duration was measured at the half maximum of the slow wave plateau amplitude. The inter-slow-wave interval (ISWI) was the time interval at the resting membrane potential between the end of the repolarization phase of a slow wave and

Table 4.1: *Effects of CPA on the slow wave activity*

	Krebs	+ CPA (3 μM)	+ D600 (1 μM)
Resting membrane potential (mV)	−73.9±0.6	−73.5±0.7	−72.9±1.0
Frequency (cpm)	4.8±0.4	1.8±0.2**	1.9±0.3**
Duration (s)	3.9±0.3	13.5±1.3**	2.8±0.3**,††
Inter-slow-wave-intervals (s)	7.7±0.7	20.0±2.4**	31.0±11.8**,†
Upstroke amplitude (mV)	42.3±1.1	42.5±1.6	37.9±1.8**,††
Plateau amplitude (mV)	36.5±0.8	37.8±1.5	- - -

n=11. '*' denotes statistically significant differences between the slow wave activity under the experimental conditions and that in Krebs solution. '†' denotes statistically significant differences between the activity in CPA plus D600 and that in CPA. †, * — $p < 0.05$; ††, ** — $p < 0.01$.

the initial upstroke of the next slow wave (see Figure 1.3). When a drug decreases the slow wave frequency and concurrently increases the duration, it is essential to determine the ISWI in order to reach a conclusion about whether or not the change in frequency is caused by the change in duration. Because of the temporal variation of the slow wave activity in different experimental conditions, representative slow-wave parameters were obtained from analyses over periods of at least 5 min.

4.3.6 Electron Microscopy

The organization of the ER in ICCs and smooth muscle cells was observed in conventionally prepared tissues (n=20); however, the contrast between sER and surrounding cytoplasm can be significantly improved with the procedure described as follows. The proximal colon from two dogs was fixed by immersion in a 0.1 M phosphate buffer (pH 7.2), containing 2% glutaraldehyde, for several hours. After removing the mucosa, the tissue was cut into small pieces (2×2 mm serosal surface). The specimen were rinsed in 0.12 M sodium cacodylate buffer, postfixed for 1 hour in 0.12 M sodium cacodylate buffer, containing 0.5% osmic acid and 0.05 M potassium ferricyanide [152], dehydrated in a graded series of ethanol, and then taken through propylene oxide to Epon (Merck). Ultrathin sections were collected on Formvar-coated nickel grids, post-stained with alkaline bismuth after Shinji [169] alone, or followed by lead citrate. This procedure is known to increase the contrast of ER in various cells by staining glycoproteins and to reduce the staining of background cytoplasm. The specimen were examined in a Philips 300 electron microscope operated at 60 kV.

4.4 Results

4.4.1 Effects of cyclopiazonic acid on the slow wave activity

Cyclopiazonic acid, CPA, (3 μM) decreased the slow wave frequency, and prolonged the slow wave plateaus and the inter-slow wave interval (ISWI), without significant effects on other slow wave parameters (n=11, Table 4.1, Figure 4.1a). The effects of CPA on the slow wave activity became steady after 10–20 min perfusion. The slow wave frequency decreased by 63% whereas the duration and the ISWI were increased

Figure 4.1: *Effects of cyclopiazonic acid (CPA) on the slow wave activity*
a. CPA (3 μM, added at arrow) increased the duration and decreased the frequency of slow waves. Reduction in the frequency was independent of the increase in duration since abolition of the slow wave duration by either D600 or hyperpolarization did not restore the frequency. The same amount of hyperpolarization in Krebs solution also diminished the plateaus without any significant effect on the frequency. After addition of D600, the slow wave plateaus gradually collapsed and a second component during the repolarization phase of slow waves was intermittently observed. Similar observations were found in 3 (out of 11) other experiments. The resting membrane potential remained the same throughout the entire experiment. Traces show a continuous recording, except for a gap of 11 min between the second and third panel, from the same cell.
b. Continuation of the recording shown in (a) illustrating the reversibility of the CPA effects. At the arrow, CPA was removed from the perfusate leaving only D600 (1 μM) in Krebs solution. Note that upon removal of CPA, the second component during the repolarization phase disappeared and that the slow wave frequency recovered to the control value.

---

by 246% and 160%, respectively. Unlike in Krebs solution, the slow wave frequency and the ISWI in the presence of CPA were variable. Within one experiment, the frequency could vary from 1.7 to 3.7 cpm and the ISWI from 10 to 31 s. The effects of 3 μM CPA were reversible in all experiments by washing with Krebs solution for about 30 min (Figure 4.1b).

Consistent with the effects of CPA on the slow wave activity, CPA significantly decreased the frequency, and increased the amplitude and duration of phasic contractions (Figure 4.2). The basal tone of the muscle strips was not statistically different from the control value which was in agreement with the absence of an effect of CPA

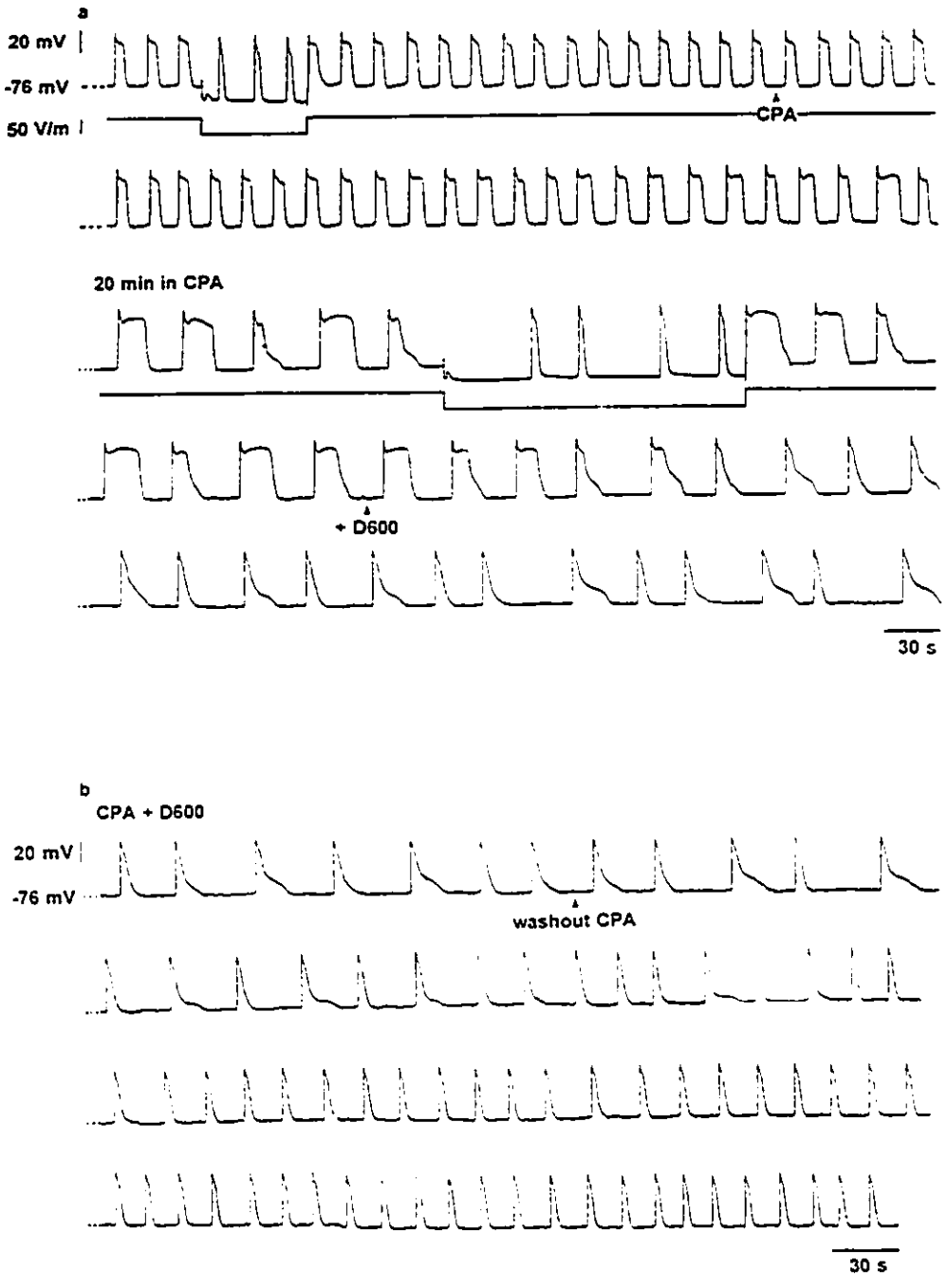
a
20 mV
-76 mV
50 V/m
CPA
20 min in CPA
+ D600
30 s
b
CPA + D600
20 mV
-76 mV
washout CPA
30 s

Figure 4.1

on the resting membrane potential.

Although the ISWI was increased, it was not clear if the reduction in slow wave frequency could be in part caused by the increase in duration. Since the slow wave plateaus can be abolished by L-type Ca^{2+} channel blockers [7, 93, 105, 194], the effect of D600 on the CPA induced activity was studied.

4.4.2 Reduction in the slow wave frequency by CPA was independent of an increase in slow wave duration

The prolonged plateaus in the presence of CPA started to collapse within 2 min of perfusion with D600 (1 μM) in all preparations (n=11, Figure 4.1b). However, the slow wave frequency remained the same (Table 4.1) indicating that the reduction in the slow wave frequency by CPA was not associated with the increase in duration. Similarly, when the prolonged plateaus were abolished by hyperpolarization (Figure 4.1a), the reduction in the slow wave frequency remained.

Consistent with the effects on electrical activity, in the presence of D600, the CPA-enhanced amplitude and duration of phasic contractions were significantly reduced below the control level (Figure 4.2). The reduction in frequency of phasic contractions by CPA remained unchanged in the presence of D600 when the duration was reduced.

4.4.3 Dose dependent effects of CPA in the presence of D600

The effects of D600 (1 μM) on the slow wave activity in Krebs solution was consistent with previously published results [7, 112]. D600 did not change the resting membrane

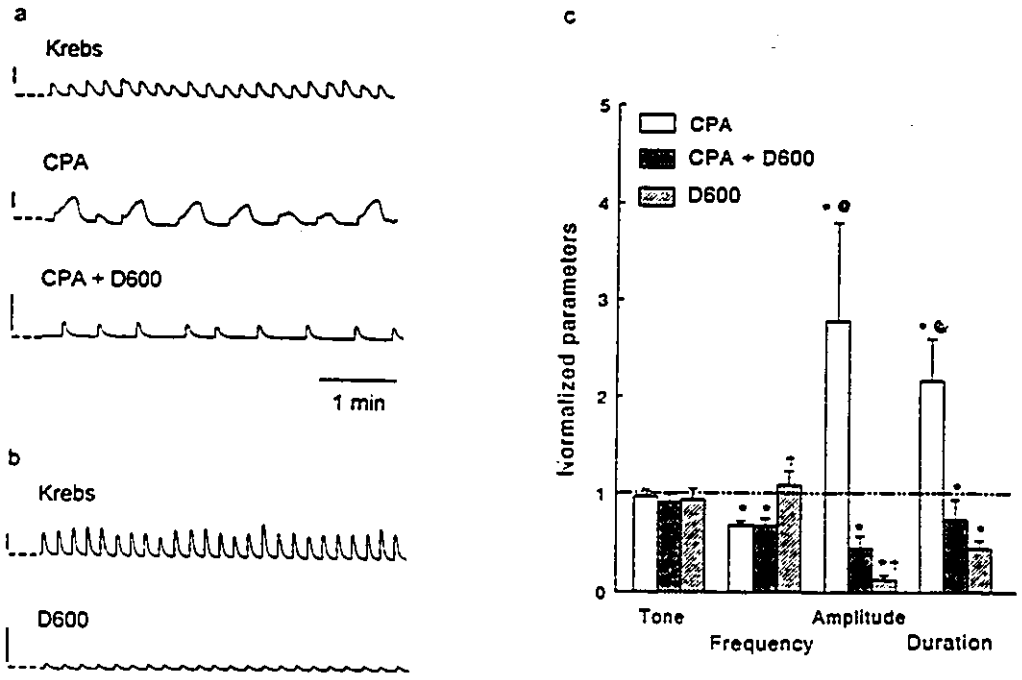

Figure 4.2: *Effects of CPA on the phasic contractions*

a. Consistent with the effects on the slow wave activity, CPA (3 μM) decreased the frequency of phasic contractions, and increased the amplitude and duration. 1 μM D600 abolished the amplitude and duration of phasic contractions induced by CPA. Reduction in the frequency remained in the presence of D600. Calibration bars represent 1 mN/mm^2.

b. Without CPA, D600 diminished the amplitude of the phasic contractions to approximately 15 % of that in Krebs solution. Calibration bars represent 1 mN/mm^2.

c. Parameters describing the characteristics of phasic contractions in different experimental conditions were normalized to the corresponding parameters in Krebs solution (control). The dash-dot line represents the control level. '*' denotes statistically significant differences between the parameters in experimental conditions with those in control. '†' denotes statistically significant differences between the parameters in D600 and those in CPA+D600. '@' denotes statistically significant differences between the parameters in CPA and those in CPA+D600. * ,†, and @ represent $p < 0.01$.

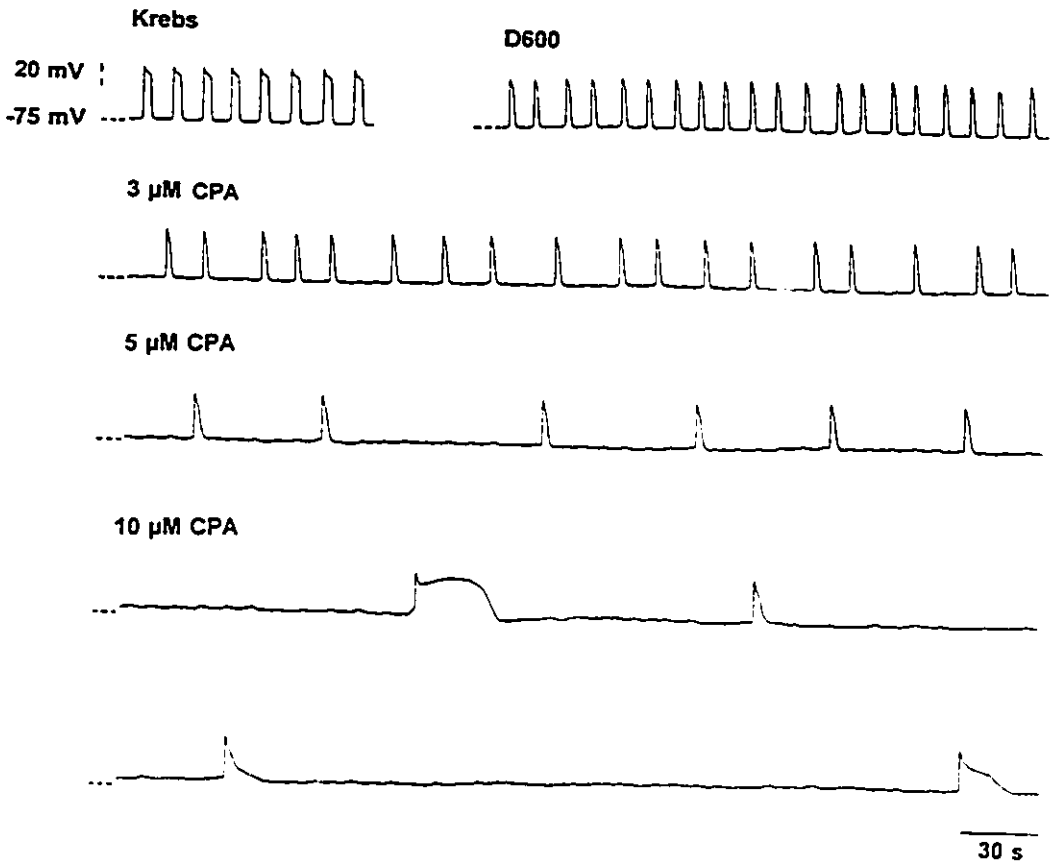

Figure 4.3: *Dose dependent effects of CPA on the upstroke potential*
After perfusion with 3 μM CPA for 20 min (beginning of the second panel), the frequency was reduced from 6 cpm (in D600) to 3 cpm without any significant effect on other slow wave parameters. 5 μM CPA (additional 20 min perfusion; beginning of the third panel) further decreased the frequency (to 1.2 cpm) and increased the duration (from 1.5 s to 2.5 s). Perfusion of 10 μM CPA for an additional 20 min (beginning of the fourth panel) substantially decreased the frequency (to 0.3 cpm). After the last slow wave shown in the recording, there was not another slow wave in the next 10 min. This figure shows sections of a continuous recording from the same cell.

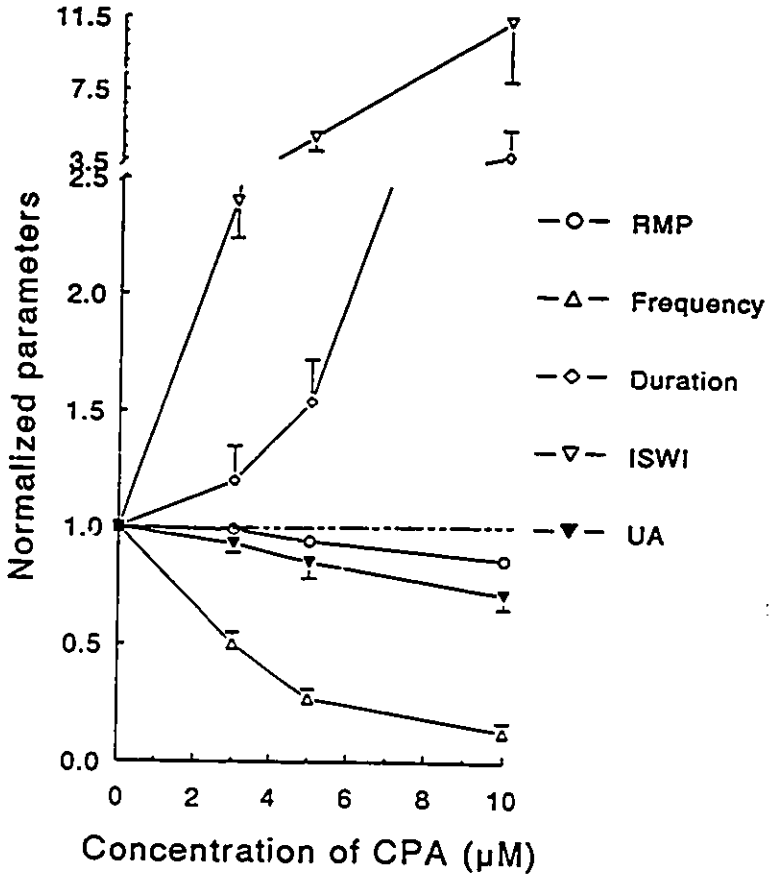

Figure 4.4: *Concentration response relationships of the effects of CPA on the upstroke potential*

The upstroke potential parameters in different concentrations of CPA were normalized to the corresponding parameters in 1 μM D600 (control). The dash-dot line represents the control level. Note the difference in scales between the upper and lower portion of the y-axis. In 2 preparations, after 30 min perfusion of 10 μM CPA , the upstroke potential frequency was reduced to less than 1 oscillation per 10 min. The parameters were obtained from the average of the last 4 oscillations observed. All values in CPA, except the resting membrane potential and upstroke amplitude in 3 μM CPA, were statistically different from control values ($p < 0.01$). ISWI — inter-slow wave interval; RMP — resting membrane potential; and, UA — upstroke potential amplitude.

potential (−73.3± 1.4 mV, n=4) and increased the slow wave frequency (from 5.0±0.3 to 5.9±0.4 cpm, $p < 0.05$), which was associated with the reduction of the duration (from 3.0±0.2 to 1.6±0.1 s, $p < 0.01$) because the values for the ISWI (from 7.6±0.4 to 7.1±0.7 s) were not significantly different. In addition, the upstroke amplitude was significantly decreased from 50.1±2.5 to 46.5±1.7 mV ($p < 0.05$). The L-type Ca^{2+}-channel-blocker insensitive component of the slow waves is termed the "upstroke potential" (see Figure 1.3), which reflects the periodicity of the biochemical clock [92], and serves as control activity in the following experiments, unless otherwise specified.

Addition of 3 μM CPA in the presence of D600 decreased the slow wave frequency by 50% while the duration was increased by 25 % (n=4, Figures 4.3 and 4.4). Increasing the CPA concentration to 5 μM further decreased the frequency by 73% and increased the duration by 54%. In 10 μM CPA, the frequency was reduced to 13% of that in D600; the duration was increased to 388% (Figure 4.4). In 2 experiments, the frequency was reduced to less than one oscillation in 10 minutes after perfusing with 10 μM CPA for 30 min. Increase in duration was observed in all preparations before oscillations were abolished. The decrease in the frequency was not caused by an increase in duration as the ISWI was increased by 2.4-, 4.9- and 11.3-fold, in 3 μM, 5 μM and 10 μM CPA, respectively.

These effects of CPA indicated that a decrease in the ER Ca^{2+} refilling rate caused a reduction in the frequency of activation of the upstroke potentials. This hypothesis was further investigated from a different perspective. We postulated that delaying the ER Ca^{2+} uptake by reducing the cytosolic Ca^{2+} concentration would produce a similar effect on the pacemaker frequency. This hypothesis was examined using BAPTA/AM. BAPTA/AM, after entering the cell, is hydrolysed into the active tetra-anionic salt form of BAPTA — a chelator of cytosolic free Ca^{2+}.

Table 4.2: *Effects of BAPTA/AM on the upstroke potentials*

	Krebs	+ D600	+BAPTA/AM	Krebs +BAPTA/AM§	+D600+CPA
Resting membrane Potential (mV)	−70.8±2.0	−70.3±1.8	−69.0±1.6	−76.5±1.5	−75.5±2.5
Frequency (cpm)	4.0±0.4	5.0±0.4*	3.0±0.4††	4.1±0.1	0.6±0.1**
Duration (s)	3.8±0.7	2.1±0.1**	3.9±0.6††	3.5±0.5	5.8±0.3**
Inter-slow-wave interval (s)	10.1±2.7	8.. ±1.6	12.5±4.6†	10.25±1.3	84.3±2.7**
Upstroke amplitude (mV)	37.3±2.0	32.9±2.6*	30.5±1.6**	47.4±1.3	43.0±3.0*
Plateau amplitude (mV)	34.3±2.1	- - -	- - -	44.0±1.5	36.9±1.7**

n=4; §: n=3. Results in the presence of BAPTA/AM (25 μM) were analyzed 30 min after the perfusion started. In 1 preparation, in the presence of D600 (1 μM) + CPA (3 μM) + BAPTA/AM (25 μM), the frequency was reduced to less than 1 oscillation in 15 min after 30 min of perfusion. The parameters were obtained from the average of the last 4 oscillations observed. '*' denotes statistically significant differences between the slow wave activity under the experimental conditions and that in Krebs solution. '†' denotes statistically significant differences between the activity in BAPTA/AM and that in D600. †, * — $p < 0.05$; ††, ** — $p < 0.01$.

4.4.4 Effects of BAPTA/AM on the electrical activity

The dose dependent effects of BAPTA on the slow wave activity could be observed over time since BAPTA is membrane impermeable. As the intracellular concentration of BAPTA was increasing over time, the decrease in frequency was more and more profound. In addition, the rate of rise of the slow waves decreased gradually as the perfusion period with BAPTA/AM increased. Therefore, in all experiments, the effects of BAPTA/AM were analyzed after a perfusion time of 30 min.

After 30 min perfusion with 25 μM BAPTA/AM in the presence of D600 (1 μM), the upstroke potential frequency was reduced by 40% and the duration and ISWI increased by 86% and 47%, respectively (n=4, Table 4.2). The effect of BAPTA/AM was reversible over a washout period of 30-45 min but only when the incubation period was not longer than 45 min (n=3).

In another set of experiments, when the Ca^{2+} uptake into the ER was further suppressed by CPA (3 μM) in the presence of BAPTA/AM, the slow wave frequency was reduced to 0.6±0.1 cpm (n=3, Table 4.2, Figure 4.5). In one preparation, the frequency was reduced to less than 1 oscillation in 15 min. The upstroke potentials were abolished before any observable changes in the resting membrane potential.

The additive effects of CPA and BAPTA/AM were consistent with the hypothesis that the rate of Ca^{2+} refilling is part of the pacemaker frequency regulatory mechanism. It was therefore of interest to study the endogenous mechanism through which Ca^{2+} was released from the ER.

4.4.5 Effects of neomycin on the upstroke potentials

One of the most common mechanisms to release Ca^{2+} from the ER is the activation of IP_3-sensitive Ca^{2+} channels. To influence the intrinsic IP_3 production, we

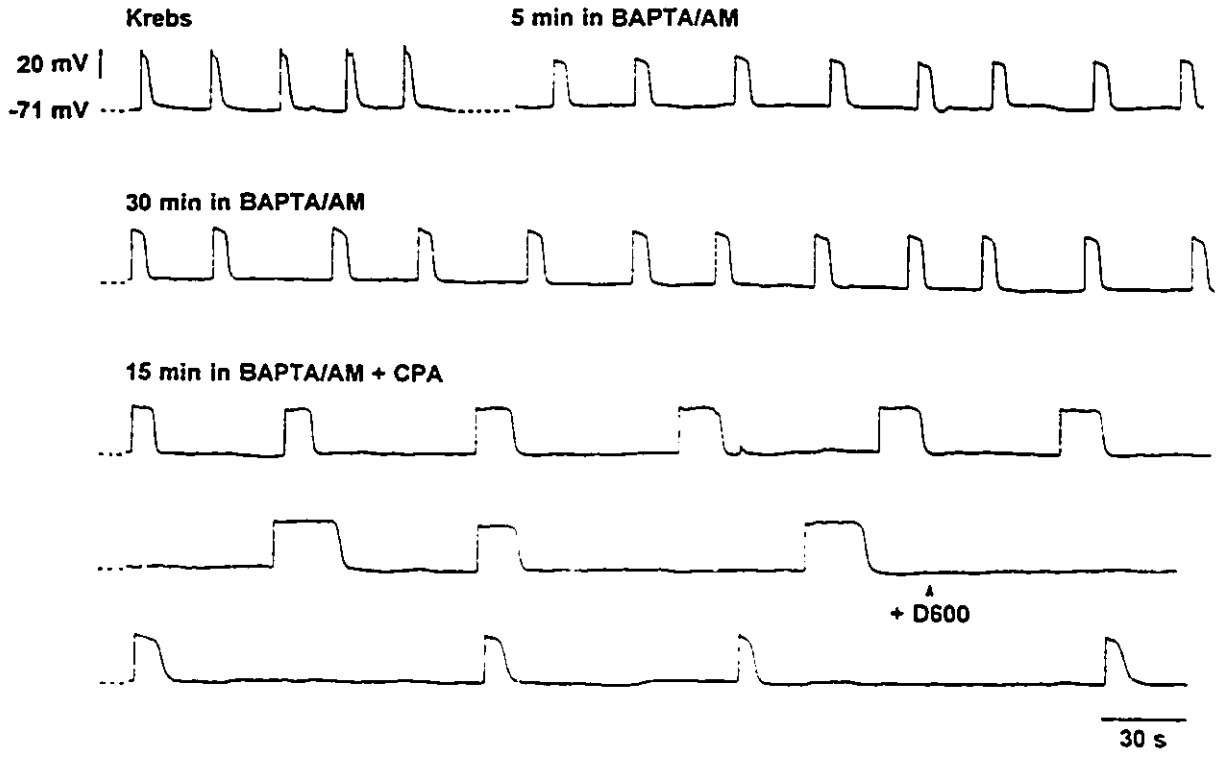

Figure 4.5: *Effects of BAPTA/AM on the slow wave activity*
BAPTA/AM (25 μM) decreased the frequency and increased the duration of slow waves. Addition of CPA (3 μM) further reduced the frequency and increased the duration of slow waves. Addition of D600 reduced the slow wave duration but the reduction in frequency remained. Recording was obtained from the same cell throughout the entire experiment.

Figure 4.6: *Effects of neomycin and caffeine on the upstroke potential*
a. In the presence of D600, neomycin (4 mM) reduced the upstroke potential frequency which was accompanied by a small depolarization of 4 mV. Repolarization did not produce any significant difference except that the uptake potential amplitude was restored.
b. Caffeine (5 mM) reduced the frequency of the upstroke potentials and slightly decreased the resting membrane potential. Increasing the concentration of caffeine to 10 mM further reduced the upstroke potential frequency and decreased the resting membrane potential. Repolarizing the cells to a similar resting membrane potential as that in D600 did not restore the frequency but the amplitude was restored (the third and the fifth panels, above bars). It indicates that the reduction in frequency, unlike the upstroke amplitude, is not caused by depolarization. Note that without caffeine, the electrical activity during repolarization (bottom panel above bar) was the same as that in D600 in the beginning of the experiment. A continuous recording (except that 5 min between the activity in Krebs and D600, and 30 s between the end of the fifth and the beginning of the sixth panel, were omitted) from the same cell is shown. Amplitudes of electric field stimulations (denoted by bars): 45 mV/mm, third panel; 170 mV/mm, fifth panel; and, 80 mV/mm, sixth panel.

---

studied the effect of neomycin which binds to polyphosphoinositides and makes them unhydrolysable by phospholipase C, thus, blocking inositide formation [190].

In the presence of D600 (1 μM), neomycin (4 mM) decreased the resting membrane potential from -70.9 ± 0.8 to -64.3 ± 1.7 mV and the upstroke potential frequency from 5.3 ± 0.2 to 3.2 ± 0.4 cpm (n=8, $p < 0.01$). Reduction in frequency was not caused by depolarization as repolarization of the cells did not restore the upstroke potential frequency (Figure 4.6a). In addition, in all preparations, a reduction in frequency was observed before depolarization appeared. Accompanying the depolarization, the upstroke amplitude was decreased from 35.5 ± 1.4 mV to 21.5 ± 3.4 mV.

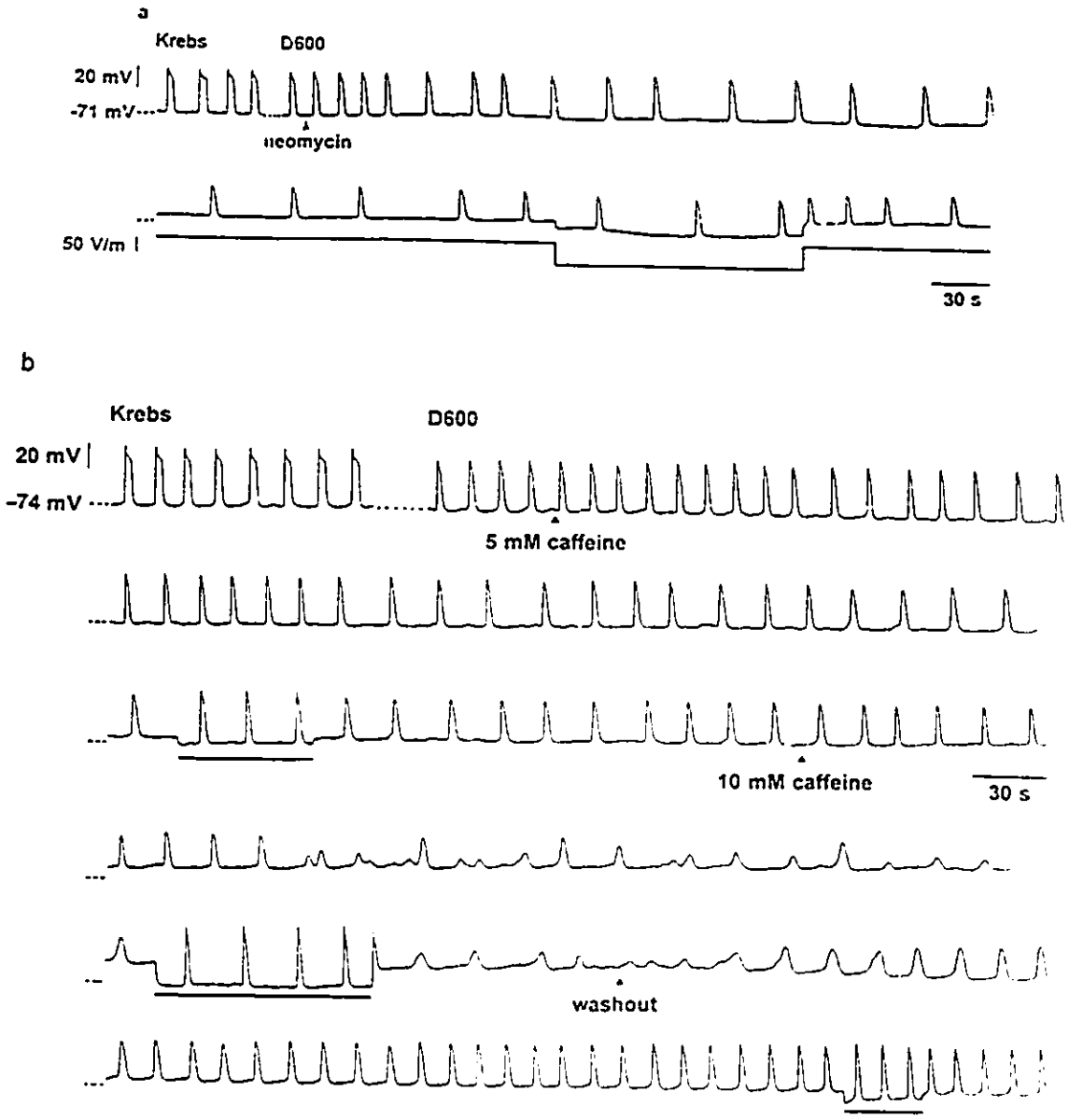
a
Krebs
D600
20 mV
-71 mV
neomycin
50 V/m
30 s
b
Krebs
D600
20 mV
-74 mV
5 mM caffeine
10 mM caffeine
30 s
washout

Figure 4.6

Table 4.3: *Effects of caffeine on the upstroke potentials*

	D600 (1 μM)	+5 mM Caffeine		+10 mM Caffeine	
		without repolarization	with repolarization§	without repolarization	with repolarization§
Resting Membrane Potential (mV)	−72.5±1.5	−67.1±1.8**	−72.2±1.6†	−58.3±2.3**	−71.3±1.6††
Frequency (cpm)	5.7±0.4	3.6±0.3**	3.5±0.5**	2.3±0.3**	2.5±0.5**
Duration (s)	1.8±0.2	1.5±0.3	1.7±0.2	2.3±0.3**	1.2±0.1**,††
Inter-slow wave interval (s)	7.1±0.8	12.7±1.1**	15.4±3.1**	25.4±4.7**	24.6±5.2**
Upstroke Amplitude (mV)	42.8±2.3	36.2±1.9**	41.2±2.9†	19.8±4.4**	40.5±2.9††

n=6; §: n=4. Caffeine was added to the perfusate in the presence of D600. Repolarization of the resting membrane potential to approximately the same value as that in control (D600) was achieved by applying appropriate potential differences across the Ag/AgCl stimulation plate in the partition chamber. '*' denotes statistically significant differences between the upstroke potentials under the experimental conditions and that in D600. '†' denotes statistically significant differences between the activity with and without repolarization in the same caffeine concentration. †, * — $p < 0.05$; ††, ** — $p < 0.01$.

Upon repolarization, the upstroke amplitude was restored to the control value.

4.4.6 Effects of ryanodine on the upstroke potentials

Ryanodine has been shown as an effective agent to deplete Ca^{2+} from ER [30, 158, 192]. However, in the ICC-CM preparations, perfusing the preparations with ryanodine (up to 60 μM) in the presence of 1 μM D600 (n=3) for 1.5 hours produced no observable effects on the upstroke potentials. These results indicate that a ryanodine-sensitive Ca^{2+} compartment, if it exists, is not involved in the generation of the

Figure 4.7: *Comparison of the density of the ER in different cell types at the submucosal border of the circular muscle layer*

a. A process of an interstitial cell of Cajal (ICC) and a circular muscle cell (CM) are cross sectioned. In addition to post-staining after Shinji, this specimen was post-stained with lead citrate. The density of sER (er) is much more abundant in the ICC than in circular muscle cells. Arrow heads are pointing at the subsurface cisternae. Glycogen granules and ribosomes are darkly stained (similar in b). x 40,700; bar = 0.5 μm. b. The density of sER (er) is lower in branching smooth muscle cells (bSM) than in ICCs but still substantially higher than in circular muscle cells. x 25,000; bar = 0.5 μm.

---

upstroke potential of slow waves.

4.4.7 Effects of caffeine on the upstroke potentials

In the presence of D600, caffeine (up to 1 mM) did not produce any observable effects on the upstroke potentials. 5 mM caffeine significantly decreased the upstroke-potential frequency, accompanied by a decrease in resting membrane potential (n=6, Figure 4.6b and Table 4.3); repolarizing the preparation to the control resting membrane potential did not alter the effect of caffeine on the upstroke- potential frequency. The decrease in upstroke amplitude was associated with a decrease in resting membrane potential since it was completely restored by repolarization (Table 4.3). Increasing the concentration of caffeine to 10 mM further reduced the upstroke-potential frequency which was again independent of depolarization (Figure 4.6b, Table 4.3). The effects of caffeine on the upstroke-potential frequency were completely reversible; however, in two preparations, the resting membrane potential did not recover, causing an apparent reduction in the upstroke amplitude (Figure 4.6b).

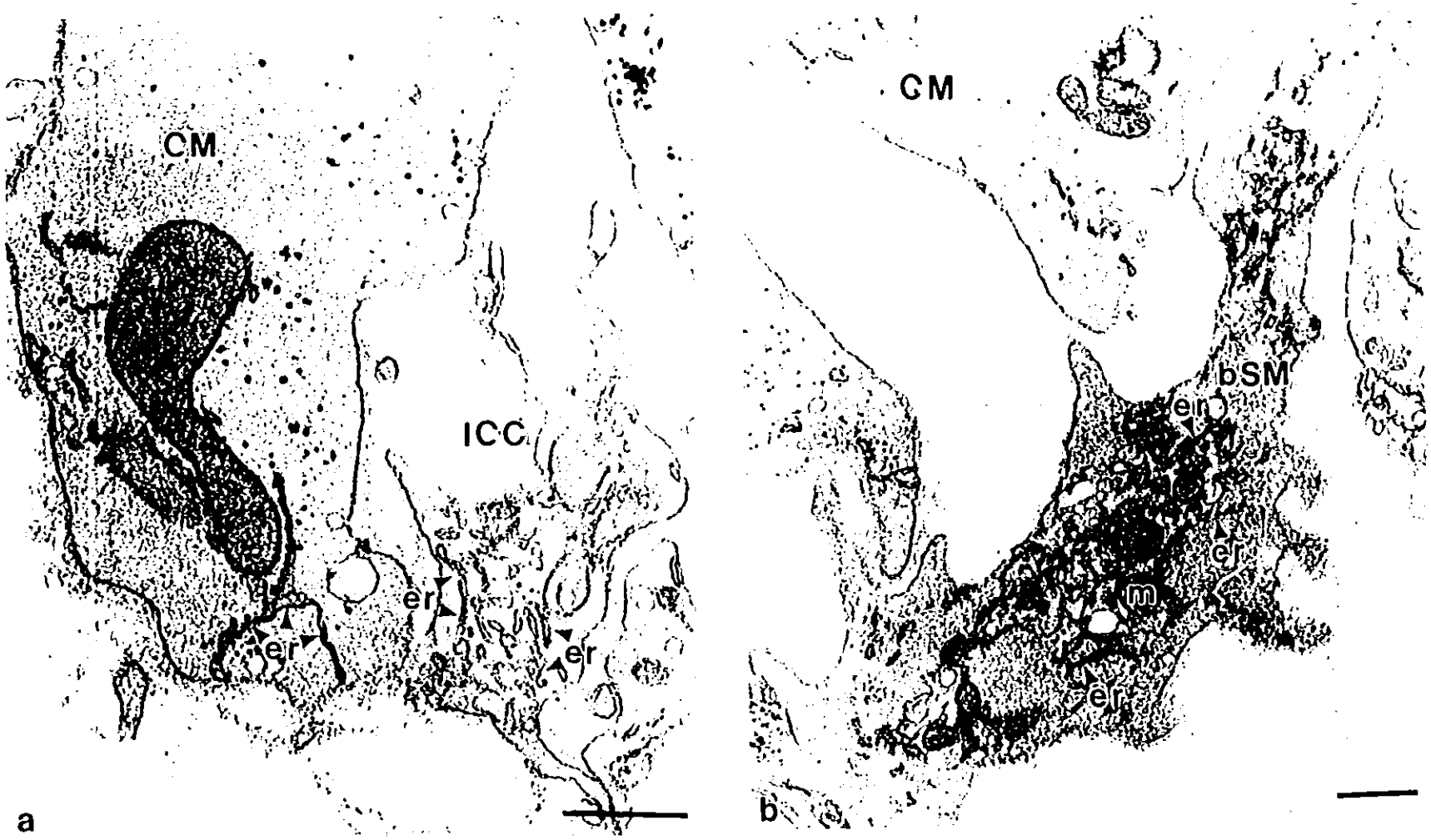

Figure 4.7

Figure 4.8: *Distribution of plasma-membrane associated endoplasmic reticulum in an interstitial cell of Cajal at the submucosal border*

a. An interstitial cell of Cajal (ICC) was tangentially sectioned very close to the plasma membrane as indicated by numerous cross-sectioned caveolae. A large amount of sER in the ICC is found to be very close to the membrane (arrows) as subsurface cisterna (arrow heads) and around the caveolae (c). Direct connections between the plasma membrane and sER are inconspicuous. × 40,700; bar = 0.5 μm. b. A higher magnification of (a). The arrows and arrow heads in (a) and (b) are pointing at the same locations. The plasma membrane associated sER was often found to be separated from the plasma membrane by a narrow gap over a long distance. × 104,000; bar = 0.1 μm.

4.4.8 Distribution of the plasma-membrane associated ER in different cell types at the submucosal border

Similar to the smooth endoplasmic reticulum (sER) in other cell types, such as epithelial cells [149], the true extent of the presence of this organelle is often not apparent in various cells of the canine colon musculature prepared by routine methods. This is caused by a lack of contrast between elements of the sER and surrounding cytosol. Potassium ferricyanide block-staining [152, 149] in combination with post-staining of ultrathin sections after Shinji [169] strongly increases this contrast.

Since the objective was to look for a structural basis for interaction between the ER Ca^{2+} and the electrical activity manifested at the plasma membrane, the plasma-membrane associated ER was of the highest interest. We have recently observed a layer of branching smooth muscle (bSM) cells sandwiched between the submuscular ICC network and the circular muscle (CM) proper [119]. Hence, densities of the plasma-membrane associated ER in ICCs, bSM and CM were investigated.

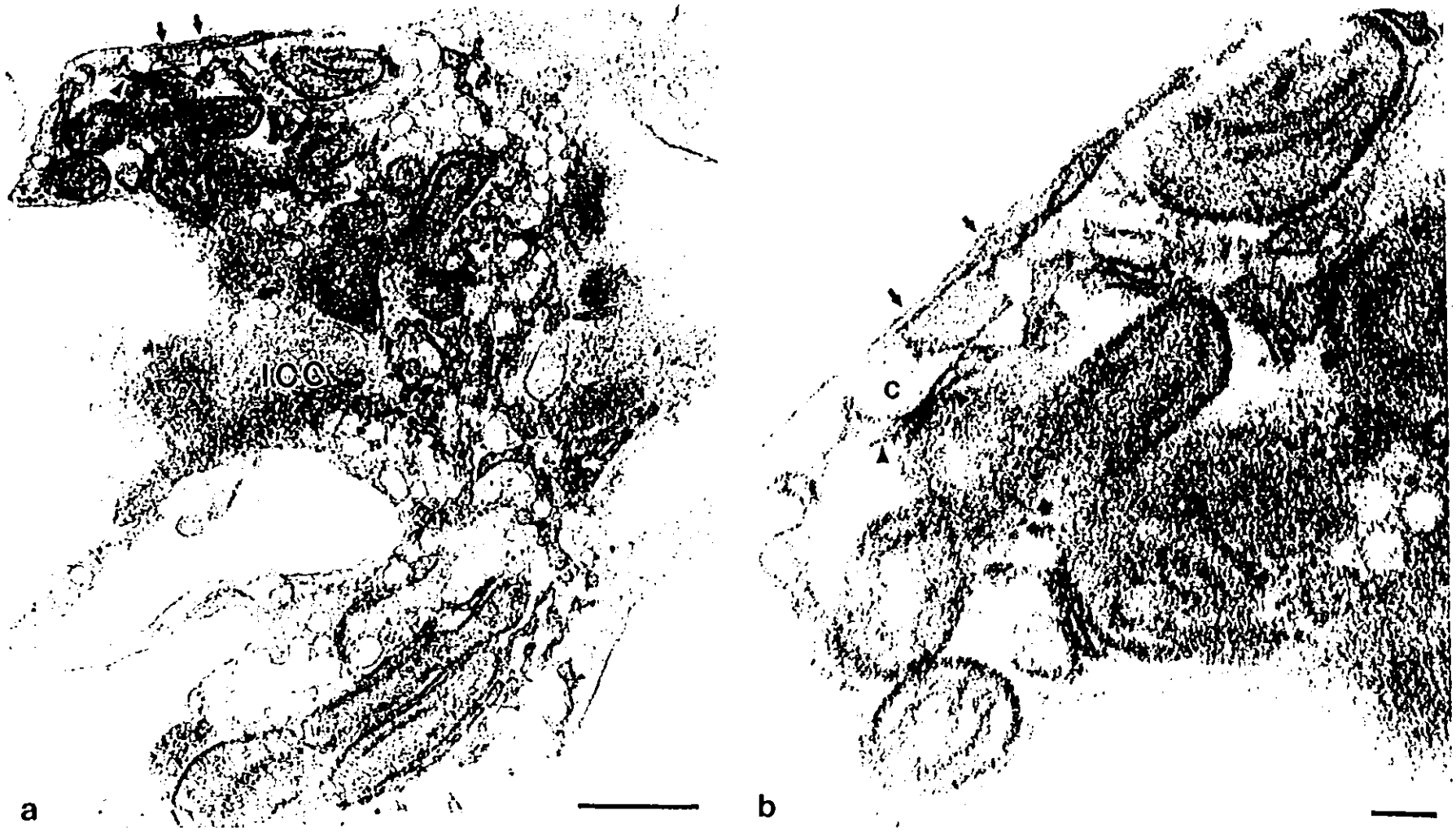

Figure 4.8

Densities of the sER cisternae in CM cells (Figure 4.7), bSM cells (Figure 4.7b), and ICCs (Figures 4.7a and 4.8) were distinctly different: in the order CM $\ll$ bSM $<$ ICC. In all three cell types, flattened sER cisternae in continuity with cisternae of rough endoplasmic reticulum (rER) were observed. The rER closely enveloped mitochondria, and was connected with a network of partly flattened, partly tubular extensions of sER.

The sER regularly formed subsurface cisternae, separated from the plasma membrane by a uniform gap of $\simeq$ 10 nm over long distances. In some areas of these gaps, irregularly-spaced thin strands bridging the plasma membrane and subsurface cisternae were observed though these strands of electron dense materials could not be further identified. Subsurface cisternae were smaller in CM cells than in bSM cells (arrow head, Figure 4.7) and commonly very extensive in ICCs (arrow heads, Figure 4.8). In all three cell types, subsurface cisternae closely approached (CM, bSM) and enveloped (ICCs, Figure 4.8) caveolae. A cross-section tangentially cut very close to the plasma membrane illustrated that the subsurface cisternae covered a large area right underneath the plasma membrane of ICCs (Figure 4.8a).

4.5 Discussion

4.5.1 Regulation of the colonic pacemaker frequency by ER calcium

The consistent, reversible and dose dependent effects of CPA on the upstroke-potential frequency provide strong evidence for our hypothesis that the rate of refilling of Ca^{2+} into the plasma-membrane associated ER is in synchrony with the rate of initiation of the upstroke potentials, hence the pacemaker activity (Figure 4.9). This hypoth-

esis is based on the observations that: (i) CPA, a specific ER Ca^{2+}-pump ATPase inhibitor [56, 80, 102] thus inhibiting Ca^{2+} uptake into the ER, decreases the pacemaker frequency; and (ii) BAPTA, a cytosolic free-Ca^{2+} chelator, similarly decreases the pacemaker frequency likely by reducing the rate of Ca^{2+} refilling into the ER as a consequence of a decrease in the cytosolic Ca^{2+} concentration ($[Ca^{2+}]$).

4.5.2 Involvement of IP_3-induced ER Ca^{2+} release in the biochemical clock

The effect of neomycin on the pacemaker frequency suggests that IP_3 is involved in the biochemical clock, regulating Ca^{2+} release. In primary cultured neurons from rat frontal cortices, neomycin significantly inhibits the action of antidepressant drugs, such as amitriptyline and imipramine, which increase IP_3 content by 20–50% leading to an elevation of cytosolic $[Ca^{2+}]$ by releasing Ca^{2+} from the IP_3-sensitive Ca^{2+} stores [168]. Hence, in the canine colon, neomycin likely decreases the pacemaker frequency by inhibiting IP_3 synthesis. Reduction in the pacemaker frequency could be caused by prolonging the time required for the IP_3 concentration ($[IP_3]$) to reach its threshold to stimulate Ca^{2+} release, implying a cytosolic $[IP_3]$ oscillation [20]. It could also be caused by a decrease in the steady level of $[IP_3]$; a mathematical model has illustrated that such a decrease in the $[IP_3]$ level can reduce the frequency of cytosolic Ca^{2+} oscillations [19]. In addition, in the smooth muscle cell line, A7r5, the timing of the IP_3-induced Ca^{2+} release is determined by the ER intraluminal $[Ca^{2+}]$ [130]. Further experimentation, involving direct measurement of $[IP_3]$, is required to differentiate between these hypotheses.

In contrast to many other smooth muscle tissues, in which caffeine evokes contraction by releasing Ca^{2+} from the ER, in canine-colon circular muscle, 10 mM

Figure 4.9: *A hypothesis of the regulation of the pacemaker frequency by Ca^{2+} in the buffer barrier zone*

a. A hypothesis on the association between the slow-wave-type action potentials and the ER [Ca^{2+}]

The dotted line in the control panel depicts the full slow-wave-type action potentials. The L-type Ca^{2+}-channel blocker insensitive component (the upstroke potential) is outlined by the solid line. For simplicity, the upstroke potentials are schematically depicted to be superimposed on the corresponding full slow waves without correcting the change in the inter-slow wave interval. The upstroke potentials are initiated at the points (•: control, □: CPA) at which the ER Ca^{2+} is released through activation of IP_3-sensitive Ca^{2+} channels (see text). Hence, the ER [Ca^{2+}] is decreased simultaneously with the initiation of each upstroke potential. When the refilling rate of Ca^{2+} into the ER is decreased (such as in presence of CPA), schematically illustrated by a more gentle slope (dash-dot line in the ER [Ca^{2+}] panel) as compared to the control refilling rate (solid line), the frequency of the upstroke potentials is decreased.

b. A hypothetical model of the interaction between Ca^{2+} in the buffer barrier zone, and the pacemaker channel, the ER and the contractile filaments

Ca^{2+} is released from the ER through IP_3-sensitive Ca^{2+} channels, causing an abrupt increase in [Ca^{2+}] in the buffer barrier zone the cytosolic space between the plasma membrane (PM) and the ER. This increase in [Ca^{2+}] may serve to activate the pacemaker channels to initiate the slow waves. When the [Ca^{2+}] in the buffer barrier zone surpasses the Ca^{2+} sequestration ability of the ER and the PM, Ca^{2+} will diffuse into the inner cytoplasm to activate contractile filaments. CPA, inhibiting the ER Ca^{2+} pumps, decreases the Ca^{2+} refilling rate and the slow wave frequency. Neomycin inhibits IP_3 synthesis. Caffeine decreases the opening probability of the IP_3-sensitive Ca^{2+} channels. Both neomycin and caffeine decrease the slow wave frequency by delaying the Ca^{2+} release.

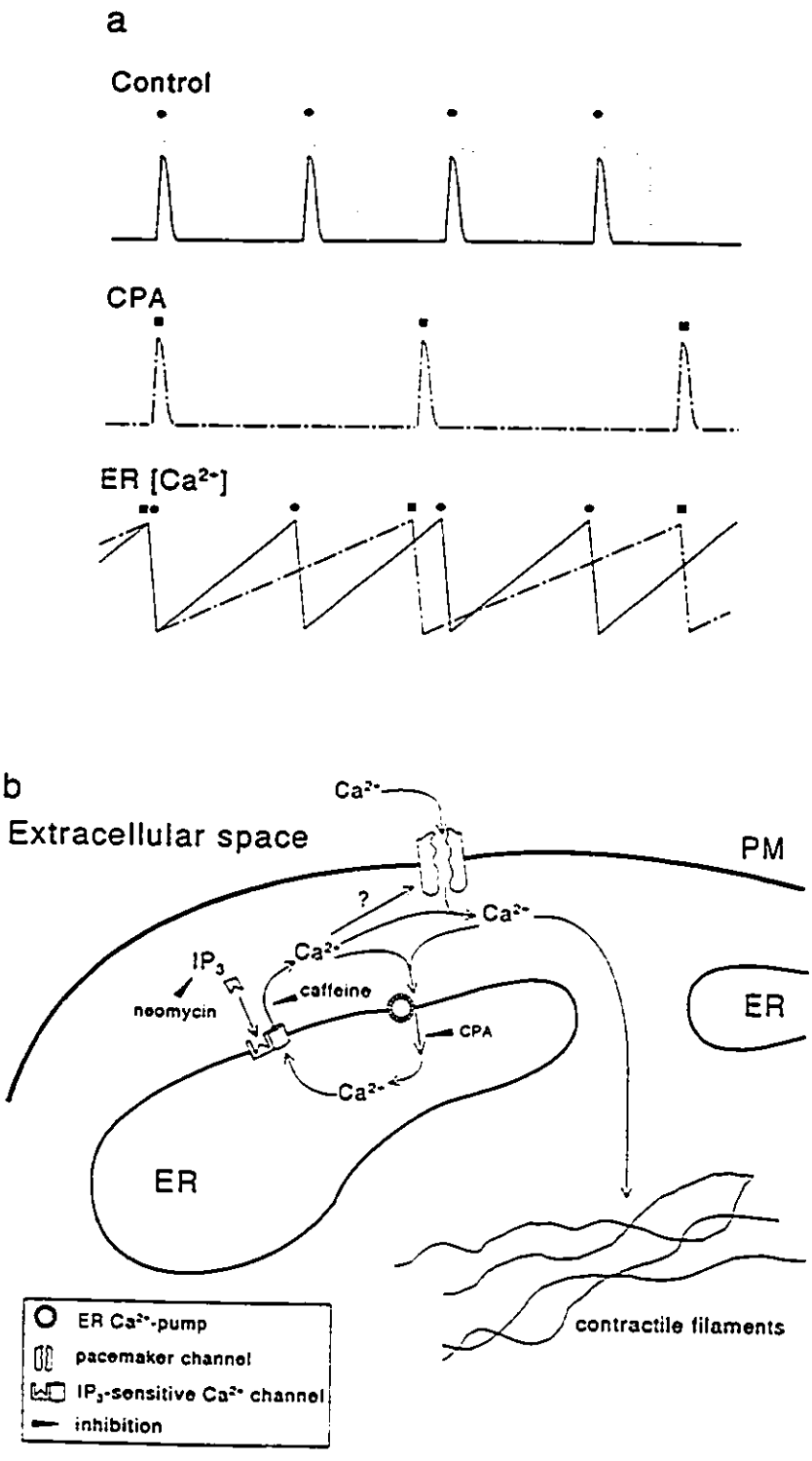
a
Control
CPA
ER [Ca2+]
b
Extracellular space
Ca2+
PM
?
Ca2+
IP3
Ca2+
caffeine
neomycin
ER
CPA
Ca2+
ER
contractile filaments
ER Ca2+-pump
pacemaker channel
IP3-sensitive Ca2+ channel
inhibition

Figure 4.9

caffeine does not cause contraction but instead completely abolishes the spontaneous phasic contractions in Krebs solution (result not shown). It indicates that, in the canine colon, reduction in the pacemaker frequency by caffeine is not caused by depletion of Ca^{2+} from caffeine-sensitive stores. We hypothesize that caffeine decreases the pacemaker frequency through an inhibition of IP_3- induced Ca^{2+} release. This interpretation is supported by studies showing that caffeine inhibits IP_3-induced Ca^{2+} release in *Xenopus* oocytes [141], cerebellar microsomes [35] and permeablized smooth muscle cells [95]; it is further substantiated by a recent study showing that 10 mM caffeine decreases the frequency of opening of the IP_3-sensitive ER Ca^{2+}-channels [23]. Furthermore, in rat hepatocytes, caffeine (6 mM), without itself releasing ER Ca^{2+}, antagonized IP_3- induced Ca^{2+} release at very low IP_3 concentrations [132].

Periodic Ca^{2+} release is unlikely to come from ryanodine-sensitive Ca^{2+} stores since ryanodine did not produce any effect on the upstroke potentials. In enzymatically dispersed canine colonic cells, identified as interstitial cells, ryanodine did not change the frequency of spontaneous Ca^{2+} oscillations although the amplitude of Ca^{2+} oscillations was decreased; this study suggests the presence of a ryanodine-sensitive Ca^{2+} compartment which is not coupled to the frequency regulatory mechanism of the Ca^{2+} oscillations [148]. Our results do not exclude the existence of ryanodine-sensitive Ca^{2+} stores in this preparations because such ER stores could exist but not be coupled to the mechanism for generating the upstroke potentials.

4.5.3 Regulation of pacemaker activity within the buffer barrier zone

The hypothesis developed above implies the presence of IP_3-sensitive Ca^{2+} stores in the vicinity of the plasma membrane such that the released Ca^{2+} can effectively mod-

ulate the ionic conductances in the plasma membrane. It has recently been demonstrated that upon release of Ca^{2+} from the CPA-sensitive stores in enzymatically dispersed canine colonic circular muscle cells, the Ca^{2+}-activated potassium channel is activated [134]. In the present study, extensive investigation at the electron microscopic level proved the existence of large areas of close associations between the ER and the plasma membrane. Remarkably, the density of such associations was very much larger in ICCs than in common smooth muscle cells. The presence of large areas separated by a narrow space of 10 nm proves the physical existence of a buffer barrier as proposed by van Breemen and colleagues [39, 40, 191]. Interestingly, under certain conditions, methylene blue accumulates exclusively in ICCs and exclusively in the ER of ICCs. Upon exposure to light, the methylene blue becomes toxic and slow wave activity is abolished [117].

The functional existence of the buffer barrier zone is demonstrated by comparing the force of phasic contractions and characteristics of the upstroke potentials in the presence of D600 with that in D600 plus CPA. Although the characteristics of each single upstroke potential are almost identical in the presence of either D600 or D600 plus 3 μM CPA, the force of the corresponding phasic contractions is significantly larger in the latter situation. Thus, when the ER Ca^{2+}-pump is inhibited by CPA, Ca^{2+}, entering the cells during the rising phase of the upstroke potentials, saturates the buffering capacity of the buffer barrier, and then overflows the buffer barrier and diffuses into the inner cytoplasm to activate contractile filaments (Figure 4.9b).

Because of the physical barrier, it is conceivable that the $[Ca^{2+}]$ is very much higher in the buffer barrier zone than in the inner cytoplasm when Ca^{2+} is released from the stores. Our hypothesis is that such an abrupt increase in $[Ca^{2+}]$ activates (directly or indirectly through subsequent interaction with second messenger pathways)

the pacemaker channels to initiate a slow wave (Figure 4.9).

4.5.4 Induction of slow wave plateaus after blockade of L-type Ca^{2+} channels

Slow wave plateaus can be abolished by organic L-type Ca^{2+} channel blockers [7, 93]. It is intriguing that the slow wave plateaus can be re-evoked by CPA (10 μM) after blockade of L-type Ca^{2+} channels by D600. The increase in duration was not due to a decrease in the Ca^{2+}-dependent maxi-K^+ conductance; in fact, in the presence of CPA, the Ca^{2+}-activated K^+ current was increased by $\simeq$ 25 % (at 20 mV) as measured in enzymatically dispersed canine-colon circular smooth muscle cells using the nystatin-perforated patch configuration [111]. It is known that depletion of intracellular Ca^{2+} stores can promote Ca^{2+} influx [30, 47, 124, 151, 170, 192]. In the A7r5 smooth muscle cells, the filling state of the IP_3-sensitive Ca^{2+} store regulates the entry of Ca^{2+} through a pathway different from voltage- operated Ca^{2+} channels since 10 μM of verapamil could not block the Ca^{2+} influx [131]. Hence, the prolonged plateaus induced by CPA (10 μM) in the presence of D600 are possibly carried by a non-L- type Ca^{2+} current evoked by depletion of the IP_3-sensitive Ca^{2+} stores. This observation demands further experimentations to investigate the characteristics of conductances that determine the duration of the slow wave plateaus.

4.5.5 Relative roles of ICC, bSM and CM in the generation of the pacemaker component

In canine colon, the submuscular ICCs are extensively coupled to adjacent smooth muscle cells by gap junctions [12]. We have recently provided evidence that the pace-

maker component of the slow waves is generated in the submuscular ICC-smooth-muscle network and that action potentials intrinsically generated by circular muscle lack such a component [112, 113]. It would be quite a challenge for ICCs to generate sufficient current by themselves to initiate the upstroke potentials in a low-resistantly coupled network [146]. Hence, the branching smooth muscle (bSM) cells have been proposed to possess the pacemaker channels as well and work synchronously with ICCs [117]. The likelihood of this hypothesis relies on extensive metabolic coupling such that the metabolically regulated biochemical clock can be synchronized between the ICCs and bSM cells. The tremendous extent of neurobiotin spread at the submucosal surface reveals that these cells are indeed very well metabolically coupled [67]. Furthermore, the morphological data presented in this study provide a structural basis for bSM cells being involved in the generation of the pacemaker activity by demonstrating the extensive amount of plasma-membrane associated sER in the bSM cells. This observation demonstrates the need to look for the pacemaker channels in the bSM cells.

In conclusion, this study provides strong evidence that pacemaker channels of the colonic ICCs are triggered periodically by an intracellular biochemical clock. Specifically, the current electrophysiological and morphological results put forward the hypothesis that the pacemaker frequency is coupled to the Ca^{2+} refilling cycle of the $I\Gamma_3$-releasable Ca^{2+} stores in the plasma-membrane associated ER.

Chapter 5

Ontogenesis of Pacemaker Activity and Interstitial Cells of Cajal in Mouse Small Intestine

5.1 Epitome

The essential role of the interstitial cells of Cajal (ICCs) associated with the myenteric plexus in the generation of the pacemaker activity, which regulates the periodicity of the slow waves, has recently been ascertained in the mouse small intestine. In this study, the ontogenesis of the pacemaker activity and the ICCs in the small intestine of neonatal mice were investigated. The pacemaker component of the slow waves has been fingerprinted by its insensitivity to L-type Ca^{2+}-channels blockers and sensi-

This chapter is in the editing process for journal submission (authored by Louis Liu, Lars Thuneberg and Jan Huizinga). Contributions of Lars Thuneberg are discussed in section 2.3 of Chapter 2.

tivity to cyclopiazonic acid (CPA), a specific inhibitor of the endoplasmic reticulum (ER) Ca^{2+}-pump ATPase. Development of this component was therefore studied electrophysiologically. The distribution of the ICCs in the neonatal mouse small intestine was studied with methylene blue. All isolated musculature of the neonatal mouse small intestine (new-born, unfed–7 days old) spontaneously generated action potentials. In new-born, unfed neonates, the action potentials were irregular in frequency and amplitude. Both the frequency and amplitude of the action potentials were significantly reduced by verapamil. 5 μM CPA completely abolished all action potentials. Quiescent spots were observed in approximately 50% of impalements. In 2–6 hours, the slow wave frequency and amplitude became regular and a well-defined plateau phase was observed. Verapamil decreased the upstroke amplitude and the rate of rise, and had no effect on the frequency, similar effects were observed in the 24–48 hours and the 2–7 days groups. 5 μM CPA decreased the slow wave frequency to 10%, 23% and 40% in 2–6 hours, 24–48 hours and 2–7 days, respectively. The effects of CPA on the pacemaker frequency in the 2–7 days group was identical to adult mice. In 2 hours old neonates, methylene-blue stained ICCs were scattered. In 48 hours, a complete ICC network covering the entire myenteric plexus was formed. In conclusion, this is the first documentation of the ontogenesis of the pacemaker activity in the gastrointestinal tract. More specifically, we demonstrated the presence of spontaneous action potentials in the small intestine of newly born, unfed neonatal mice. In addition, the pacemaker component of the slow waves was identified in neonates as early as 6 hours after birth. The pacemaker component was fully developed 2 days after birth. The correlation of the development of ICC network and the progressive decrease in the quiescent spots consistently suggests that the methylene-blue stained ICCs are the source of the pacemaker activity.

5.2 Introduction

Knowledge of the control mechanism of the gastrointestinal (GI) motility is based upon the identification of the origin of the pacemaker activity by which the slow-wave-type action potentials (slow waves) are triggered. Electrophysiological evidence, acquired from different isolated and intact muscle strip preparations, demonstrates that the slow waves launch from the myenteric plexus of the stomach [9] and of the small intestine [82, 85, 175, 183], and from the submuscular plexus of colon [38, 43, 60, 58, 62, 110, 115, 172]. Interstitial cells of Cajal (ICCs) are always identified in areas where the slow waves originate [70, 179, 184]. These observations are consistent with the hypothesis that ICCs are crucial in the generation of the pacemaking activity in the GI tract.

The role of ICCs in regulating the GI motility is challenged by an inference acquired from results of individual studies on neonates. Gershon and Thompson demonstrated that the contractile apparatus and the neural innervations have been developed in foetuses at 17 days of gestation in rabbit and 16 days of gestation in mouse [78]; several contraction recordings presented in that study indicate spontaneous periodic phasic contractions in foetal rabbit small intestine as early as 17 days of gestation. In addition, spontaneous sustained rhythmic contractions were consistently observed in cultured explants of the musculature isolated from the small intestine of neonatal mice, age between 2–7 days old [136, 182]. In both term and preterm infants, the intestine produces similar and appropriate contractile responses to the first feeding [22, 137]. These studies clearly demonstrate that the neonatal intestine is capable of generating rhythmic phasic contractions. However, morphological studies illustrated that the cytodifferentiation of ICCs was incomplete, though precursor cells have been identified, until 2-3 weeks after birth in the mouse small intestine [68] and

colon [69]. A recent study showed that development of the pacemaker activity and ICCs associated with the myenteric plexus of the small intestine was impaired when an anti-c-kit antibody was injected intraperitoneally into neonatal mice over the first 4 days after birth [189]; the first injection was made within the first 24 hours after birth. These observations lead to an interrogation of the mechanism by which the periodic phasic contractions are controlled in new-born neonates.

The objective of this study was to investigate the ontogenesis of the pacemaker activity and the ICCs in the small intestine of neonatal mice starting from the age of new-born, unfed. The pacemaker component of the slow waves has been fingerprinted by its resistance to L-type Ca^{2+}-channels blockers [85, 93, 194] and sensitivity to cyclopiazonic acid [118], a specific inhibitor of the endoplasmic reticulum (ER) Ca^{2+}-pump ATPase. Development of this component was therefore studied electrophysiologically. The ICCs associated with the myenteric plexus in the mouse small intestine have been depicted at the light microscopic level after their selective accumulation of methylene blue [179]. The distribution of the ICCs in the neonatal mouse small intestine was studied with methylene blue.

5.3 Materials and methods

5.3.1 Electrophysiological measurements

Tissue acquisition and preparation

Neonatal mice (at birth to 7 days) were sacrificed by decapitation. Pregnant mice (CD1) were purchased from Charles River Laboratories at 15–16 days of gestation and monitored for delivery (time zero) after 19–20 days of gestation. The GI tract,

starting from the lower oesophagus to the colon, of the sacrificed neonatal mouse was removed with the intact mesenteric vascular bed to minimize stretch when the gut was transferred to a dissecting dish filled with pre-warmed Krebs solution. After releasing the gut from the mesenteric vascular bed, the gut was mounted, without stretching, on the Sylgard (184 silicone elastomer, Dow Corning Corporation) surface with insect pins (Fine Science Tools Inc., 0.1 mm in diameter) at the stomach and the ileo-caecal junction. The musculature of the small intestine (20–50% of the entire length as measured between the pylorus and the ileo-caecal junction) was carefully dissected from the submucosa without opening the gut under a dissection microscope (Zeiss) at 40x. Electron microscopic examinations of the dissected tissue revealed that the musculature cleaved along the deep muscular plexus leaving the outer circular muscle layer, myenteric plexus and longitudinal muscle layer healthily intact.

The isolated musculature was mounted, with the serosal surface facing up, in a Sylgard trap (Figure 5.1) customarily designed for obtaining stable microelectrode impalements in this preparation. The diameter of the exposed area for microelectrode impalements was approximately 1 mm. Before experimentation started, all preparations were equilibrated for at least 2 hours at 37.0±0.5 °C in a tissue chamber with continuously aerated (95% O_2 and 5% CO_2) Krebs solution perfusing at a rate of 500 ml/h (Pharmacia LKB·Pump P-1).

Microelectrode recordings

Intracellular recordings were made by microelectrodes (50–80 MΩ) filled with 3 M KCl. A microelectrode was inserted into a microelectrode holder which was connected to an electrometer (WPI Duo773). Microelectrodes were driven into the tissue vertically by a micromanipulator (Narishige, MN-151). The output of the electrometer

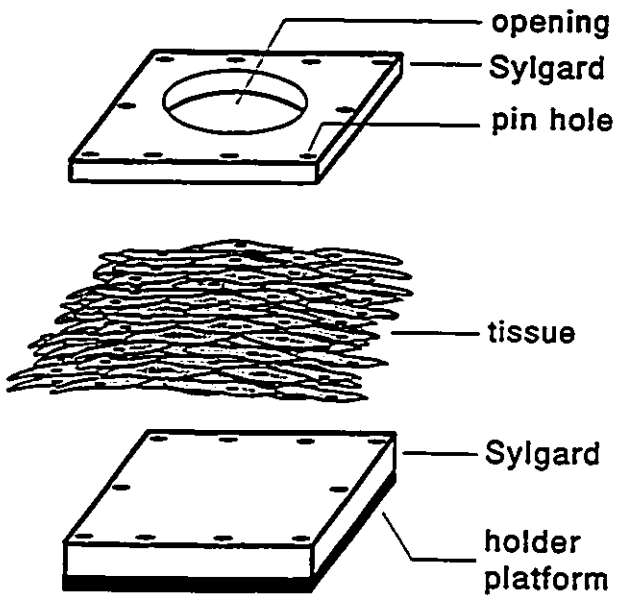

Figure 5.1: *Schematic illustration of the Sylgard trap*

The Sylgard trap consists of two pieces of Sylgard between which the tissue is trapped. The two pieces of Sylgard and the tissue are anchored by insect pins. Since the tissue is held in place by the Sylgard with a large surface area over which pressure is distributed, the tissue can be stabilized with only a few insect pins sparsely inserted along edges of the Sylgard. The top piece of Sylgard possesses a circular opening, approximately 1 mm in diameter, through which microelectrodes were able to access the tissue.

Table 5.1: *Spontaneous slow wave activity in neonatal mouse small intestine*

	new-born, unfed †	6–12 hour ‡	24–48 hour §	2–7 days ξ
Resting membrane potential (mV)	−63.1±2.8	−61.5±1.7	−62.0±2.3	−64.8±2.1
Frequency (cpm)	14.1±0.4	17.4±1.1**	19.1±0.9**	19.8±0.8**
Duration (s)	0.9±0.2	1.1±0.1	1.2±0.1	1.2±0.1
Upstroke amplitude (mV)	22.1±3.8	20.3±3.5	23.2±3.5	24.7±2.6
Plateau amplitude (mV)	- - -	14.9±3.3	16.7±2.6	19.6±2.4
Rate of rise (mV/s)	119.2±26.3	146.5±20.9*	136.3± 21.6*	157.1±28.9*

The n numbers for different sets of experiments are: † = 5, ‡ = 8 (only five animals showed slow wave plateaus), § = 5, ξ = 13. Statistically significant difference of different age groups were compared to the new-born, unfed group (*, $p < 0.05$ and **, $p < 001$).

was displayed on a Gould oscilloscope (1421) and recorded on a Gould ink- writing recorder (2400S).

Drugs and solutions

All solutions perfused into the partition chamber were prewarmed to 37.0±0.5°C and equilibrated with 95% O_2 and 5% CO_2. The composition (in mM) of the Krebs solution was: NaCl — 120.3; KCl — 5.9; $CaCl_2$ — 2.5; $MgCl_2$ — 1.2; $NaHCO_3$ — 20.2; NaH_2PO_4 — 1.2 and glucose — 11.5. The nominal calcium concentration

($[Ca^{2+}]_{nom}$) Krebs solution was prepared by omitting $CaCl_2$ in the Krebs solution formula. Cyclopiazonic acid (CPA; Sigma, St. Louis) was dissolved in dimethyl sulfoxide (DMSO, Sigma, St. Louis) to prepare a stock solution of 10 mM. Verapamil (verapamil hydrochloride, Sigma, St. Louis) stock solution (1 mM) was prepared in deionized distilled water. Vehicles in the concentrations applied did not have any effect on the electrical activity.

Result Presentation & Statistical Analysis

All data were expressed as mean ± S.E.M. 'n' represented the number of neonatal mice used in each set of experiments. Statistically significant differences between data sets were determined by one-way repeated measures ANOVA (KWIKSTAT 4, TexaSoft). The slow wave duration was measured at the half maximum of the slow wave plateau amplitude. Because of the temporal variation of the slow wave activity in the presence of CPA, representative slow wave parameters were obtained from analyses over periods of at least 5 min.

5.3.2 Light microscopy

Procedure for the light microscopic examination employed in this study was the same as that described in Chapter 3 except that neonatal mouse small intestine was used instead of the dog colon.

5.4 Results

5.4.1 Compendium of contractile activity in isolated musculature of neonatal mouse small intestine

Isolated musculature from the small intestine of all neonates (new-born, unfed to 7 days) contracted spontaneously in Krebs solution. Contractions in new-born, unfed neonates were usually more sluggish and less spatially co-ordinated. The frequency of contractions was not quite regular. Regular rhythmic contractions were observed in neonates 6 hours after birth. In 24 hours, regular and forceful contractions were observed. In 48 hours, spatially co-ordinated, regular and forceful contractions had been developed.

5.4.2 Electrical activity of neonatal mouse small intestine

New-born, unfed

All the isolated musculature from the small intestine of new-born, unfed neonatal mice exhibited spontaneous action potentials in Krebs solution (Table 5.1, Figure 5.2a). Neonates would be discarded if traces of milk could be found in any part of the GI tract when the gut was exposed. Spontaneous action potentials were irregular in both frequency and upstroke amplitude (Figure 5.2a). No plateau phase was observed in all 47 stable impalements from 6 different muscle strips of 5 neonates. In all preparations, many quiescent spots (53 out of 112 impalements (or should I say 50%)) were observed with resting membrane potentials ranging from -72 to -58 mV.

Verapamil (1 μM) decreased the frequency, the upstroke amplitude and the rate of rise of the action potentials without significantly affecting other parameters

Figure 5.2: *Effects of verapamil on the electrical activity in neonatal mouse small intestine of different age groups*

a. In Krebs solutions, the spontaneous electrical oscillations in the small intestine of newborn, unfed neonatal mice were various in amplitude and frequency (top panels). The plateau phase of action potentials had not been developed. 1 μM verapamil, a L-type Ca^{2+} channel blocker, decreased both the amplitude and the frequency without affecting other parameters (bottom panels). Right panels show recordings at a faster chart speed.

b. In the 6–12 hours group, both the frequency and amplitude became steady. The plateau phase of the slow wave activity was well-defined which is better illustrated by recording shown at a faster chart speed (right top panel). Recordings were made from a neonate of 8 hours old. Verapamil (1 μM) decreased the upstroke amplitude and rate of rise (bottom panels).

c. Recordings were made from a 30 hours old neonate. In Krebs solution, the electrical activity of this age group was not significantly different from the 6–12 hours group. Consistent with other age groups, verapamil (1 μM) decreased the upstroke and rate of rise of the slow waves.

d. Recordings were made from a 7 days old mouse. Spikes superimposed on the plateau phase of slow waves started to observed in 2 days old mice. To better illustrate the spike activity, traces are shown in different time scales (note different calibrations). Verapamil (1 μM) abolished all spiking activity, and decreased the amplitude and rate of rise of the slow waves.

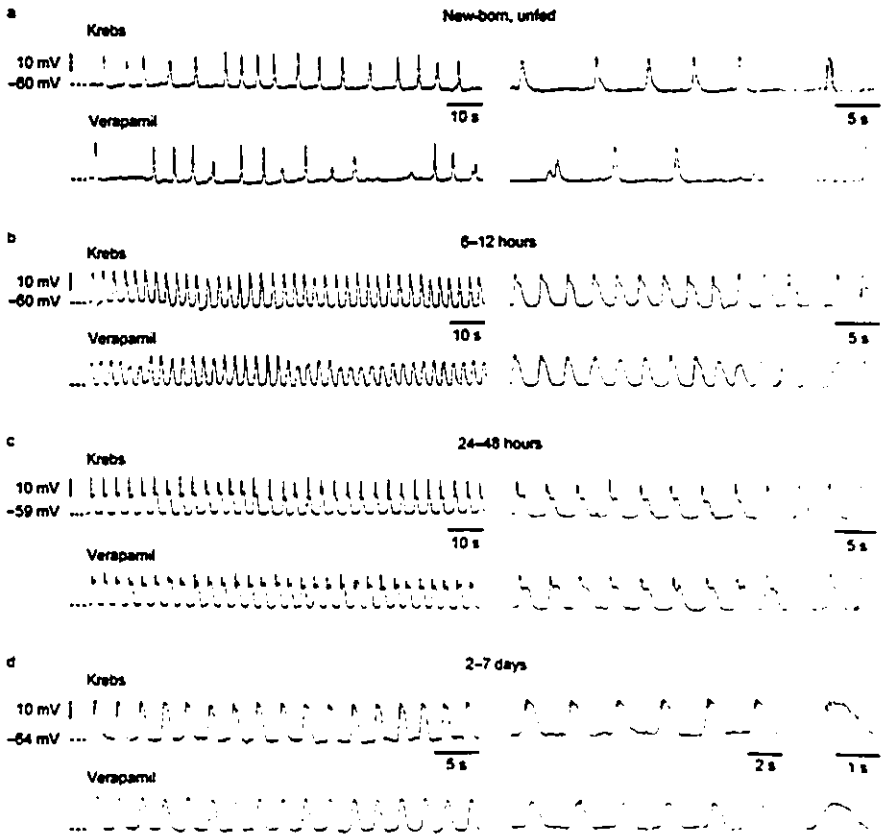
a
New-born, unfed
Krebs
10 mV
-60 mV
10 s
5 s
Verapamil
b
6–12 hours
Krebs
10 mV
-60 mV
10 s
5 s
Verapamil
c
24–48 hours
Krebs
10 mV
-59 mV
10 s
5 s
Verapamil
d
2–7 days
Krebs
10 mV
-64 mV
5 s
2 s
1 s
Verapamil

Figure 5.2

(Table 5.2, Figure 5.2a). 5 μM CPA, within 1 minute of perfusion, completely abolished all electrical oscillations (Table 5.3). The effects of CPA were completely reversible (Fig 3a). Ni^{2+} (1 mM), with or without the presence of verapamil, completely abolished all electrical activity with a slight decrease in membrane potential (2–4 mV).

6–12 hours

Unlike the new-born, unfed neonates, electrical activity of this group exhibited well-defined upstroke and plateau phases which were characteristic to the slow-wave-type action potentials (slow waves) of the GI tract. Both the frequency and the amplitude became regular (Figure 5.2b). The rate of rise at this age group was significantly larger than new-born, unfed animals (Table 5.1). Verapamil (1 μM) decreased the upstroke amplitude and the rate of rise (Table 5.2). The frequency was not affected by the addition of verapamil (Table 5.2, Figure 5.2b).

Addition of CPA (5 μM) in the presence of verapamil significantly decreased the slow wave frequency to 10% of that in verapamil (Table 5.3, Figure 5.3b). Both the amplitude and the rate of rise were also decreased. The effects of CPA were completely reversible (Figure 5.3b). 1 mM Ni^{2+} completely abolished all electrical oscillations which was accompanied with a depolarization of 2–3 mV (Figure 5.4).

24–48 hours

The spontaneous slow wave activity of this age group was not significantly different from that in the 6–12 hour group. The quiescent spots were no longer distinguishably identified. Verapamil (1 μM) decreased the upstroke amplitude and the rate of rise (Table 5.2, Figure 5.2c). Addition of 5 μM CPA decreased the slow wave frequency to 23% (Table 5.3, Figure 5.3c). In the presence of verapamil, 1 mM Ni^{2+} abolished all

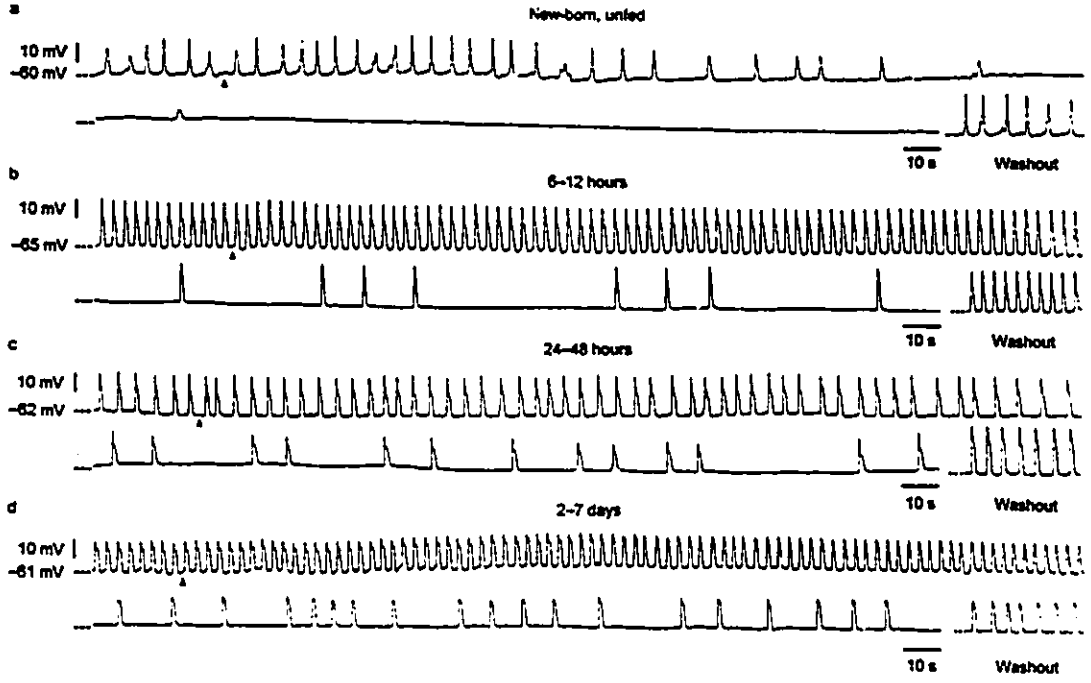

Figure 5.3: *Effects of cyclopiazonic acid, CPA, on the electrical activity in neonatal mouse small intestine of different age groups*

Beginning of all tracings show electrical activities in the presence of 1 μM verapamil for at least 20 minutes. CPA (5 μM), a specific inhibitor of the endoplasmic reticulum Ca^{2+}-pump ATPase, was added to the perfusion solution at arrows. Washout segments show electrical activities after removing CPA from the perfusion solution for 30 minute. Experiments shown were obtained from impalements of the same cell. The effects of CPA were reversible after washout for 30 minutes. a. In the presence of verapamil, similar to Figure 5.2, action potentials were irregular in amplitude and frequency. CPA first reduced the frequency and then decreased the amplitude gradually. Activity was completely abolished within 5 minute of perfusion with CPA. b. Recordings were made from a neonate of 10 hours old. 10 minutes of the recording was omitted between the first and the second panel. CPA significantly reduced the slow wave frequency. Unlike in the new-born, unfed group, the upstroke amplitude only reduced slightly. c. The neonate used in this experiment was 42 hours old. There was a gap of 17 min between the first and the second panel. CPA slightly depolarized the cells and subsequently decreased the upstroke amplitude. The frequency was significantly reduced. d. Experiment was preformed on a 5 days old neonate. 20 min of the recording was omitted between the first and the second panel. Similar to other age group, CPA significantly decreased the frequency and slightly depolarized the tissue.

Table 5.2: *Effects of verapamil on the electrical activity of neonatal mouse small intestine*

	new-born, unfed †		6–12 hour ‡		24–48 hours §		2–7 days ξ	
	Krebs	verapamil	Krebs	verapamil	Krebs	verapamil	Krebs	verapamil
Resting membrane potential (mV)	-59.9 ± 1.4	-58.8 ± 1.3	-61.3 ± 1.0	-61.3 ± 1.0	-59.5 ± 2.1	-58.5 ± 1.5	-59.3 ± 0.5	-58.8 ± 0.6
Frequency (cpm)	13.9 ± 0.5	9.9 ± 1.2**	18.4 ± 1.3	18.0 ± 1.1	18.9 ± 1.2	18.4 ± 1.4	20.7 ± 1.7	19.3 ± 1.6
Duration (s)	1.1 ± 0.2	0.9 ± 0.1	1.2 ± 0.3	1.1 ± 0.2	1.2 ± 0.2	1.1 ± 0.1	1.2 ± 0.1	1.1 ± 0.1
Upstroke amplitude (mV)	21.4 ± 5.4	16.3 ± 5.3*	18.5 ± 2.8	16.8 ± 1.8*	15.8 ± 1.1	12.7 ± 1.4*	16.4 ± 1.4	14.3 ± 1.1*
Plateau amplitude (mV)	------	------	11.2 ± 0.6	11.3 ±0.8	11.1 ± 0.6	9.8 ± 0.8	12.8 ± 0.8	11.2 ± 1.1
Rate of rise (mV/s)	103.2 ± 29.1	50.3 ± 16.8**	146.4 ± 34.8	121.9 ± 34.0*	129.3 ± 20.7	98.3 ± 23.3*	134.7 ± 15.7	89.2 ± 13.9**

The n number for different sets of the experiments are: † = 4, ‡ = 4, § = 4, ξ = 6. Activity in the presence of verapamil was compared with the corresponding activity in Krebs solution in the same age group (*, $p < 0.05$; ** = $p < 0.01$). Oscillations with amplitude less than 2 mV were neglect.

Table 5.3: *Effects of CPA on the electrical activity of neonatal mouse small intestine*

	new-born, unfed †		6–12 hour †		24–48 hour §		2–7 days ξ	
	verapamil	CPA	verapamil	CPA	verapamil	CPA	verapamil	CPA
Resting membrane potential (mV)	-59.8 ± 1.3	-57.2±0.9*	-62.7 ± 1.3	-60.0 ± 1.2*	-60.0 ± 0.8	-59.0 ± 1.0	-59.5 ± 0.6	-57.8 ± 0.7*
Frequency (cpm)	9.9 ± 1.2	-------	18.6 ± 1.2	1.9 ± 0.1**	20.7 ± 0.5	4.8 ± 0.7**,■	19.6 ± 1.9	7.8 ± 1.5**,□
Duration (s)	0.9 ± 0.1	-------	1.2 ± 0.2	1.0 ± 0.3	1.0 ± 0.1	1.3 ± 0.3	1.2 ± 0.2	1.1 ± 0.1
Upstroke amplitude (mV)	16.3 ± 5.3	-------	21.5 ± 3.3	19.0 ± 3.5	15.2 ± 0.4	13.3 ± 0.8*	15.8 ± 1.2	12.2 ± 1.4*
Plateau amplitude (mV)	------	-------	12.7 ± 1.5	-------	10.1 ± 0.5	10.4 ± 0.3	11.5 ± 1.5	11.2 ± 1.1
Rate of rise (mV/s)	50.3 ± 16.8	-------	169.2 ± 35.0	102.5 ± 7.5**	110.0 ± 16.7	67.5 ± 27.5**	103.6 ± 21.7	71.2 ± 11.9**

The n number for different sets of the experiments are: † = 4, ‡ = 4, § = 4, ξ = 5. ‡: only 1 animal exhibited the plateau phase, thus, plateau amplitude was not included in the table. §, ξ: the plateau phase was observed in 3 animals of each experimental group. Activity in the presence of CPA (5 μM) was compared with the corresponding activity in Krebs solution containing 1 mM verapamil in the same age group (*, $p < 0.05$; ** = $p < 0.01$). ■ represents significantly larger than that in the bathing solution in the 6–12 hours group. □ represents significantly larger than that in the same bathing solution in the 6–12 hours and the 24–48 hours groups. The effects of CPA were completely reversible in all experiments.

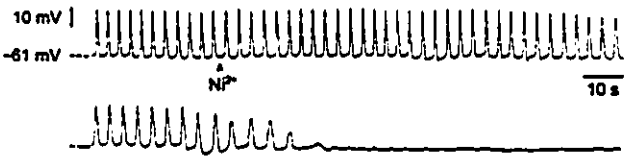

Figure 5.4: *Effects of Ni^{2+} on the slow wave activity of the small intestine of a 10 hours old neonate*

Beginning of the top panel shows electrical activity in the presence of 1 mM verapamil. The top and the bottom panels show continuous recording from the same cell. Ni^{2+} (1 mM) completely abolished all electrical oscillations with a depolarization of 2 mV. The effects of Ni^{2+} was not reversible even after washing with verapamil-Krebs solution for 30 min.

Figure 5.5: *Effects of removal of extracellular Ca^{2+} on the slow wave activity of small intestine of two 3 days old neonates*

Both experiments were performed in the presence of 1 μM verapamil. Verapamil had been perfused for at least 20 min before the perfusion solution was switched to nominal Ca^{2+} concentration ($[Ca^{2+}]_{nom}$) Krebs solution containing 1 μM verapamil. Experiments shown were continuous recordings made from the same cell. a. Removal of extracellular Ca^{2+} from Krebs solution containing 1 μM verapamil resulted in slow reduction of the upstroke frequency and amplitude. Small oscillations of approximately 3–4 mV were observed at a lower frequency after 18 min perfusion with $[Ca^{2+}]_{nom}$-Krebs solution containing 1 μM verapamil. The effects were reversible after 30 minutes washout with Krebs solution containing 1 μM verapamil. b. Addition of 1 mM EGTA to the $[Ca^{2+}]_{nom}$-Krebs solution containing 1 μM verapamil accelerated the effects of removal extracellular Ca^{2+}. Reduction in the frequency was observed after 4 minutes of perfusion. In 10 min, oscillations were completely abolished.

---

the oscillations in 2 of 5 preparations; in the remaining three preparations, periodic oscillations of 2–4 mV in amplitude were observed at a frequency of 12.1±2.2 cpm (18.2±1.0 cpm in verapamil). 2 mM Ni^{2+} was required to completely abolished the remaining oscillations.

2–7 days

Spikes superimposed on the plateau phase on the slow waves started to be observed in neonatal mice of two days old (in 11 out of 13 neonates) although the appearance of spikes was progressively more frequent in older neonates. The frequency and amplitude of these spikes were 148.5±21.9 cpm and 3.5±0.5 mV, respectively (n = 11).

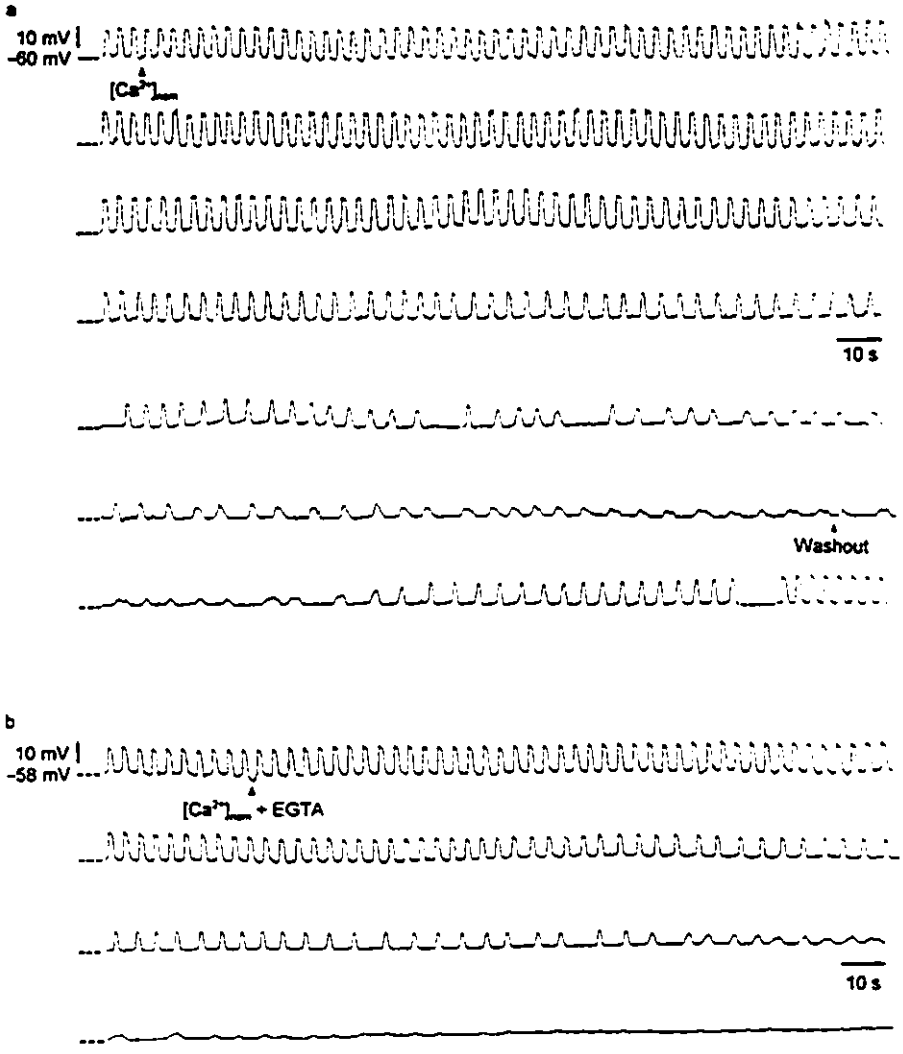

Figure 5.5

These spikes were completely abolished by 1 μM verapamil (Figure 5.2d). Similar to other age groups, verapamil consistently decreased the upstroke amplitude and the rate of rise (Table 5.2).

The effects of CPA in the presence of verapamil were similar to the 24–48 hours group except the effects on frequency (Table 5.3). The frequency was reduced to 40 % of that in verapamil (Figure 5.3d). The effects of CPA on the frequency in 2–7 days old neonates were identical to that in adult mice (results not shown). Electrical activity was abolished by 2 mM Ni^{2+} in 3 out of 4 preparations; in the remaining one, 5 mM Ni^{2+} was needed to completely abolished the activity (cells depolarized by 4 mV).

These results suggested that the upstroke depolarization, representing the pacemaker activity, is mediated by a Ca^{2+}-dependent inward current. This hypothesis was further verified by removing Ca^{2+} ($[Ca^{2+}]_{nom}$) from the Krebs solution. $[Ca^{2+}]_{nom}$ first decreased the frequency and then decreased the amplitude to 2–6 mV (n = 4, Figure 5.5a); in another three preparations, all oscillations were abolished. The resting membrane potentials were changed from -61.8 ± 0.5 to -59.5 ± 0.6 mV ($p < 0.05$). There was a time delay of 10–26 minutes for $[Ca^{2+}]_{nom}$ to take effect. Addition of 1 mM EGTA to $[Ca^{2+}]_{nom}$ Krebs solution reduced the oscillation amplitude to less than 2 mV in 8–15 min (n = 4, Figure 5.5b). The effects of $[Ca^{2+}]_{nom}$,with or without EGTA, were completely reversible, though the washout period was longer with a previous challenge with EGTA.

5.4.3 Distribution and identification of ICCs in neonatal mouse small intestine

Incubation of the neonatal mouse small intestine with methylene blue (1–10 μM) for 30 min resulted in selective staining of the ICCs associated with the myenteric plexus. At the light microscopic level, after incubation with methylene blue, it became conspicuous that the ICCs of 2 hours old neonates were scattered (Figure 5.6a). In 12 hours, the staining pattern of the ICCs were almost identical, though less dense, to that in 48 hours old neonates (Figure 5.6b) whose staining pattern was indistinguishable from that in the adult mouse.

5.5 Discussion

5.5.1 Ontogeny of the pacemaker activity and ICCs

This study provides the first documentation of the ontogeny of the pacemaker component of the slow waves in the neonatal mouse small intestine. The pacemaker component was reflected by the verapamil-insensitive and ER-Ca^{2+} dependent component of the slow wave activity. Such component had qualitatively been developed as early as 6 hours after birth. After 2 days, the pacemaker component has fully been developed, as indicated by the effects of 5 μM CPA on the pacemaker frequency (the amount of decrease is the same as that in adult mice (unpublished observations, Richardson and Huizinga)).

In neonates of 2 hours old, the ICCs associated with the myenteric plexus were scattered. The distribution of ICCs at this age is consistent with the presence of scattered pacemaker active spots. The occurrence of quiescent spots decreased

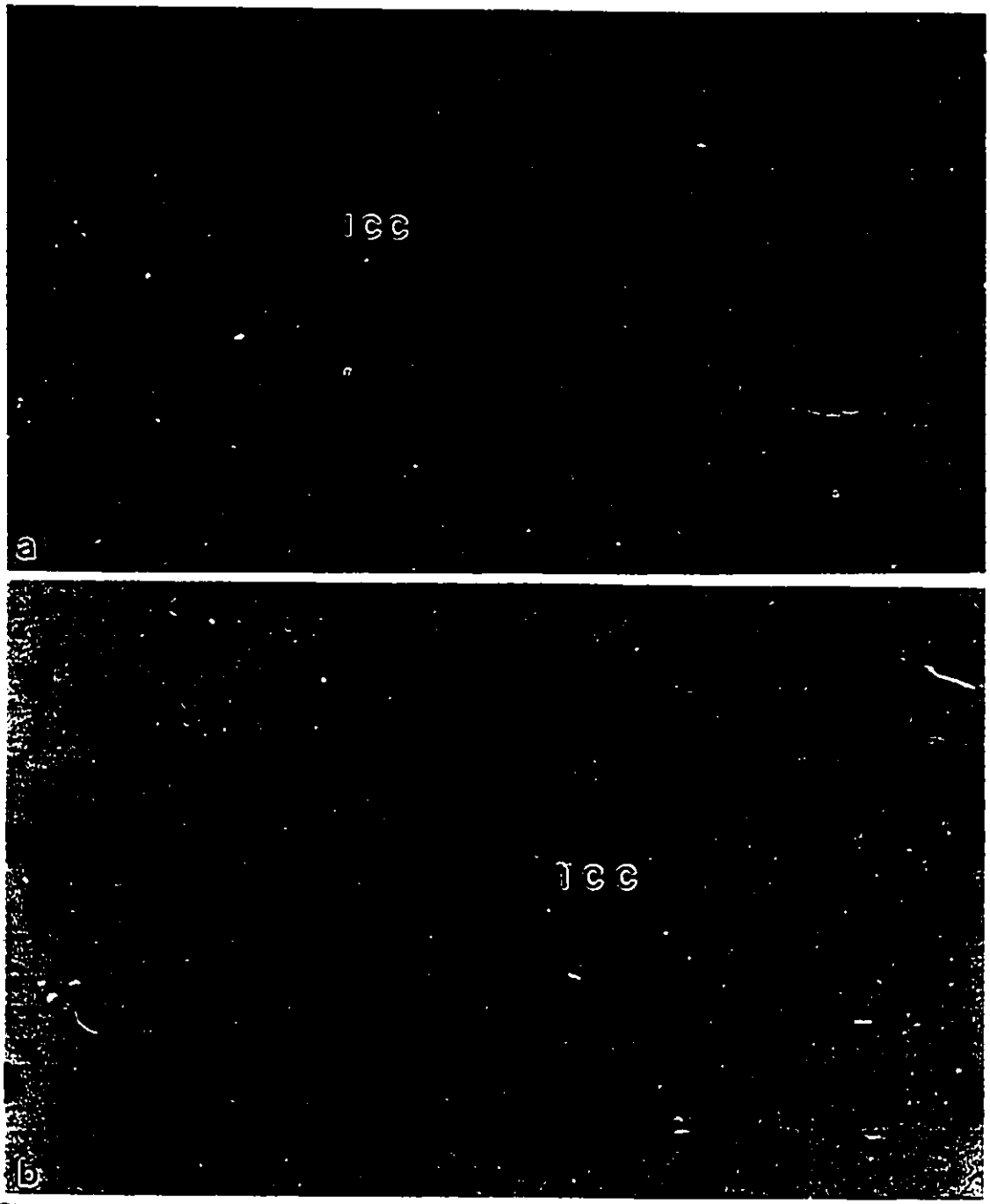

Figure 5.6: *Methylene blue staining patterns of ICCs associated with the myenteric plexus*

a. The methylene blue staining pattern of an 2 hours old neonate is shown. The ICCs (arrows) were scattered. x 420. b. The network structure of the ICCs (arrows) in an 48 hours old neonate is depicted after incubation with methylene blue. The network structure in 48 hours old neonates was fully developed. x 420.

dramatically as the neonates became older and reduced to none in the 2–7 days old group. Following the staining pattern in older neonates suggests that the ICCs were in the process of connecting up with each other. The network structure of the ICCs in 48 hours old neonates was indistinguishable from that of the adult mice. The correlation of the development of ICC distribution and the progressive decrease in the quiescent spots consistently suggests that the methylene-blue stained ICCs are the source of the pacemaker activity.

In new-born, unfed neonates, action potentials were observed. This is consistent with the occurrence of contractile activity observed in isolated musculature as explained by the excitation-contraction-coupling mechanism. This observation in neonatal mice suggests that contractile responses observed in the stomach [21, 187] and the small intestine [21, 22, 137, 187] of new-born infants may be explained by the same mechanism. The frequency of action potentials in the small intestine of new-born, unfed neonatal mice was decreased by verapamil. Although a verapamil-insensitive component remained, the reduction in frequency suggests an immature development of the pacemaker activity.

The force of contractions in the GI smooth muscle is highly dependent on the amount of calcium influx from the extracellular space [91, 176]. The appearance of spiking activity in older (2–7 days) neonates is consistent with the observation of an increase in the force of phasic contraction in the isolated musculature. The spikes superimposed on the plateau phase of the slow waves were mediated by the activation of L-type calcium channels which was positively illustrated by their inhibition by verapamil. The ontogeny of L-type calcium channels has been studied in many tissues. The amplitude of the Ca^{2+} current was increased by 38% from neonatal to adult in rat dorsal root ganglion neurons without a change in the single-channel conductance

[101], and by 4-fold from day 1 to day 30 in mouse skeletal muscle [81]. During embryonic development of chick heart, silent Ca^{2+} channels are transformed into functional Ca^{2+} channels [185], also see review [100]. In rat colonic circular smooth muscle cells, the calcium channel density increases by 100% from day 1 to day 3 [197]. In rabbit, the number of L-type Ca^{2+} channels increased in antrum where extracellular Ca^{2+} is required for contraction but remain the same in the fundus where contraction is mainly mediated by intracellular calcium stores [96]. Hence, in the mouse small intestine, the appearance of spiking activity in older neonates likely resulted from an increase in the abundance of L-type calcium channels. However, voltage-clamp and patch- clamp investigations on the ontogeny of the L-type calcium channel in isolated cells are necessary to unequivocally validate this hypothesis.

5.5.2 Pacemaker channel in neonatal mouse small intestine

The pacemaker potential in the adult mouse small intestine has been hypothesized to be mediated by a Ca^{2+}-dependent non-specific cation channel [125]. In the canine colon, a similar pacemaker channel has also been proposed [93, 194]; more specifically, it has recently been demonstrated that the frequency of activation of the pacemaker channel is entrained with the calcium refilling cycle in the endoplasmic reticulum associated with the plasma membrane [118]. The observations with CPA shows that the same coupling mechanism is operating in the mouse small intestine. The long time-delay of the decrease in the slow wave amplitude in the nominal Ca^{2+} concentration suggests that the pacemaker channel is dependent on Ca^{2+} but not permeable only to Ca^{2+}. Moreover, elimination of the Na^{+} concentration gradient almost immediately decreased the slow wave upstroke amplitude (from 14.0±0.1 to 5.8±1.3 mV) and the rate of rise (from 67.5±22.5 to 19.0±1.9 mV/s) but did not affect the rest-

ing membrane potential and frequency (unpublished observations, Liu and Huizinga). The abolition of the slow wave activity by Ni^{2+} observed in this study consistently supports the hypothesis that the pacemaker channel is a type of non-specific cation channel. Since rhythmically contracting explants of neonatal mouse small intestine have been successfully cultured, identification of the fully-developed pacemaker activity encourages us to unravel different components of the GI pacemaking mechanism in the neonatal mouse small intestine system.

In summary, this is the first documentation of the ontogenesis of the pacemaker activity in the GI tract. More specifically, we demonstrated the presence of spontaneous action potentials in the small intestine of newly born, unfed neonatal mice. In addition, the pacemaker component of the slow waves was identified in neonates as early as 6 hours after birth. The pacemaker component was fully developed 2 days after birth.

Chapter 6

Assessing Cell to Cell Communication: An Alternate Method to Determine the Space Constant

6.1 Epitome

Cell to cell communication is fundamental for tissue functions. The space constant has been widely employed to characterize passive electrical properties of numerous tissues under physiological and pathophysiological conditions. The conventional method determines the space constant by fitting the amplitude of electrotonic potentials, measured at various distances from a stimulation source, to a one-dimensional exponential decay function. This method is based on the assumption that during the entire experiment, all stimulation potentials evoked at the origin are identical. However, this

condition is very difficult to achieve. In this communication, a method has been developed to determine the space constant using a double-electrode technique such that the dependence on the electrotonic potentials evoked at the origin by a potentially variable stimulation source is eliminated. This method is simple, less time consuming and takes into account tissue variabilities during experiments.

6.2 Introduction

Almost all aspects of bodily functions depend on cell to cell communication. One of the major mechanisms by which intercellular communication occurs is the propagation of electrical signals, most commonly action potentials. Examples are the transmission of sensory information to the central and peripheral nervous system, propagation of cardiac action potentials from the sinoatrial node to the rest of the myocardium, synchronization of action potentials in the myometrium to produce propulsive contractions during delivery. In the gastrointestinal tract, the pacemaker activity is believed to originate from specific network of cells, the interstitial cells of Cajal (ICCs) [85]. To produce peristalsis, action potentials are required to propagate from the ICCs into smooth muscle layers. In general, electrical coupling between cells is critical for a tissue to function as a whole. Hence, knowledge about passive electrical properties of a tissue is essential for the understanding of the physiology and pathophysiology of biological systems.

The space constant is one of the most widely used quantitative parameters of passive electrical properties of a tissue. It is defined as the distance at which the amplitude of a passively propagating electrotonic signal decays to 1/e of its original amplitude. The space constant has been used to characterize passive electrical prop-

erties of various tissues, such as the pancreas, the sinoatrial node, the myometrium, the intestinal organs, and bladder smooth muscle in normal and pathological situations [1, 28, 89, 139, 165]. Furthermore, the space constant is a frequently used parameter in theoretical signal conduction models of most physiological systems.

In all previously described studies, the space constant was determined by fitting a single exponential function to the amplitude of electrotonic pulses measured at various distances away from the stimulation origin. In spite of its wide acceptance, there are inherent weaknesses in this method. The accuracy of this method requires consistency of the stimulation source and recording conditions. Even if the amplitude of stimulation pulses can be controlled completely, responses of the tissue to the same stimulation may not be the same at different times. Hence, the amplitude of the source signal (generated by the tissue in response to the stimulus) evoked at the origin is uncertain unless it can be measured directly. In general, ideal conditions are almost impossible to achieve in constantly varying biological systems.

In this communication, a more precise and reliable method has been developed to determine the space constant without the need to employ the above assumptions.

6.3 Materials and methods

6.3.1 Preparation of muscle strips

Mongrel dogs were killed by an overdose of sodium pentobarbital (100 mg/kg) given intravenously. Approximately 5 cm of the proximal colon was taken from 5 cm distal to the ileocecal junction. The colon was opened flat. Colonic contents were carefully removed in a beaker containing Krebs solution equilibrated with 95% O_2/5% CO_2. The mucosa, submucosa and longitudinal muscle layer were carefully removed

in a dissecting dish which was filled with continuously aerated Krebs solution. These preparations, composed of the circular muscle with the intact submuscular ICC network, were referred to as *ICC-CM preparations.*

Approximately 3×6 mm of the tissue, with the ICC network facing up, was pinned onto the Sylgard of a transfer holder. A free strip of 10 mm in length was extended from one pinned edge and placed in the stimulation chamber of a partition chamber (Figure 6.1) allowing voltage control of the muscle strips [1, 112]. The length of the mounted strips was parallel to the long axis of circular muscle cells.

6.3.2 Double electrode set-up

Intracellular recordings were made simultaneously by two microelectrodes (30–50 MΩ tip resistances) connected to an electrometer (WPI Duo773). Microelectrodes were filled with 3 M KCl. Locations of impalements were measured by the vernier scale of a micromanipulator (Narishige, MN-151) with an accuracy of ± 35 μm. The outputs of the electrometer were displayed on a Gould oscilloscope (1421) and recorded on a Graphtec thermal arraycorder (WR 7700). Segments of the electrical activity were sampled at 100 Hz with AxoTape 1.2 (Axon Instruments, Inc) through a TL-1 DMA interface (Axon Instruments, Inc.). The muscle strips were allowed to equilibrate with continuously aerated Krebs solution in the partition chamber for at least 2 hours at 37.0±0.5 °C before the start of experiments.

Electrotonic pulses were introduced into the muscle strips through a Grass isolation unit (SIU5) by applying potential differences (generated by a Grass stimulator (S88)) across a pair of Ag/AgCl plates separated by 10 mm. The field strength was measured by a pair of recording electrodes, 2 mm apart, located in the middle of the stimulating chamber (Figure 6.1). Because of the syncytial property of the prepara-

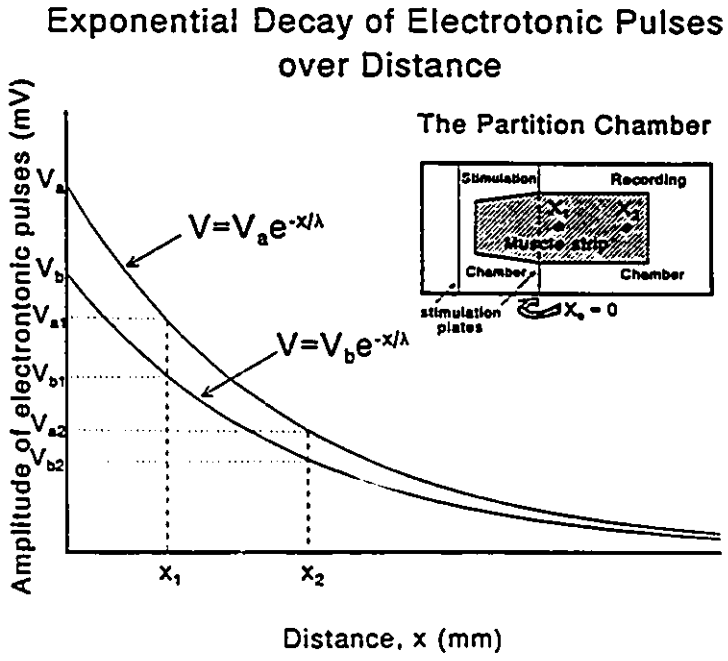

Figure 6.1: *Schematic illustrations of the double-electrode technique and the partition chamber*

Using a pair of Ag/AgCl stimulation plates in the partition chamber, two electrotonic potentials, V_a and V_b, are evoked at x_o and propagate electrotonically to x_1 and x_2. The amplitude of the electrotonic pulse at various distances is estimated by the one-dimensional exponential decay function, $V = V_o \exp(-x/\lambda)$, where λ is the space constant.

tion under study, point source stimulations failed to evoke any membrane potential deflections as the injected current immediately shunted to neighbouring cells through the low resistance network. Hence, large extracellular electrodes were used to apply a relatively uniform field stimulation to introduce electrotonic pulses at x_o.

6.4 Mathematical derivation

When a stimulation potential, V_s, is applied across the pair of Ag/AgCl plates, an electrotonic potential, V_o, is evoked in the muscle strip at x_o (Figure 6.1). The amplitude of V_o evoked at x_o is proportional to the input resistance of the tissue [112]. Consider that two distinct stimulations are applied across the stimulation plates, producing electrotonic pulses of V_a and V_b, respectively, at x_o. If the space constant of the muscle strip equal to λ, the amplitude of the electrotonic pulses, V_{a1} and V_{b1} at x_1, and V_{a2} and V_{b2} at x_2, can be deduced from one-dimensional single exponential decay functions. That is,

at x_1	$V_{a1} = V_a \cdot e^{\frac{-x_1}{\lambda}}$	
and	$V_{b1} = V_b \cdot e^{\frac{-x_1}{\lambda}}$	
Therefore,	$V_{a1} - V_{b1} = (V_a - V_b) \cdot e^{\frac{-x_1}{\lambda}}$	
	$\Delta V_1 = V_{a1} - V_{b1}$	
Hence,	$\Delta V_1 = (V_a - V_b) \cdot e^{\frac{-x_1}{\lambda}}$	[6.1]
Similarly, at x_2,	$\Delta V_2 = V_{a2} - V_{b2}$	
Therefore,	$\Delta V_2 = (V_a - V_b) \cdot e^{\frac{-x_2}{\lambda}}$	[6.2]
$\frac{[6.1]}{[6.2]}$	$\frac{\Delta V_1}{\Delta V_2} = e^{\frac{x_2 - x_1}{\lambda}}$	
	$S_{12} = e^{\frac{\Delta x}{\lambda}}$	[6.3]

where Δx = distance between the two microelectrodes, $x_2 - x_1$; and,

S_{12} = slope of the graph of V_1 against V_2

Since both Δx and λ are constants, it is obvious that the graph of V_1 against V_2 is going to be a straight line. The slope, S_{12}, can be obtained by linear regression using the least-squares method. Thus, from equation [6.3]:

$$\lambda = \frac{\Delta x}{ln(S_{12})} \qquad [6.4]$$

Observing that for any electrotonic pulse, V_i, evoked at x_o, the amplitude of the electrotonic pulse is:

at x_1, $V_{i1} = V_i \cdot e^{\frac{-x_1}{\lambda}}$

and at x_2, $V_{i2} = V_i \cdot e^{\frac{-x_2}{\lambda}}$

Therefore the voltage transfer function, defined as V_{i2}/V_{i1}, is:

$$\frac{V_{i2}}{V_{i1}} = e^{\frac{x_1 - x_2}{\lambda}}$$

hence, $$ln(V_{i1}) - ln(V_{i2}) = \frac{x_2 - x_1}{\lambda}$$

$$\lambda = \frac{\Delta x}{ln(V_{i1}) - ln(V_{i2})} \qquad [6.5]$$

According to the mathematic derivation, the space constant can be determined either from the relative change of the voltage measured at x_2 to the corresponding voltage measured at x_1 (equation [6.4]) or from the instantaneous voltage transfer function (equation [6.5]).

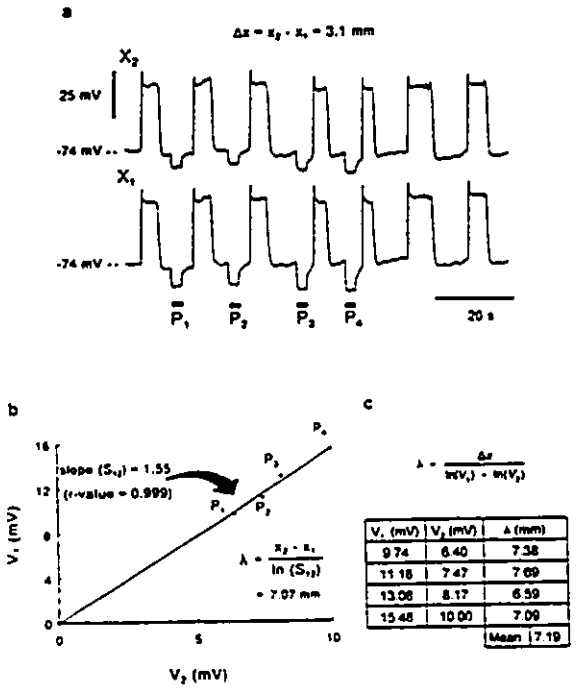

Figure 6.2: *Determination of the space constant of an ICC-CM preparation*

a. Simultaneous intracellular recording of the slow-wave type action potentials at the submuscular surface of an ICC-CM preparation. Separation of the two microelectrode was 3.1 mm. Electrical stimulations of increasing amplitude were applied during P_1, P_2, P_3, and P_4.

b. Plotting the amplitudes of the electrotonic pulses recorded at x_1 against those recorded at x_2 yielded a straight line with slope, S_{12}, as determined by linear regression using the least-squares method. The r-value was equal to 0.999 for this fit. The space constant, λ, determined by equation [6.4], was 7.07 mm.

c. The space constant was also determined by the instantaneous voltage transfer function (equation [6.5]) without the need of curve fitting. The average (7.19 mm) was very similar to that obtained by equation [6.4].

6.5 Electrophysiological results

Simultaneous recordings were made by a pair of microelectrodes at the submuscular surface of ICC-CM preparations. Pairs of microelectrodes were positioned 1.3–3.1 mm apart. Simultaneous recordings of the electrotonic potentials at x_1 and x_2 upon a series of field stimulations revealed the space constant, λ, to be equal to 8.96±1.55 mm as determined by equation [6.4] (n=11, Figure 6.2). The r-values of the linear regression used to determine the slope of the graphs of V_1 against V_2 were larger than 0.985 in all fits indicating a linear relationship within the voltage range over which stimulations were applied. In 52 sets of simultaneous measurements in the same 11 strips, λ was equal to 8.84±1.35 mm when determined by equation [6.5] (Figure 6.2). Blockade of the gap junction conductance by 1–2 mM octanol reduced the space constant of the muscle strips below any detectable level.

6.6 Discussion

6.6.1 Theoretical basis for determining the space constant with the double-electrode technique

The present communication provides a new alternative to determine the space constant using the one-dimensional exponential approximation for passive propagation of electrotonic potentials. In a single exponential function, $V(x) = V_o exp(\frac{-x}{\lambda})$, there are three unknowns, namely the amplitude of the initial electrotonic pulse, V_o, the distance over which the pulse has propagated, x, and the space constant, λ. Using the conventional method, a recording electrode is placed at various distances from the stimulation source (varying x). The space constant is then determined with the

assumption that V_o is constant throughout the entire experiment. However, the amplitude of V_o is determined by both the size of the stimulation potential and the input resistance of the tissue [112] which are rarely constant throughout an experiment. In our study, it was observed that the amplitude of stimulation pulses measured across the stimulation plates in the stimulation chamber varied ($\pm$ 5–25%) despite a constant voltage output from the Grass stimulator indicating a continuous change of stimulation electrode conditions, such as depletion of the Ag/AgCl surface. Furthermore, constant amplitude stimulations applied across the stimulation plates did not always produce identical amplitudes of electrotonic pulses at x_1 and x_2 indicating a temporal variation of the passive electrical properties of the muscle strips. Employing equation [6.4] or [6.5] with a double-electrode set-up, the space constant can be determined independent of V_o since V_o is the same for the electrotonic pulses arriving at both x_1 and x_2. Therefore, V_o can be eliminated in the mathematic derivation of equations [6.4] and [6.5].

6.6.2 Independence of the origin of electrotonic pulses

This independence is particularly important when large extracellular electrodes, such as Ag-AgCl plates used in the partition chamber, are required to evoke electrotonic potentials in tissue because it is difficult to precisely determined the site where V_o is evoked. This method is usually required for tissues that behave as an electrical syncytium. The method developed in this communication allows one to determine the space constant without the need to identify the location at which electrotonic potentials are initiated.

6.6.3 Specific applications of the double-electrode technique

The methodology developed in this communication to determine the space constant has the advantages of simplicity. It is readily applicable to a double-electrode experiment in which one of the microelectrodes is used simultaneously to inject current and to record the electrotonic pulse evoked. With the measurement of the amplitude of the electrotonic pulse at the other electrode, the space constant can be determined using either equation [6.4] or equation [5.5] depending on experimental protocols. This kind of experimental set-up has been widely employed in studies of the passive electrical properties of cardiac tissue [139]; however, experiments have always been performed by repositioning the second microelectrode at various distances from a presumably constant stimulation source. In the islet of Langerhans from the mouse, Eddlestone *et al.* [61] studied the effects of glucose on electrical coupling. The extent of electrical coupling was characterized by a "coupling ratio" defined as V_2/V_1 which is similar to the voltage transfer function defined in this study. However, the relationship between the space constant and the "coupling ratio" was not presented.

The instantaneous voltage transfer function is particularly beneficial to systems which show inward rectification such that there is only a narrow window of linear current- voltage relationship. To determine the space constant with the conventional method, stimulation pulses with a large enough amplitude would need to be applied to obtain recordable electrotonic potentials at various distances so that a good exponential fit can be acquired. Using the instantaneous voltage transfer function, the space constant can be determined by a reasonably small amplitude stimulation since only one set of electrode position is required. Under these conditions, the space constant computed from equation [6.5] with repetitive stimulations yields a representable space constant of the tissue. Taking an average of several stimulations takes

into account the temporal variations of passive electrical properties of the tissue and measurement uncertainties.

The space constant along the long axis of the circular muscle cells at the submucosal surface of the ICC-CM preparations had previously been determined to be 3 mm using a conventional signal recording electrode technique [89]. It was acknowledged that the location of the origin of the electrotonic potentials could not be precisely determined. Furthermore, because of the need to apply high amplitude stimulations so that electrotonic potentials at far enough distances could be recorded, the amplitude of stimulations sometimes fell within the rectification range of the tissue. This may, in part, account for the difference. In addition, temporal variations of recording conditions and tissue responses were also observed as indicated by large deviations of datum points from the best fit linear regression line.

In summary, the methodology presented in this communication represents a classical way of eliminating an uncertain input by simultaneously obtaining the input-output relationship of the double-electrode system. The advantages offered by this method will lead to more accurate estimations of electrotonic coupling in biological systems.

Chapter 7

Interstitial Cells of Cajal: Mediators of Communication Between Longitudinal and Circular Muscle Cells of Canine Colon

7.1 Epitome

The network of interstitial cells of Cajal (ICC) in the myenteric plexus of the canine colon was shown to facilitate communication between the circular and longitudinal

This chapter was submitted to Cell and Tissue Research (authored by Louis Liu, Laura Farraway, Irene Berezin and Jan Huizinga). Contributions of co-authors are discussed in section 2.3 of Chapter 2.

muscle layer. The cellular mechanisms of this communication in the colon are particularly intriguing because the electrical activities of the two muscle layers are distinctly different. Through electrophysiological measurements with microelectrodes, the study of neurobiotin spread using confocal microscopy and the investigation of the cellular structure at the electron-microscopic level, we have demonstrated the existence of low-resistance pathways which facilitate intercellular communication between the two muscle layers across the myenteric plexus of canine colon. Electrical coupling between the muscle layers was demonstrated by propagating extracellularly evoked electrotonic pulses from circular to longitudinal muscle cells very close to the myenteric border. As a result of hyperpolarizations of the longitudinal muscle, the spiking activity generated spontaneously by the longitudinal muscle was abolished. Propagation of electrotonic pulses from circular to longitudinal muscle cells was not observed when the impaled longitudinal muscle cell was situated more than 100 μm away from the myenteric border. The existence of cytoplasmic continuity across the myenteric plexus, creating low-resistance pathways for electrotonic coupling, was proven by the ability of neurobiotin to spread from a single injected cell to interstitial cells of Cajal, and circular and longitudinal muscle cells. Importantly, direct neurobiotin spread between circular and longitudinal muscle cells was not observed even when they were directly apposing each other as determined by confocal microscopy. However, when neurobiotin spread across the two muscle layers, the ICCs were always visible at the border where the two muscle layers met. Electron-microscopic examination of the narrow myenteric plexus regions revealed frequent presence of close apposition contacts, and extremely infrequent presence of small gap junctions between ICCs and smooth muscle cells from either the longitudinal or the circular muscle layer. Neither gap junctions nor close apposition contacts were observed between directly appos-

ing longitudinal and circular smooth muscle cells. These observations demonstrate the existence of cytoplasmic continuity between the two muscle layers through ICCs, which facilitate electrotonic coupling across the myenteric border. This special arrangement for electrotonic coupling across the myenteric border suggests controlled coupling between the two muscle layers explaining the preservation of their distinct electrical activities.

7.2 Introduction

Peristalsis was first described by Bayliss and Starling [11] in the dog small intestine *in vivo*. In the colon, 6 cycles per minute (cpm) phasic contractions were first demonstrated in cats by Cannon [37] using radiography. Similar contractile patterns were subsequently observed in other species such as dogs, ferrets, guinea pigs, hedgehogs, rabbits and rats by Elliott and Barclay-Smith [65]. Peristaltic movement requires coordinated motility of the circular and the longitudinal muscle layers. Since the contractile activity of muscle layers is associated with the electrical activity through excitation-contraction coupling, it is of interest to search for electrical communication between the two muscle layers that would serve to produce coordinated contractions.

In the small intestine, electrical interaction between the circular and the longitudinal muscle layers has been observed [25, 98]. Specifically, electrotonic coupling between the two muscle layers was demonstrated in the cat jejunum by the propagation of extracellularly evoked electrotonic potentials from the circular into the longitudinal muscle layer [64]. In addition, gap junctions, which constitute low resistance pathways to facilitate electrotonic coupling, have been observed connecting the "connective tissue cells" (probably equivalent to interstitial cells of Cajal) to lon-

gitudinal and circular muscle cells of the cat jejunum [178]. In the guinea pig small intestine, gap junctions were found to be rare but present between circular and longitudinal muscle cells [74]. However, in the colon, no direct evidence is available as to the mechanism by which communication between the two muscle layers occurs.

The mechanism of communication between the circular and the longitudinal muscle layers of the colon is particularly intriguing because the electrical activities of the two muscle layers are distinctly different. This was first demonstrated in the cat colon where Christansen documented slow wave activity in the circular muscle, and bursts of spiking activity without slow waves in the longitudinal muscle [44]. In the canine colon, the activity of the longitudinal muscle is similar when recorded from isolated longitudinal muscle strips or from longitudinal muscle strips with circular muscle attached. The longitudinal muscle layer generates spike-like action potentials (SLAPs) of 16–24 cpm from a resting membrane potential of −45 mV [41, 110]. SLAPs are not always regular in frequency and can appear in bursts of variable duration and frequency. The *isolated* circular muscle layer has an intrinsic resting membrane potential of -62 mV and is spontaneously quiescent [112, 113]. Coupled to the submuscular network of interstitial cells of Cajal (ICCs), where slow wave-type action potentials (slow waves) originate, slow waves with or without superimposed spikes are recorded throughout the entire circular muscle layer [4, 87, 110, 171].

When electrical activity across the myenteric plexus was studied both in isolated strips and in intact tissue, the hypothesis emerged that the resting membrane potential gradient in the circular muscle layer near the myenteric plexus is caused by *electrical coupling* of the circular to the more depolarized longitudinal muscle layer [110]. In a dual sucrose gap apparatus, the circular and the longitudinal muscle layers exhibited their characteristic electrical and motor activities quite independently

without a pharmacological stimulus, but contracted synchronously upon carbachol stimulation [157]. Although phasic contractions in the two muscle layers were synchronized, their electrical activities remained distinct. These observations indicate that the mechanism of communication between the two muscle layers must be quite special in that it allows sufficient electrical coupling to produce co-ordinated motility, yet preserves the distinct intrinsic electrical activities of the two muscle layers.

The structural basis for communication between the two muscle layers across the myenteric plexus of the colon has not been determined. The myenteric plexus consists of a network of inter-linked ganglia and nerve strands. This includes a primary plexus of ganglia and major nerve trunks, a secondary plexus of circumferentially running thinner nerve strands, and a tertiary plexus of thin fibre bundles which constitute a network within the meshes of the primary plexus [120]. In the dog colon, an electron-microscopic examination of the myenteric plexus characterized components of the plexus, focusing on the ICCs and their association with nerve tissue [13]. This study was performed on areas of 10 μm or wider where all components of the plexus can be found. In these regions, the longitudinal and circular muscle cells do not appose each other; whereas the ICCs are coupled by gap junctions with each other and with either circular or longitudinal muscle cells [13]. This observation has recently been confirmed [188]. However, it is not known whether these gap junctions lead to low resistance pathways for electrical coupling from one muscle layer to the other.

The objectives of this study were (i) to demonstrate electrotonic coupling by propagating extracellularly evoked hyperpolarizing pulses from circular into longitudinal muscle cells, (ii) to characterize the pathway of cytoplasmic continuity across the myenteric plexus through the study of neurobiotin spread, and (iii) to identify cell to cell contacts responsible for this communication using electron microscopy.

7.3 Materials and methods

7.3.1 Tissue acquisition and preparation

Mongrel dogs of either sex were killed by an overdose of sodium pentobarbital (100 mg/kg) given intravenously. Approximately 5 cm of proximal colon, starting from 5 cm distal to the ileocecal junction, was removed. The colon was opened flat. Colonic contents were carefully removed in Krebs solution equilibrated with 95% O_2/5% CO_2. The composition of the Krebs solution was (mM): NaCl — 120.3; KCl — 5.9; $CaCl_2$ — 2.5; $MgCl_2$ — 1.2; $NaHCO_3$ — 20.2; NaH_2PO_4 — 1.2 and glucose — 11.5. The clean segment was then pinned flat onto the Sylgard of a dissecting dish which was filled with continuously aerated Krebs solution. After removing the mucosa and the submucosa, the segment was turned over and approximately 80–90% of the longitudinal muscle layer was carefully removed. This is referred to as the *LCM preparation*. The thickness of the remaining longitudinal muscle layer in the LCM preparations was measured by a microscopic ruler marked on the objective of a dissection microscope (Nikon, SMZ-1) with a resolution of ± 15 μm at 30×. *ICC-CM preparations* were obtained by removing the entire longitudinal muscle layer. Experiments were also performed on isolated longitudinal muscle strips (*LM preparations*) from which the entire circular muscle layer was removed.

The tissue was pinned onto the Sylgard of a transfer holder with the longitudinal muscle of LCM preparations facing up. LM preparations were mounted with either the myenteric or serosal surface facing up. The size of the mounted area varied from 2×2 to 2×4 mm, depending on the type of experiment undertaken. At one side, the tissue strip extended to10 mm in length along the long axis of either circular muscle cells in LCM preparations or longitudinal muscle cells in LM preparations,

unless otherwise specified. The holder was transferred to a partition chamber [112, 1] with the pinned section in the recording chamber and the free strip in the stimulation chamber.

7.3.2 Electrophysiology

Intracellular recordings were made by microelectrodes with tip resistances of 30–50 MΩ. Microelectrodes were filled with 3M KCl and connected to an electrometer (WPI Duo773). The output of the electrometer was displayed on a Gould oscilloscope (1421) and recorded on a Gould ink-writing recorder (2400S). Electrotonic pulses were introduced, through a Grass isolation unit (SIU5), into the muscle strips by applying potential differences (generated by a Grass stimulator (S88)) across a pair of Ag-AgCl plates separated by 10 mm. The field strength was measured by a pair of electrodes, 2 mm apart, located in the middle of the stimulation chamber. The electric field strength (represented by the voltage gradient across the recording electrodes) was displayed on the Gould oscilloscope and recorded on the Gould ink-writing recorder. Stimulus artifacts, which occurred during the rising and falling phases of the hyperpolarization pulses, were removed. Experimental results were sampled at 100 Hz by AxoTape (Axon Instruments, Inc.) through an TL-1 DMA Interface (Axon Instruments, Inc.) and stored in a computer. The hyperpolarization pulses were applied to the muscle strips either along the long axis of the circular muscle cells in the LCM and the ICC-CM preparations or along the long axis of the longitudinal muscle cells in the LM preparations. The depth of impalements was determined from the rotatory vernier scale calibrated for the vertical movement of the micromanipulator (Narishige, MN-151); the resolution is better than $\pm$ 2.5 μm. All muscle strips were allowed to equilibrate with continuously aerated Krebs solution in the partition chamber for at

least 2 hours at 37.0±0.5 °C before experimentation started.

7.3.3 Measurement of space constants

Space constants were determined by a double-electrode technique described previously (Chapter 6). In summary, the space constant, λ, was determined by simultaneous measurements of voltage deflections at two locations (x_1 and x_2, $x_1 < x_2$) in response to a series of field stimulations applied through the Ag-AgCl plates in the stimulation chamber (see Figures 7.5 and 6.1). The locations of impalements were determined from the vernier scale of the micromanipulator with an accuracy of ± 35 μm. The space constant refers to the distance at which the size of an electrotonic pulse decreases to 1/e of the amplitude of the electrotonic pulse induced in the muscle strip at the Ag/AgCl plate facing the recording chamber (x = 0). It is not possible to record very close to the source of stimulation because of the space occupied by the thickness of the stimulation plate and the diameter of the mounting pins (0.3–0.4 mm); thus, this set-up cannot determine space constants of less than 0.5 mm with considerable precision. The formula used to determine the space constant was (see Chapter 6):

$$\lambda = \frac{\Delta x}{ln(S_{12})}$$

where Δx = distance between the two microelectrodes ($x_2 - x_1$),

S_{12} = slope of the graph, V_1 versus V_2;

V_1 = amplitude of voltage deflection at x_1; and,

V_2 = amplitude of voltage deflection at x_2.

Slopes (S_{12}) were obtained by the least-squares method based on at least four sets of independent measurements recorded simultaneously at both x_1 and x_2 (see

Figure 7.5). The r-squared value (square root of the coefficient of determination) was better than 0.985 in all fits.

The nomenclature used for space constants in different locations was:

$\lambda_{L,l}$ — space constant along the long axis of longitudinal muscle cells in the LM preparations;

$\lambda_{L,s}$ — space constant along the short axis of longitudinal muscle cells in the LM preparations;

$\lambda_{C,l}$ — space constant along the long axis of circular muscle cells at the myenteric surface of ICC-CM preparations; and

$\lambda_{LC,s}$ — *apparent* space constant along the short axis of the longitudinal muscle in LCM preparations.

7.3.4 Confocal Microscopy

Microelectrode impalements were made in single cells of LCM preparations. Preparations were always approached from the longitudinal muscle side. Stable impalements were obtained using microelectrodes (electrode resistances: 200–500 MΩ) filled with 0.25 mM LiCl containing 3% neurobiotin (MW 323, Dimension Labs). Neurobiotin was injected into the impaled cell with 0.5 nA depolarizing current, 2 Hz, 150 ms. Continuous monitoring of the electrical activity ensured that the microelectrode remained sealed in a single cell during neurobiotin injection [67]. If microelectrodes dislodged from cells prematurely, experiments were discarded.

In order to ensure that all visible fluorescence was a result of specific binding of Texas Red-conjugated streptavidin to injected neurobiotin, tissues not injected with neurobiotin were carried through the incubation procedure used to visualize the

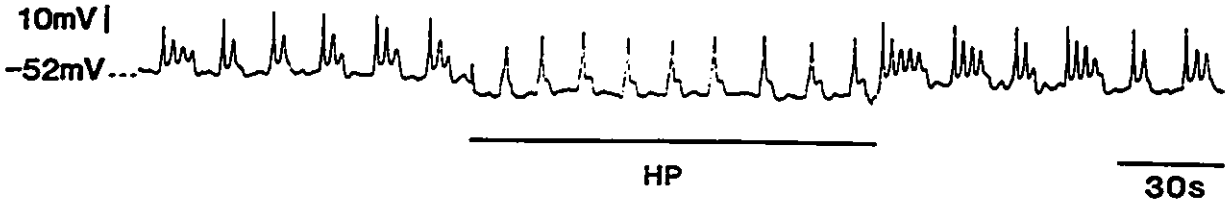

Figure 7.1: *Effects of hyperpolarizing stimulations on circular muscle cells of a LCM preparation*

To allow access to circular muscle cells, the LCM preparation was mounted sideways so that the entire circular muscle layer was exposed, similar to the mounting method described previously [110]. An impalement was made in a circular muscle cell approximately 150 μm away from the myenteric plexus. The electrical activity revealed spikes superimposed on the slow wave plateaus. A hyperpolarization pulse of 150 mV/mm (during bar) abolished the spikes but not the slow wave component. HP — hyperpolarizing pulse.

tracer. Tissues in which injections were purposefully made between cells were also included in order to investigate the possibility of extracellular uptake of neurobiotin.

All tissues were fixed overnight in freshly prepared 4% para-formaldehyde (Sigma) in 0.1 M phosphate buffer (pH 7.4), washed several times and stored in PBS. They were then permeablized in 0.4% Triton X-100 in PBS for 2 hours and subsequently incubated in Texas Red-conjugated streptavidin (BIO/CAN Scientific) for 36 hours. After a two hour wash in PBS, tissues were dehydrated in an ethanol series. Thereafter, tissues were cleared in methyl salicylate (Sigma) for 2 hours. During dehydration and clearing, tissues remained pinned to Sylgard 184 (Dow Corning)

to maintain shape and to prevent damage due to handling of the tissue which was rendered transparent. Preparations were then mounted on slides in Entellan (BDH) and observed using a Zeiss LSM-10 confocal microscope with a helium-neon laser (543 nm). The thickness of each optical section was 0.2 μm. The reconstructed overlays were composed of 0.2 μm thick optical sections with a constant gap in between each sections of an overlay. The width of the gap was various and depended on the thickness of images under investigation.

7.3.5 Electron Microscopy

Four mongrel dogs were anaesthetized with sodium pentobarbital (30 mg/kg i.v.). Segments of the proximal colon were fixed by local perfusion through the mesenteric terminal artery with 2% glutaraldehyde in 0.075 M cacodylate buffer (pH 7.4) containing 4.5% sucrose and 1 mM $CaCl_2$, as previously described [12, 13]. Following fixation, circular and longitudinal strips of muscularis externa were cut, washed overnight in 0.1 M cacodylate buffer, containing 6% sucrose and 1.24 mM $CaCl_2$ (pH 7.4) at 4 °C, postfixed with 2% OsO_4 in 0.05 M cacodylate buffer (pH 7.4) at room temperature for 90 minutes, stained with saturated uranyl acetate, and embedded in Epon 812. Tissues were oriented in moulds to cut the circular muscle layer either across or in longitudinal direction. To locate narrow regions of the myenteric plexus, 0.5 μm thick serial and semi-serial sections were cut and stained with 2% toluidine blue. Both the longitudinal and circular strips of colonic muscularis externa were used for this study. After suitable areas were found on the toluidine blue stained sections, ultra-thin sections were cut, mounted on either 200 mesh grids or 400 mesh ultra light transmission grids, and double stained with uranyl acetate and lead citrate. The grids were examined in a JEOL-1200 EX Biosystem electron microscope

at 80 kV.

7.4 Results

7.4.1 Electrotonic current spread

Within the CM layer

When impalements were made in circular muscle cells 100–150 μm away from the myenteric border of LCM preparations, slow waves of 4–7 cycles/min (cpm) at a resting membrane potential of −55 mV were recorded (Figure 7.1), consistent with data published previously [110]. In addition, spikes superimposed on the plateau phase of slow waves were frequently observed. Electrotonic current, causing hyperpolarization of 4–6 mV, did not significantly affect the slow wave component but abolished superimposed spikes (Figure 7.1, n=2). To determine the space constant at the myenteric border of the circular muscle, $\lambda_{C,l}$, simultaneous electrical recordings were made from the myenteric surface of ICC-CM preparations at less than 50 μm from the surface (see Figure 7.5). $\lambda_{C,l}$ was determined to be 6.9 $\pm$ 0.5 mm (n=3).

Within the LM layer

Spike-like action potentials (SLAPs) were generated spontaneously both at the myenteric (Figure 7.2) and at the serosal (Figure 7.3) surface of all LM preparations. SLAPs appeared as continuous oscillations in all preparations (n=12) except two in which SLAPs appeared in bursts (38.5$\pm$4.9 s in duration and the time interval between bursts varied from 22 to 75 s). The characteristics of an individual SLAP occurring in either oscillatory pattern were not significantly different. SLAPs were

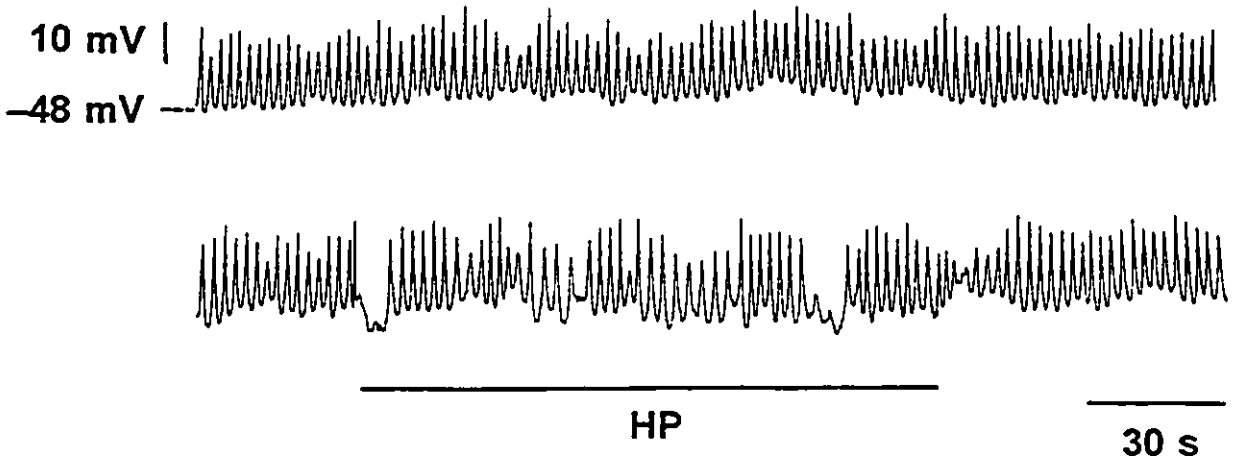

Figure 7.2: *Effects of hyperpolarizing pulses on isolated LM preparations: recording made at the myenteric surface*

Spike-like action potentials (SLAPs) are spontaneously generated at the myenteric surface of the LM preparations. The first panel illustrates electrical activity recorded 1.2 mm away from the stimulation plate of a LM preparation. A hyperpolarization pulse of 225 mV/mm was applied during the length of the bar. No effect on the electrical activity was observed. When the impalement was made at 0.65 mm away from the stimulation plate in the same preparation, the SLAPs became more burst-like with small amplitude oscillations appearing intermittently during a hyperpolarization pulse of 220 mV/mm (during bar). The average amplitude of the SLAPs was reduced.

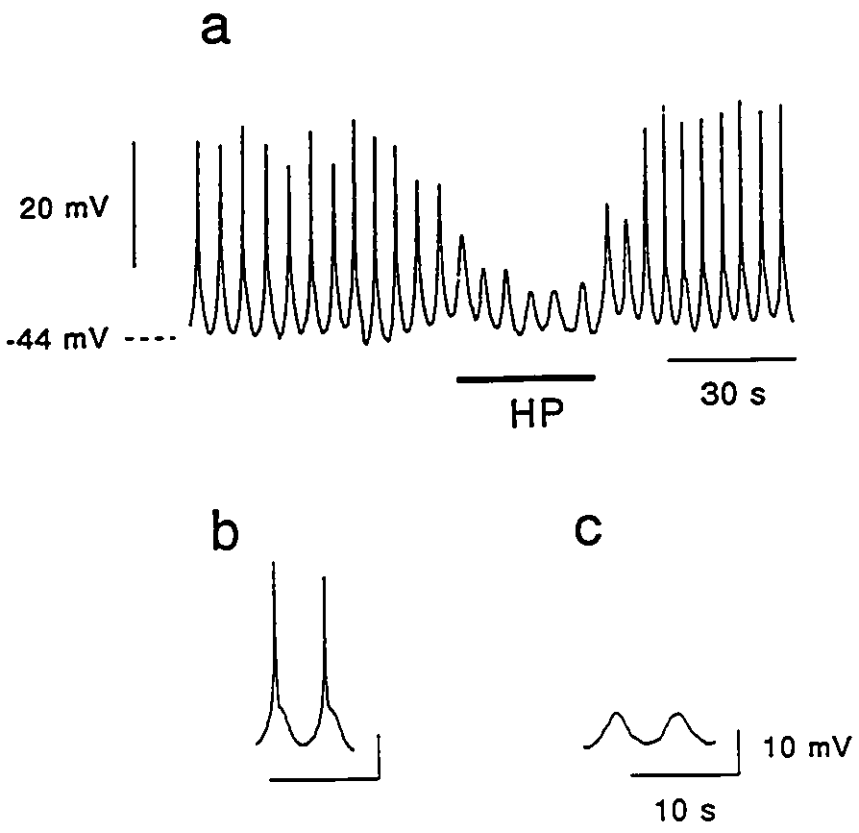

Figure 7.3: *Effects of hyperpolarizing pulses in isolated LM preparations: recording made at the serosal surface*

The fast spike component of the SLAPs were abolished during a hyperpolarization pulse of 230 mV/mm (during bar). (b) and (c) show portions of recording in (a) at an expanded time scale. (b) — without hyperpolarization; (c) — during hyperpolarization.

observed to be oscillating at a frequency of 20.7±1.3 cpm starting from a resting membrane potential of −44.5±0.7 mV; the amplitude, duration and rate of rise were 12.4±0.6 mV, 1.1±0.1 s and 17.8±2.8 mV/s, respectively. In 5 preparations, a fast spike component (15.8±1.1 mV in amplitude, 0.20±0.03 s in duration and 108 ± 16 mV/s in rate of rise) was observed (Figure 7.3c; n=3 at the serosal surface and n=2 at the myenteric surface).

In all LM preparations (n=12), when hyperpolarization pulses, up to 250 mV/mm, were applied along the long axis of longitudinal muscle cells in the stimulation chamber, no significant electrotonic current spread was observed, suggesting that the space constant along the long axis of longitudinal muscle cells, $\lambda_{L,l}$, was less than 0.5 mm. Hence, the space constant along the short axis of longitudinal muscle cells, $\lambda_{L,s}$, would be approximately 10 times smaller ($\leq$ 0.05 mm) than $\lambda_{L,l}$ based on the cell length ratio of the two axes.

Despite the fact that no hyperpolarization was observed, when impalements were made as close as possible ($\leq$ 0.5 mm) to the stimulation plate, effects of hyperpolarizing stimulations on the electrical activity were noted: (i) a change from a continuous to a burst-like activity (Figure 7.2; n=2); and, (ii) abolition of the fast spike component of the SLAPs (Figure 7.3; n= 3). No observable effects on the electrical activity could be recorded in all preparations when impalements were made at a distance greater than 1 mm away from the stimulation plate.

From circular into longitudinal muscle cells

Propagation of electrotonic pulses from the circular muscle layer into longitudinal muscle cells were observed in the LCM preparations (n=5, Figure 7.4) when electrotonic pulses were applied along the long axis of circular muscle cells while recording

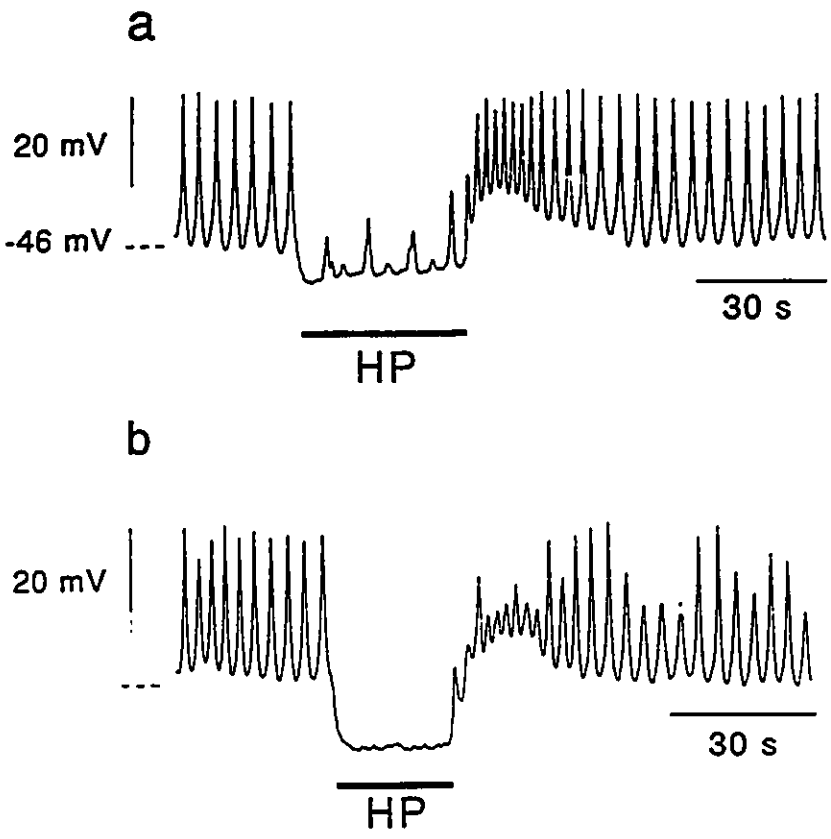

Figure 7.4: *Effects of hyperpolarizing stimulations on a LCM preparation*
Hyperpolarizing pulses were initiated by Ag/AgCl plates in the stimulation chamber and propagated along the circular muscle layer of an LCM preparation. The microelectrode was positioned at $\simeq$100 μm from the myenteric plexus in a longitudinal muscle cell.
a. A hyperpolarizing pulse of 85 mV/mm (during bar) caused a marked hyperpolarization of the membrane potential of the impaled longitudinal cell. Concomitantly, both the amplitude and the frequency of the SLAPs were decreased.
b. When the amplitude of the hyperpolarization pulse was increased to 110 mV/mm (during bar), causing the resting membrane potential to reach -59 mV, the SLAPs were completely abolished. Recordings were obtained from impalements of the same cell.

electrodes were placed in longitudinal muscle cells. The thickness of longitudinal muscle remaining on these LCM preparations was approximately 150 μm. Impalements in longitudinal muscle cells were recognized by the typical electrical activity and by monitoring the depth of impalement — no impalements were made deeper than 50 μm from the surface. The characteristics of SLAPs recorded in these cells were not different from that in isolated LM preparations. The resting membrane potential, frequency, duration and amplitude were -47.2 ± 1.7 mV, 18.4 ± 2.9 cpm, 1.1 ± 0.3 s, 14.9 ± 2.7 mV, respectively (n=5). When hyperpolarization pulses of 25–175 mV/mm in amplitude were applied along the long axis of the circular muscle cells, the impaled longitudinal muscle cells ($\simeq$ 100 μm from the myenteric border) were hyperpolarized (Figure 7.4). Depending on the degree of hyperpolarization, the SLAPs first decreased in amplitude and frequency (Figure 7.4a) and were completely abolished when the resting membrane potential was hyperpolarized to -58.4 ± 3.2 mV (Figure 7.4b; n=5). The absence of slow waves under these conditions further substantiated that impalements were made in longitudinal muscle cells.

When two impalements were made simultaneously into longitudinal muscle cells, and when electrotonic pulses were applied along the long axis of the circular muscle cells, the *apparent* space constant along the short axis of the longitudinal muscle, $\lambda_{LC,s}$, was 4.8 ± 1.6 mm (Figure 7.5; n = 3). Since $\lambda_{LC,s}$ could only be revealed when intact circular muscle was present and when stimulation pulses were applied along the long axis of circular muscle cells, the value of $\lambda_{LC,s}$ reflects the electrical properties of circular muscle rather than longitudinal muscle. The difference between $\lambda_{LC,s}$ and $\lambda_{C,l}$ suggests an abrupt degradation of electrotonic pulses as they propagate passively from the circular muscle into the high resistance longitudinal muscle. Consistently, in LCM preparations with a thicker remaining longitudinal

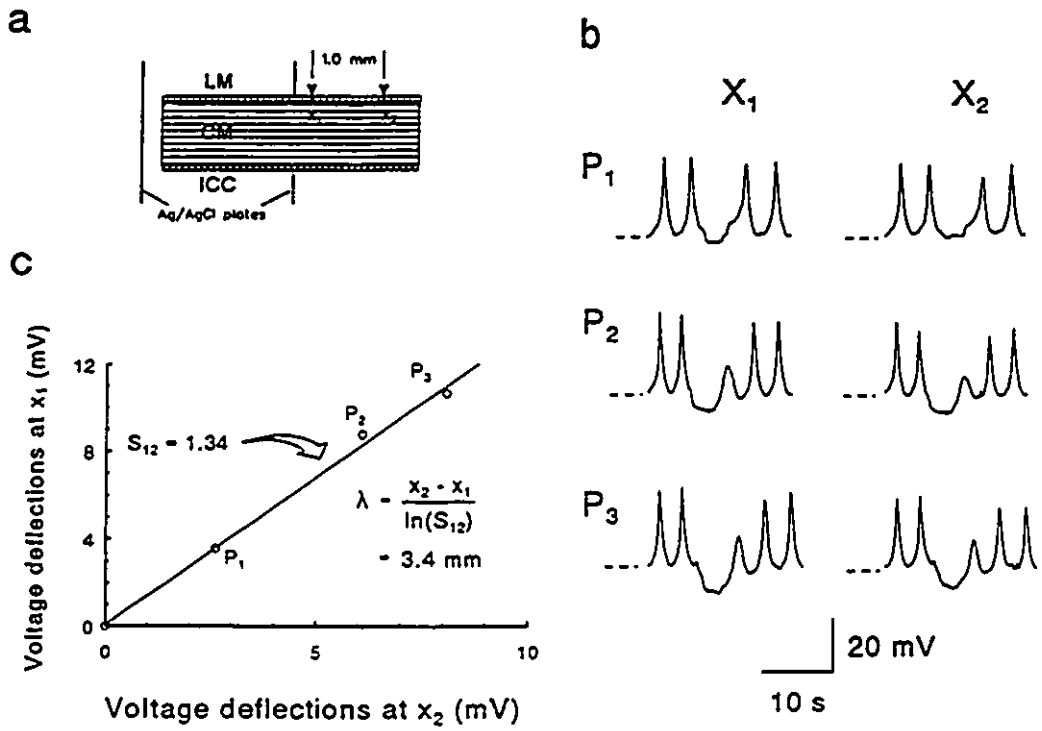

Figure 7.5: *Determination of the space constant in a LCM preparation with a double-electrode technique*

a. Schematically illustrates the orientation of a LCM preparation in the partition chamber with two microelectrodes, positioned in longitudinal muscle cells, separated by 1.0 mm along the short axis of longitudinal muscle cells. The first microelectrode was 0.9 mm (x_1) away from the stimulation plate.

b. Recordings at x_1 and x_2 in response to 3 different amplitudes of hyperpolarizing stimulations. Dashed lines denote the resting membrane potentials.

c. The amplitudes of the electrotonic voltage deflections at x_1 and x_2 were plotted. The slope of the plot was determined by linear regression using the least squares method. The r-squared value of this fit was 0.998. The apparent space constant along the short axis of the longitudinal muscle in this LCM preparation, $\lambda_{LC,s}$, was 3.4 mm.

muscle layer ($\simeq$ 0.35 mm), no effects of hyperpolarizing current was observed until microelectrodes were driven into the longitudinal muscle to approximately 120-150 μm from the myenteric border. Furthermore, when the LCM preparations were reoriented such that hyperpolarization pulses were applied along the short axis of circular muscle cells (i.e. the long axis of longitudinal muscle cells), effects of hyperpolarization stimulations in longitudinal muscle cells close to the myenteric border impaled at a distance of $\geq$ 0.5 mm from the stimulation plate were not observed (17 impalements in 3 preparations).

The presence of electrotonic coupling between longitudinal and circular muscle layers across the myenteric border illustrates the existence of low-resistance pathways. This was further substantiated by the study of the spread of neurobiotin.

7.4.2 Neurobiotin spread

Neurobiotin injections were made in cells close to the myenteric plexus whose position was judged by the same criteria used for electrotonic coupling measurements (n=11). After fixation and binding of Texas Red-conjugated streptavidin to neurobiotin, the identity and the location of cells was revealed using confocal microscopy.

Neurobiotin was injected into single circular muscle cells in 2 of 11 preparations. No spread was seen to occur into longitudinal muscle cells or ICCs. Because of the low level nonspecific background fluorescence in the longitudinal muscle, both the neurobiotin-marked circular muscle cells and the adjacent longitudinal muscle cells were observed. Since both the injected circular and the longitudinal muscle cells were visible in an optical section of 0.2 μm in thickness, the neurobiotin containing circular muscle cells were within 0.2 μm of the longitudinal muscle cells into which neurobiotin did not diffuse (Figure 7.6a). A 1.5 min injection applied intermittently

Figure 7.6: *Different neurobiotin spread patterns at the myenteric plexus*

a. Neurobiotin spread was restricted to circular muscle cells when neurobiotin was injected into a circular muscle cell close to the myenteric border. The fluorescent region measured 963 μm long, 17 μm wide and 54 μm deep following a 4 minute intermittent injection with 7.5 minutes allowed for further diffusion. Note the non-specific background fluorescence of longitudinal muscle cells (arrow heads). Both the longitudinal and the circular muscle cells (with the brightest fluorescent intensity) could be identified in one optical section of 0.2 μm in thickness; therefore, the neurobiotin-injected circular muscle cells were directly apposing the longitudinal muscle cells. (a) Bar — 100 μm.

b. Neurobiotin spread was restricted to longitudinal muscle cells when neurobiotin was injected into a longitudinal muscle cell close to the myenteric border. Tracer spread was slower in the longitudinal muscle layer than in the circular muscle layer. The fluorescent region measured 369 μm long, 20 μm wide and 26 μm deep following a 4 minute intermittent injection with 7.5 min to allow further diffusion. Bar — 50 μm.

c. Higher magnification of the frame in (b). Thorn-like protrusions are visible near in longitudinal muscle cells. Bar — 10 μm.

d. Neurobiotin injected into a cell at the myenteric border rapidly diffused within in ICC network as well as bordering longitudinal and circular muscle cells. The fluorescent region measured 352 μm along the long axis of the circular muscle, 1416 μm along the long axis of the longitudinal muscle (to the edges of the tissue) and approximately 62 μm in depth following a 2 minute intermittent injection with 7 minutes for further diffusion. Longitudinal muscle cells (vertical in this figure), circular muscle cells and ICCs contain neurobiotin. Bar — 50 μm.

e. The branching morphology of the ICCs is illustrated at higher magnification. Their processes were seen connecting adjacent ICCs and smooth muscle cells. Bar — 25 μm.

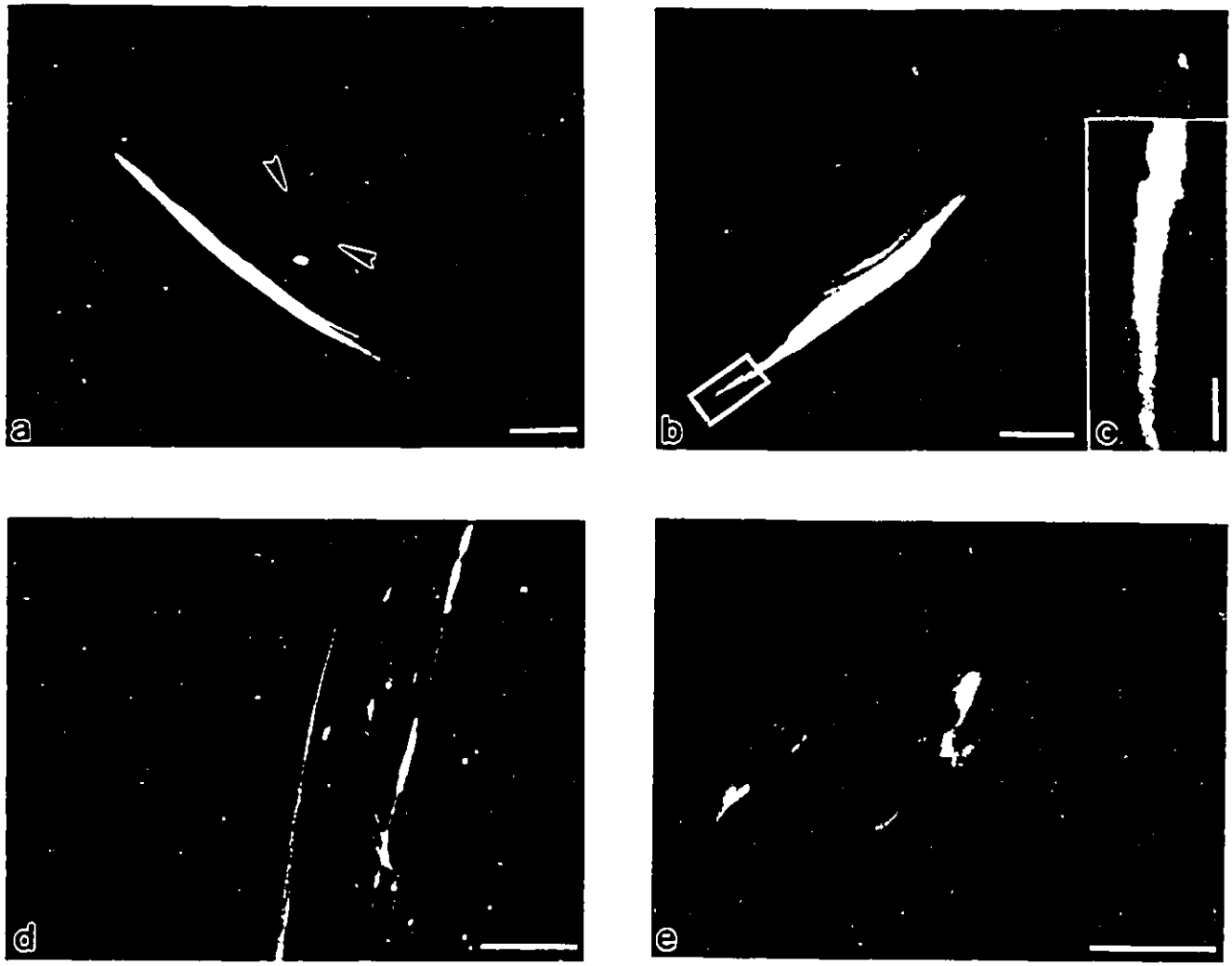

Figure 7.6

over 4 min, followed by an additional 5 min diffusion period resulted in an area of fluorescence made up of 6 to 10 circular muscle cells.

In 7 of 11 preparations, neurobiotin was injected into longitudinal muscle cells. A 4 min intermittent injection, including a total injection period of 1.5 min, followed by an additional 5 min diffusion period resulted in an area of fluorescence made up of approximately 4 to 6 longitudinal muscle cells (Figure 7.6b). No neurobiotin was observed to diffuse into circular muscle cells and ICCs. Short projections were frequently observed in neurobiotin-marked longitudinal muscle cells (Figure 7.6c).

In the remaining 2 preparations, the pattern of neurobiotin spread was completely different from that observed in the preparations described above; neurobiotin spread was rapid and extensive. Fluorescence could be found in longitudinal muscle cells, ICCs and circular muscle cells. In one of the preparations, the fluorescent area, resulting from a total of 2 min injection applied intermittently over a period of 4 min and followed by a 5 minute diffusion period, measured 352 μm along the long axis of circular muscle cells (limited by the tissue size at one edge), 1416 μm along the long axis of the longitudinal muscle (to the edges of the tissue) and approximately 62 μm in depth (Figure 7.6d). Optical sections in various depths of the preparation showed close association of the two muscle layers with the ICCs lying between them. At a higher magnification, ICCs were able to be identified by their characteristic branching morphology, their network structure and their close association with smooth muscle cells. Processes of the ICCs were seen in contact with each other and with adjacent smooth muscle cells (Figure 7.6e).

The study of neurobiotin spread revealed only one route of communication between longitudinal and circular muscle cells — indirectly through ICCs. Direct communication between smooth muscle cells of the two muscle layers was not

Figure 7.7: *Close apposition of the longitudinal and circular muscle layers*

a. Cross section through circular muscle. Narrow gaps (arrows) of 0.1–3 μm in width were frequently observed between the two muscle layers (more than 200 μm in length). c – capillaries. × 440, Bar — 25 μm.

b. Longitudinal section through circular muscle. In narrow regions of the myenteric plexus, the main body of nerves of the tertiary plexus (N), associated with ICCs (arrowheads), frequently enters the longitudinal muscle (LM) layer following the direction of the capillary plexus (c) forming a small inner subdivision of the longitudinal muscle (iLM). The iLM is separated from the circular muscle layer (CM) by a thin (less than 2 μm) layer of connective tissue (arrows) containing a few small nerves and ICC processes. × 530, Bar — 20 μm.

c. Cross section through the circular muscle. Nerve fibres of the tertiary plexus (N), associated with ICCs, are occasionally seen to be embedded in the circular muscle (CM) forming a small outer subdivision of circular muscle (oCM) separated from the longitudinal muscle (LM) by a thin layer of connective tissue. Note circular muscle cells in the oCM are closely apposed to adjacent longitudinal muscle cells (large arrows; approximately 100 nm in width). The small arrow indicates a close contact between an ICC and an outer circular muscle cell. × 5,100, Bar — 2 μm.

d. High power micrograph showing the area of close apposition (arrow) between a longitudinal muscle (LM) cell projection and a circular muscle (CM) cell. The gap (65 nm) between the two cells is filled with electron dense material. No specialized structures are observed on the apposed plasma membranes. × 52,500, Bar — 200 nm.

e. High power micrograph showing a close apposition contact between an ICC process and a thorn-like process (arrowhead) of a longitudinal muscle cell (LM). At this magnification, the ICC process can easily be distinguished from a smooth muscle process by the presence of numerous intermediate filaments (circle) and microtubules (mt), as well as a mitochondrion (m). × 60,000, Bar — 200 nm.

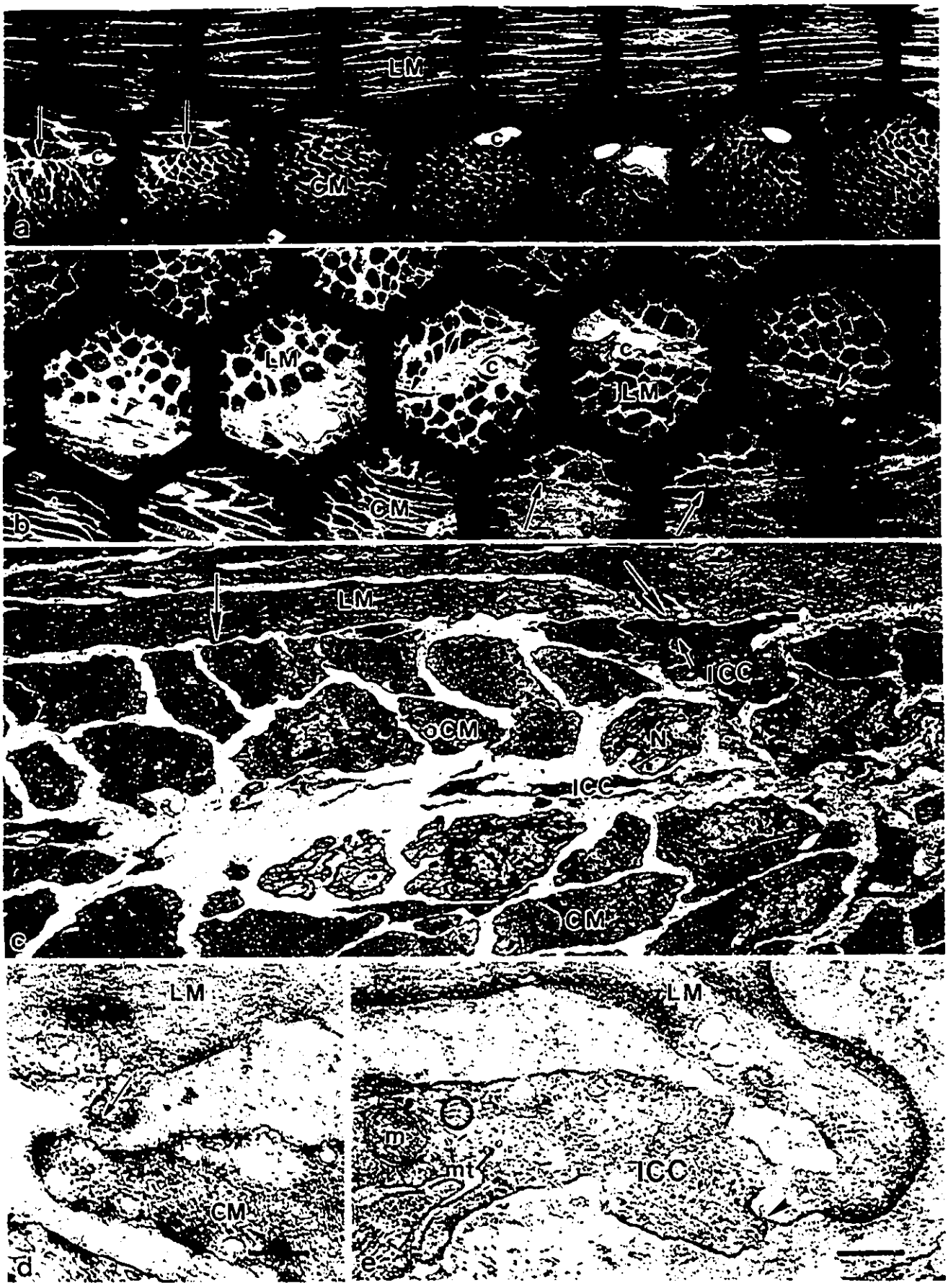

Figure 7.7

observed. The structural basis for the provision of cytoplasmic continuity to facilitate low-resistance electrotonic coupling was further investigated by electron microscopy.

7.4.3 Transmission electron microscopy

Electron microscopic examination of the myenteric plexus revealed frequent long stretches (200 μm or longer) of narrow gaps of less than 7μm (typically 50 nm–3 μm) in width separating the two muscle layers (Figure 7.7a–c). Only the tertiary myenteric plexus was present in these narrow areas. ICCs were abundantly present and closely associated with small nerves (Figure 7.7c). The ICCs were interconnected by gap junctions. A conspicuous characteristic of the ICCs was the frequent occurrence of close apposition contacts with neighbouring smooth muscle cells (Figures 7.7e and 7.8). In addition, longitudinal muscle cells extended small protrusions where close apposition contacts with ICCs were observed (Figure 7.7e). Such thorn-like protrusions were similarly noticeable in the neurobiotin-marked longitudinal muscle cells (Figure 7.6e). Gap junctions between ICCs and smooth muscle cells were present but rare.

The tertiary plexus was not always observed to be positioned between the two muscle layers. Its main branches, accompanied by the capillary plexus and ICCs, often diverged into either the longitudinal or the circular muscle layer and then rejoined the main branches (Figure 7.7b & c). Such branching of the tertiary plexus created areas where the two muscle layers directly apposed each other by gaps of 100–120 nm in width, occasionally as small as 50 nm. The gaps were filled with loose collagen fibres and basal lamina of both types of smooth muscle cells. No distinguishable cell-to-cell membrane specializations such as gap junctions or close apposition contacts were present but caveolae condensations were commonly observed in closely apposing

Figure 7.8: *A cross section through the narrow intermuscular region*

a. In some slightly wider regions of the tertiary plexus (5 μm–8 μm in width), smooth muscle profiles (SM) were occasionally seen oriented in such a way that they did not appear to belong to either muscle layer. They were located at some distance from both the circular muscle (CM) and longitudinal muscle (LM) layers. It was common for these smooth muscle cells to form close contacts with ICC processes (arrowheads). N — nerve. × 11,700, Bar — 1 m.

b. High magnification micrograph of the frame in (a) showing two ICC processes forming close contact (arrow) to one another. Each ICC process makes extended close apposition contacts (arrowheads) with overlapping smooth muscle (SM) processes. At this magnification, ICC processes can be distinguished from smooth muscle processes by the presence of abundant mitochondria (m), intermediate filaments (small circle), as well as subsurface cisternae of smooth endoplasmic reticulum (sER). The cytoplasm of smooth muscle processes is dominated by thin filaments (large circle). × 37,300, Bar — 500 nm.

---

plasma membranes. ICC processes were abundant in these areas and observed to form close apposition contacts with both muscle cells.

A few smooth muscle cell profiles of unidentifiable orientation were occasionally observed in these narrow areas (Figure 7.8). These cells had the spindle-like shape of smooth muscle cells. However, based on the orientation of contractile filaments in sections, it was not possible to identify with certainty the muscle layer from which these smooth muscle cells originated. They were separated from the two main muscle layers by connective tissue and nerve fibres. The distinctive feature of these smooth muscle cells was the frequent occurrence of close apposition contacts with ICC processes.

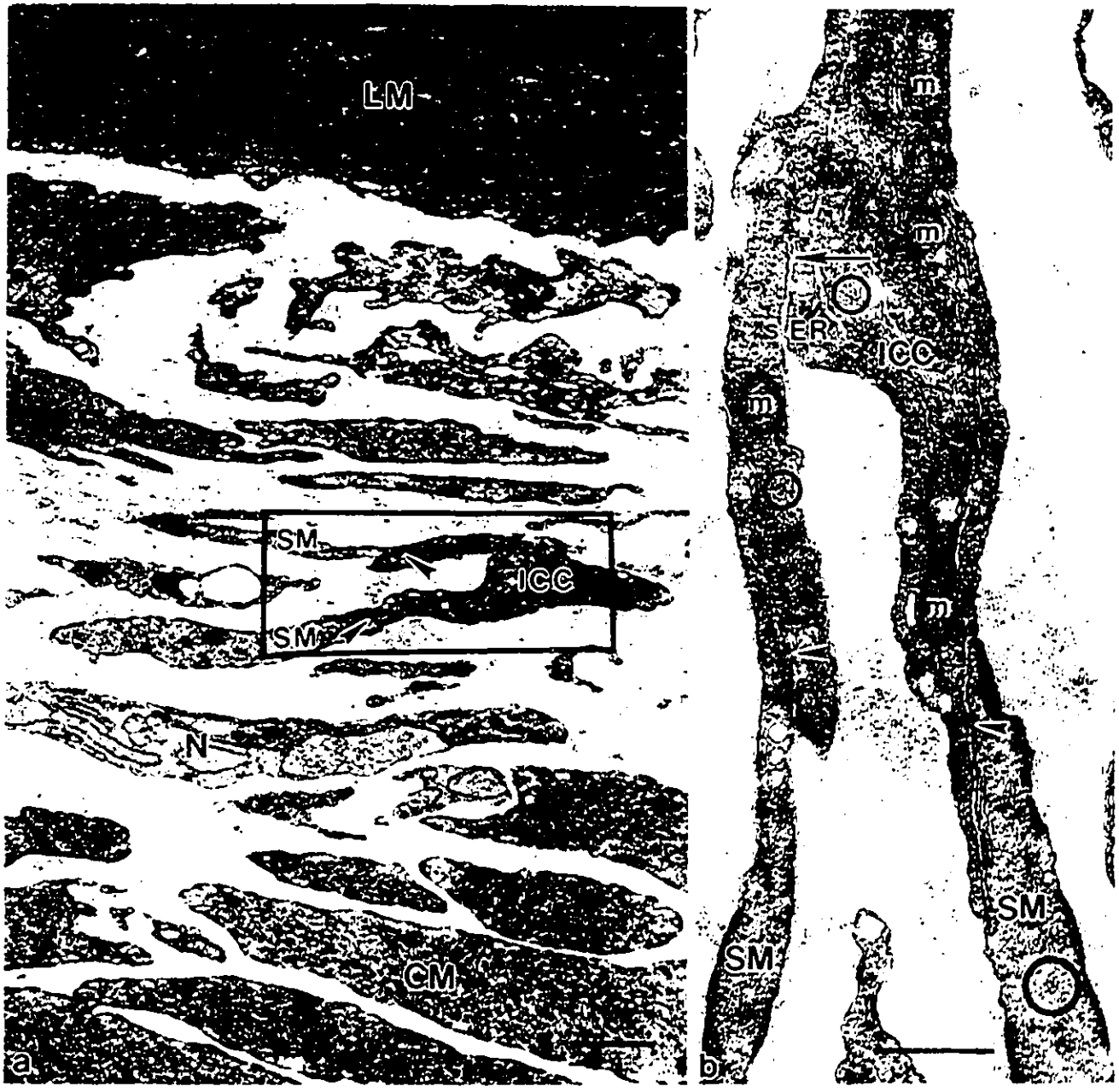

Figure 7.8

7.5 Discussion

The existence of low resistance pathways between smooth muscle cells of the longitudinal and the circular muscle layers was demonstrated by electrotonic current spread. Evidence from the study of neurobiotin spread and from electronmicroscopic observations indicate that the circular and longitudinal muscle cells are coupled to a network of interstitial cells of Cajal (ICCs), covering the entire myenteric border of the two muscle layers, primarily by an abundance of close apposition contacts. There are regions, scattered throughout the myenteric plexus, in which circular muscle cells are closely apposing longitudinal muscle cells (with gaps as narrow as 50 nm) mainly resulting from branching of the tertiary myenteric plexus into one of the muscle layers. ICC processes are frequently present in these regions but no direct cell-to-cell contacts between muscle cells are observed.

Electrotonic coupling between circular and longitudinal muscle cells was positively demonstrated by injecting current into the circular muscle layer and subsequently recording the electrotonic pulse in a longitudinal muscle cell. Effective hyperpolarization of the muscle strips was illustrated by the abolition of voltage-sensitive SLAPs generated by the longitudinal muscle cells when hyperpolarizing electrotonic pulses of 5–8 mV were injected along the long axis of circular muscle cells. The space constant along the long axis of the circular muscle cells at the myenteric surface, $\lambda_{C,l}$, is comparable with the apparent space constant along the short axis of the longitudinal muscle of LCM preparations, $\lambda_{LC,s}$. It is consistent with the proposition that electrotonic pulses propagated along the circular muscle cells. A similar hypothesis has been proposed in the cat jejunum [64].

Coupling between longitudinal muscle cells is of relatively high resistance. Evidence includes: (i) the small space constant along the long axis of the longitudinal

muscle, $\lambda_{L,I}$; (ii) the fast spike superimposed on the peaks of the SLAPs can be abolished without a recordable change in the resting membrane potential; and (iii) electrotonic pulses reached longitudinal muscle cells only within 100–120 μm from the myenteric border. This confined region of electrotonic coupling of the longitudinal muscle layer to the circular muscle conceivably provides controlled electrotonic coupling of the two muscle layers with preservation of their distinct electrical activities.

The spread of neurobiotin from a single injected cell to neighbouring cells, including ICCs and circular and longitudinal muscle cells, proves the existence of cytoplasmic continuity among these three cell types. The most abundant intercellular junctions between circular or longitudinal muscle cells and ICCs are close apposition contacts. Since the spread of neurobiotin and electrotonic current infers the existence of gap junction-like structures to facilitate low-resistance coupling, it seems logical to propose that close apposition contacts constitute a gap junction-like structure. The electron-dense material often seen in the gaps of the close apposition contacts could reflect connexons. Electron microscopy cannot identify gap junctions in these structures since a large plaque of connexons is needed to reveal the typical seven-line structure [126]. Furthermore, slightly oblique sectioning would already prevent the observation of small gap junctions.

The type of connexin protein constituting close apposition contacts is not known. Connexin 43 (Cx 43) has not been identified in the myenteric plexus region using immunohistochemical methods; however, it is quite possible that fluorescent signals of fine structures, like close apposition contacts, are below the detection limit of this method [128]. Nevertheless, Cx 43 is still a strong candidate since Cx 43 protein as well as Cx 43 mRNA have been identified in this area [106].

7.5.1 Network of ICCs as mediators of communication

This study puts forth a significant physiological role for the ICCs located in the myenteric plexus of the colon. The highly branched ICCs together with their long processes are organized in a network [13, 188] spanning the entire myenteric plexus effectively constituting low- resistance pathways to facilitate electrical coupling between the two muscle layers. This allows for electrical interaction between the muscle layers to coordinate their contractile activity to create propulsive contractions. There is another network of ICCs situated at the submuscosal surface of the circular muscle layer [12, 119]. The submuscular ICC network is crucial to the generation of the pacemaker component of the slow waves [60, 110, 112, 117, 172] which synchronizes with the phasic contractions generated in the circular muscle. There is no evidence that the ICC network in the myenteric plexus can generate such a pacemaker component. Furthermore, there is, thus far, no evidence that the myenteric ICCs are essential for the generation of SLAPs recorded spontaneously in the longitudinal muscle, as proposed previously [171]. SLAPs are a characteristic electrical activity of the circular [112] and the longitudinal [41, 62, 110, 157] muscle layers as well as of isolated circular smooth muscle cells [143].

In the human colon, obliquely oriented smooth muscle bundles have been observed running from one muscle layer into the other [72, 94, 103, 140]. It was first observed by Landau [103] who suggested that these bundles serve to conduct electrical impulses across the two muscle layers to bring harmonious motility in the human colon. A recent study suggested that similar oblique smooth muscle bundles existed between the circular and the longitudinal muscle layers of canine proximal colon and hypothesized that these bundles serves to electrically coupled the circular and the longitudinal muscle cells [99]; however, it did not show any communication pathways

between the oblique muscle cells and either muscle layers, and also failed to recognize the presence of the interstitial cells of Cajal in this area. Nevertheless, oblique smooth muscle bundles could be correlated to the smooth muscle cells of unidentifiable orientation found in the narrow areas described in the present study (see Figure 7.8). Thorough electron microscopic examination revealed no evidence of direct communication between circular or longitudinal muscle cells and these oblique smooth muscle cells. ICCs were always present connecting these oblique smooth muscle cells to either circular or longitudinal muscle cells.

In the small intestine, recordings from different isolated muscle strips of the cat jejunum with pressure- and micro-electrodes revealed that slow waves originated from the boundary between the longitudinal and the circular muscle layers [25, 49, 98], likely initiated by the ICCs in the myenteric plexus [175, 179, 180]. In the small intestine, the slow wave activity recorded simultaneously in both muscle layers is similar and has a constant phase lag. Furthermore, electrotonic coupling between the two muscle layers has been demonstrated by the propagation of extracellularly evoked electrotonic potentials from the circular to the longitudinal muscle [64, 178]. In the cat jejunum, gap junctions have been observed between the interstitial cells, longitudinal muscle cells and circular muscle cells near the myenteric plexus [178]. Hence, unlike in the colon, the myenteric ICCs in the small intestine may serve as both communicating and pacemaking cells. It is interesting to note that in the small intestine of the W/W^v mutant mice, where the ICC network in the myenteric plexus is absent, there is a 1700% increase in areas of directly apposing smooth muscle cells from both muscle layers [85]. The identity of communication pathways in this tissue has not yet been elucidated.

In the small and large intestine, in vivo patterns of motility are prominently

modulated by nerves [161]. Observations from this and previous [12, 13, 46, 50, 72, 140, 156, 188] studies illustrate that the ICCs, as mediators of communication between the two muscle layers, are extensively innervated. The hypothesis emerges that neural control of motility through the ICC network is an important aspect of normal gastrointestinal motility.

Chapter 8

Electrical Coupling Between Longitudinal Muscle Cells of Canine Colon: Involvement of Close Apposition Contacts

8.1 Epitome

Knowledge of the intercellular communication between longitudinal muscle cells is essential for advancing our understanding of the role of the longitudinal muscle layer in gastrointestinal motility. No positive evidence has been presented to demonstrate the existence of electrical coupling between longitudinal muscle cells. The objective

This chapter is in the editing process for journal submission (authored by Louis Liu, Irene Berezin and Jan Huizinga). Contributions of Irene Berezin are discussed in section 2.3 of Chapter 2.

of this study was to examine the characteristics of intercellular communication in the longitudinal muscle layer of canine colon with electrophysiological and electron microscopic investigations. The characteristics of electrical coupling were characterized by the input resistance, the space constant and the phase relationship of simultaneously recorded electrical activities. The input resistance, R_i, of the longitudinal muscle layer was equal to 32.1±2.6 MΩ (n = 20) in Krebs solution; the R_i was negligible at the submucosal surface of the circular muscle layer. In the presence of 1 mM octanol, which blocked gap junction conductance, the R_i was increased to 49.7±1.9 MΩ (n = 5) in the longitudinal muscle layer and increased to 63.4±3.1 MΩ at the submucosal surface of the circular muscle layer (n = 9). The space constant along the long axis of smooth muscle cells was negligible in the longitudinal muscle layer and equal to 8.1±1.1 mm (n = 12) at the submucosal surface of the circular muscle layer. Spike-like action potentials (SLAPs) recorded simultaneously in the longitudinal muscle layer were entrained over 90% of the time with a 2–8 mV difference in resting membrane potential. Separations of the recording electrodes were 1–2.8 mm along the long axis of longitudinal muscle cells. At the submucosal surface of the circular muscle layer, slow waves were perfectly synchronized with an identical resting membrane potential for a separation as far as 3.5 mm along the long axis of circular muscle cells. A detailed electron microscopic investigation revealed the absence of gap junctions in the longitudinal muscle layer. Whereas, numerous close apposition contacts were observed. Unlike the circular muscle cells, the longitudinal muscle cells were highly branched with many processes which interdigitated into adjacent longitudinal muscle cells. In interdigitations, close apposition contacts were frequently observed. This study provides the first positive demonstration of electrical communication, as indicated by entrainment of SLAPs, in the longitudinal muscle layer of

canine colon. The intercellular communication pathways between longitudinal muscle cells are hypothesized to be constituted by close apposition contacts.

8.2 Introduction

The *muscularis externa* of the gastrointestinal (GI) tract consists of the circular and the longitudinal muscle layers. The ring-like contractions generated in the circular muscle are believed to be fundamental for peristaltic movement. In the circular muscle layer of the GI tract, gap junctions have been consistently observed in various species [12, 75, 128]. It is widely accepted that gap junctions constitute the structural basis for intercellular communication [52, 77, 84] through which individual cells can function in harmony as a tissue. The physiological roles of the longitudinal muscle are not completely understood but two main hypotheses exist: (i) aiding in propulsive activity by periodic shortening, and (ii) serving as a pathway for the local circuit current spread to provide electrical coupling between circular muscle bundle in the long axis of the intestine [27]. For both proposed functions of the longitudinal muscle, adequate electrical coupling between smooth muscle cells is essential. However, in the longitudinal muscle layer, gap junctions have never been observed in the colon [76, 184], and, only a single study has illustrated the presence of a tiny gap junction in an obliquely cut thin section of the cat small intestine [178].

Studies of spread of low molecular weight substances, such as Lucifer Yellow and neurobiotin, from a single injected cell to neighbouring cells provide important information on intercellular communication. Despite the absence of identifiable gap junctions in the longitudinal muscle layer, spread of Lucifer Yellow has been observed in the longitudinal muscle layer of the guinea pig small intestine [199]. Furthermore,

a recent study consistently observed the spread of neurobiotin from a single injected cell to neighbouring cells in the longitudinal muscle of canine colon [67]. These observations positively demonstrate the existence of cytoplasmic continuity between smooth muscle cells of the longitudinal muscle layer.

Characteristics of electrical coupling between longitudinal smooth muscle cells is presently unknown. Simultaneous intracellular recordings from the myenteric and the serosal surface of the longitudinal muscle of the canine colon prefatorily indicate that smooth muscle cells are not electrically coupled at these two sites [171]. Thus far, positive physiological evidence on electrical communication of longitudinal muscle cells has not been presented.

In this study, an attempt was made to thoroughly examine the properties of intercellular communication between longitudinal muscle cells of canine colon. The objective was implemented by electrophysiological and electron microscopic investigations. Properties of electrical coupling were determined by three parameters, namely the input resistance revealed by intracellular current injections, the space constant as measured by the double-electrode technique, and the phase relationship of simultaneously recorded electrical activities. Three issues could be addressed as to the significance of this study: (a) physiological significance of tissue with marked difference in gap junction density; (b) relative importance of gap junctions versus close apposition contacts; and (c) appropriateness of various methods in determining electrical coupling.

8.3 Method and materials

8.3.1 Preparation of muscle strips

Dogs of either sex were killed by an overdose of sodium pentobarbital (100 mg/kg) given intravenously. Approximately 10 cm of proximal colon was taken from 5 cm distal to the ileocecal junction. The colon was opened flat. Colonic contents were carefully removed in a beaker containing Krebs solution equilibrated with 95% O_2 and 5% CO_2. The preparation procedures of different muscle strips, namely ICC-circular muscle (ICC-CM) preparations [112], circular muscle (CM) preparations [113], and longitudinal muscle (LM) preparations [41, 110] had previously been described.

The tissue was pinned onto the Sylgard bottom of a transfer holder which was then placed in a partition chamber allowing voltage control of muscle strips [112]. Muscle strips were allowed to equilibrate with continuously aerated (95% CO_2 and 5% O_2) Krebs solution in the partition chamber for at least 2 hours at 37.0±0.5 °C before experimentations started. The composition of the Krebs solution was (mM): NaCl — 120.3; KCl — 5.9; $CaCl_2$ — 2.5; $MgCl_2$ — 1.2; $NaHCO_3$ — 20.2; NaH_2PO_4 — 1.2 and glucose — 11.5. Octanol (1-octanol, Sigma, St. Louis) was added directly to Krebs solution to reach final concentrations of 1–2 mM before it perfused to the partition chamber.

8.3.2 Intracellular recordings

Intracellular recordings were made by microelectrodes with 30–50 MΩ pipette resistances. Microelectrodes were filled with 3 M KCl. A microelectrode was inserted into a microelectrode holder which was connected to an electrometer (WPI Duo773). The output of the electrometer was displayed on a Gould oscilloscope (1421) and recorded

on a Graphtec thermal arraycorder (WR 7700). Parts of the experimental results were also sampled at 100 Hz by AxoTape (Axon Instruments, Inc.) through an TL-1 DMA Interface (Axon Instruments, Inc.) and stored in a computer.

8.3.3 Measurements of electrical coupling

Input resistance determined by intracellular current injection

The input resistance, R_i, was determined by injecting a known current source, I, into an impaled cell. With the measurement of the voltage deflection, V, registered at the impaled cell in response to I, R_i can be determined according to Ohm's Law ($R_i = V/I$). The microelectrode resistance was balanced by a bridge circuit (WPI Duo 773) before each impalement. Proper balancing of the microelectrode resistance during each experiment was ensured by injecting the same amount of current into the microelectrode after it was withdrawn from the impaled cell.

Determination of space constants with the double-electrode technique

The space constant is defined as the distance at which the size of an electrotonic pulse decreases to 1/e of the amplitude of the electrotonic pulse induced in the muscle strip at the Ag-AgCl plate facing the recording chan. ($x = 0$). Hyperpolarizing electrotonic pulses were induced extracellularly by a pair of Ag-AgCl plates. Space constants were determined by a double-electrode technique as described in Chapter 6. This method has been shown to be more sensitive and accurate than the conventional single-electrode method. The space constants were determined by (see Chapter 6):

$$\lambda = \frac{\Delta x}{ln(S_{12})}$$

where Δx = distance between the two microelectrodes at locations x_1 and x_2,
S_{12} = slope of the graph, V_1 versus V_2;
V_1 = amplitude of voltage deflection at x_1; and,
V_2 = amplitude of voltage deflection at x_2.

Slopes (S_{12}) were obtained by the least-squares method based on at least four sets of independent measurements recorded simultaneously at both x_1 and x_2 (see Figure 6.1). The r-squared value (square root of the coefficient of determination) was better than 0.980 in all fits. The locations of impalements were determined from the vernier scale of the micromanipulator with an accuracy of $\pm$ 35 μm. As discussed previously, this set-up cannot determine space constants of less than 0.5 mm with any considerable precision.

Phase relationship of simultaneously recorded electrical activities

The degree of electrical coupling was also determined by the phase relationship of electrical activities recorded simultaneously at two sites with known separations, Δx. Microelectrodes were always positioned along the long axis of smooth muscle cells. The phase difference is defined by the time lag, Δt, between the appearance of the half-maximum amplitude during the upstroke phase of action potentials at the two recording sites. The extent of electrical coupling was measured by the *apparent* propagation velocity (v_p) which was defined as $\Delta x/\Delta t$.

8.3.4 Electron Microscopy

Mongrel dogs (n = 4) were anaesthetized with sodium pentobarbital (30 mg/kg i.v.). Segments of the proximal colon were fixed by local perfusion through the mesenteric terminal artery with 2% glutaraldehyde in 0.075 M cacodylate buffer (pH 7.4) containing 4.5% sucrose and 1 mM $CaCl_2$, as previously described [12]. Following fixation, circular and longitudinal strips of muscularis externa were cut, washed overnight in 0.1 M cacodylate buffer, containing 6% sucrose and 1.24 mM $CaCl_2$ (pH 7.4) at 4 °C, postfixed with 2% OsO_4 in 0.05 M cacodylate buffer (pH 7.4) at room temperature for 90 minutes, stained with saturated uranyl acetate for 60 min, and embedded in Epon 812. Tissues were oriented in moulds to cut the longitudinal muscle layer either across or in longitudinal direction. After suitable areas were found on the toluidine blue stained 0.5 μm thick sections, ultra-thin sections were cut, mounted on either 200 mesh grids or 400 mesh ultra light transmission grids, and double stained with uranyl acetate and lead citrate. The grids were examined in a JEOL-1200 EX Biosystem electron microscope at 80 kV.

8.4 Results

8.4.1 Measurements of electrical coupling

Input resistances

When either depolarizing or hyperpolarizing current pulses (1 nA in amplitude and 0.5–1 s in duration) were injected into the impaled cells through intracellular electrode at the serosal surface of the LM preparations, an input resistance, R_i, of 32.1±2.6 MΩ was revealed (n = 20, Figure 8.1a). Rectification of injected current was not noticeable

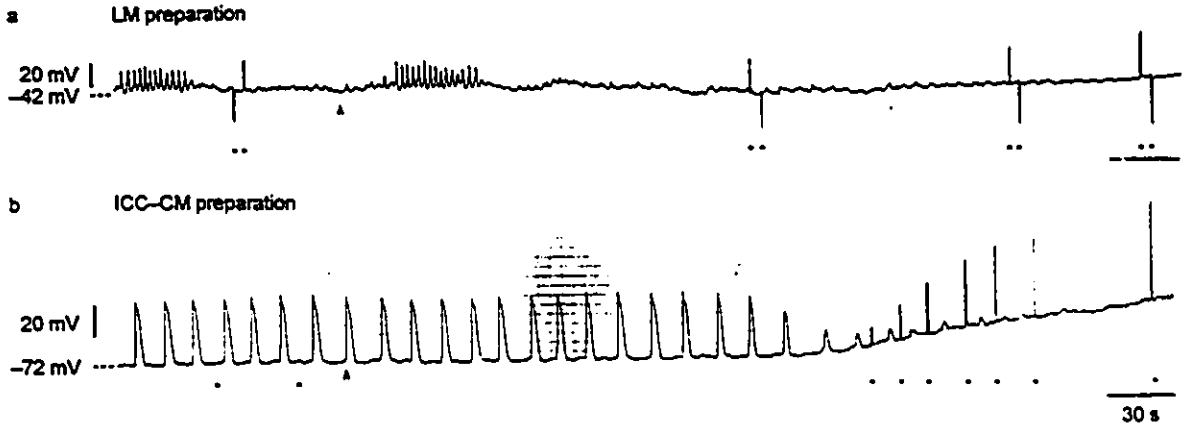

Figure 8.1: *Effects of octanol on input resistances of LM and ICC-CM preparations*
a. In Krebs solution, longitudinal muscle cells spontaneously generated spike-like action potentials (SLAPs). Impalement was made at the serosal surface. Burst-type oscillations were observed in this preparation. Either depolarizing or hyperpolarizing current pulses (squares) were delivered to the impaled longitudinal muscle cell of an LM preparation. Rectification to current stimulations (0.5 or 1 s in durations) was not observed. In this experiment, the input resistance, R_i, was 26 MΩ in Krebs solution. Addition of 1 mM octanol (at arrow), which blocks gap junction conductance, increased R_i to 38 MΩ.
b. In the ICC-CM preparation, the slow waves were generated spontaneously at the submucosal surface in Krebs solution. Current pulses of 1 nA (squares) were applied to the impaled cell, no observable membrane potential deflection were registered. In the presence of 1 mM octanol (add at arrow), R_i increased to 61.5 MΩ (the last square). Octanol also depolarized the tissue and concomitantly abolished the slow wave activity.

with the applied current amplitude. Addition of octanol (1 mM), which effectively blocked gap junction conductance, increased the R_i to 49.7±1.9 MΩ (n=5). The input resistance of the longitudinal muscle at the serosal surface was not significantly different from that in the middle of the layer.

When impalements were made at the submucosal surface of the ICC-CM preparations, current pulses of 1-5 nA in either the depolarizing or hyperpolarizing direction did not generate any recordable membrane potential perturbation in 58 impalements of 27 different ICC-CM preparations (Figure 8.1b). In the presence of 1 mM octanol, the R_i was increased to 65.2±3.1 MΩ (n = 9, Figure 8.1b).

When the submuscular ICC-smooth-muscle layer was removed from ICC-CM preparations, the CM preparations were obtained. When 1 nA depolarizing pulses were injected into the cell impaled near the submuscular surface, R_i between 0 and 4 MΩ (2.4±0.3 MΩ) were observed in 37 impalements of 8 different preparations. In the presence of 1 mM octanol, the R_i was increased to 51.7±4.3 MΩ (n = 4). The effects of octanol in all different preparations were completely reversible.

Space constants

In parallel with the high input resistance in the longitudinal muscle which suggested that longitudinal muscle cells were more electrically isolated than circular muscle cells, it was not feasible to detect any electrotonic current spread in the longitudinal muscle.

In contrast, the space constant, λ, determined by the equation derived from the double-electrode technique, was equal to 8.1±1.1 mm at the submucosal surface of the ICC-CM preparations (n = 12). The CM preparations were spontaneously quiescent with a resting membrane potential of 63.4±0.8 mV (n = 8). Resting membrane

Figure 8.2: *Simultaneous recordings of electrical activities in the LM and ICC-CM preparations*

a. Simultaneous intracellular recordings were made at the serosal surface of a LM preparation. Continuous SLAPs were observed. The distance between the two microelectrodes, Δx, was 1.4 mm (along the longitudinal axis of smooth muscle cells). The SLAPs in the two recording sites were very well entrained over a time course of 10 min (only a segment of the activity is shown). There was a difference of 4 mV in the resting membrane potentials at the two sites.

b. Simultaneous surface electrode recordings were made at the serosal surface of a LM preparation. The surface electrode technique employed in this experiment has previously been described [113]. Separations between adjacent electrodes, Δx, were 3.0 mm. Electrodes were placed along the longitudinal axis of smooth muscle cells. Burst-type activity was observed. It is conspicuous that the appearance of bursts is well co-ordinated but not synchronized.

c. Simultaneous intracellular recordings of slow wave activities at the submucosal surface of an ICC-CM preparation is shown. Slow wave activities at the two recording sites, separated by 2.0 mm, were perfectly synchronized at an identical resting membrane potential. The waveform of slow wave activities at the two sites were almost identical.

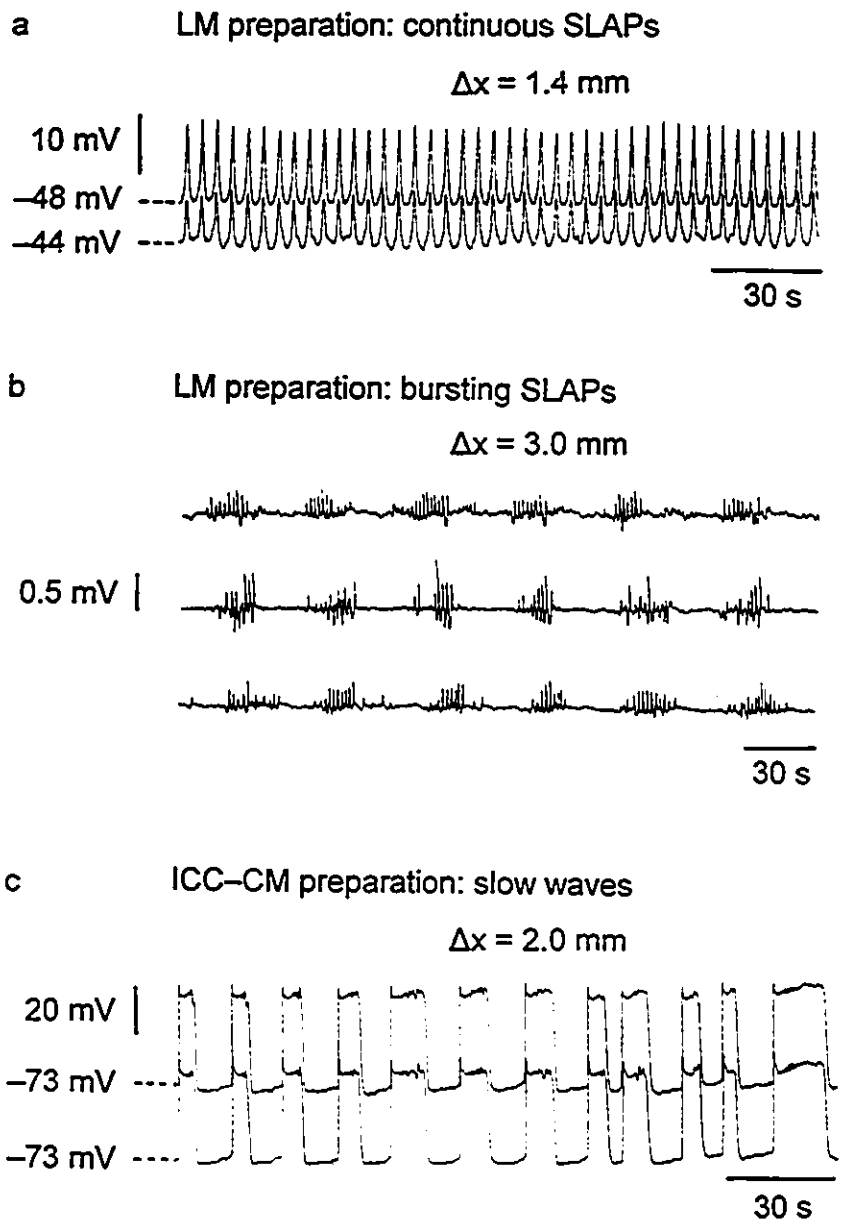
a
LM preparation: continuous SLAPs
Δx = 1.4 mm
10 mV
–48 mV
–44 mV
30 s
b
LM preparation: bursting SLAPs
Δx = 3.0 mm
0.5 mV
30 s
c
ICC–CM preparation: slow waves
Δx = 2.0 mm
20 mV
–73 mV
–73 mV
30 s

Figure 8.2

potentials at both recording sites were very often identical but a difference of less than 2 mV had occasionally observed (5 out of 27 paris of simultaneous impalements in 8 preparations). The space constant of the CM preparations was equal to 8.3±1.4 mm (n = 5) which was not statistically different from the space constant of the ICC-CM preparations. When approximately half of the circular muscle layer was removed from the CM preparations, space constant was determined to be 7.1±2.2 mm (n=3). Space constants were determined along the long axis of circular muscle cells in both the ICC-CM and CM preparations. Blockade the electrotonic current spread by 1 mM octanol reduced the space constant below any detectable level.

Phase relationship of electrical activities

The spike-like action potentials (SLAPs) generated spontaneously in the longitudinal muscle could appear in bursts (Figure 8.2b) or as continuous oscillations (Figure 8.2a). During the continuous oscillatory pattern, the SLAPs exhibited a frequency of 17.6±0.9 cpm at a resting membrane potential of −46.3±0.7 mV (n=14). The amplitude and duration of SLAPs were 16.5±1.1 mV and 1.7±0.2 s, respectively. In the burst-type activity, the burst durations ranged from 12 to 40 s with a bursting frequency of 1.6±0.4 burst/min (n=4). The characteristics of SLAPs within bursts were not significantly different from that appeared as continuous oscillations.

Although electrotonic coupling between longitudinal muscle cells was insignificant, the SLAPs generated spontaneously in the longitudinal muscle layer were coordinated. Simultaneous intracellular recordings illustrated that the SLAPs occurred at different resting membrane potentials (ranged 2–8 mV, n=18). The phase relationship of the SLAPs at the two recording sites were not constant but in the same direction (entrainment) over 90% of the time in all experiments (Figures 8.2a and

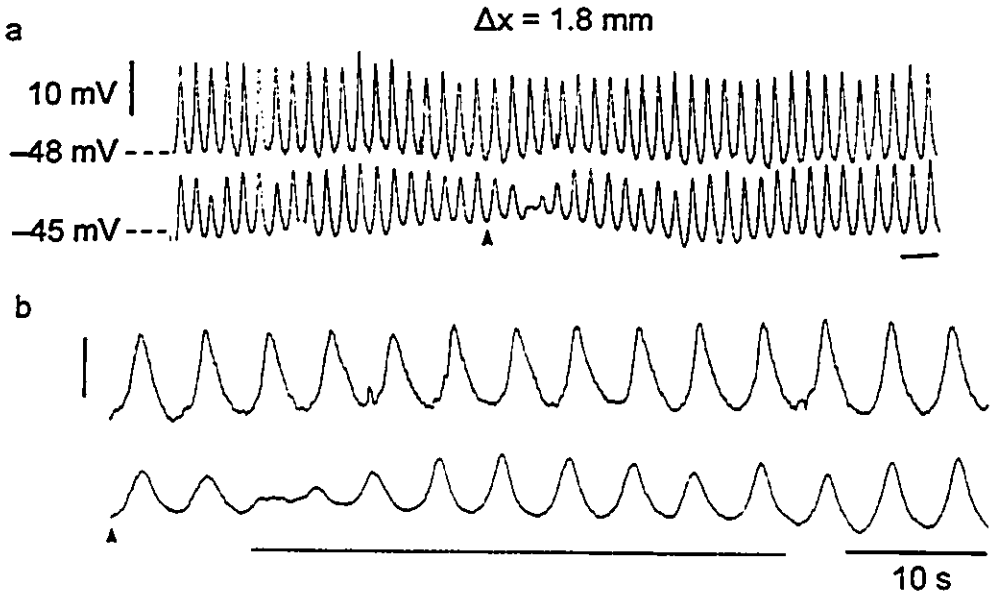

Figure 8.3: *Effects of oscillation amplitude on entrainment of SLAPs*

a. Simultaneous recordings were made at the myenteric surface of a LM preparation. Microelectrodes were separated by 1.8 mm (Δx). SLAPs were exhibited at a 3 mV difference of the resting membrane potential. The SLAPs were well entrained in the entire experiment except when (and shortly after) the amplitude of SLAPs reduced substantially at one recording site (the third oscillation after the arrow).

b. A segment of the simultaneous recordings shown in a. Arrow heads in a and b point at the same point. In the beginning of the dotted line, entrainment of the SLAPs at the two sites started to lose when the amplitude at one site (the bottom recording) was reduced significantly. As the amplitude of the SLAPs restored, the SLAPs gradually entrained. At the end of the dotted line, entrainment was restored and remained for the rest of the experiment (5 more min).

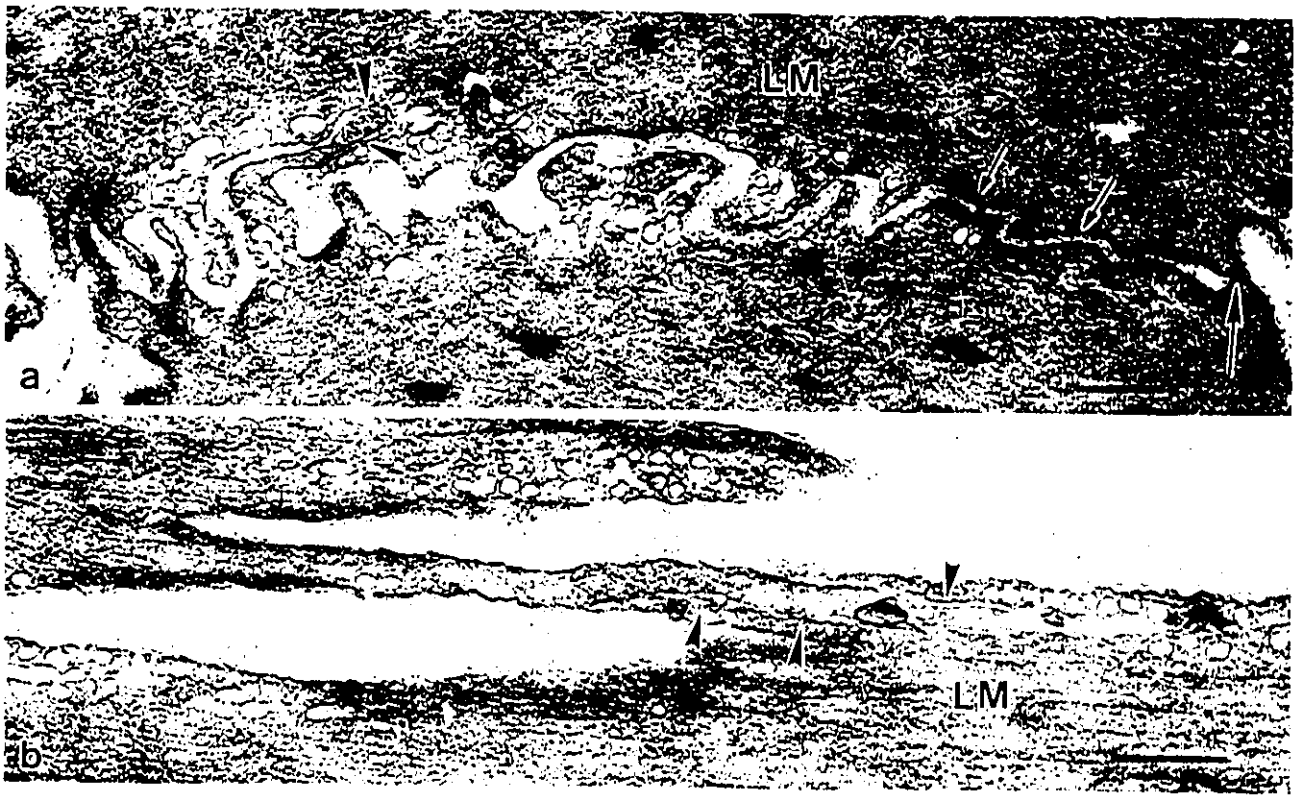

Figure 8.4: *Electron micrographs showing various intercellular contacts frequently observed between longitudinal muscle cells of canine proximal colon*

a. A cross section through two longitudinal muscle cells (LM). Three common types of intercellular contacts are shown: intermediate contacts (small arrows), a close apposition contact (large arrow; a close approximation between two cells, less than 10 nm), and a small interdigitation (arrowheads; a finger-like protrusion of the cell below invaginates into an indentation of the top cell). × 22000, bar 0.5 μm.

b. A longitudinal section through longitudinal muscle cells. A deep interdigitation junction (arrowheads) is formed by insertion of a long protrusion of a branched longitudinal muscle cell into an adjacent muscle cell. Multiple close apposition contacts (arrowheads) were observed in the extended areas of the cell protrusion with the indented cell. × 31,000, bar — 0.5 μm.

8.3). Separations of the two microelectrodes ranged from 1.0 to 2.8 mm (size limit of the mounted area). A direct correlation between the difference in resting membrane potential and the electrode separation was not observed (compare Figure 8.2a to Figure 8.3). Transient asynchronizations of the simultaneously recorded activities were observed when there was a change in the characteristics, such as amplitude, of the electrical activity in either one or both of the recording sites (Figure 8.3). Electrical activities were always re-entrained when the original characteristics of the activities were restored. During the burst-type activity, the appearance of bursts were, albeit asynchronized, very well co-ordinated (Figure 8.2b). Entrainment and co-ordination of SLAPs in either oscillatory pattern were affected neither by TTX nor by storing the tissue at 4°C for 24 hours.

In all ICC-CM preparations, the slow-wave-type action potentials (slow waves) recorded simultaneously at the submucosal surface were perfectly synchronized at an identical resting membrane potential (Figure 8.2c). In all preparations examined (n = 20), there were a constant phase lag between slow waves in each pair of recordings (separated by 1.4–3.5 mm) during the entire experiment (ranged from 4–35 min). The apparent propagation velocity of slow wave was 29.7±0.9 mm/s along the long axis of the circular muscle cells. Furthermore, the waveform of slow waves were almost identical in both recording sites (Figure 8.2c).

8.4.2 Electron microscopic observations

In the longitudinal muscle layer of the canine colon, extensive electron microscopic examinations revealed no identifiable gap junctions. Other intercellular junctions were therefore investigated to explore their roles in facilitating intercellular communication. Close apposition contacts and intermediate contacts were frequently observed.

Figure 8.5: *Electron micrographs showing the distribution of ICCs in the longitudinal muscle layer*

a. A cross section through longitudinal muscle cells at approximately half of the depth of the longitudinal muscle layer. Scattered ICCs were frequently observed in this region. × 4500, bar — 2 μm.

b. A medium magnification micrograph of an ICC interposed between two longitudinal muscle cells (LM). The phenotype of ICCs within the longitudinal muscle layer is identical to those associated with the myenteric plexus. A close apposition contact (large arrow) is observed between the ICC and an adjacent longitudinal muscle cell. Small arrows point at caveolae, a cellular feature distinguished ICCs from fibroblasts. × 18,500, bar — 1 μm.

c. An ICC-nerve bundle in the innermost subdivision of the longitudinal muscle layer. In this region, ICCs form close contacts (arrowhead) with nerves (N). ICC processes are connected to each other by gap junctions (double arrows), and to longitudinal muscle cells (LM) by close apposition contacts (arrow). × 12,300, bar — 1 μm.

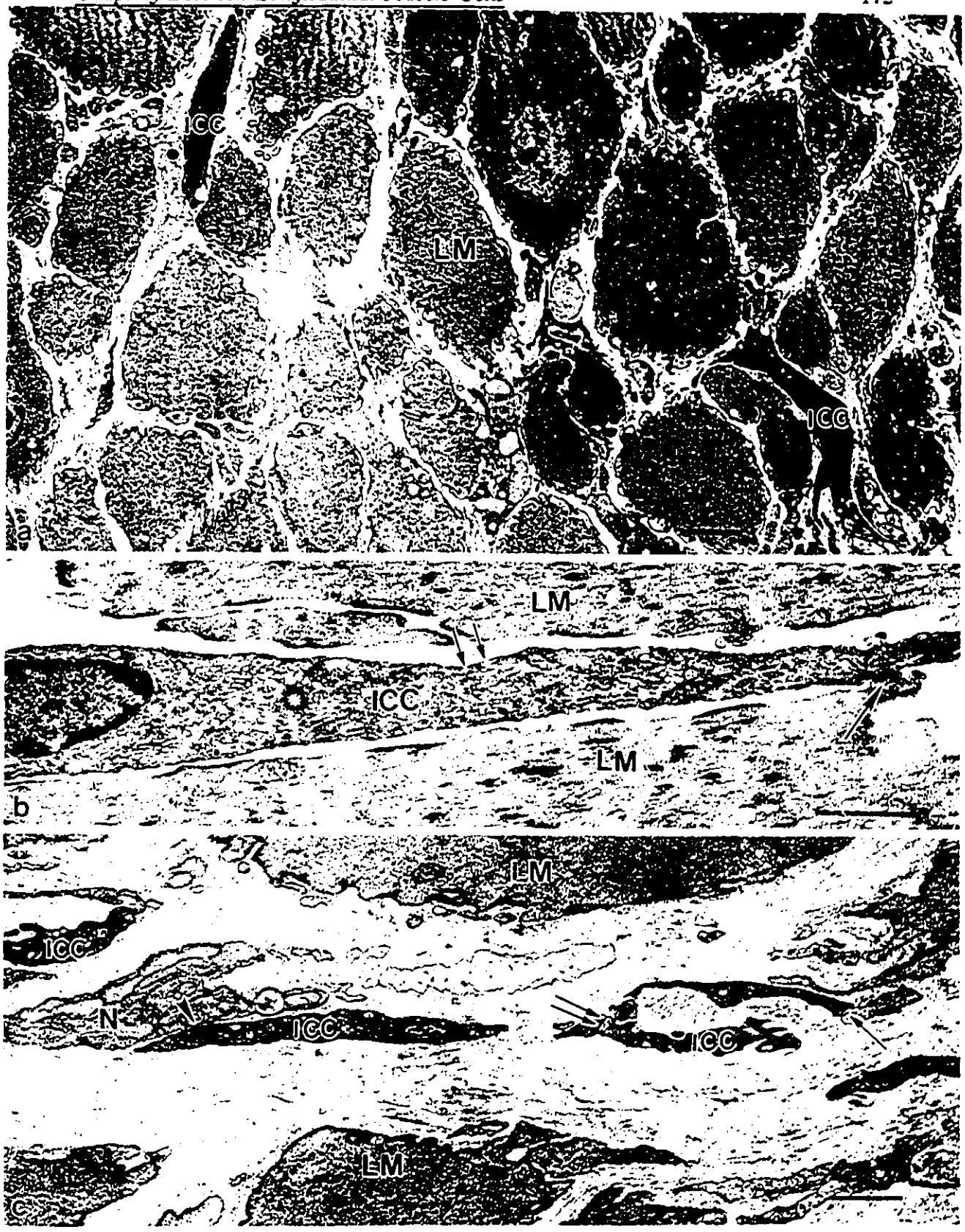

Figure 8.5

The longitudinal muscle cells were highly branched (Figures 8.4 and 8.5a). Long cylindrical projections, up to 4–5 μm in length (Figure 8.4b), very often invaginated into neighbouring longitudinal muscle cells forming extended interdigitation contacts (Figure 8.4b). In the interdigitations, multiple close apposition contacts between apposed membranes were often found (Figure 8.3b). Short thorn-like protrusions were numerous in longitudinal muscle cells (Figure 8.4a). Simple close apposition contacts (point-type, less than 10 nm) between membranes of adjacent thorn-like protrusions were frequently identified (Figure 8.4a). The contour of the membrane of longitudinal muscle cells were highly convoluted (Figure 8.4a). This convoluted contour created long stretches of extracellular gaps as narrow as 35 nm in width and running 2–8 μm in length. In these convoluted areas, intermediate contacts and close apposition contacts were abundantly observed on apposing membranes (Figure 8.4).

ICCs were frequently observed within the inner portion of the longitudinal muscle layer, up to half of its depth (Figure 8.4). These ICCs had a similar phenotype (Figure 8.5b) as that described in the myenteric plexus region previously [13]. ICCs within the longitudinal muscle layer were in gap junction contacts with each other (Figure 8.5c), and formed close contacts with smooth muscle cells and small nerves (Figure 8.5b, c). Some nerves, and their associated ICCs, were observed to connect to the nearby myenteric plexus (Figure 8.5c).

8.5 Discussion

8.5.1 Electrical communication between longitudinal muscle cells

Electrical communication between longitudinal muscle cells of canine colon was positively demonstrated. Spike-like action potentials (SLAPs) generated spontaneously in the longitudinal muscle cells were entrained 90% of the time over a distance of up to 2.8 mm along the long axis of the longitudinal muscle cells.

Entrainment of SLAPs was observed with a 2–8 mV difference of the resting membrane potential. Such a difference at two nearby recording sites (1–2.8 mm) indicates that electrotonic current spread between longitudinal muscle cells is minimal. This postulation is justified by the negligible space constant in the longitudinal muscle layer measured along the long axis of smooth muscle cells. In contrast, the space constant in the circular muscle layer is approximately 7–8.5 mm. The larger the space constant, the better the electrotonic coupling of the tissue is. The large space constant in the circular muscle layer constitutes a supportive evidence to substantiate our recently proposed hypothesis that the resting membrane potential gradient in the circular muscle layers is caused by electrical coupling of the circular muscle cells to the submuscular interstitial cells of Cajal (ICCs) and longitudinal muscle cells [110]. In addition, the largest space constant at the submucosal surface provides a electrical basis for the observation of a uniform resting membrane potential near the submucosal border of the circular muscle layers.

The input resistance, R_i, reflects the degree of electrical coupling of cells in the tissue. If the cells are three-dimensionally coupled by low resistance pathways via gap junctions, the injected current would dissipate into the coupled network and con-

sequentially no voltage deflection could be registered (i.e. $R_i = 0$). Thus, the higher the input resistance, the more electrically isolated cells in the tissue are. The R_i was 32.1 MΩ in the longitudinal muscle layer, 2.4 MΩ in the middle of the circular muscle layer and negligible at the submucosal surface of the circular muscle layer. These observations are consistent with the morphological observations that gap junctions are found abundantly only in the first 5–7 cells layers of the circular muscle layers [12, 13], are small and rare in the body of the circular muscle layer [13, 188, 114] and absence in the longitudinal muscle layer.

In the presence of octanol, after blockade of the gap junction conductance [142], the R_i relates closely to the input resistance of the impaled cell. The R_i of the impaled cell is larger at the submucosal surface than either in the body of the circular muscle layer or in the longitudinal muscle layer. R_i in the circular and longitudinal muscle layers are not significantly different. At the submucosal surface, a network of ICCs with associated branching smooth muscle cells (bSM) has been found to cover the entire submucosal border of the circular muscle layer [119]. Both ICCs and bSM consist of long slender processes and smaller cell bodies than ordinary smooth muscle cells in the circular and the longitudinal muscle layers. In the presence of octanol, gap junction channels were blocked. The measured R_i reflects mostly the input resistance of the impaled cell. The R_i of highly branched ICCs and bSM are conceivably to be larger than circular and longitudinal muscle cells. Hence, the difference of R_i of the impaled cell observed in the presence of octanol is consistent with the observations of the heterogeneity of cell morphology in the musculature.

Because SLAPs can be recorded in small isolated areas of longitudinal muscle. Each small piece of longitudinal muscle possesses an intrinsic oscillations whose characteristics vary from one area to another. That is, each small isolated piece of

the longitudinal muscle is an oscillator. Successful entrainment of the SLAPs in the longitudinal muscle depends on the characteristics of the local intrinsic oscillations. It was conspicuous from our experimental observation that oscillation amplitude is a critical determinant for proper entrainment.

8.5.2 Morphological basis for intercellular communication in the longitudinal muscle layer

In the longitudinal muscle layer of canine colon, no gap junctions has been identified. However, the existence of cytoplasmic continuity has been demonstrated by the spread of neurobiotin from a single injected longitudinal muscle cells to neighbouring cells [67]. In this study, close apposition contacts has been abundantly observed between longitudinal muscle cells. It is conceivable that these close apposition contacts constitute gap-junction-like structures which facilitate neurobiotin spread and electrical coupling. The hypothesis of the presence of gap- junction-like structures in the longitudinal muscle layer is consistent with the facts that in the presence of octanol (i) the spread of neurobiotin was inhibited and (ii) the input resistance was increased. These effects of octanol on the longitudinal muscle can be explained by the blockade of gap junction conductance. The electron-dense material observed in the gaps of close apposition contacts could embody connexons. Although Connexin 43 (Cx 43) has not been identified in the longitudinal muscle of canine colon using immunohistochemical methods, Cx 43 protein as well as Cx 43 mRNA have been identified in this area [106]. Because fluorescent signals of fine structures, like close apposition contacts, are likely below the detection limit of this method [128], Cx 43 still remains a legitimate candidate to constitute close apposition contacts.

In conclusion, electrical coupling between longitudinal muscle cells is first documented in the canine colon by direct demonstration of the entrainment of SLAPs. The mechanism of electrical coupling in the longitudinal muscle layer is unlikely the same as that in the circular muscle layer. In the circular muscle layer, intercellular communication is facilitated by low resistance pathways, constituting by electron microscopically identified gap junctions. The intercellular junctional resistance is considerably higher between longitudinal muscle cells than between circular muscle cells as indicated by the negligible electrotonic current spread, large input resistance, and entrainment of SLAPs with a different resting membrane potential in the longitudinal muscle layer. Such high resistance pathways are likely to be constituted by close apposition contacts.

Chapter 9

Communication Between Circular Muscle Lamellae of Canine Colon

9.1 Epitome

The circular muscle (CM) layer of canine colon is divided into circumferentially oriented lamellae separated by connective tissue septa. Communication between CM lamellae is necessary to generate propulsive phasic contractions which facilitate peristalsis. The submuscular ICCs are organized in a network covering the entire submucosal border of the CM layer. These submuscular ICCs are extensively coupled to the underlying branching smooth muscle (bSM) cells forming an ICC-bSM network. There is also an ICC network located in the myenteric plexus. The roles of the submuscular ICC-bSM network, the myenteric ICC network and the longitudinal

This chapter is in the final editing process and to be submitted to the Canadian Journal of Physiology and Pharmacology (authored by Louis Liu, Russell Ruo and Jan Huizinga. Contributions of Russell Ruo are discussed in section 2.2 of Chapter 2.

muscle layer in mediating communication across the CM lamellae were studied by simultaneous recordings with three surface electrodes using different types of muscle strip preparations. When the ICC-bSM network was intact, slow-wave-type action potentials (slow waves) were observed to be entrained both along and across CM lamellae. The CM layer devoid of the ICC-bSM network, the myenteric plexus and the longitudinal muscle (CM preparation) was spontaneously quiescent. Spike- like action potentials (SLAPs) evoked in the CM preparations by Ba^{2+} (0.5 mM) were entrained along CM lamellae (n = 3) but were not co-ordinated and even oscillated with different frequencies across the CM lamellae (n = 9). In the LM-CM preparations, in which the longitudinal muscle and the myenteric ICC network were intact, the Ba^{2+}-evoked SLAPs were not co-ordinated across CM lamellae but entrained within CM lamellae. In a step preparation, in which the ICC-bSM network was removed in part of the muscle strip, slow waves were observed to be entrained in areas with and without the ICC-bSM network when electrodes were positioned along a CM lamella. Separation of the muscle strip at the boundary where the ICC- bSM network was removed while the electrodes were still in place resulted in immediate disappearance of the slow waves in the area devoid of the ICC-bSM network indicating that the slow waves were propagated from the area with intact ICCs (n = 4). When electrodes were positioned across CM lamellae, synchronized slow wave activity was observed only in areas with the intact ICC-bSM network and quiescent activity was recorded in areas devoid of the ICC-bSM network (n = 9). These results demonstrate that CM cells are electrically coupled along a CM lamella, oriented circumferentially around the canine colon, but electrically insulated across CM lamellae. The submuscular ICC-bSM network, but not the longitudinal muscle nor the myenteric plexus, is essential for mediating communication between CM lamellae such that co-ordinated motility can

be exhibited in neighbouring CM lamellae through excitation-contraction coupling.

9.2 Introduction

In the gastrointestinal (GI) tract, the pacemaker activity originates in the myenteric plexus of the stomach [9] and the small intestine [82, 175], and in the submuscular plexus of the colon [38, 58, 60, 62, 110, 172]. Once the pacemaker activity is generated, it requires to propagate to the rest of the musculature where the contractile force is generated for propulsive movement. Responses of the circular muscle layer upon receipt of the pacemaker potential depend on the structural organization and characteristics of electrical coupling in the musculature. Propagation of the ring-like contraction generated in the circular muscle layer is cardinal for the peristaltic movement in the GI tract.

Septa, consist of connective tissue, have been identified in the circular muscle layer of the colon [140, 155] and the small intestine [153]. In the canine colon, connective tissue septa have also been observed in the circular muscle layer at the light microscopic level [67, 119, 193]. A recent study [119] observed a smooth ridge-and-groove contour at the submuscular surface of the circular muscle layer at the light microscopic level after selective accumulation of methylene blue by the submuscular interstitial cells of Cajal (ICCs). This observation leads to a postulation that the circular muscle layer is divided into circumferentially orientated lamellae separated by connective tissue septa. Using confocal microscopy, physical boundaries of circular muscle lamellae have recently been demonstrated by the discernable and abrupt boundaries of neurobiotin spread when neurobiotin was injected in a single cell at the myenteric border of the circular muscle layer [67].

In the canine colon, the slow-wave-type action potentials (slow waves) originate from the submucosal surface of the circular muscle layer [60, 62, 110, 172], and are phase-locked along the longitudinal axis [193]. Along the submucosal surface, the submuscular ICCs form a complete network covering the entire submuscular border of the circular muscle [45, 119]. These submuscular ICCs are intimately coupled to each other and to the underlying branching smooth muscle (bSM) cells with numerous gap junctions [12, 184], forming an ICC-bSM network. The nature of electrical interaction between circular muscle lamellae is unclear: are circular muscle lamellae electrically insulated by the connective tissue septa, and if so, what are the mediators for inter-lamellar communication? Knowledge to these questions is of particular importance because it is conceivable that communication between circular muscle lamellae is a fundamental necessity for the gut to produce co-ordinated motility for fulfilling its physiological functions.

The physical appearance of the submuscular ICC-bSM network suggests its possible role in mediating communication across the circular muscle lamellae in the longitudinal direction of the colon. There is another ICC network located at the myenteric plexus [13, 188] whose function in communication has recently been investigated. Evidence has been presented that the myenteric ICC-network is responsible for mediating communication between the circular and the longitudinal muscle layers (Chapter 7). However, its role in inter-lamellar communication has not been explored. In this study, we examined if the circular muscle lamellae of canine colon were discrete, electrically insulated units. Furthermore, the roles of the submuscular ICC-bSM network, the myenteric-ICC network and the longitudinal muscle layer in mediating inter-lamellar communication between circular muscle lamellae were investigated by simultaneous surface-electrode recordings using different types of muscle

strip preparations.

9.3 Materials and methods

9.3.1 Tissue acquisition and preparation

Mongrel dogs of either sex were killed by an overdose of sodium pentobarbital (100 mg/kg) given intravenously. Approximately 10 cm of proximal colon, starting from 5 cm distal to the ileocecal junction, was removed. The colon was opened flat. Colonic contents were carefully removed in Krebs solution equilibrated with 95% O_2/5% CO_2. The clean segment was then pinned flat onto the Sylgard (184 silicone elastomer, Dow Corning Corporation, Michigan, U.S.A.) of a dissecting dish which was filled with continuously aerated Krebs solution. The mucosa and the submucosa were carefully removed by sharp dissection. Removal of the submuscular ICC network and a few layers of adjoining smooth muscle cells (ICC-bSM network) resulted in the *LM-CM preparation* which is composed of the longitudinal and the circular muscle layers. The *CM preparation* was prepared by further removal of the longitudinal muscle layer. The *step preparation* was prepared by removing part of the submuscular ICC-bSM network of the full thickness musculature (see schematic illustrations in Figures 9.4 and 9.5).

9.3.2 Surface electrode set-up

The dissected tissue was pinned onto the Sylgard of an organ bath, filled with 500 ml of continuously aerated Krebs solution. The organ bath was incubated by a warm water bath which kept the bathing solution at 37.0±0.5°C. Suction electrodes were used to measure electrical activities in different muscle strip preparations. Gentle

suction was provided by a mechanical pump (Cast: D0A-P161-AA, Benton Harbour, Michigan). Both the recording and the ground electrodes were chloridized silver (Ag-AgCl) wires (0.38 mm in diameter). The tip of the Ag-AgCl wire was tapered to less than 0.1 mm in diameter. The recording electrode was insulated by a flexible plastic tubing with outer and inner diameters of 1.5 mm and 0.5 mm, respectively. The electrical activities were recorded by a Gould inkwriting recorder (2800S).

9.3.3 Drugs and solutions

The composition of the Krebs solution was (mM): NaCl — 120.3; KCl — 5.9; $CaCl_2$ — 2.5; $MgCl_2$ – 1.2; $NaHCO_3$ — 20.2; NaH_2PO_4 — 1.2 and glucose — 11.5. Stock solutions of Ba^{2+} (0.1 M $BaCl_2$; Fisher Scientific Company, Fair Lawn, N.J., U.S.A.) and verapamil (1 mM verapamil hydrochloride; Sigma, St. Louis) stock solution were prepared with de- ionized distilled water. In the Ba^{2+} experiments, Ba^{2+} stock solution was added to Krebs solution in the tissue bath reaching a concentration, ranged from 0.5 to 2 mM, until steady electrical activity was observed.

9.3.4 Result presentation and statistical analysis

The electrical activity was characterized by the frequency, duration (measured at the half maximum amplitude) and amplitude. All the data were expressed as mean±SEM. 'n' represents the number of dogs used. The statistical significant differences between data sets were determined by Student's t-tests.

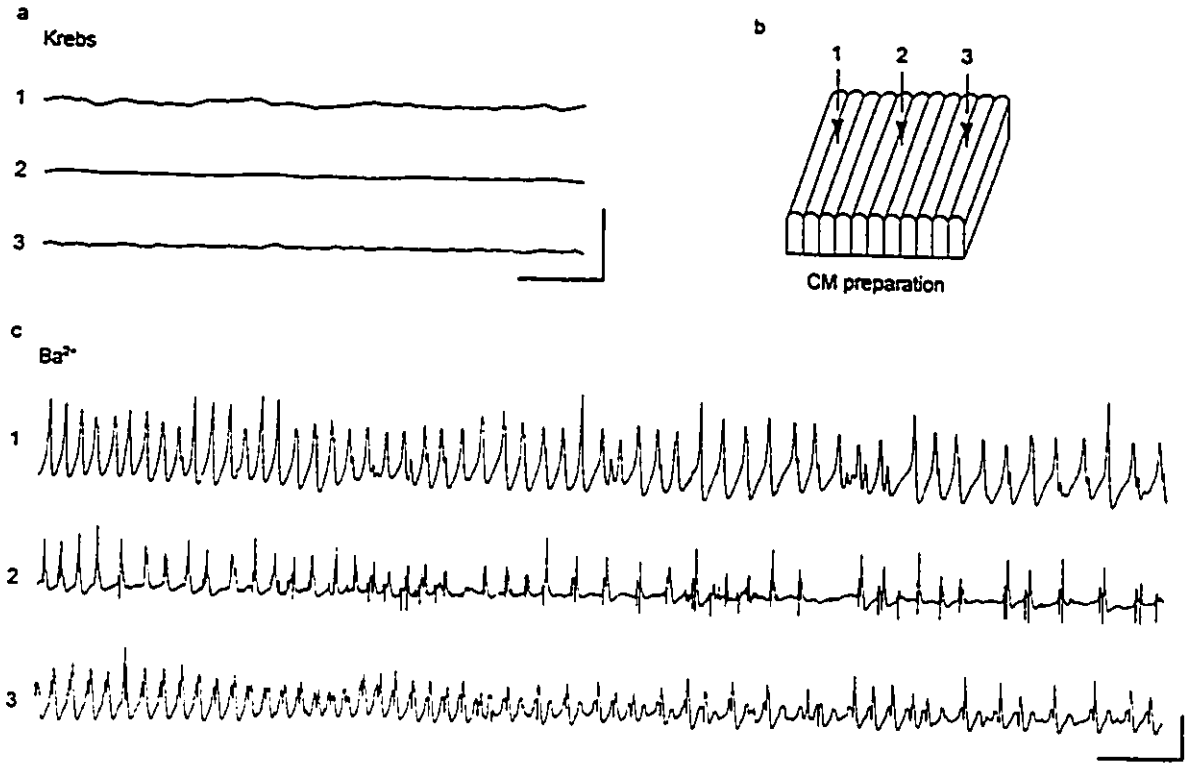

Figure 9.1: *Simultaneous recordings across circular muscle lamellae*
Electrical activity of the CM preparations was spontaneously quiescent in Krebs solution (a). Three electrodes (arrows in b) were placed on the surface of a CM preparation which is schematically illustrated in b. Distances between adjacent electrodes were 5 mm. In the presence of 0.5 mM Ba^{2+}, spike-like action potentials (SLAPs) were evoked (c). During the experiment, SLAPs were first evoked at electrode 1, approximately 10 min before SLAPs appeared in the other two recording sites (traces not shown). When the Ba^{2+}-evoked SLAPs became steady in all three recording sites (c), the SLAPs were not co-ordinated. Calibration bars: horizontal – 30 s; vertical – 1 mV.

9.4 Results

9.4.1 Electrical isolation between circular muscle lamellae

The hypothesis that the circular muscle lamellae were discrete units, hence electrically isolated, was examined in the CM preparation, in which the submuscular ICC-bSM network, the longitudinal muscle layer and the myenteric plexus were removed. The CM preparations were spontaneously quiescent, similar to previously documented observations [113, 171]. Blockade of potassium conductance by Ba^{2+} evoked characteristic electrical activity [112]. The Ba^{2+}- evoked spike-like action potentials (SLAPs) in the circular muscle layer oscillated at 5.8±1.4 cycles/min (cpm) with amplitude and duration equal to 0.9±0.4 mV and 2.8±0.5 s, respectively (n = 9). The Ba^{2+}-evoked SLAPs were abolished by 1 μM verapamil.

When electrodes were placed across circular muscle lamellae, the SLAPs recorded simultaneously by three electrodes were distinctly unco-ordinated (Figure 9.1) even at a separation as close as 3.5 mm. When the preparations were cut such that the three recording sites were physically isolated while the electrodes were still in place, the association and characteristics of the Ba^{2+}-evoked SLAPs did not significantly change at the these recording sites, indicating no electrical interaction between CM lamellae in intact CM preparations.

9.4.2 Electrical coupling within circular muscle lamellae

When the three surface electrodes were placed within a circular muscle lamella of the CM preparations, the Ba^{2+}-evoked SLAPs at the three recording sites were entrained with a constant phase relationship for as long as 45 min during the entire experiment (Figure 9.2). Entrainment of electrical activity was observed for a separation as far

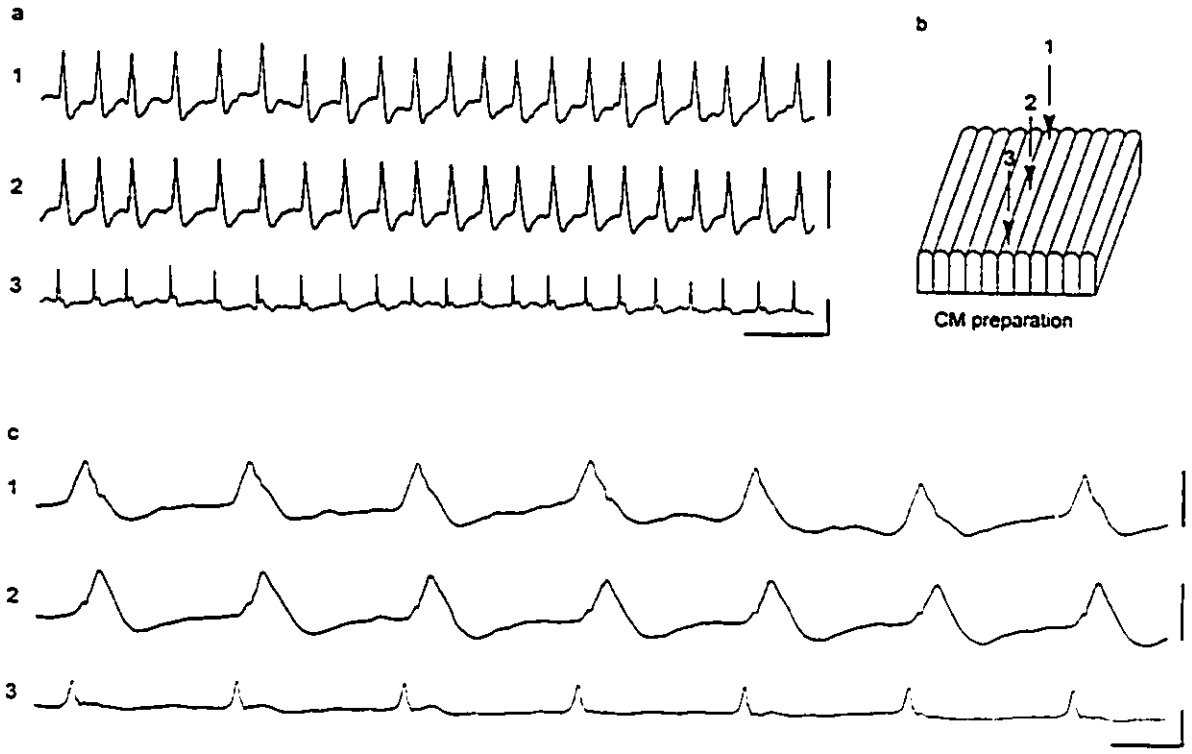

Figure 9.2: *Simultaneous recordings along circular muscle lamella*
The CM preparation were spontaneously quiescent in Krebs solution. Beginning of (a) shows Ba^{2+}-evoked SLAPs along a circular muscle lamella. The three electrodes (arrows in b) were placed on the surface of a CM preparation along a circular muscle lamella as schematically illustrated in b. Distances between adjacent electrodes were 5 mm. The SLAPs evoked at the three recording sites were entrained with a constant phase relationship as illustrated in (c) with a faster chart speed. Note that SLAPs in both electrodes 1 and 3 lead SLAPs in electrode 2. Calibration bars: horizontal – (a) 30 s, (c) 5 s; vertical – 1 mV.

as 16 mm. The characteristics of the Ba^{2+}-evoked SLAPs were the same as the last experimental group. The frequency, amplitude and duration were 5.6±0.8 cpm, 1.2±0.3 mV, and 3.1±0.4 s, respectively (n = 3). These observations suggested that circular muscle lamellae were electrically insulated from one another but electrically coupled within each lamella.

9.4.3 Does the myenteric ICC network play a role in communication between circular muscle lamellae?

Electrical insulation between circular muscle lamellae was also observed in LM-CM preparations in which the longitudinal muscle, the circular muscle (with the submuscular ICC-bSM network removed) and the myenteric ICC-network were intact. In Krebs solution, all LM-CM preparations (n = 4) were spontaneously quiescent at the submucosal surface of the circular muscle layer. When three electrodes were placed in a L-orientation, such that two electrodes were within a CM lamella and two were across CM lamellae (see Figure 9.3), the Ba^{2+}-evoked SLAPs were entrained within the same circular muscle lamella (with electrode separation up to 18 mm) and unco-ordinated when recordings were made from different lamellae (n = 4). The characteristics of the Ba^{2+}-evoked SLAPs in the LM-CM preparations were not different from that evoked in the CM preparations although burst-type activity was more frequently observed in the LM-CM preparations.

Since the LM-CM preparations were composed of the intact longitudinal muscle layer and myenteric plexus, it was clear that these structures did not play a role in mediating communication between circular muscle lamellae. The role of the submuscular ICC-bSM network to facilitate inter-lamellar communication in the circular muscle layer was studied with step preparations.

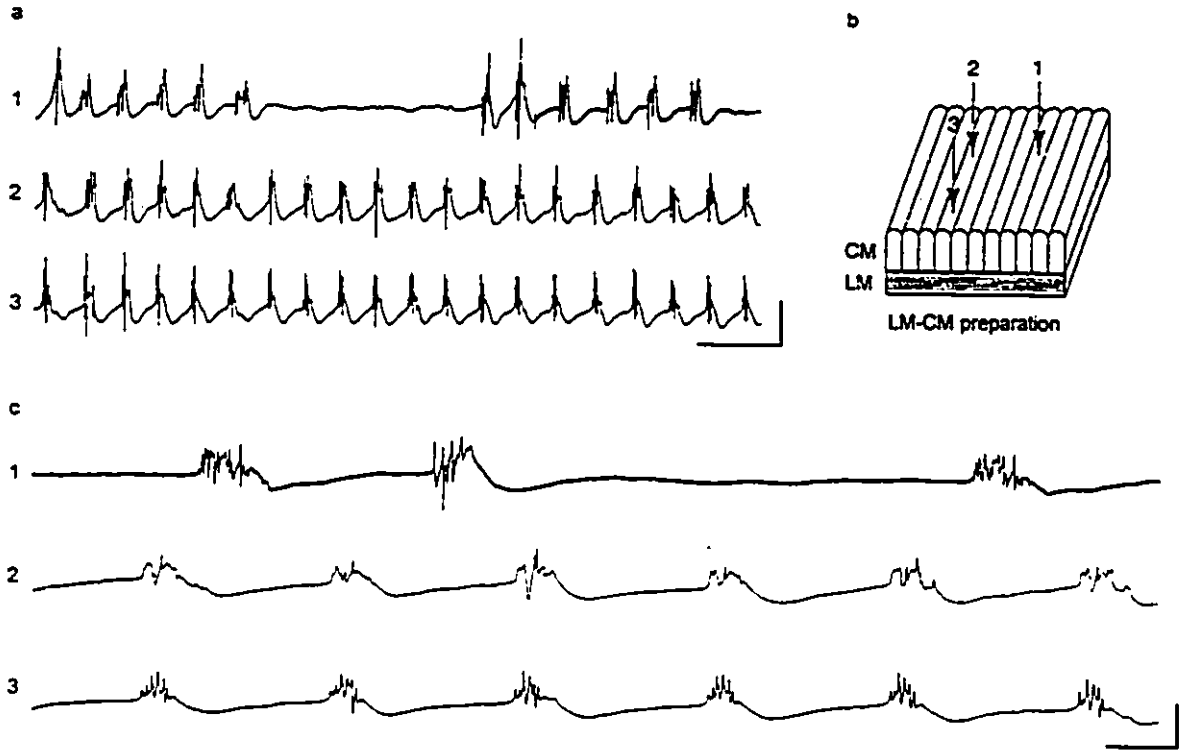

Figure 9.3: *Simultaneous recordings of electrical activity across and along circular muscle lamellae*

Three electrodes were placed in a L-orientation (b) to study electrical coupling across and along lamellae simultaneously. The LM-CM preparations, schematically illustrated in b, were spontaneously quiescent in Krebs solution when recordings were made at the submucosal surface of the circular muscle layer. In the presence of 0.5 mM Ba^{2+}, the Ba^{2+}-evoked SLAPs were not co-ordinated across lamellae (electrodes 1 and 2; 3.5 mm apart) and generally exhibited different patterns of electrical activity (a). Note that burst-type activity was observed at electrode 1. The Ba^{2+}-evoked SLAPs were very well synchronized along a circular muscle lamella (electrodes 2 and 3; 12.5 mm apart). Synchronization of the SLAPs recorded by electrodes 2 and 3 are clearly illustrated in c with a faster chart speed. Calibration bars: horizontal — (a) 30 s, (c) 5 s; vertical — 1 mV.

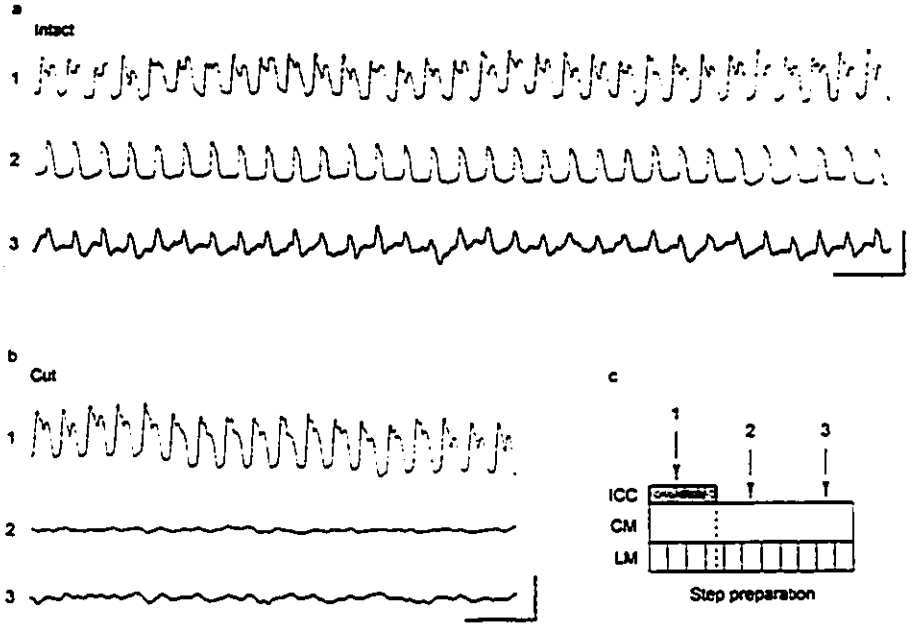

Figure 9.4: *Electrical activities recorded simultaneously along a circular muscle lamella of a step preparation*

The submuscular ICC-bSM network was removed from part of the preparation resulting in an area with the circular muscle layer exposed. Electrical activity was recorded along a circular muscle lamella. Electrode 1 was recorded from the intact submuscular ICC-bSM network area; whereas, electrodes 2 and 3 were recorded from the circular muscle exposed area. The distance between electrodes 1–2 and 2–3 were 8 mm and 7 mm, respectively. The configuration of the step preparation and electrode orientation are schematically illustrated in c. When the step preparation was intact, electrical activity was observed to be entrained at all three recording sites (a). The area with the intact ICC-bSM network was separated completely (along the dotted-line shown in c) from the circular muscle area while electrodes were still in place. Electrical activity at the same recording sites as in (a) is demonstrated in (b). This procedure immediately resulted in complete abolition of the slow wave activity in the circular muscle area devoid of the submuscular ICC- bSM network (electrodes 2 and 3 in b). Hence, the slow wave activity recorded in the circular muscle exposed area in the beginning of the experiment was propagated from the intact submuscular ICC-bSM network area. Calibration bars: horizontal — 30 s; vertical — 1 mV.

Table 9.1: *Characteristics of the slow wave activity in the step preparations*

	along lamellae		across lamellae	
	ICC	CM	ICC	CM
Frequency (cpm)	6.1±0.9	6.0±0.9	6.1±0.3	- - -
Amplitude (mV)	1.1±0.4	0.9±0.3	1.9±0.6	- - -
Duration (s)	4.2±0.8	3.5±0.5	3.6±0.3	- - -

n=4. ICC: recorded from the submuscular ICC-bSM network area; CM: recorded from the circular muscle exposed areas with the ICC-bSM network removed. Electrical activity was recorded in step preparations with three surface electrodes placed either along or across circular muscle lamellae. Surface electrodes were placed at the submucosal surface of the circular muscle layer. Spontaneous slow waves were observed in all recording sites when electrodes were placed along lamellae. However, the slow waves did not propagate across lamellae into the areas without intact submuscular ICC-bSM network. Electrical acitivty in the intact ICC-bSM network areas is not statistically significant difference from that in the CM areas.

9.4.4 Role of the submuscular ICC-bSM network in communication between circular muscle lamellae

In the step preparations, in which the submuscular ICC-bSM network was removed in part of the preparations, three electrodes were placed either along a lamella or across septa in different lamellae to study electrical coupling of the electrical activity.

Along a circular muscle lamella

Simultaneous recordings within a circular muscle lamella with the electrodes oriented circumferentially revealed the occurrence of slow-wave-type action potentials (slow waves) in the areas with and without an intact submuscular ICC- bSM network. Slow waves recorded simultaneously at the three recording sites within a circular muscle lamella were observed to be entrained (Figure 9.4) with an apparent propagation velocity (v_p) of 8.1±0.9 mm/s (n = 4).

When the portion devoid of the ICC-bSM network was separated from the portion with the intact network while keeping the surface electrodes in place, the slow wave activity in the area devoid of the ICC-bSM network immediately disappeared (Figure 9.4). This illustrated that the slow waves recorded in the area devoid of the ICC-bSM network propagated from the area with the intact submuscular ICC-bSM network.

Across septa in different circular muscle lamellae

When electrodes were positioned across circular muscle lamellae, the slow waves were synchronized only in areas with the intact ICC-bSM network but quiescent in all preparations with the ICC-bSM network removed (n = 9; Figure 9.5a). The apparent propagation velocity (v_p) of the slow wave activity in areas with the intact ICC-bSM network was 1.5±0.2 mm/s. The viability of the preparations at the quiescent spots was verified by their ability to generate Ba^{2+}-evoked SLAPs. In the presence of 0.5 mM Ba^{2+}, the characteristics of the SLAPs were similar to that in the CM preparations (see Table 9.1), despite the more frequent occurrence of burst-type activity. The SLAPs were not synchronized with the slow wave activity recorded in the area with the intact ICC-bSM network. In some preparations, both the frequency and the

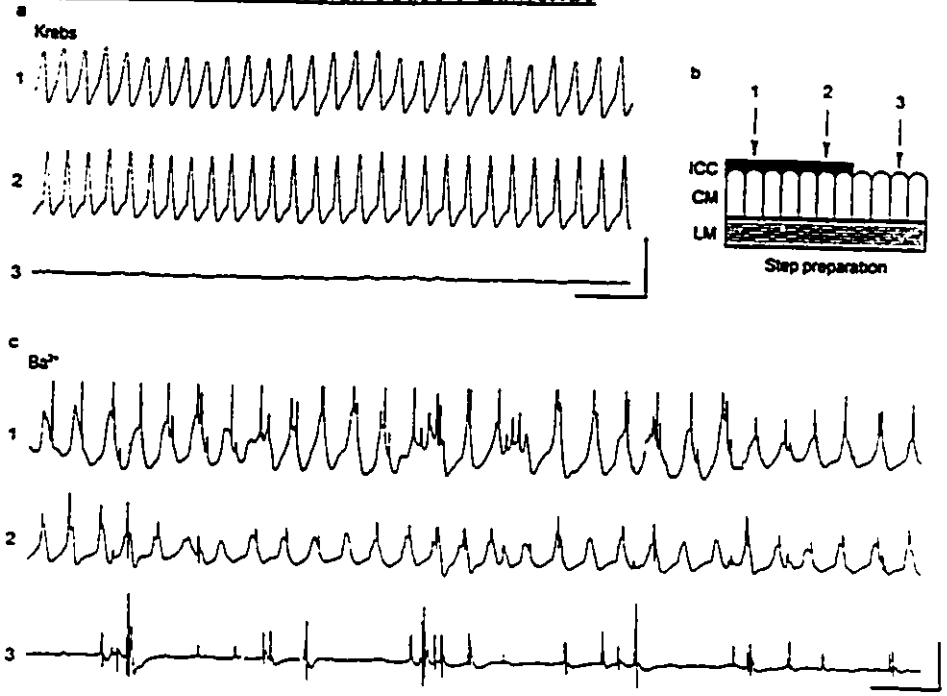

Figure 9.5: *Electrical activity recorded simultaneously across circular muscle lamellae of a step preparation*

Electrodes 1 and 2 were placed on the surface of the step preparation where the submuscular ICC-bSM network was intact. Electrode 3 recorded from the area with the circular muscle exposed. Distances between electrodes 1–2 and 2–3 were 4.5 and 6 mm, respectively. The configuration of the preparation and electrode orientation are schematically depicted in b. The slow wave activity recorded from the intact ICC-bSM network was synchronous with an apparent propagation velocity of 1.7 mm/s (a). In Krebs solution, the circular muscle was spontaneously quiescent and the slow wave activity did not propagate across circular muscle lamellae from the intact ICC-bSM network area into the circular muscle (a). In the presence of 0.5 mM Ba^{2+}, the slow wave activity with superimposed spikes remained entrained in the area with intact ICC-bSM network; whereas, Ba^{2+}-evoked SLAPs were observed in the circular muscle exposed area (c). Note that, at electrode 3, burst-type activity was observed which was distinctly different from the continuous slow wave activity at electrodes 1 and 2. Hence, the SLAPs were not electrically coupled to the slow wave activity recorded by electrodes 1 and 2. Calibration bars: horizontal — 30 s; vertical — 1 mV.

oscillatory pattern in the area with the intact ICC-bSM network were different from that in the area without the ICC-bSM network (Figure 9.5b).

9.5 Discussion

9.5.1 Submuscular ICC-bSM network mediates inter-lamellar communication

Simultaneous recordings in different muscle strip preparations demonstrate that the circular muscle lamellae are electrically insulated from each others and that the intact submuscular ICC-bSM network, but not the myenteric ICC-network, is essential for inter-lamellar communication across circular muscle lamellae.

Structural investigations at the light microscopic level suggest that the width of circular muscle lamellae in the dog colon ranges from 0.5 to 2 mm [67, 193]. Since the Ba^{2+}-evoked SLAPs in the CM preparations were not co-ordinated when recordings electrodes were placed across circular muscle lamellae, these lamellae were electrically insulated. However, within a circular muscle lamella, circular muscle cells were electrically coupled as indicated by synchronized Ba^{2+}-evoked SLAPs along circular muscle lamella. Hence, a functional definition of the circular muscle lamella can be proposed as an electrically insulated circular muscle bundle oriented circumferentially around the gut. Because the Ba^{2+}-evoked SLAPs were not co-ordinated across circular muscle lamellas at a distance as close as 3.5 mm (limited by the physical dimension of the surface electrodes used), the width of a circular muscle lamella must be less than 3.5 mm.

In the LM-CM preparations, in which the longitudinal muscle and the myenteric plexus are intact, electrical activities recorded across septa are not coupled, il-

lustrating that neither the myenteric plexus nor the longitudinal muscle is responsible for inter-lamellar communication in the circular muscle layer. When the submuscular ICC-bSM network is intact, both the slow waves and the Ba^{2+}- evoked SLAPs are entrained across circular muscle lamellae. Hence, the submuscular ICC-bSM network is essential and sufficient for mediating communication across circular muscle lamellae. Consistent with our observations, in the cat colon, it has been reported that longitudinal coupling of the slow wave activity requires the integrity of "the interface between the submucosa and muscularis propria [48]."

The ICC-network at the myenteric plexus has recently been demonstrated to mediate communication between the circular and the longitudinal muscle layers (Chapter 7). It was observed during the course of this study that in the LM-CM and the step preparations, in which the longitudinal muscle layer and the myenteric plexus are intact, burst-type spiking activity was more likely to be observed in the presence of Ba^{2+} (compare Figure 9.1 to Figure 9.5). Burst-type activity is more characteristic for longitudinal muscle [41, 62, 157]. It is likely that in the presence of Ba^{2+}, the burst-type activity recorded in the circular muscle is under the influence of the longitudinal muscle activity. However, it still remains obscure why the ICC-network at the submucosal border of the circular muscle layer is more effective for inter-lamellar communication than the ICC-network at the myenteric border which is responsible for inter-muscle-layer communication. This difference may relate to their different associations with the adjacent smooth muscle cells since the ICC-bSM network observed only at the submucosal but not at the myenteric border.

9.5.2 Apparent slow wave propagation along and across circular muscle lamellae

Since the slow wave activity can be recorded from small isolated areas when the submuscular ICC-bSM network is intact, the phase difference between the slow waves at various recording sites does not indicate propagation of the slow waves from one recording site to another site. Such a difference is a consequence of entrainment of electrical oscillations with different intrinsic characteristics at nearby sites (see [51, 161] for discussion). This theoretical prediction is consistent with our experimental observation that the phase lag relationship of electrical activities at different recording sites is not always lagging in the same direction; that is, if activity in electrode 1 lags activity in electrode 2, it does not necessarily imply that activity in electrode 2 would also lag activity in electrode 3 (see Figure 9.2). The leading site is arbitrarily defined as the hot spot from which the activity originates in the temporal sense. This hot spot may shift in time as the characteristics of the intrinsic oscillations vary. A parallel discussion on the origin of the slow waves from discrete, multiple pacemaker foci has been documented in the canine stomach [9]. The term, *apparent* propagation velocity (v_p, as discussed previously [48, 162]), is employed to describe the phase lag relationship of electrical activities at adjacent recording sites.

The slow waves (with or without superimposed spikes on the plateaus) are coherent with the phasic contractions of the circular muscle layer [4, 62, 176]. Thus, the v_p of slow waves is associated with the propagation of the contractile wave *in vivo*. The v_p of slow waves of the dog colon was 8.1 mm/s in the circumferential direction and 1.5 mm/s in the longitudinal direction. These results are consistent with v_p's obtained from the dog colon with the microelectrode technique [159], and are in the same order of magnitude as those in the cat colon [43, 48]. It is conceivable that

the larger v_p in the circumferential than in the longitudinal direction ensures near simultaneous contraction around the circumference to facilitate ring-like contractions during peristalsis.

9.5.3 Physiological significances of the lamellar structure in the circular muscle layer

The notion that the low-resistantly coupled submuscular ICC-bSM network could serve to dissipate local active current such that differentiation of motor activity in the longitudinal direction of the gut can be achieved has recently been discussed [107]. ICCs are extensively innervated [12, 45, 70, 180]. Their roles in neural modulation of smooth muscle excitation has been addressed [147]. Recently, a nerve-ICC-smooth-muscle functional unit in the GI tract has been proposed based on the morphological association among these three cell types [70]. Having the same structure to mediate communication between circular muscle lamellae probably makes the neural modulation of GI motility to be more effective. Hence, the electrically insulated circular muscle lamellae can facilitate regional neural excitations or relaxations without interfering either the upstream or the downstream motility of the GI tract.

In summary, this documentation presents the first evidence for the existence of discrete, electrically insulated circular muscle lamellae oriented around the circumference of the canine colon where the inter-lamellar communication is mediated by the submuscular ICC-bSM network. The lamellar structure of the circular muscle layer conceivably facilitates differentiation of motor activity in the longitudinal axis of the intestine.

Chapter 10

Concluding Remarks

10.1 Pacemaker roles of ICCs in the intestine

Although the absolute proof that ICCs are the pacemaker cells of the gastrointestinal tract is awaiting the results from studies using isolated single ICCs, experimental evidence presented in this dissertation ascertain their role in the generation of pacemaker activity. During the course of my Master's studies, I demonstrated that the circular smooth muscle cells are excitable and play an active role in conducting the colonic slow waves which are triggered by the pacemaker potentials originating from the submuscular ICC-bSM network. Observations presented in Chapter 3 of this dissertation positively correlate the disruption of the pacemaker activity to the selective lesioning of the submuscular ICCs. The cellular resolution of this study is probably the highest one can attain in tissue because only ICCs, but not nerves nor smooth muscle cells, are selectively removed (lesioned) from the pacemaker activity generating system. Nevertheless, studies using isolated cells are indispensable to unequivocally prove ICCs as the gastrointestinal pacemaker cells since the possibility of

inconspicuous damage imposed on other cell types cannot be absolutely eliminated in the methylene blue study.

In the canine colon, branching cells, tentatively identified as ICCs, have been enzymatically dispersed from the circular muscle layer near the submucosal border. Although spontaneous voltage [104] and calcium [148] oscillations have been observed in these branching cells, these oscillations not only lack the characteristic pacemaker frequency but also are completely abolished by L-type Ca^{2+}-channel blockers. Hence, the spontaneous oscillations identified in these isolated branching cells do not possess the properties of the pacemaker activity observed in the same tissue. Therefore, it is either not yet able to isolate the pacemaker cells or the isolated pacemaker cells are not in the condition that the pacemaker activity can be recorded, as generation of the pacemaker activity may rely on interaction between more than one cell.

10.2 The nature of the intestinal pacemaker activity

The rhythmicity of the intestinal slow waves has previously been hypothesized to be regulated by a biochemical clock sensitive to the concentration of intracellular cAMP [92]. An advancement in characterizing the frequency regulatory mechanism of the intestinal pacemaker activity has been made in Chapter 4 where the L-type calcium channel blocker insensitive upstroke potentials have been demonstrated to be sensitive to Ca^{2+} released from the endoplasmic reticulum (ER). Specifically, the frequency of the upstroke potentials, which are triggered by the pacemaker component (see Figure 1.3), is in phase with the rate of Ca^{2+} release from the ER. This L-type Ca^{2+}-channel-blocker insensitive but ER-Ca^{2+} dependent pacemaker component of

the slow wave activity is consistently found in both the canine colon (Chapter 4) and the mouse small intestine (Chapter 5). Although similar experiments should be repeated in other systems to establish a generalized theory, it is not inconceivable that the pacemaker activity of the gastrointestinal tract is fingerprinted by such an component.

10.3 Pacemaker channels for the generation of the intestinal slow waves

In the canine colon, the pacemaker component is hypothesized to be initiated by activation of a type of non-specific cation channels [135, page 229]. The hypothesis is put forward with the observations that the pacemaker component is: (i) resistant to organic L-type calcium channel blockers, such as nifedipine, D600, verapamil, nitrendipine, etc. [7, 93, 194], (ii) inhibited by metal ions, such as Ni^{2+} and Cd^{2+} [92, 7], and (iii) resistant to voltage changes from -120 to -40 mV. The pacemaker component is also aboiished by removal of extracellular Ca^{2+} [7, 93]. Furthermore, evidence presented in Chapter 4 indicate that activation of the pacemaker component is dependent on the Ca^{2+} released from the endoplasmic reticulum. All of the above described characteristics of the pacemaker channels in the canine colon are the exact descriptions of the type of non-selective cation channels identified by Loirand *et al.* [122] in smooth muscle cells isolated from the rat portal vein. This study encourages the search for a similar type of channels in isolated cells of the dog colon.

The L-type calcium channel blockers resistant property of the pacemaker channels has recently been challenged by a study which argues that the "nifedipine resistance of the upstroke depolarization could be due to the voltage dependence of the

block of Ca^{2+} channels by dihydropyridines." [194, page 321] However, initiation of the pacemaker component persists in the presence of glucamine and nitredipine even when the resting membrane potential of the tissue was depolarized by increasing the extracellular K^+ (see Figure 3.2B) or by extracellular field stimulation using the partition chamber (personal communication, Farraway, L.); under these conditions, the resting membrane potential decreased to approximately where the plateau potential of the slow wave activity in the control condition. Hence, it is unlikely that nifedipine, verapamil or nitredipine, can abolish the slow wave plateaus but cannot block the initiation of the slow waves at the same membrane potential if they are both mediated by L-type Ca^{2+} channels. Until more direct and unequivocal evidences of classes of ion channels can be characterized from positively identified isolated ICCs (or other cell types which possess ion channels sharing the same properties of the pacemaker channels observed in tissue), a type of non-specific cation channels is still the most likely candidate as the intestinal pacemaker channels.

10.4 Role of ICCs as communicating cells

While studies devoted to the investigation of the pacemaker role of ICCs are abundant in the literature, evidence for the role of ICCs in facilitating intercellular communication is negligible. Because of the branching morphology of ICCs and their topographical relationship to nerves and smooth muscle cells, ICCs present themselves as ideal communicating cells. In my Master's thesis [108], the resting membrane potential gradient observed near the myenteric border of the circular muscle is hypothesized to be caused by electrical coupling of the circular muscle cells to the more depolarized longitudinal muscle cells situated at the other side of the myenteric plexus. The validity

of this hypothesis requires communication between the longitudinal and the circular muscle cells across the myenteric plexus. Chapter 7 of this dissertation provides electrophysiological evidence that the two muscle layers are electrotonically coupled across the myenteric border of the canine colon. Furthermore, the low-resistance pathways, which facilitate electrotonic coupling, is shown to be mediated by the ICCs associated with the myenteric plexus. The ICC network located at the submucosal border of the circular muscle layer, apart from generating the pacemaker activity, also plays a significant role in facilitating inter-lamellar communication across circular muscle lamellae (Chapter 9).

10.5 Final remarks

10.5.1 On pacemaker activity

During the last decade, ICCs have become recognized as central players in the generation of pacemaker activity in most circular muscle layers of the gut. The evidence may be summarized as follows: (i) in areas where electrophysiological evidence exists for the origin of pacemaking activity, the presence of a network of ICCs has been demonstrated [60, 82, 110, 172]; (ii) removal of the ICC network abolishes the slow wave activity [60, 82, 112, 113, 172]; (iii) slow wave activity has been recorded from cells in the submuscular ICC network of the colonic circular muscle [5, 166]; (iv) selective methylene blue uptake by ICCs and subsequent specific destruction of ICCs by intense illumination abolished the slow wave activity [183, 119, 117, Chapter 3]; (v) the pacemaker activity is immature as long as the ICC network is not fully developed (Chapter 5); and (vi) the ability to generate the pacemaker activity was disrupted in W/W^v mutant mice whose ICCs associated with the myenteric plexus are absent

[85, 196].

10.5.2 On intercellular communication

Intercellular communication is essential for individual cells to function in harmony as a tissue. The mechanism through which electrical coupling is achieved depends, in part, on the morphological organization of the cells in the tissue. It is obvious that gap junctions provide low-resistance pathways for electrical coupling. However, there are areas in which the density of gap junctions is so abundant that it is far beyond the need for electrical coupling. It has been mathematically estimated that ≈ 20 open connexons are already sufficient to electrically couple adjacent smooth muscle cells in a two-cell model [146]. As discussed previously, in canine colon, the pacemaker potential of the slow waves is likely to be triggered by a metabolically regulated event sensitive to cAMP and intracellular calcium. The large density of gap junctions at the submuscular surface of the circular muscle may be essential for metabolic coupling of the submuscular ICCs (possibly including the branching smooth muscle cells) in which the pacemaker component of the slow waves is generated.

It is noteworthy to realize that electrical field coupling between cells arises naturally when the cellular orientation is favourable. In the longitudinal muscle of canine colon, the spike-like action potentials can be perfectly synchronized despite the lack of detectable electrotonic current spread [114]. Furthermore, no electron-microscopically identifiable gap junctions has yet been found; instead, plasma membranes of adjacent longitudinal muscle cells are closely apposed to one another over a long distance with highly convoluted contour (Chapter 9). This organization is auspicious for electric field coupling. Nonetheless, neurobiotin has been observed to spread from an injected longitudinal muscle cell to a few adjacent cells with a slow diffusion rate; this is in

sharp contrast with the fast and extensive neurobiotin spread at the submuscular surface of the circular muscle [66]. Not only does the canine colonic musculature possess a tremendous heterogeneity in intercellular junctions, but it also exhibits distinct intrinsic electrical oscillations in different parts of the musculature. The overall electrical activity, which governs the motility through excitation-contraction coupling, *in situ* is caused by electrical interaction of the different intrinsic electrical activities of different cell types.

Bibliography

[1] Abe, Y. and Tomita, T. Cable properties of smooth muscle. *J. Physiol.(Lond)*, 196:87–100, 1968.

[2] Alvarez, W.C. and Mahoney, L.J. Action current in stomach and intestine. *Am. J. Physiol.*, 58:476–493, 1922.

[3] Barajas-López, C. and Huizinga, J.D. Heterogeneity in spontaneous and tetraethylammonium induced intracellular electrical activity in colonic circular muscle. *Pflugers Arch.*, 412:203–210, 1988.

[4] Barajas-López, C. and Huizinga, J.D. Different mechanisms of contraction generation in circular muscle of canine colon. *Am. J. Physiol.*, 256:G570–G580, 1989.

[5] Barajas-López, C., Berezin, I., Daniel, E.E. and Huizinga, J.D. Pacemaker activity recorded in interstitial cells of Cajal of the gastrointestinal tract. *Am. J. Physiol.*, 257:C830–C835, 1989.

[6] Barajas-López, C., Chow. E., Den Hertog, A. and Huizinga, J.D. Role of the sodium pump in pacemaker generation in dog colonic smooth muscle. *J. Physiol.(Lond)*, 416:369–383, 1989.

[7] Barajas-López, C., Den Hertog, A. and Huizinga, J.D. Ionic basis of pacemaker generation in dog colonic smooth muscle. *J. Physiol.(Lond)*, 416:385–402, 1989.

[8] Barbosa, P. and Peters, T.M. The effects of vital dyes on living organisms with special reference to methylene blue and neutral red. *Histochem-J.*, 3:71–93, 1971.

[9] Bauer, A.J., Publicover, N.G. and Sanders, K.M. Origin and spread of slow waves in canine gastric antral circular muscle. *Am. J. Physiol.*, 249:G800–G806, 1985.

[10] Bauer, A.J., Reed, J.B. and Sanders, K.M. Slow wave heterogeneity within the circular muscle of the canine gastric antrum. *J. Physiol.(Lond)*, 366:221–232, 1985.

[11] Bayliss, W. M. and Starling, E. H. The movement and innervation of the small intestine. *J. Physiol.(Lond)*, 24:99–143, 1899.

[12] Berezin, I., Huizinga, J.D. and Daniel, E.E. Interstitial cells of Cajal in the canine colon: a special communication network at the inner border of the circular muscle. *J. Comp. Neurol.*, 273:42–51, 1988.

[13] Berezin, I., Huizinga, J.D. and Daniel, E.E. Structural characterization of interstitial cells of Cajal in myenteric plexus and muscle layers of canine colon. *Can. J. Physiol.Pharmacol.*, In press, 1991.

[14] Berkson, J. Electromyographic studies of the gastrointestinal tract. IV. an inquiry into the origin of the potential variations of rhythmic contraction in the intestine; evidence in disfavor of muscle action currents. *Am. J. Physiol.*, 104:67–72, 1932.

[15] Berkson, J. Electromyograpic studies of the gastrointestial tract. III. observations on excised intestine. *Am. J. Physiol.*, 104:62–66, 1932.

[16] Berkson, J. Electromyographic studies of the gastrointestinal tract. VI. recovery of characteristic electropotential variations of the small intestine following application of nicotine, by restoration of circulation. *Am. J. Physiol.*, 105:454–456, 1933.

[17] Berkson, J. Further inquiries into the origin of potential variations of the small intestine by means of certain drugs. *Am. J. Physiol.*, 105:450–453, 1933.

[18] Berkson, J., Baldes, E.J. and Alvarez, W.C. Electromyographic studies of the gastrointestinal tract. I. the correlation between mechanical movement and changes in electrical potential during rhythmic contraction of the intestine. *Am. J. Physiol.*, 102:683–692, 1932.

[19] Berridge, M. J. Cytoplasmic calcium oscillations: a two pool model. *Cell Calcium*, 12:63–72, 1991.

[20] Berridge, M. J. and Dupont, G. Spatial and temporal signalling by calcium. *Curr. Opin. Cell Biol.*, 6:267–274, 1994.

[21] Berseth, C. L. . Gestational evolution of small intestine motility in preterm and term infants. *J. Ped.*, 115:646–651, 1989.

[22] Berseth, C. L. . Neonatal small intestinal motility: motor responses to feeding in term and preterm infants. *J. Ped.*, 117:777–782, 1990.

[23] Berseth, C. L. . Caffeine-induced inhibition of inositol(1,4,5)-trisphosphate-gated calcium channels from cerebellum. *Molecular Biology of the Cell*, 5:97–103, 1994.

[24] Bortoff, A. . Slow potential variation of small intestine. *Am. J. Physiol.*, 201:203–208, 1961.

[25] Bortoff, A. Electrical transmission of slow waves from longitudinal to circular intestinal muscle. *Am. J. Physiol.*, 209(6):1254–1260, 1965.

[26] Bortoff, A. Myogenic control of intestinal motility. *Curr. Topics Physiol.*, 56:418–433, 1976.

[27] Bortoff, A., Michaels, D. and Mistretta, P. Dominance of longitudinal muscle in propagation of intestinal slow waves. *Am. J. Physiol.*, 240:C135–C147, 1981.

[28] Bouman, L. N., Duivenvoorden, J. J., Bukauskas, F. F. and Jongsma, H. J. Anisotropy of electrotonus in the sinoatrial node of the rabbit heart. *J. Mol. Cell Cardiol.*, 21:407–418, 1989.

[29] Bourreau, J. P., Kwan, C. Y. and Daniel E. E. . Distinct pathways to refill ACh-sensitive internal Ca^{2+} stores in canine airway smooth muscle. *Am. J. Physiol.*, 265:C28–C35, 1993.

[30] Bourreau, J. P.,Abela, A. P., Kwan, C. Y. and Daniel E. E. . Acetylcholine ca^{2+} stores refilling directly involves a dihydropyridine-sensitive channel in dog trachea. *Am. J. Physiol.*, 261:C497–C505, 1991.

[31] Bozler, E. Electric stimulation and conduction of excitation in smooth muscle. *Am. J. Physiol.*, 122:614–623, 1938.

[32] Bozler, E. Electrophysiological studies on the motility of the gastrointestinal tract. *Am. J. Physiol.*, 127:301–307, 1939.

[33] Bozler, E. The action potentials accompanying conducted responses in visceral smooth muscles. *Am. J. Physiol.*, 136:553–560, 1941.

[34] Bozler, E. The activity of the pacemaker previous to the discharge of a muscular impulse. *Am. J. Physiol.*, 136:543–552, 1942.

[35] Brown, G. R., Sayers, L. G., Kirk, C. J., Michell, R. H. and Michelangeli F. The opening of the inositol 1,4,5-trisphosphate-sensitive ca^{2+} channel in rat cerebellum is inhibited by caffeine. *Biochem. J.*, 282:309–312, 1992.

[36] Bueno, L., Fioramonti, J., Ruckebusch, Y., Frexinos, J. and Coulom, P. Evaluation of colonic myoelectrical activity in health and functional disorders. *Gut*, 21:480–C485, 1980.

[37] Cannon, W.B. The movements of the intestines: Studies by means of the Rõntgen rays. *Am. J. Physiol.*, 6:251–277, 1902.

[38] Caprilli, R. and Onori, L. Origin, transmission and ionic dependence of colonic electrical slow waves. *Scand. J. Gastroenterol.*, 7:65–74, 1972.

[39] Chen, Q., M. Cannell, and van Breemen, C. The superficial buffer barrier in vascular smooth muscle. *Can. J. Phys. Pharm.*, 70:509–541, 1992.

[40] Chen, Q., M. Cannell, and van Breemen, C. The superficial buffer barrier in venous smooth muscle: Sarcoplasmic reticulum refilling and unloading. *Br. J. Pharmacol.*, 109:336–343, 1993.

[41] Chow, E. and Huizinga, J.D. Myogenic electrical control activity in longitudinal muscle of human and dog colon. *J.Physiol.(Lond)*, 392:21–34, 1987.

[42] Christensen, J. A commentary on the morphological identification of interstitial cells of Cajal in the gut. *J. Auton. Nerv. Sys.*, 37:75–88, 1992.

[43] Christensen, J. and Rasmus, S.C. Colon slow waves: Size of oscillators and rates of spread. *Am. J. Physiol.*, 223:1330–1333, 1972.

[44] Christensen, J., Caprilli, R. and Lund, G.F. Electric slow waves in circular muscle of cat colon. *Am. J. Physiol.*, 217:771–776, 1969.

[45] Christensen, J., Rick, G. A., and Lowe, L. S. Distributions of interstitial cells of Cajal in stomach and colon of cat, dog, ferret, opossum, rat, guinea pig and rabbit. *J. Auton. Nerv. Sys.*, 37:47–56, 1992.

[46] Christensen, J., Rick, G. A. and Soll, D. J. Intramural nerves and interstitial cells revealed by the Champy-Maillet stain in the opossum esophagus. *J. Auton. Nerv. Sys.*, 19:131–151, 1987.

[47] Clapham, D. E. A mysterious new influx factor? *Nature*, 364:763–764, 1993.

[48] Conklin, J.L. and Du, C. Pathways of slow-wave propagation in proximal colon of cats. *Am. J. Physiol.*, 258:G894–G903, 1990.

[49] Connor, J. A., Kreulen, D., Prosser, C. L. and Weigel, R. Interaction between longitudinal and circular muscle in intestine of cat. *J. Physiol. (Lond)*, 273:665–689, 1977.

[50] Daniel, E. E. and Daniel, V. Posey. Neuromuscular structures in opossum esophagus: role of interstitial cells of Cajal. *Am. J. Physiol.*, 246:G305–G315, 1984.

[51] Daniel, E. E., Bardakjian, B. L., Huizinga, J. D. and Diamant, N. E. Relaxation oscillators and core conductor models are needed for understanding of gastrointestinal electrical activities. *Am. J. Physiol.*, 266:G485–G496, 1994.

[52] Daniel, E. E.,Daniel, V. P., Duchon, G., Garfield, R. E., Nichols, M., Malhotra, S. K. and Oki, M. Is the nexus necessary for cell-to-cell coupling of smooth muscle? *J. Membr. Biol.*, 28:207–239, 1976.

[53] Daniel, E.E. and Chapman, K.M. Electrical activity of the gastrointestinal tract as an indication of mechanical activity. *Am. J. Digest. Disease.*, 8:54–102, 1963.

[54] Daniel, E.E., Honour, A.J. and Bogoch, A. Electrical activity of the longitudinal muscle of dog small intestine studied *in vivo* using microelectrodes. *Am. J. Physiol.*, 198:113–118, 1960.

[55] Darby, P. J., Kwan, C. Y. and Daniel, E. E. Use of calcium pump inhibitors in the study of calcium regulation in smooth muscle. *Biol. Signals*, 2:293–304, 1993.

[56] Deng, H. W. and Kwan, C. Y. Cyclopiazonic acid is a sarcoplasmic reticulum Ca^{2+}-pump inhibitor of rat aortic muscle. *Chung. Kuo. Yao. Li. Hsueh. Pao.*, 12:53–58, 1991.

[57] Dewey, M.M. and Barr, L. Intercellular connection between smooth muscle cells: the nexus. *Science*, 137:670–672, 1962.

[58] Du, C. A. and Conklin, J. L. Origin of slow waves in the isolated proximal colon of the cat. *J. Auton. Nerv. Sys.*, 28:167–177, 1989.

[59] Duchon, G.,Henderson, R. and Daniel, E. E. Circular muscle layers in the small intestine. In E. E. Daniel., editor, *Proceedings of the Fourth International Symposium on Gastrointestinal Motility*, pages 635–646. Mitchell Press, Vancouver, 1974.

[60] Durdle, N.G., Kingma, Y.J., Bowes, K.L. and Chambers, M.M. Origin of slow waves in the canine colon. *Gastroenterology*, 84:375–382, 1983.

[61] Eddlestone, G. T., Goncalves, A., Bangham, J. A. and Rojas, E. Electrical coupling between cells in islets of Langerhans from mouse. *J. Membr. Biol.*, 77:1–14, 1984.

[62] El-Sharkawy, T.Y. Electrical activities of the muscle layers of the canine colon. *J. Physiol.(Lond)*, 342:67–83, 1983.

[63] El-Sharkawy, T.Y. and Szurszewski, J. H. Modulation of canine antral circular smooth muscle by acetylcholine, noradrenaline and pentagastrin. *J. Physiol.(Lond)*, 279:309–320, 1978.

[64] Elden, L. and Bortoff, A. Electrical coupling of longitudinal and circular intestinal muscle. *Am. J. Physiol.*, 246(9):G618-G626, 1984.

[65] Elliott, T.R. and Barclay-Smith, E. Antiperistalsis and other muscular activities of the colon. *J. Physiol. (Lond.)*, 31:272–304, 1904.

[66] Farraway, L. and Huizinga, J.D. Heterogeneity of metabolic and electrical communication within the colonic musculature. *J. Gastroint. Motil.*, 5:190, 1993.

[67] Farraway, L., Ball, A. and Huizinga, J.D. Intercellular metabolic coupling in canine colon musculature. *Am. J. Physiol.*, 268:C1492–C1502, 1995.

[68] Faussone Pellegrini, M. S. Cytodifferentiation of the interstitial cells of Cajal related to the myenteric plexus of mouse intestinal muscle coat. *Anat. Embryol. (Berl)*, 171:163–169, 1985.

[69] Faussone Pellegrini, M. S. Cytodifferentiation of the interstitial cells of Cajal of mouse colonic circular muscle layer. *Acta Anat*, 128:98–109, 1987.

[70] Faussone Pellegrini, M. S. Histogenesis, structure and relationships of interstitial cells of Cajal (ICC): from morphology to functional interpretation. *Eur. J. Morphol.*, 30:137–148, 1992.

[71] Faussone Pellegrini, M. S.,Cortesini, C. and Romagnoli, P. Sull'ultrasturttura della tunica muscolare della porzione cardiale dell'esofago e dello stomaco umano con particolare riferimento alle cosiddette cellule interstiziali di Cajal. *Arch. Ital. Anat. Embriol.*, 82:157–177, 1977.

[72] Faussone Pellegrini, M. S.,Pantalone, D., and Cortesini, C. Smooth muscle cells, interstitial cells of Cajal and myenteric plexus interrelationships in the human colon. *Acta. Anat. (Basel).*, 139:31–44, 1990.

[73] Fioramonti, J., Garcia Villar, R., Bueno, L and Ruckebusch Y. Colonic myoelectrical activity and propulsion in the dog. *Dig. Dis. Sci.*, 25:641–646, 1980.

[74] Gabella, G. Intercellular junctions between circular and longitudinal intestinal muscle layers. *Z. Zellforsch. Mikrosk. Anat.*, 125:191–199, 1972.

[75] Gabella, G. Nexuses between the smooth muscle cells of the guinea-pig ileum. *J. Cell Biol.*, 82:239–247, 1979.

[76] Gabella, G. Gap junctions of the muscles of the small and large intestine. *Cell Tissue Res.*, 219:469–488, 1981.

[77] Garfield, R. E., Thilander, G., Blennerhassett, M. G. and Sakai, N. An update on the question: are gap junctions necessary for cell to cell coupling of smooth muscle? *Can. J. Phys. Pharm.*, 70:481–490, 1992.

[78] Gershon, M. D. and Thompson, E. B. The maturation of neuromuscular function in a multiply innervated structure: development of the longitudinal smooth muscle of the foetal mammalian gut and its cholinergic excitatory, adrenergic inhibitory, and non-adrenergic inhibitory innervation. *J. Physiol. (Lond)*, 234:257–277, 1973.

[79] Gill, W.B., Taja, A., Chadbourne, D.M., Roma, M. and Vermeulen, C.W. Inactivation of bladder tumor cells and enzymes by methylene blue plus light. *J. Urol.*, 138:1318–1320, 1987.

[80] Goeger, D. E., Riley, R. T., Dorner, J. W. and Cole, R. J. Cyclopiazonic acid inhibition of the Ca^{2+}-transport ATPase in rat skeletal muscle sarcoplasmic reticulum vesicles. *Biochem. Pharmacol.*, 37:978–981, 1988.

[81] Gonoi, T. and Hasegawa S. Post-natal disappearance of transient calcium channels in mouse skeletal muscle: effects of denervation and culture. *J. Physiol. (Lond)*, 401:617–637, 1988.

[82] Hara, Y., Kubota, M. and Szurszewski, J.H. Electrophysiology of smooth muscle of the small intestine of some mammals. *J. Physiol.(Lond)*, 372:501–520, 1986.

[83] Huizinga, J. D. and Liu, L. W. C. Role of calcium channels in pharmacological modulation of gastrointestinal motility. In M. O. Christen and R. P. Dordrecht, editors, *Calcium Antagonists in Gastroenterology Research and Perspectives*, pages 31–39. Kluwer Academic Publishers, The Netherlands, 1993.

[84] Huizinga, J. D., Liu, L. W. C., Blennerhassett, M. G., Thuneberg, L. and Molleman, A. . Intercellular communication in smooth muscle. *Experientia*, 48:932–941, 1992.

[85] Huizinga, J. D., Thuneberg, L., Kluppel, M. Malysz, J., Mikkelsen, H. B. and Bernstein, A. The *w-kit* gene is required for interstitial cells of Cajal and intestinal pacemaker activity. *Nature*, 373:347–349, 1995.

[86] Huizinga, J. D.,Tomlinson, J. and Pintin-Quezada, J. Involvement of nitric oxide in nerve mediated inhibition and action of VIP in colonic smooth muscle. *J. Pharmacol. Exp. Ther.*, 260:803–808, 1992.

[87] Huizinga, J.D. Action potentials in gastrointestinal smooth muscle. *Can. J. Physiol. Pharmacol.*, 69:1133–1142, 1991.

[88] Huizinga, J.D. and Barajas-López, C. Ionic and cellular basis for slow-wave-type and spike-like action potentials. *Prog. Clin. Biol. Res.*, 327:605–615, 1990.

[89] Huizinga, J.D. and Chow, E. Electrotonic current spread in colonic smooth muscle. *Am. J. Physiol.*, 254:G702–G710, 1988.

[90] Huizinga, J.D., Barajas-López, C. and Chow, E. Generation of spiking activity in circular muscle cells of the canine colon. *Can. J. Physiol. Pharmacol.*, 65:2147–2150, 1987.

[91] Huizinga, J.D., Chang, G., Diamant, N.E. and El-Sharkawy, T.Y. Electrophysiological basis of excitation of canine colonic circular muscle by cholinergic agents and substance P. *J. Pharmacol. Exp. Ther.*, 231:692–699, 1984.

[92] Huizinga, J.D., Farraway, L. and Den Hertog, A. Effect of voltage and cyclic AMP on frequency of slow wave type action potentials in canine colonic smooth muscle. *J. Physiol. (Lond)*, 442:31–45, 1991.

[93] Huizinga, J.D., Farraway, L. and Den Hertog, A. Generation of the slow wave type action potentials in colonic smooth muscle involves a non-L-type Ca^{2+} conductance. *J. Physiol. (Lond)*, 422:15–29, 1991.

[94] Huizinga, J.D., Stern, H.S., Chow, E., Diamant, N.E., and El-Sharkawy T.Y. Electrophysiologic control of motility in the human colon. *Gastroenterology*, 88:500–511, 1985.

[95] Huizinga, J.D., Stern, H.S., Chow, E., Diamant, N.E., and El-Sharkawy T.Y. Caffeine inhibits Ca^{2+}-mediated potentiation of inositol 1,4,5-trisphosphate-induced Ca^{2+} release in permeabilized vascular smooth muscle cells. *Biochem. Biophys. Res. Commun.*, 194:726–732, 1993.

[96] Hyman, P. E., Martin, M. G., Tomomasa, T., Jing, J. and Snape, W. J., Jr. Development of calcium channels in gastric smooth muscle. *Pediatr. Res.*, 25:600–604, 1989.

[97] Jessen, H. andThuneberg, L. Interstitial cells of Cajal and auerbach's plexus. a scanning electron microscopical study of guinea-pig small intestine. *J. Submicrosc. Cytol. Pathol.*, 23:195–212, 1991.

[98] Kobayashi, M., Nagai, T. and Prosser, C. L. Electrical interaction between muscle layers of cat intesine. *Am. J. Physiol.*, 211(6):1281–1291, 1966.

[99] Kobayashi, S., Torihashi, S., Iino, S. and Sanders, K. M. Oblique smooth muscle bundles between the circular and longitudinal muscle layers in the canine proximal colon. *Arch. Histol. Cytol.*, 57:29–45, 1994.

[100] Kojima, M., Sperelakis, N. and Sada, H. Ontogenesis of transmembrane signaling systems for control of cardiac Ca^{2+} channels. *J. Dev. Physiol.*, 14:181–219, 1990.

[101] Kostyuk, P., Pronchuk, N., Savchenko, A and Verkhratsky, A. Calcium currents in aged rat dorsal root ganglion neurones. *J. Physiol. (Lond)*, 461:467–483, 1993.

[102] Kurebayashi, N. and Ogawa, Y. Discrimination of Ca^{2+}-ATPase activity of the sarcoplasmic reticulum from actomyosin-type ATPase activity of myofibrils in skinned mammalian skeletal muscle fibres: Distinct effects of cyclopiazonic acid on the two ATPase activities. *J. Muscle Res. Cell Motil.*, 12:355–365, 1991.

[103] Landau, E. Über Zusammenhnge zwischen beiden Schichten der Tunica muscularis des Darmes. *Z. Mikrosk. Anat. Forsch.*, 14:441–446, 1928.

[104] Langton, P., Ward, S. M., Carl, A., Norell, M. A. and Sanders, K. M. Spontaneous electrical activity of interstitial cells of Cajal isolated from canine proximal colon. *Proc. Natl. Acad. Sci. U. S. A.*, 86:7280–7284, 1989.

[105] Langton, P.D., Burke, E.P. and Sanders, K.M. Participation of Ca currents in colonic electrical activity. *Am. J. Physiol.*, 257:C451–C460, 1989.

[106] Li, Z., Z. Zhou, and Daniel, E. E. Expression of gap junction connexin 43 and connexin 43 mRNA in different regional tissues of intestine in dog. *Am. J. Physiol.*, 265:G911–G916, 1993.

[107] Liu, L. W. C., Sperelakis, N. and Huizinga, J. D. Pacemaker activity and intercellular communication in the gastrointestinal musculature. In J. D. Huizinga, editor, *Pacemaker Activity and Intercellular Communication*, pages 159–174. CRC Press, Ann Arbor, 1995.

[108] Liu, L.W.C. Electrical Communication between Different Cell Types in the Colonic Musculature. Master's thesis, McMaster University, Hamilton, Ontario, Canada, 1991.

[109] Liu, L.W.C., and Huizinga, J.D. Colonic circular muscle generates action potentials without the pacemaking component of slow waves. *FASEB J.*, 7(4):A6781, 1993.

[110] Liu, L.W.C., and Huizinga, J.D. Electrical coupling of circular muscle to longitudinal muscle and interstitial cells of Cajal in canine colon. *J. Physiol. (Lond)*, 470:445–461, 1993.

[111] Liu, L.W.C., and Huizinga, J.D. Role of the calcium activated potassium channel in repolarization of colonic electrical activity. *J. Gastroint. Motil.*, 5:201, 1993.

[112] Liu, L.W.C., and Huizinga, J.D. Canine colonic circular muscle generates action potentials without the pacemaker component. *Can. J. Phys. Pharm.*, 72(1):70–81, 1994.

[113] Liu, L.W.C., Daniel, E.E. and Huizinga, J.D. Excitability of canine colon circular muscle disconnected from the network of interstitial cells of Cajal. *Can. J. Phys. Pharm.*, 70:289–295, 1992.

[114] Liu, L.W.C., Mikkelsen, H. B., Thuneberg, L., Berezin, I. and Huizinga, J.D. Electrical communication in areas with and without gap junctions in canine colon. *Gastroenterology*, 103:1391, 1992.

[115] Liu, L.W.C., Thuneberg, L., and Huizinga, J.D. Methylene blue and light selectively lesioned interstitial cells of Cajal in canine colon. *Gastroenterology*, 103:1377, 1992.

[116] Liu, L.W.C., Thuneberg, L., and Huizinga, J.D. Regulation of colonic pacemaker frequency by intracellular calcium in sarcoplasmic reticulum. *J. Gastroint. Motil.*, 5:201, 1993.

[117] Liu, L.W.C., Thuneberg, L., and Huizinga, J.D. Selective lesioning of interstitial cells of Cajal by methylene blue and light leads to loss of slow waves. *Am. J. Physiol.*, 266:G485–G496, 1994.

[118] Liu, L.W.C., Thuneberg, L., and Huizinga, J.D. Cyclopiazonic acid, inhibiting the endoplasmic reticulum calcium pump, reduces the canine colon pacemaker frequency. *J. Pharmacol. Exp. Ther.*, in press, 1995.

[119] Liu, L.W.C., Thuneberg, L., Daniel, E. E.and Huizinga, J.D. Selective accumulation of methylene blue by interstitial cells of Cajal in canine colon. *Am. J. Physiol.*, 264:G64–G73, 1993.

[120] Llewellyn-Smith, Costa, I. J., M., Furness, J. B. and Bornstein, J. C. Structure of the tertiary component of the myenteric plexus in the guinea-pig small intestine. *Cell Tissue Res.*, 272:509–516, 1993.

[121] Locke, F. R. and Rosenheim, O. Contributions to the physiology of the isolated heart: The consumption of dextrose by mammalian cardiac muscle. *J. Physiol. (Lond)*, XXXVI:205–220, 1907.

[122] Loirand G., Pacaud P., Baron A., Mironneau C., and Mironneau J. Large conductance calcium-activated non-selective cation channel in smooth muscle cells isolated from rat portal vein. *J. Physiol. (Lond)*, 437:461–475, 1991.

[123] Low, A. M., Kwan, C. Y. and Daniel, E. E. Evidence for two types of internal Ca^{2+} stores in canine mesenteric artery with different refilling mechanisms. *Am. J. Physiol.*, 262:H31–H37, 1992.

[124] Luckhoff, A. and Clapham, D. E. Calcium channels activated by depletion of internal calcium stores in A431 cells. *Biophys. J.*, 67:177–182, 1994.

[125] Malysz, J., Richardson, D., Farraway, L., Christen, M. O. and Huizinga, J. D. Initiation of slow wave type action potentials in the mouse small intestine involves a non-L-type calcium channel. *J. Gastroint. Motil.*, in press, 1995.

[126] McNutt, N. S. and Weinstein, R. S. . Membrane ultrastructure at mammalian intercellular junctions. *Prog. Biophys. Mol. Biol.*, 26:47–101, 1973.

[127] Menezes, S., Capella, M. A. and Caldas, L. R. Photodynamic action of methylene blue: repair and mutation in Escherichia coli. *J. Photochem. Photobiol. B.*, 5:505–517, 1990.

[128] Mikkelsen, H. B.,Huizinga, J. D., Thuneberg, L. and Rumessen, J. J. Immunohistochemical localization of a gap junction protein (connexin 43) in the muscularis externa of murine, canine and human intestine. *Cell Tissue Res.*, 274:249–246, 1993.

[129] Mines, G.R. On functional analysis by the action of electrolytes. *J. Physiol. (Lond)*, XLVI:188–235, 1913.

[130] Missiaen, L., De Smedt, H., Droogmans, G. and Casteels, R. Luminal Ca^{2+} controls the activation of the inositol 1,4,5-trisphosphate receptor by cytosolic Ca^{2+}. *J. Biol. Chem.*, 267:22961–22966, 1992.

[131] Missiaen, L., Declerck, I., Droogmans, G., Plessers, L., DeSmedt, H. and Raeymaekers, L. Agonist-dependent Ca^{2+} and Mn^{2+} entry dependent on state of filling of Ca^{2+} stores in aortic smooth muscle cells of the rat. *J. Physiol. (Lond)*, 427:171–186, 1990.

[132] Missiaen, L., Taylor, C. W. and Berridge, M. J. Luminal Ca^{2+} promoting spontaneous Ca^{2+} release from inositol trisphosphate-sensitive stores in rat hepatocytes. *J. Physiol. (Lond)*, 455:623–640, 1992.

[133] Modica-Napolitano, J. S. and Aprille, J. R. Basis for selective cytotoxicity of Rhodamine 123. *Cancer Res.*, 47:4361–4365, 1987.

[134] Molleman, A. and Huizinga, J. D. Carbachol activated membrane currents in canine colon circular smooth muscle cells. *J. Gastroint. Motil.*, 5:206, 1993.

[135] Molleman, A., Sims, S., Lee, J.C.F. and Huizinga, J.D. Ion channels involved in gastrointestinal action potential generation. In J. D. Huizinga, editor, *Pacemaker Activity and Intercellular Communication*, pages 223–236. CRC Press, Ann Arbor, 1995.

[136] Molleman, A.,Thuneberg, L. and Huizinga, J. D. Characterization of the outward rectifying potassium channel in a novel intestinal smooth muscle preparation. *J. Physiol. (Lond)*, 470:211–229, 1993.

[137] Morriss, F. H., Jr. Neonatal gastrointestinal motility and enteral feeding. *Seminars in Perinatology*, 15:478–481, 1991.

[138] Nagai, T. and Prosser, C.L. Patterns of conduction in smooth muscle. *Am. J. Physiol.*, 204:910–914, 1963.

[139] Noble, D., Brown, H. F. and Winslow, R. L. Propagation of pacemaker activity: interaction between pacemaker cells and atrial tissue. In J. D. Huizinga, editor, *Pacemaker Activity and Intercellular Communication*, pages 73–92. CRC Press, Ann Arbor, 1995.

[140] Pace, J. L. and Williams, I. Organization of the muscular wall of the human colon. *Gut*, 10:352–359, 1969.

[141] Parker, I. and Ivorra, I. Caffeine inhibits inositol trisphosphate-mediated liberation of intracellular calcium in Xenopus oocytes. *J. Physiol. (Lond)*, 433:229–240, 1991.

[142] Perez Armendariz, M., C. Roy, D. C. Spray, and M. V. Bennett. . Biophysical properties of gap junctions between freshly dispersed pairs of mouse pancreatic beta cells. *Biophys. J.*, 59:76–92, 1991.

[143] Post, J. M. and Hume, J. R. Ionic basis for spontaneous depolarizations in isolated smooth muscle cells of canine colon. *Am. J. Physiol.*, 263:C691–C699, 1992.

[144] Prosser, C.L., and Sperelakis, N. Transmission in ganglion-free circular muscle from the cat intestine. *Am. J. Physiol.*, 187:536–545, 1956.

[145] Prosser, C.L., Burnstock, G. and Kahn, J. Conduction in smooth muscle: comparative structural properties. *Am. J. Physiol.*, 199:545–552, 1960.

[146] Publicover, N. G. Generation and propagation of rhythmicity in gastrointestinal smooth muscle. In J. D. Huizinga, editor, *Pacemaker Activity and Intercellular Communication*, pages 175–192. CRC Press, Ann Arbor, 1995.

[147] Publicover, N. G., Hammond, E. M. and Sanders, K. M. Amplification of nitric oxide signaling by interstitial cells isolated from canine colon. *Proc. Natl. Acad. Sci. U. S. A.*, 90:2087–2091, 1993.

[148] Publicover, N. G., Horowitz, N. N. and Sanders, K. M. Calcium oscillations in freshly dispersed and cultured interstitial cells from canine colon. *Am. J. Physiol.*, 262:C589–C597, 1992.

[149] Qvortrup, K. and Rostgaard, J. Three-dimensional organization of a transcellula tubulocisternal endoplasmic reticulum in epithelial cells of Reissner's membrane in the guinea-pig. *Cell Tissue Res.*, 261:287–299, 1990.

[150] Ramón Y Cajal, S. Sur les ganglions et plexus nerveux de l'intestin. *Compt. Rend. Soc. Biol. Paris*, 45:217–223, 1893.

[151] Randriamampita, C. and Tsien, R. Y. Emptying of intracellular Ca^{2+} stores releases a novel small messenger that stimulates Ca^{2+} influx. *Nature*, 364:809–814, 1993.

[152] Rostgaard, J. and Moller, O. Localization of Na^{+}, K^{+}-ATPase to the inside of the basolateral cell membranes of epithelial cells of proximal and distal tubules in rabbit kidney. *Cell Tissue Res.*, 212:17–28, 1980.

[153] Rumessen, J. J., and Thuneberg, L. Interstitial cells of Cajal in human small intestine. Ultrastructural identification and organization between the main smooth muscle layers. *Gastroenterology*, 100:1417–1431, 1991.

[154] Rumessen, J. J., Mikkelsen, H. B., and Thuneberg, L. Ultrastructure of interstitial cells of Cajal associated with deep muscular plexus of human small intestine. *Gastroenterology*, 102:56–68, 1992.

[155] Rumessen, J. J., Peters, S. and Thuneberg, L. Light- and electron microscopical studies of interstitial cells of Cajal (ICC) and muscle cells at the submucosal border of human colon. *Laboratory Investigation*, 68(4):481–495, 1993.

[156] Rumessen, J. J., Thuneberg, L., and Mikkelsen, H. B. Plexus muscularis profundus and associated interstitial cells. II. Ultrastructural studies of mouse small intestine. *Anat. Rec.*, 203:129–146, 1982.

[157] Sabourin, P.J., Kingma, Y.J. and Bowes, K.L. Electrical and mechanical interactions between the muscle layers of canine proximal colon. *Am. J. Physiol.*, 258:G484–G491, 1990.

[158] Sakai, T., Terada, K., Kitamura, K. and Kuriyama, H. Ryanodine inhibits the Ca-dependent K current after depletion of Ca stored in smooth muscle cells of the rabbit ileal longitudinal muscle. *Br. J. Pharmacol.*, 95:1089–1100, 1988.

[159] Sanders, K. M., Stevens, R., Burke, E. and Ward, S. W. Slow waves actively propagate at submucosal surface of circular layer in canine colon. *Am.J.Physiol.*, 259:G258–G263, 1990.

[160] Sanders, K.M. Colonic electrical activity: concerto for two pacemakers. *N. I. P. S.*, 4:176–180, 1989.

[161] Sarna, S. K. and Otterson, M. F. Myoelectric and contractile activities. In M. M. Schuster, editor, *Atlas of Gastrointestinal Motility in Health and Disease*, pages 3–42. Williams & Wilkins, Baltimore, Maryland, USA, 1993.

[162] Sarna, S. K., Daniel, E. Ξ. and Kingma, Y. J. Simulation of the electric-control activity of the stomach by an array of relaxation oscillators. *Am. J. Dig. Dis.*, 17:299–310, 1972.

[163] Sarna, S.K., Condon, R. and Cowles, V. Colonic migrating and nonmigrating motor complexes in dogs. *Am. J. Physiol.*, 246:G355–G360, 1984.

[164] Schang, J. C., Hemond, M., Hebert, M. and Pilot, M. Myoelectrical activity and intraluminal flow in human sigmoid colon. *Dig. Dis. Sci.*, 31:1331–1337, 1986.

[165] Seki, N., Karim, O. M. A. and Mostwin, J. L. Changes in electrical properties of guinea pig smooth muscle membrane by experimental bladder outflow obstruction. *Am. J. Physiol.*, 262:F885–F891, 1992.

[166] Serio, R., Barajas-López, C., Daniel, E.E., Berezin, I., and Huizinga, J.D. Slow wave activity in colon: Role of network of submucosal interstitial cells of Cajal. *Am. J. Physiol.*, 260:G636–G645, 1991.

[167] Shima, H. and Blaustein, M. P. Modulation of evoked contractions in rat arteries by ryanodine, thapsigargin, and cyclopiazonic acid. *Circ. Res.*, 70:968–977, 1992.

[168] Shimizu, M., Nishida, A., Hayakawa, H. and Yamawaki, S. Ca^{2+} release from inositol 1,4,5-triphosphate-sensitive Ca^{2+} store by antidepressant drugs in cultured neurons of rat frontal cortex. *J. Neurochem.*, 60:595–601, 1993.

[169] Shinji, Y., Shinji, E. andMizuhira, V. . A new electron-microscopic histocytochemical staining method-demonstration of glycogen particles. *Acta. Histochem. Cytochem.*, 8(2):139–149, 1975.

[170] Shuttleworth, T. J. and Thompson, J. L. Modulation of inositol (1,4,5) trisphosphate-sensitive calcium store content during continuous receptor activation and its effects on calcium entry. *Cell Calcium*, 13:541–551, 1992.

[171] Smith, T.K., Reed, J.B. and Sanders, K.M. Interaction of two electrical pacemakers in muscularis of canine proximal colon. *Am. J. Physiol.*, 252:C290–C299, 1987.

[172] Smith, T.K., Reed, J.B. and Sanders, K.M. Origin and propagation of electrical slow waves in circular muscle of canine proximal colon. *Am. J. Physiol.*, 252:C215–C224, 1987.

[173] Stach, W. Der Plexus entericus extremus des Dickdarmes und seine Beziehungen zu den interstitiellen Zellen (Cajal). *Z. Mikrosk. Anat. Forsch. Leipzig.*, 85:245–272, 1972.

[174] Suzuki, M., Muraki, K., Imaizumi, Y., and Watanabe, M. Cyclopiazonic acid, an inhibitor of the sarcoplasmic reticulum Ca^{2+}-pump, reduces Ca^{2+}-dependent K^+ currents in guinea-pig smooth muscle cells. *Br. J. Pharmacol.*, 107:134–140, 1992.

[175] Suzuki, N., Prosser, C.L. and Dahms, V. Boundary cells between longitudinal and circular layers: essential for electrical slow waves in cat intestine. *Am. J. Physiol.*, 250:G287–G294, 1986.

[176] Szurszewski, J.H. Electrophysiological basis of gastrointestinal motility. In L.R. Johnson, editor, *Physiology of the Gastrointestinal Tract, Volume 1*, pages 383–422. Raven Press, New York, 1987.

[177] Taxi, J. Cellules de Schwann et 'cellules interstitielles de Cajal' au niveau des plexus nerveux de la musculeuse intestinale du cobaye: retour aux definitions. *Arch. Anat. Microsc. Morphol. Exp.*, 41(1):281–304, 1953.

[178] Taylor, A.B., Kreulen, D. and Prosser, C.L. Electron microscopy of the connective tissue between longitudinal and circular muscle of small intestine of cat. *Am. J. Anat.*, 150:427–442, 1977.

[179] Thuneberg, L. Interstitial cells of Cajal: Intestinal pacemaker cells? *Adv. Anat. Embryol. Cell Biol.*, 71:1–130, 1982.

[180] Thuneberg, L. Interstitial cells of Cajal. In G. S. Schultz, J. D. Wood, and B. B. Rauner, editors, *Handbook of Physiology, the Gastrointestinal System*, pages 349–386. American Physiological Society, Bethesda, U.S.A., 1989.

[181] Thuneberg, L. Vital methylene blue (MB): (I) preservation of MB for electron microscopy; (II) selectivity for interstitial cells of Cajal (ICC); (III) selective accumulation of MB in the endoplasmic reticulum of ICC. *Gastroenterology*, 103(4):1388, 1992.

[182] Thuneberg, L. and Peters, S. Primary cultures of intestinal musculature: correlation of intestinal rhythmicity and presence of interstitial cells of Cajal. *Dig. Dis. Sci.*, 32:930, 1987.

[183] Thuneberg, L., Johansen, V., Rumessen, J.J. and Andersen, B.G. Interstitial cells of Cajal: Selective uptake of methylene blue inhibits slow wave activity. In C. Roman, editor, *Gastrointestinal Motility*, pages 495-502. MTP Press Limited, Lancaster, 1983.

[184] Thuneberg, L., Rumessen, J. J., Mikkelsen, H. B., Peters, S. and Jessen, H. Structural aspects of interstitial cells of Cajal as intestinal pacemaker cells. In J. D. Huizinga, editor, *Pacemaker Activity and Intercellular Communication*, pages 193–222. CRC Press, Ann Arbor, 1995.

[185] Tohse, N., Meszaros, J. and Sperelakis, N. Developmental changes in long-opening behavior of L-type Ca^{2+} channels in embryonic chick heart cell. *Circ. Res.*, 71:376–384, 1992.

[186] Tomita, T. Electrical activity (spikes an slow waves) in gastrointestinal smooth muscles. In E. Buldbring, editor, *Smooth Muscle*, pages 127–156. Arnold, London, 1981.

[187] Tomomasa, T., Itoh, Z., Koizumi, T. and Kuroume, T. Nonmigrating rhythmic activity in the stomach and duodenum of neonates. *Biology of the Neonate*, 48:1–9, 1985.

[188] Torihashi, S., Gerthoffer, W. T., Kobayashi, S. and Sanders, K. M. Identification and classification of interstitial cells in the canine proximal colon by ultrastructure and immunocytochemistry. *Histochemistry*, 101:169–183, 1994.

[189] Torihashi, S., Ward, S. M., Nishi, K., Kobayashi, S. and Sanders, K. M. *c-kit*-dependent development of interstitial cells and electrical activity in the murine gastrointestinal tract. *Cell Tissue Res.*, in press, 1995.

[190] Tysnes, O., Steen, V. and Holmsen, H. Neomycin inhibits platelet functions and inositol phospholipid metabolism upon stimulation with thrombin, but not with ionomycin or 12-O-tetradecanoyl-phorbol 13-acetate. *Eur. J. Biochem.*, 177:219–223, 1988.

[191] van Breemen, C., Chen, Q. and Laher, I. Superficial buffer barrier function of smooth muscle sarcoplasmic reticulum. *TIPS*, 16:98–105, 1995.

[192] van Breemen, C.,and Saida, K. Cellular mechanisms regulating $[Ca^{2+}]_i$ smooth muscle. *Annu. Rev. Physiol.*, 51:315–329, 1989.

[193] Ward, S.M. and Sanders, K.M. Pacemaker activity in septal structures of canine colonic circular muscle. *Am. J. Physiol.*, 259:G264–G273, 1990.

[194] Ward, S.M. and Sanders, K.M. Upstroke component of electrical slow waves in canine colonic smooth muscle due to nifedipine-resistant calcium current. *J. Physiol. (Lond)*, 455:321–337, 1992.

[195] Ward, S.M., Burke, E. P. and Sanders, K.M. Use of rhodamine 123 to label and lesion interstitial cells of Cajal in canine colonic circular muscle. *Anat. Embryol. (Berl)*, 182:215–224, 1990.

[196] Ward, S.M. Burns, A.J., Torihashi, S. and Sanders, K.M. Mutation of the proto-oncogene c-kit blocks development of interstitial cells and electrical rhythmicity in murine intestine. *J. Physiol. (Lond.)*, 480:91–97, 1994.

[197] Xiong, Z., Sperelakis, N., Noffsinger, A. and Fenoglio-Preiser, C. Changes in calcium channel current densities in rat colonic smooth muscle cells during development and aging. *Am. J. Physiol.*, 265(1):C617–C625, 1993.

[198] Yu, D. S.,Chang, S. Y. and Ma, C. P. Ultrastructural changes of bladder cancer cells following methylene blue-sensitized photodynamic treatment. *Eur-Urol.*, 19:322–326, 1991.

[199] Zamir, O. and Hanani, M. Intercellular dye-coupling in intestinal smooth muscle. Are gap junctions required for intercellular coupling? *Experientia*, 46:1002–10050, 1990.

List of Publications

Journal Articles

1. Liu, L. W. C., L. Thuneberg and J. D. Huizinga. Cyclopiazonic acid, inhibiting the endoplasmic reticulum calcium pump, reduces the canine colonic pacemaker frequency. *J. Pharmacol. Exp. Ther.*, 275: 1058–68, 1995.

2. Liu, L. W. C., L. Thuneberg, and J. D. Huizinga. Selective lesioning of interstitial cells of Cajal by methylene blue and light leads to loss of slow waves. *Am. J. Physiol.*, 266: G485–G496, 1994.

3. Liu, L. W. C. and J. D. Huizinga. Canine colonic circular muscle generates action potentials without the pacemaker component. *Can. J. Physiol. Pharm.*, 72(1), 70–81, 1994.

4. Liu, L. W. C. and J. D. Huizinga. Electrical coupling of circular muscle to longitudinal muscle and interstitial cells of Cajal in canine colon. *J. Physiol.(Lond.)*, 470: 445–461, 1993.

5. Liu, L. W. C., L. Thuneberg, E. E. Daniel, and J. D. Huizinga. Selective accumulation of methylene blue by interstitial cells of Cajal in the canine colon. *Am. J. Physiol.*, 264: G64–G73, 1993.

6. Huizinga, J. D., L. W. C. Liu, M. Blennerhassett, L. Thuneberg, and A. Molleman. Intercellular communication in smooth muscle. *Experientia*, 48: 932–940, 1992.

7. Liu, L. W. C., E. E. Daniel, and J. D. Huizinga. Excitability of canine colon circular muscle disconnected from the network of interstitial cells of Cajal. *Can. J. Physiol. Pharmacol.* 70(2): 289–295, 1992.

8. Liu, L. W. C., L. Farraway, I. Berezin, and J. D. Huizinga. Interstitial cells of Cajal: Mediators of communication between longitudinal and circular muscle cells of canine colon. *Cell & Tissue Research*, submitted.

Book Chapters

1. Liu, L. W. C., N. Sperelakis, J. D. Huizinga. Pacemaker activity and intercellular communication in the gastrointestinal musculature, in *Intercellular Communication and Pacemaking Activity*, edited by J. D. Huizinga. CRC press: Ann Arbor, pp 159–174, 1995.

2. Huizinga, J. D., and L. W. C. Liu. Role of calcium channels in pharmacological modulation of gastrointestinal motility, in *Calcium Antagonists in Gastroenterology Research and Perspectives*, edited by Christen, M. O. and Paoletti, R. Kluwer Academic Publishers: Boston, pp 31–39, 1993.

Abstracts

1. Liu, L. W. C., L. Thuneberg and J. D. Huizinga. Simultaneous development of pacemaker activity and interstitial cells of Cajal network in neonatal mouse small intestine. *J. Gastroint. Motil.*, in press, 1995. (presented in the XV International Symposium on Gastrointestinal Motility, Rome Italy.)

2. Liu, L. W. C., L. Farraway, I. Berezin and J. D. Huizinga. Interstitial cells of Cajal: Mediators of communication between longitudinal and circular muscle cells of canine colon. J. Gastroint. Motil., in press, 1995. (presented in the XV International Symposium on Gastrointestinal Motility, Rome Italy.)[S]

3. Liu, L. W. C., R. L. Ruo and J. D. Huizinga. Submuscular interstitial cells of Cajal mediate communication between circular muscle lamellae of canine colon. *J. Gastroint. Motil.*, in press, 1995. (presented in the XV International Symposium on Gastrointestinal Motility, Rome Italy.)

4. Liu, L. W. C. and J. D. Huizinga. Role of the calcium activated potassium channel in repolarization of colonic electrical activity. *J. Gastroint. Motil.*, 5:201, 1993. (presented in the 14^{th} International Symposium on Gastrointestinal Motility, Muskoka, Ontario, Canada.)

5. Liu, L. W. C., L. Thuneberg and J. D. Huizinga. Regulation of colonic pacemaking frequency by intracellular calcium in sarcoplasmic reticulum. *J. Gastroint. Motil.*, 5:201, 1993. (presented in the 14^{th}International Symposium on Gastrointestinal Motility, Muskoka, Ontario, Canada.)

6. Liu, L. W. C., and J. D. Huizinga. Colonic circular muscle generates action potentials without the pacemaking component of slow waves. *FASEB J.* 7(4), A678, 1993. (presented in FASEB 93, New Orlean, Louisanna, U. S. A.)^S

7. Liu, L. W. C., I. Berezin and J. D. Huizinga. Gradient of membrane potential in circular muscle of canine colon is caused by electrical interaction between different cell types. *Gastroenterology*, 103(4): 1378, 1992. (presented in the 7^{th} Biennial Meeting of American Motility Society, Lake Tahoe, California, U. S. A.)

8. Liu, L. W. C., L. Thuneberg and J. D. Huizinga. Methylene blue and light selectively lesioned interstitial cells of Cajal in canine colon. *Gastroenterology*, 103(4): 1377, 1992. (presented in the 7^{th} Biennial Meeting of American Motility Society, Lake Tahoe, California, U. S. A.)^S

9. Liu, L. W. C., H, Mikkelsen, L. Thuneberg, I. Berezin and J. D. Huizinga. Electrical communication in areas with and without gap junctions in canine colon. *Gastroenterology*, 103(4): 1391, 1992. (presented in the 7^{th} Biennial Meeting of American Motility Society, Lake Tahoe, California, U. S. A.)^S

10. Huizinga, J. D., A. Molleman, L. W. C. Liu, L. Farraway and J. Tomlinson. Autorhythmicity in gut smooth muscle is mediated by second messenger operated calcium channels. 5^{th} *International Symposium on Calcium Antagonists*, Houston, 1991.

11. Liu, L. W. C., I. Berezin, and J. D. Huizinga. Electrical and morphological communication between the longitudinal and circular muscle cells of the canine colon. 34^{th} *Annual Meeting of Canadian Federation of Biological Society*, 1991.

12. Liu, L. W. C., E. E. Daniel, and J. D. Huizinga. Colonic circular muscle without the network of interstitial cells of Cajal can generate slow waves through different mechanisms. *Gastroenterology* 99(II): 1215, 1990. (presented in the 6^{th} Biennial Meeting of American Motility Society, Newport, Rhode Island, U. S. A.)

S denotes awards winning abstracts